INAUGURAL DISSERTATION

for

obtaining the doctoral degree

of the

Combined Faculty of Mathematics, Engineering and Natural Sciences

of the

Ruprecht - Karls - University

Heidelberg

Presented by

M.Sc. Bastienne Zaremba

Born in Schongau, Germany

Oral examination: February 10th 2025

DEVELOPMENT AND EVOLUTION OF PALLIAL CELL TYPES AND STRUCTURES IN AMNIOTES

Referees: Prof. Dr. Henrik Kaessmann

Prof. Dr. Ana Martin- Villalba

SUMMARY

Within the clade of amniotes (including mammals, birds, and non-avian reptiles), two lineages—birds and mammals—are renowned for their remarkable cognitive abilities. These capabilities likely evolved through innovations in the forebrain, particularly in the dorsal telencephalon, or pallium. Since the last common ancestor of amniotes approximately 320 million years ago, the pallium has undergone extensive morphological diversification. In mammals, the pallium is dominated by layered structures like the isocortex, whereas birds and reptiles primarily feature nuclear-organized regions, such as the dorsal ventricular ridge (DVR). While non-avian reptiles possess a small layered cortex, birds lack a layered cortex entirely and instead possess the hyperpallium, a unique nuclear-organized dorsal structure. These profound differences have sparked debates about pallial evolution, leading to competing hypotheses—some emphasizing homology of cell types performing analogous roles in a conserved neural microcircuit, while others focus on shared developmental origins in distinct pallial domains.

In my dissertation, I addressed these debates by investigating the cellular composition, development, and evolution of the pallium across amniotes. To this end, I generated spatially resolved cell type atlases of the entire adult chicken pallium and its developmental stages using single-nucleus RNA sequencing and spatial transcriptomics. I compared these data to equivalent datasets from mammals and reptiles, including those I generated, as well as publicly available datasets, to reconstruct the evolutionary history of pallial structures and cell types.

Within chickens, I found remarkable similarity between neurons in the hyperpallium and the nidopallium (ventral DVR), despite their topologically distinct locations. This similarity likely arises from extensive gene expression convergence during late development, suggesting that embryonic topological location does not always dictate the gene expression programs underlying adult functional properties in birds.

Across species, my findings confirm conserved gene expression patterns in inhibitory neurons, but reveal an expansion of a cell type predominantly found in the mammalian amygdala that is distributed throughout the avian pallium. I also identified conserved excitatory neuron types in the hippocampal regions of birds, non-avian reptiles, and mammals, as well as homologous populations of claustrum-like neurons in the mesopallium (anterior DVR) of birds. Additionally, certain cell types in the avian mesopallium resemble neurons in the deep layers of the mammalian isocortex. In contrast, some populations in the hyperpallium and nidopallium show substantial divergence. Developmental analyses suggest these neurons evolved distinct identities in birds, diverging significantly from their mammalian counterparts.

These findings challenge previous circuitry-based models, which propose homologies largely unsupported by my observations. Although my results align more closely with development-based homology hypotheses, they also argue against the notion of simple one-to-one

correspondences between pallial regions. Instead, they reveal a mosaic pattern of evolution: some excitatory cell types are conserved across species, even when located in different pallial domains, whereas others have diverged significantly.

This dissertation also includes an investigation into the cellular evolution of the mammalian isocortex across major mammalian lineages. For example, I highlight the conservation of the principal claustral cell type across mammals, setting the stage for future studies on pan-mammalian cellular features of the pallium.

Overall, this work provides critical insights into the anatomy, development, and evolution of the amniote pallium—particularly the avian pallium. It confirms previously suggested homologies, such as those among inhibitory or hippocampal excitatory neurons, while uncovering novel relationships, such as those between avian mesopallial excitatory neurons and mammalian deep-layer isocortical neurons. My findings underscore the importance of developmental data in testing evolutionary models and challenge longstanding assumptions about regional homology in the amniote pallium. By highlighting conserved, divergent, and convergent aspects of pallial evolution, this dissertation lays the foundation for understanding the molecular mechanisms underlying advanced cognitive abilities in birds.

ZUSAMMENFASSUNG

Innerhalb der Gruppe der Amnioten – zu der Säugetiere, Vögel und nicht-avische Reptilien gehören – zeichnen sich insbesondere Vögel und Säugetiere durch ihre bemerkenswerten kognitiven Fähigkeiten aus. Diese Fähigkeiten haben sich wahrscheinlich durch evolutionäre Innovationen im Vorderhirn, insbesondere im dorsalen Telencephalon oder Pallium, entwickelt. Seit dem letzten gemeinsamen Vorfahren der Amnioten vor etwa 320 Millionen Jahren hat das Pallium eine beeindruckende morphologische Vielfalt hervorgebracht. Während bei Säugetieren das Pallium durch geschichtete Strukturen wie den Isocortex dominiert wird, findet man bei Vögeln und Reptilien vor allem clusterartig aufgebaute Regionen wie den dorsalen ventrikulären Kamm (DVR). Nicht-avische Reptilien besitzen zwar einen kleinen geschichteten Kortex, doch Vögeln fehlt dieser vollständig; stattdessen haben sie das Hyperpallium, eine einzigartige clusterartig aufgebaute dorsale Struktur. Diese grundlegenden Unterschiede haben große Debatten über die Evolution des Palliums ausgelöst, die zu unterschiedlichen Hypothesen geführt haben. Einige Theorien betonen die Homologie von Zelltypen, die ähnliche Funktionen in einem konservierten neuronalen Mikroschaltkreis erfüllen, während andere den Fokus auf gemeinsame Entwicklungsursprünge in verschiedenen Regionen des Palliums legen.

In meiner Dissertation habe ich verschiedene Theorien evaluiert, indem ich die zelluläre Zusammensetzung, Entwicklung und Evolution des Palliums bei Amnioten untersucht habe. Dafür habe ich räumlich aufgelöste Atlanten der Zelltypen im adulten Hühnerpallium und seiner Entwicklungsstadien mithilfe von Einzelkern-RNA-Sequenzierung und räumlicher Transkriptomik erstellt. Diese Daten habe ich mit entsprechenden Datensätzen von Säugetieren und Reptilien verglichen – einschließlich meiner eigenen Ergebnisse sowie öffentlich zugänglicher Daten –, um die Evolutionsgeschichte der Strukturen und Zelltypen des Palliums nachzuvollziehen.

Im Hühnerpallium fand ich eine bemerkenswerte Ähnlichkeit zwischen den Neuronen des Hyperpalliums und des Nidopalliums (ventraler DVR), obwohl diese topologisch getrennt sind. Diese Ähnlichkeit ist wahrscheinlich auf eine weitgehende Konvergenz der Genexpression während der späten Entwicklung zurückzuführen. Das deutet darauf hin, dass die Position der Neuronen und ihrer Vorläuferzellen im Embryo nicht immer die Genexpressionsprogramme vorgibt, die letztlich die funktionellen Eigenschaften im adulten Tier bestimmen.

Artübergreifend zeigen meine Ergebnisse konservierte Genexpressionsmuster bei inhibitorischen Neuronen, aber auch die Ausbreitung eines inhibitorischen Zelltyps, der bei Säugetieren nur in der Amygdala vorkommt, bei Vögeln jedoch über das gesamte Pallium verteilt ist. Außerdem habe ich konservierte glutamaterge Neuronentypen in den Hippocampus-Regionen von Vögeln, nicht-avischen Reptilien und Säugetieren identifiziert sowie homologe Populationen von claustrum-ähnlichen Neuronen im Mesopallium (anteriores DVR) der Vögel. Interessanterweise ähneln einige Zelltypen des Mesopalliums von Vögeln den Neuronen in den tiefen Schichten des Isocortex bei Säugetieren. Im Gegensatz

dazu zeigen Populationen im Hyperpallium und Nidopallium erhebliche Unterschiede, die darauf hindeuten, dass diese Neuronen bei Vögeln einzigartige Genexpressionsmuster entwickelt haben, die sich stark von denen der potentiell korrespondierenden Zelltypen in Säugetieren unterscheiden.

Diese Ergebnisse stellen bisherige Hypothesen in Frage, die Homologien auf Grundlage von Schaltkreisfunktionen vorgeschlagen, da sie von meinen Beobachtungen weitgehend nicht gestützt werden. Während meine Ergebnisse entwicklungsbasierte Homologiehypothesen eher unterstützen, widersprechen sie auch der Idee einer einfachen Eins-zu-eins-Entsprechung zwischen verschiedenen Regionen des Palliums. Stattdessen zeigt sich ein mosaikartiges Muster der Evolution: Einige glutamaterge Zelltypen sind über Arten hinweg konserviert, auch wenn sie in unterschiedlichen Regionen des Palliums lokalisiert sind, während andere deutliche Divergenz aufweisen.

Zusätzlich habe ich in meiner Dissertation die zelluläre Evolution des Isokortex der Säugetiere über verschiedene Säugetiergruppen hinweg untersucht. Dabei konnte ich beispielsweise die Konservierung eines claustralen Zelltyps bei Säugetieren nachweisen und eine Grundlage für zukünftige Studien zu säugetierübergreifenden zellulären Merkmalen des Palliums schaffen.

Insgesamt liefert diese Arbeit wichtige Einblicke in die Anatomie, Entwicklung und Evolution des Palliums bei Amnioten, insbesondere bei Vögeln. Sie bestätigt bereits vermutete Homologien, etwa bei inhibitorischen Neuronen oder glutamatergen Hippocampus-Zelltypen, und deckt zugleich neue Verbindungen auf, etwa zwischen Neuronen im Mesopallium von Vögeln und Neuronen in tiefen Schichten des Säugetierkortex. Meine Ergebnisse unterstreichen die Bedeutung von Daten zur zellulären Entwicklung für die Überprüfung evolutionärer Modelle und stellen etablierte Annahmen über die regionale Homologie im Pallium der Amnioten infrage. Indem sie konservierte, divergente und konvergente Aspekte der Evolution des Palliums beleuchtet, legt diese Dissertation einen wichtigen Grundstein für das Verständnis der molekularen Mechanismen, die den fortgeschrittenen kognitiven Fähigkeiten von Vögeln zugrunde liegen.

PUBLICATIONS

Bastienne Zaremba, Amir Fallahshahroudi, Céline Schneider, Julia Schmidt, Ioannis Sarropoulos, Evgeny Leushkin, Bianka Berki, Enya Van Poucke, Per Jensen, Rodrigo Senovilla-Ganzo, Francisca Hervas-Sotomayor, Nils Trost, Francesco Lamanna, Mari Sepp, Fernando García-Moreno, Henrik Kaessmann. **Developmental origins and evolution of pallial cell types and structures in birds**. *bioRxiv* 2024.04.30.591857 (2024). Under review at *Science.*

Hanke Gwendolyn Bauersachs, C. Peter Bengtson, Ursula Weiss, Andrea Hellwig, Celia García-Vilela, Bastienne Zaremba, Henrik Kaessmann, Priit Pruunsild, Hilmar Bading. **N-methyl-d-aspartate Receptor-mediated Preconditioning Mitigates Excitotoxicity in Human Induced Pluripotent Stem Cell-derived Brain Organoids**. *Neuroscience* 484, 83-97 (2022).

CONTRIBUTIONS

Science is always a collaborative effort. However, to facilitate evaluation I will do my best to dissect the contributions to this thesis. Animal brain dissections were carried out by Dr. Amir Fallahshahroudi (adult chicken), Enya Van Poucke (adult chicken), Dr. Fernando García-Moreno and Rodrigo Senovilla-Ganzo (developing chicken), collaborators from the Frank Grützner lab (echidna) and me (adult chicken, mouse, opossum, green anole lizard). Quality control of tissues and all nuclei isolations for single-nucleus RNA-sequencing and single-nucleus multiome ATAC and RNA sequencing were carried out by me, most of the subsequent library preparation was carried out by Céline Schneider and Julia Schmidt. Library sequencing was mostly performed by Céline Schneider and me. A subset (~10%) of the single-nucleus RNA-sequencing dataset presented for the adult chicken pallium, and single-nucleus RNA-sequencing datasets for the murine isocortex were generated as part of my master's thesis. Tissue sectioning for In Situ Sequencing (ISS) and Visium spatial transcriptomics was carried out by me. Imaging of ISS sections was carried out by Cartana, Sweden. Visium libraries were prepared by Dr. Bianka Berki at the Heidelberg Deep Sequencing core facility. All analyses, except for analysis of single nucleus ATAC sequencing, which was carried out by Dr. Ioannis Sarropoulos, were performed by me. However, I had support in form of some shared code mainly from Dr. Francesco Lamanna and Nils Trost. Conceptual contributions are close to impossible to dissect, but I received major input from Dr. Mari Sepp, Dr. Fernando García-Moreno and of course Prof. Henrik Kaessmann. Most results are available in a preprint (*1*), for which I wrote the initial draft and made and assembled all figures, except for one supplementary figure. ChatGPT was used for language editing to improve the readability of certain sections.

ACKNOWLEDGEMENTS

I firmly believe that our life experiences shape who we are and what we can achieve. In that sense, completing this project would not have been possible without the remarkable people who have accompanied me throughout my life and during this PhD journey. Some provided hands-on support and invaluable guidance, others brightened my daily life, and a few inspired me profoundly with just a few words.

First and foremost, I am deeply grateful to Prof. Dr. Henrik Kaessmann, my PhD supervisor, for granting me this exceptional opportunity and placing his trust in me to tackle this extensive, yet incredibly exciting project. His enthusiasm, kindness, guidance, and encouragement over the years have been invaluable, and I am so glad I chose to apply for my master's thesis in his group.

I would also like to express my heartfelt gratitude to Dr. Fernando García-Moreno, who joined this project at just the right moment. His expertise and support in interpreting the data and his guidance in navigating the complexities of the chicken brain field were absolutely invaluable and he reignited my excitement and motivation at a time when I really needed it.

I am sincerely thankful to Prof. Dr. Ana Martin-Villalba for her valuable insights during my TAC meetings and for serving as my secondary PhD supervisor. I also extend my thanks to Dr. Lauren Saunders and Dr. Simon Anders for dedicating their time to serve as examiners on my defense committee.

To my colleagues and friends, thank you so much for making this journey a truly memorable and wonderful experience. I am immensely grateful to Dr. Mari Sepp for sharing her extensive neuroscience knowledge, her thoughtful feedback on my writings, and most importantly her unfailing kindness and encouragement. I am also so grateful to Céline Schneider and Julia Schmidt, whose practical support was essential to this project, and their impeccable organization and cheerful presence made lab work not only efficient but also much more enjoyable. My gratitude also extends to Dr. Francesco Lamanna and Dr. Evgeny Leushkin for their advice and guidance in this project. Special thanks go to Nils Trost for his invaluable help with coding, his efforts in maintaining our critical computational infrastructure, and, of course, his constant supply of memes. I would also like to thank Dr. Ioannis Sarropoulos for his critical questions and thoughtful insights, and for always being helpful, fun and inspirational. I am also very grateful to Dr. Amir Fallahshahroudi for being a great companion during sampling adventures and for sharing his expertise in all things chicken-related.

I would like to thank everyone in the Vertebrain team—Dr. Francisca Hervas-Sotomajor, Dr. Kerry Lynn Gendreau, Matthias Janeschik, and Daniel Soto-Carballo—for their phylogenetic and evolutionary insights and for their much-appreciated enthusiasm about non-human brains. Dr. Rodrigo Senovilla-Ganzo also deserves a special mention for his advice, his shared frustration over the challenges of working with chickens, and his wonderfully weird sense of humor. To Leticia Rodriguez-Montes and Dr. Xuefei Yuan, my incredible office booth mates

and friends: thank you for listening to my rants, sharing in moments of silliness and muffin time, and for being absolutely lovely and fun. Special thanks also go to Noe Mbengue, the most talented dungeon master known to man (and halflings), and to the rest of our glorious group of adventurers—Nils, Ioannis, Evgeny, Matthias, Daniel, Elena, Tetsuya, Xuefei, and others—for making Thursdays the highlight of every week.

I am especially grateful to Kathrin Hall for her unwavering enthusiasm and for keeping spirits high, even in the face of tedious timesheets and travel reimbursements. I would also like to thank everyone else I had the privilege of working with in the Kaessmann lab, including Dr. Margarida Cardoso-Moreira, Dr. Florent Murat, Dr. Kevin Leiss, Pascal Lafrenz, Dana Frank, Lea Kubitz, Alexander Stuart, and Dr. Aleksandra Kondrashkina. Each of you has contributed in your unique way, making this journey all the more wonderful.

Finally, I have no words to fully express my love and gratitude to my family, including my newly extended family, for their unwavering support throughout this process and beyond. They have celebrated every small step with boundless enthusiasm, regardless of the outcome, and their belief in me has carried me through many moments of doubt.

And to my husband Jan: thank you for listening to endless chicken brain talk, for your constant encouragement, and for always building my confidence. You consoled me during the lows and celebrated every milestone with me. With you I feel safe and inspired to explore what I can achieve.

TABLE OF CONTENTS

TABLE OF FIGURES

1 INTRODUCTION

Neuroscientists have spent centuries investigating the biological foundation for complex animal behaviors and intelligence. Several metrics have been suggested to reflect cognitive capacity, such as the brain-to-body mass ratio, relative brain size (*2*), and more recently relative neuron numbers and density across different brain structures (*3*). Among all species examined to date, two taxa stand out regarding most of these metrics - mammals and birds (*2*, *4*, *5*), separated by 320 million years of independent evolution since their last common ancestor (*6*). The massive increase in neuron numbers observed in these two lineages compared to the third major group within amniotes, non-avian reptiles, is mostly accounted for by the expansion of two specific brain structures, the cerebellum and the telencephalon (*4*). The telencephalon, the most anterior part of the brain, in particular the dorsal telencephalon, is considered to be central to advanced cognition. Consistently, birds and mammals demonstrate complex behaviors, such as intricate vocalizations (*7*) and sophisticated social structures (*8*), with certain avian clades, like corvids, exhibiting cognitive abilities comparable to those of primates and even great apes (*9*–*12*). Understanding the molecular mechanisms driving the likely independent brain expansion and evolution of advanced cognitive abilities in birds (*13*) can offer insights into how different brains have evolved to solve similar cognitive challenges. Convergent evolution of neurons, circuits and brain regions—meaning the independent evolution of similar traits in distinct lineages—may reflect developmental, genetic, and functional constraints, as well as potential positive selection shaping these structures, while evolutionary conservation can point to essential functions. Thus, a comparative analysis of the dorsal telencephalon across amniotes has the potential to uncover the fundamental principles governing the organization and function of this key brain region.

1.1 ANATOMY, FUNCTION AND CONNECTIVITY OF THE ADULT AMNIOTE PALLIUM

The telencephalon comprises two main territories, the ventrally-located subpallium and the dorsally-located pallium, which both arise from the anterior neural tube in all vertebrates (*14*). While the structure, cellular composition and development of the subpallium are largely conserved across vertebrates (*15*, *16*), the pallium has undergone dramatic morphological and molecular changes. For example, the amphibian pallium is relatively simple and comparatively small while in mammals, it is organized into various nuclei and layers and for instance in humans covers almost the entire surface of the brain (*17*–*19*).

1.1.1 THE MAMMALIAN PALLIUM

In mammals, the pallium encompasses diverse structures that can be classified using two systems: one based on laminar structure and the other based on functional roles.

The first classification system organizes pallial regions according to their laminar structure, specifically the number and appearance of cortical layers. Pallial structures are broadly divided into the isocortex (traditionally also called neocortex; Fig. 1A),

characterised by its hallmark six-layered organization, and the allocortex, which exhibits a simpler architecture with three to six layers (*20*). The allocortex includes regions such as the archicortex (e.g., hippocampus (*21*)), the paleocortex (e.g., olfactory bulb and piriform cortex (*22*)), and transitional areas collectively referred to as periallocortex (e.g., entorhinal and parts of insular the cortices (*23*)). These differences in laminar structure not only highlight architectural diversity but also reflect evolutionary trajectories, as allocortical regions are believed to predate the isocortex due to shared characteristics with reptilian cortices (*22*, *24*).

The second system classifies pallial structures based on their functional roles. For instance, the hippocampal formation —which includes the cornu ammonis, dentate gyrus, subiculum, and entorhinal cortex— is central to learning and memory (*25*, *26*). The claustrum and endopiriform nucleus though less well-studied, are implicated in diverse functions such as modulating cortical information processing to support attention and controlling the sleep-wake cycle (*27*). The olfactory bulb and olfactory (or piriform) cortex receive and process olfactory input (*22*), while the pallial nuclei of the amygdala regulate emotion and social behavior (*28*) (Fig. 1A).

The isocortex, in contrast, plays a pivotal role in sensory perception, cognition, motor command generation, and other higher-order processes (*29*). In the tangential dimension, it consists of primary sensory areas, unimodal sensory association areas (dedicated to a single sensory modality), multimodal association areas, and motor areas. Primary sensory areas receive direct input from first-order nuclei of the thalamus and are reciprocally connected with unimodal sensory association areas. These, in turn, connect to multimodal association areas, which project to other multimodal areas and/or the motor cortex (*30*). Radially, pyramidal excitatory neurons within each of the six layers, numbered from the outermost to the innermost layer, share many characteristics, including their descending and ascending connections. Neurons in layer two and three exclusively send axons to neighboring and distant cortical areas, whereas certain types of pyramidal neurons in deep layers project to subcortical targets, such as the striatum, thalamus, midbrain or brain stem. Neurons in layer four receive primary sensory input from the thalamus (*31*) (Fig. 1B).

All of the aforementioned pallial structures can be identified in all mammalian lineages, including eutherians (‘placental’ mammals), metatherians (marsupials), and egg-laying monotremes, with the exception of the claustrum and endopiriform nucleus, whose existence in monotremes is debated (*32*, *33*). The isocortex’s unique six-layered organization, as well as the relative position of primary sensory areas, are also shared among these lineages. However, there is considerable variation in the relative size of the isocortex, of isocortical areas and of molecular layers, as well as in the degree of folding (*34*, *35*).

1.1.2 THE SAUROPSID PALLIUM

While the dorsal areas of the pallium largely occupied by the isocortex are relatively expanded in mammals, the pallium in sauropsids (including birds and non-avian reptiles) is dominated by a ventro-lateral structure called the dorsal ventricular ridge (DVR). In contrast to the mammalian cortex, the DVR does not have a laminar structure, but is organized in a nuclear fashion, meaning neurons aggregate into clusters (*36*) (Fig. 1A). Still, DVR neurons were found to be arranged in functional columns meaning neurons in different areas receive and process distinct sensory inputs in a topographically discrete manner, analogous to mammalian isocortical areas and layers (*37–39*) (Fig. 1B).

In non-avian reptiles the DVR is traditionally considered to consist of two main parts, the anterior predominantly sensory recipient DVR, which is the major target of ascending thalamic projections, and the posterior mainly associative DVR, which receives extensive projections from the anterior DVR but also projects to extra-telencephalic targets (*36*, *40*). Further important subdivisions have been described, such as the claustrum-like anterior medial DVR in lizards and the corresponding pallial thickening in turtles, or an amygdala-like region in the posterior DVR in lizards and turtles (*41*, *42*). However due to limited data and discourse about the reptilian brain, there is no consensus neuroanatomical atlas defining a structural hierarchy, as in mammals.

The DVR is especially prominent in archosaurs (including crocodilians and birds; Fig. S1), where it is subdivided into three major regions, the mesopallium, nidopallium and arcopallium (*43*, *44*) (Fig. 1A). The mesopallium is an associative region forming predominantly intra-telencephalic connections (*45*), whereas the nidopallium harbors heterogeneous regions in terms of connectivity, i.e., primary sensory areas as well as highly associative areas, such as the nidopallium caudolaterale (Fig. 1B) (*36*). Several pallial and subpallial regions in the caudal telencephalon have been grouped into the arcopallium and/or avian amygdala, but the nomenclature and grouping vary across sources (*43*, *44*). In this thesis, I will refer to all pallial regions in this collection as ‘arcopallium’ in order to avoid confusion with the mammalian amygdala. The arcopallium represents the major output and motor-associated structure of the avian DVR as it projects to subpallial (e.g., striatum, pallidum) and various extra-telencephalic targets (e.g., optic tectum; Fig. 1B) (*36*, *38*).

Dorsally to the DVR, non-avian reptiles possess a three-layered cortex, organized in a similar manner as mammalian three-layered cortices. The reptilian cortex is traditionally subdivided into a medial, dorsal and lateral part, where lateral cortex receives input from the olfactory bulb similar to the piriform cortex in mammals, the dorsal cortex receives multimodal input (e.g., visual in turtles), and the medial cortex integrates information from both regions and is involved in spatial memory and learning akin to the mammalian hippocampal formation (*24*).

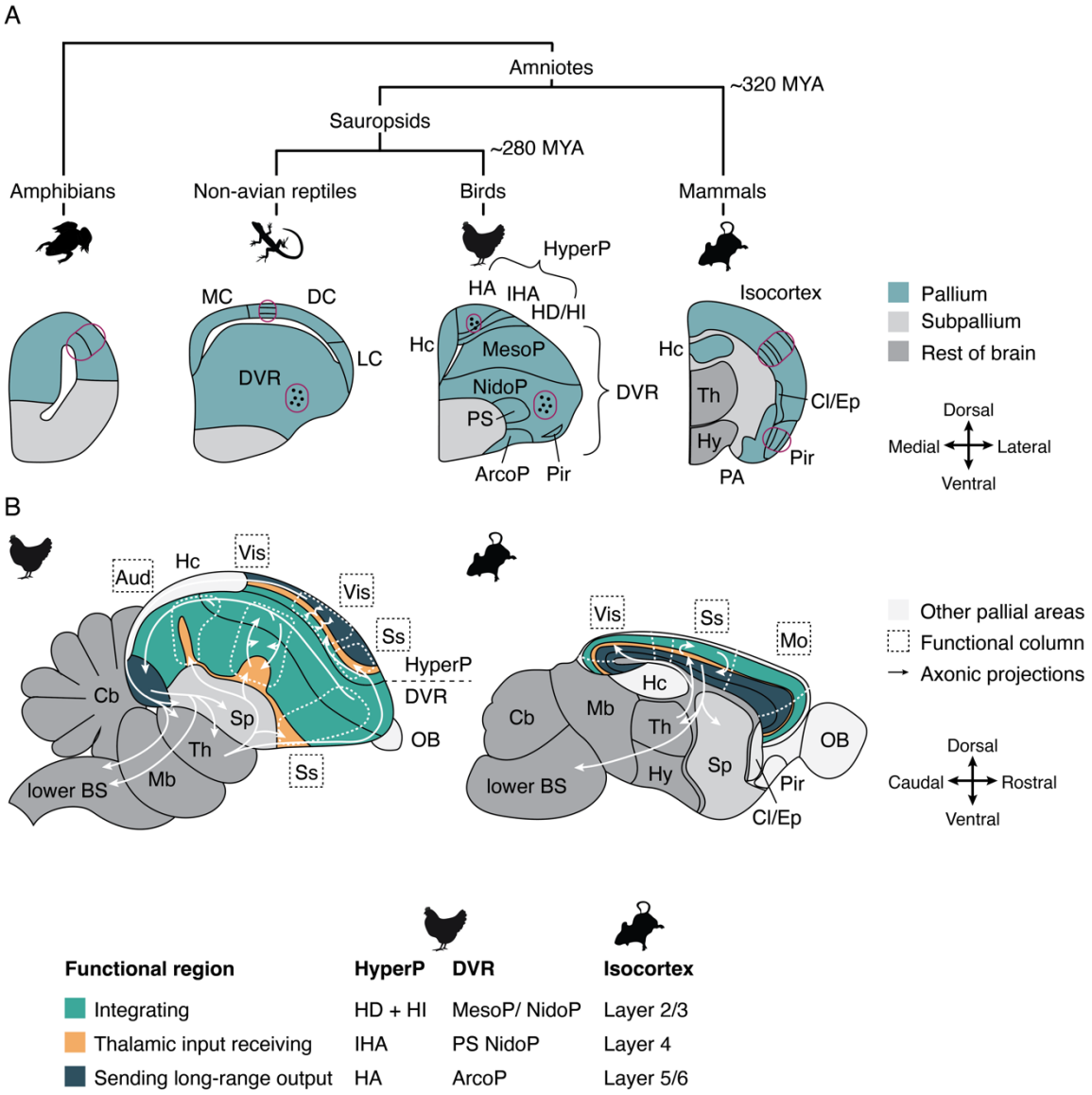

Functional region	HyperP	DVR	Isocortex
Integrating	HD + HI	MesoP/ NidoP	Layer 2/3
Thalamic input receiving	IHA	PS NidoP	Layer 4
Sending long-range output	HA	ArcoP	Layer 5/6

Figure 1 Anatomy and functional organization of the amniote pallium. (A) Schematic representation of coronal sections of the telencephalon in (left to right) frog, lizard, chicken and mouse. Molecular structure (layered or nuclear) is depicted within red circles. **(B)** Schematic representation of sagittal brain sections in birds (left) and mice (right). Sensory-motor circuits, formed by neurons in distinct brain regions and their axonal projections, are organized into functional columns processing various sensory modalities in both lineages. While projections across columns are broadly similar, only some simplified examples are shown. Analogous circuits to those in the mammalian isocortex are present in the avian hyperpallium (HyperP) and DVR. MYA, million years ago; MC, medial cortex; DC, dorsal cortex; LC, lateral cortex; DVR, dorsal ventricular ridge; Hc, hippocampal area (chicken) / hippocampus (mouse); HyperP, hyperpallium; HA, apical hyperpallium; IHA, interstitial apical hyperpallium; HD/HI, densocellular hyperpallium and intercalated hyperpallium; MesoP; mesopallium; NidoP, nidopallium; PS, primary sensory areas of the nidopallium; ArcoP, arcopallium; Pir, piriform cortex; Cl, claustrum; Ep, endopiriform nucleus; PA, pallial amygdala; Th, thalamus; Hy, hypothalamus. Aud, auditory; Vis, visual; Ss, somatosensory; Mo, motor; Cb, cerebellum; BS, brain stem; Mb, midbrain; Th, thalamus; Hy, hypothalamus; Sp, subpallium; OB, olfactory bulbs; Pir, piriform cortex; Cl, claustrum; Ep, endopiriform nucleus.

In birds, the majority of this three-layered cortex likely diversified into another nuclear structure known as the Wulst (German for ‘bulge’) or hyperpallium (*36*). The avian hyperpallium is subdivided into several mediolateral regions: the apical hyperpallium

(HA), interstitial apical hyperpallium (IHA), intercalated hyperpallium (HI), and densocellular hyperpallium (HD) (*44*) (Fig. 1A). These substructures are prominent and easily distinguishable in species with large hyperpallia, such as owls (*46*). However, in species with smaller hyperpallia, such as finches and chickens, the reduced size and absence of clear anatomical boundaries have led to debates regarding the molecular identity of HI and HD. Some studies propose that these regions belong to the neighboring mesopallium rather than the hyperpallium (*47*, *48*). Additionally, some authors have suggested to redefine the caudal border of the hyperpallium, based on the *in situ* expression of selected genes, to include the "caudal hyperpallium" (HC), which was previously categorized as a distinct region located between the hyperpallium and hippocampal areas (*44*).

Similar to the DVR, neurons within the hyperpallial substructures are arranged in functional columns, forming sensory-motor circuits independent of those in the DVR. In these circuits, neurons in the IHA receive sensory input relayed by the thalamus (e.g., visual or somato-sensory), while neurons in HA project to subpallial and extra-telencephalic targets (e.g., thalamus, brainstem). The HD and HI areas have associative functions and project mainly within the telencephalon, similar to the neighboring mesopallium (*37*, *38*, *49*) (Fig. 1B). The connectivity of the newly defined HC remains unclear (*44*).

In addition to the DVR and the hyperpallium, the avian pallium also contains a comparatively small medial hippocampal area that extends caudally where it borders the arcopallium, and an even smaller piriform cortex, the only truly cortical structure in the avian brain (*36*, *44*).

1.1.3 THE PALLIUM OF AMNIOTE LAST COMMON ANCESTOR

Paleontological evidence suggests that early amniotes had smaller brain-to-body mass ratios and relatively smaller telencephala compared to modern mammals or birds, indicating that the telencephalic expansion observed in these lineages occurred independently (*13*). To reconstruct the internal anatomical organization of the telencephalon in the amniote last common ancestor, comparative analyses of telencephalic structures across extant species are essential. The major subdivisions of the subpallium, including the striatum and pallidum, can be identified across vertebrates (*15*, *16*), indicating their likely presence in the ventral telencephalon of stem amniotes. Furthermore, the existence of a cortical structure in the dorsal pallium of both mammals and non-avian reptiles suggests that this feature may be ancestral to the amniote lineage. However, the organization and structure of the remaining pallial regions in these early amniotes remain speculative.

1.2 CELL TYPES IN THE ADULT AMNIOTE PALLIUM

The adult amniote pallium contains three major classes of cells, neurons, glia, and immune cells. Neurons and glia arise from local neuroepithelial stem cells (*50*) whereas microglia, the brain parenchyma's resident macrophages, invade the central nervous system (CNS) during development in mammals (*51*). Little is known about the ontogeny and functions of microglia outside mammals, but they have been identified in various vertebrate and invertebrate species (*52*), arguing for a certain degree of conservation of this cell type across all vertebrates. In addition to these primary cell populations, other cell types, such as fibroblasts, endothelial cells, and mural cells, which are associated with the meninges or the brain's vasculature (*53*), are frequently identified in single-cell datasets. However, these will not be discussed here in more detail.

1.2.1 GLIA

Glial cells encompass a diverse range of differentiated, as well as prenatal and adult stem/progenitor cell types which have been mostly studied in eutherians. Stem and progenitor glial cells are discussed in chapter 1.3. Key differentiated glial cell types include ependymal cells, oligodendrocytes, and astrocytes.

Ependymal cells are often ciliated and form an epithelial layer that lines the brain's ventricular system, playing a critical role in cerebrospinal fluid homeostasis (*54*, *55*). The presence of ependymal cells across various vertebrate and invertebrate species suggests that this cell type emerged before the origin of vertebrates, however a one-to-one homology of this cell type across species has not been definitely established (*56*).

Oligodendrocytes, derived from fate-restricted oligodendrocyte progenitor cells (OPCs), are responsible for the production of myelin sheaths around axons, thereby enabling saltatory conduction of action potentials (*57*, *58*). This cell type likely originated within the jawed vertebrate lineage from the diversification of an ancestral glial cell type, which transcriptomically resembles mammalian astrocytes (*16*).

Astrocytes, named for their often stellate morphology in mammals, represent a morphologically diverse group of glial cells involved in water and ion homeostasis, nutrient exchange across the blood-brain barrier, and the development and regulation of neural connectivity (*59*). Stellate astrocytes are also prevalent in the avian brain (*56*), and a glial cell type closely resembling mammalian astrocytes in morphology and function has been identified in zebrafish (*60*), suggesting that astrocytes may have already been present in the last common ancestor of extant bony vertebrates (Osteichthyes) (Fig. S1).

However, astrocytes share substantial similarities with radial glia, the primary embryonic neural stem cell type in vertebrates, and may retain some neurogenic potential in mammals (*61*, *62*). Furthermore, mammals possess astrocyte-like cells with more radial morphologies, Müller glia and Bergmann glia, that fulfil analogous roles in specific brain regions (*63*, *64*). In some other vertebrate species, for instance some amphibian species,

where bona fide astrocytes have so far not been identified, other glial cells likely perform functions analogous to those of mammalian astrocytes and ependymal cells and are therefore often called “astroglia” or “ependymoglia” (*56*), blurring the distinction between these cell types. This overlap in morphology and function between radial glia and astrocytes suggests an intertwined evolutionary relationship and further work is needed to trace their evolutionary origin and diversification across species.

1.2.2 NEURONS

Unexpected transcriptomic heterogeneity has been observed in some glial cell types across different brain regions in eutherians (*65*, *66*). However, neurons exhibit a much more pronounced regional diversity (*67*, *68*) and their numbers, in contrast to glial cell numbers, vary significantly across amniote lineages (*4*). These observations suggest that neurons are likely the primary drivers of the advanced cognitive abilities observed in mammals and birds and, consequently, this thesis primarily focuses on the study of neurons.

Neurons are excitable, post-mitotic cells that can be broadly classified into two groups based on their projection identity: interneurons and projection neurons. Interneurons have originally been defined as neurons interposed between sensory and motor neurons. However, this definition applies to an overwhelming majority of neurons in the vertebrate brain, thus ‘interneuron’ is also often used as a synonym for local circuit neurons that participate in local aspects of neural circuits by modulating only nearby neurons. In this thesis, the term "interneuron" is used in the sense of "local circuit neuron" only. In contrast to local circuit neurons, projection neurons possess axons extending between regions of the CNS, or from the CNS to receptors and effector organs, including sensory and motor neurons. Projection neurons thus form the backbone of neural circuits across the body and brain (described in chapter 1.1.1.) (*20*).

Based on neurotransmitter identity, three major neuron populations can be distinguished in the amniote telencephalon: glutamatergic, GABAergic (gamma-aminobutyric acid releasing) and cholinergic neurons (acetylcholine releasing) (*41*, *67*). Cholinergic neurons are rare in the mammalian and lizard telencephalon and their heterogeneity is best characterized in rodents, where cholinergic interneurons and projection neurons are mostly found in the subpallium, with some cholinergic interneurons also present in the pallium (*69*).

GABAergic neurons in the adult telencephalon function as inhibitory cells, typically inducing hyperpolarization in post-synaptic neurons. They can be classified into major transcriptomic groups based on their developmental origin from distinct germinal zones in the mammalian subpallium: the medial (MGE), lateral (LGE), and caudal ganglionic eminence (CGE), the embryonic septum and embryonic preoptic area (*70*, *71*) (Fig. 2). A significant number of GABAergic neurons migrate from these zones along well-defined routes, eventually populating the whole telencephalon, with the ganglionic eminences

being the primary source of GABAergic neurons in the pallium (*41*, *67*, *72*). Although corresponding structures are morphologically not easily discernible in non-mammalian embryos (*15*), GABAergic interneurons with an MGE and LGE-like transcriptomic profile were identified in the lamprey, arguing for conservation of these structures across vertebrates (*16*). CGE-like neurons were detected in the salamander (*19*) but not in teleost (*73*, *74*), where certain populations of GABAergic neurons displayed mixed MGE- and CGE-like gene expression profiles, suggesting that populations with a distinct CGE identity originated within the sarcopterygian lineage (including tetrapods, lungfishes and coelacanths; Fig. S1). In amniotes, the majority of GABAergic neurons in the pallium are interneurons, whereas the subpallium contains both GABAergic projection and interneurons. The MGE and LGE give rise to both types across amniotes, while the CGE likely gives rise to interneurons exclusively (*15*). However, the proportions of GABAergic interneurons and projection neurons derived from different ganglionic eminences vary across different amniote lineages (*41*, *75*, *76*).

In eutherians, a remarkable morphological, functional and transcriptomic diversity of GABAergic neurons has been described, extending much beyond the classification based on developmental origins (*77*). While some of these populations have been identified in other amniote lineages (*41*, *72*, *75*), the extent of conservation or diversification of GABAergic neuron populations within amniotes remains uncertain. This uncertainty largely stems from the limited morphological and functional data available for sauropsids and the lack of common criteria and methods for classifying distinct cell types within and across species.

Glutamatergic neurons, which are excitatory, comprise the majority of neurons in the amniote pallium and serve as the main group of projection neurons (*41*, *67*, *76*). The classification of glutamatergic neuron types is well established in the mammalian isocortex, where layer-specific types can be distinguished by their morphology, developmental time of origin, specific gene expression profiles, and connectivity patterns (described in chapter 1.1.1) (*31*, *78*, *79*). However, unlike GABAergic neuron types, which are largely shared across pallial regions, glutamatergic neuron types exhibit significant regional variability. Although single-cell transcriptomic data are available for the entire mouse and human brain (*67*, *68*, *76*, *80*, *81*), the diversity of glutamatergic neuron types in pallial structures outside the isocortex, as well as their variation across regions, has not yet been comprehensively characterized. According to my knowledge only one study investigated the variation across pallial regions in the context of the murine isocortex and hippocampal formation, revealing a parallel spatial and projection-identity-related transcriptomic variation of distinct, yet broadly similar glutamatergic types (*82*).

Recent single-cell studies of the non-avian reptile pallium (*41*, *72*) and specific regions of the bird pallium (*75*, *83*) provided insights into the organization of glutamatergic neurons in other amniote lineages. These studies reveal distinct transcriptomic and functional

neuron types within anatomically defined regions, broadly resembling the organization of glutamatergic neurons in the mammalian pallium. However, the relationship between glutamatergic neuron types identified in other amniote lineages and those in the mammalian pallium remains a subject of ongoing debate (further discussed in chapter 1.2).

1.3 Development of the amniote pallium

The telencephalon originates from a sheet of neuroepithelial cells in the anterior neural tube during early vertebrate development (*84*, *85*). The neural tube's inner or apical surface, adjacent to the prospective ventricles, represents the brain's germinative zone, also called ventricular zone in later development. As development progresses, the telencephalic neuroepithelium undergoes patterning into distinct progenitor regions, such as the pallium and subpallium, which are further divided into various subregions, later giving rise to specific cell populations. This patterning is directed by morphogen gradients inducing a sequence of gene regulatory networks. This process is best studied in the mouse, but seems to be conserved to various degrees across vertebrates i.e., the division into pallium and subpallium occurs in all vertebrates, while many of the subsequent steps are suggested to be conserved across tetrapods (*17*, *86*). In amniotes, slight variations of these shared patterns likely arise from quantitative differences in expression levels of signaling molecules and lead to early telencephalic subdomains differing in size across lineages. For example, the mammalian telencephalon contains an expanded dorsal pallial domain compared to an expanded ventral pallial domain observed in sauropsids (*87*).

While broad patterning of the telencephalic neuroepithelium seems to be largely conserved across amniotes, clear differences between species manifest during neurogenesis. At the onset of neurogenesis (embryonic day 10.5 in mouse (*88*), or embryonic day 4 in chicken (*89*)) neuroepithelial cells differentiate into radial glia (RG), considered to be the primary neural progenitor cells in many regions of the developing brain in various vertebrate species. However, several types of RG and other RG-derived neural progenitors have been identified in the amniote telencephalon (*90*). In eutherian mammals, the first type of RG to form in the telencephalon are apical RG characterized by their apical position, their bipolar morphology - one process of the cell contacts the apical surface, and the second process extends towards or contacts the basal pial meninges - and their specific gene expression profile. During mid-neurogenesis, these cells mainly undergo asymmetric divisions to self-renew and give rise to other types of neural progenitors, thus most of neuro- and gliogenesis occurs indirectly (*91*) (Fig. 2). Other types of neural progenitors include for example several types of outer/basal radial glia or intermediate progenitor cells, with varying morphology, proliferative capacity and fate restriction. Most of these secondary types of progenitors accumulate in an area basal to the ventricular zone, called the subventricular zone, and the extent of this zone varies across mammalian species (*91*). The expansion of secondary progenitor pools likely

enabled the expansion of the primate cortex (*92*, *93*). Although neurogenesis has not been studied to the same extent in other mammalian or amniote lineages, indirect neurogenesis is thought be much less prevalent in sauropsids compared to mammals (*90*, *94*) (Fig. 2). Some potential secondary neural progenitor cells have been identified in the pallium of birds (*95*) and turtles (*96*), however their transcriptomic identity and relationship to mammalian progenitors was largely unexplored prior to this study.

Glutamatergic neurons in the amniote telencephalon are predominantly derived from progenitors in the pallium. In the mammalian isocortex, these migrate along radial fibers towards the pial surface in an "inside-out" pattern, meaning early-born neurons populate deep layers whereas late-born neurons populate upper layers. This migration is guided by a largely transient type of cells, Cajal-Retzius cells, located in the prospective layer one of the isocortex (*97*, *98*). Glutamatergic migrations in other mammalian pallial structures besides the isocortex follow different complex patterns (*99*, *100*). Cajal-Retzius cells have been suggested to be ancestral to amniotes or even tetrapods, although the regional origin and distribution of potentially corresponding cell populations in sauropsids and amphibians differ from those in mammals (*101–104*). Consistently, migration of glutamatergic neurons in other amniote lineages predominantly occurs in a radial "outside-in" pattern, meaning early-born neurons are located closer to the pial surface while late-born neurons are located close to the ventricles, within a limited tangential range of their origin (*89*, *104*).

GABAergic and cholinergic neurons mostly originate from subpallial progenitors (Fig. 2), though it has been suggested that few GABAergic neurons derive from pallial progenitors in the human isocortex (*105*, *106*). From the subpallium they populate subpallial structures or migrate into the pallium along tangential migratory routes assumed to be largely conserved across amniotes (*15*), although this has not been studied comprehensively.

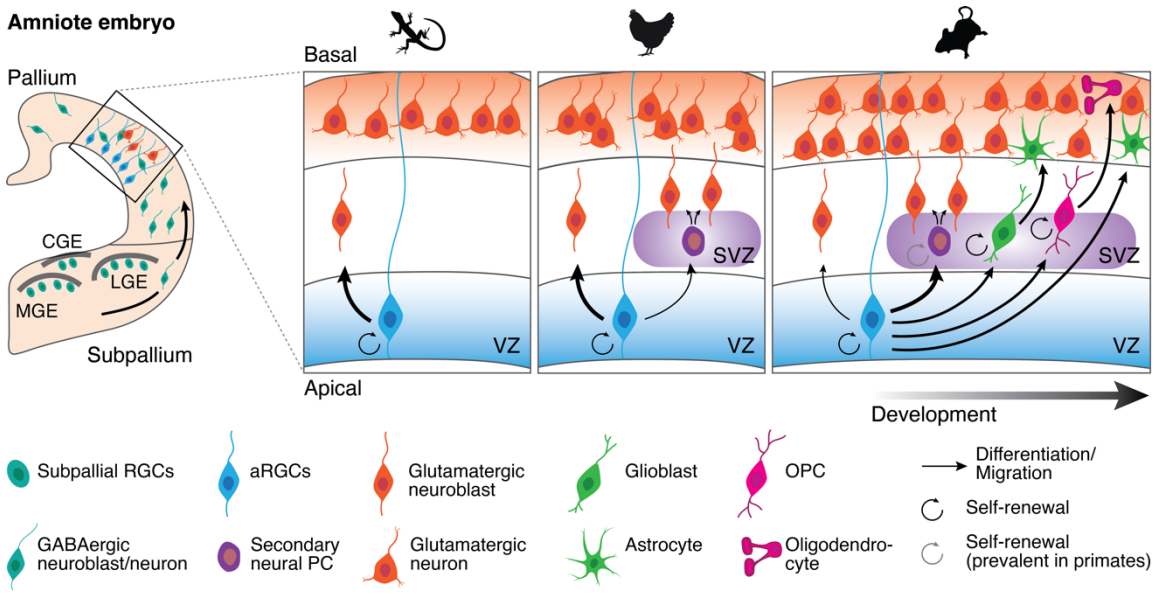

Figure 2 Development of cell types in the amniote pallium. (Left) Schematic representation of a coronal brain section from an amniote embryo, illustrating the developmental origin of GABAergic and glutamatergic neurons. (Right) Schemes depicting pallial germinal layers, progenitor cell types and modes of neurogenesis across different amniote lineages. Arrow-thickness represents relative frequency of different neurogenesis modes. Different mammalian species exhibit diverse secondary neural progenitor cell types (not shown) with varying proliferative capacity. Gliogenesis, shown only for mouse, occurs later in development, involving both direct and indirect generation of glial cell types. M/C/L GE, medial/caudal/lateral ganglionic eminence; VZ, ventricular zone; SVZ, subventricular zone; RGCs, radial glial cells; aRGCs, apical radial glial cells; PC, progenitor cell.

Like neurons, mature glial cells originate from radial glia, but gliogenesis has mostly been studied in eutherians. Specific subpopulations of progenitors are likely committed to an ependymal cell fate early in development (*54*, *107*), while oligodendrocyte progenitor cells (OPCs) and astrocytes are generated from previously neurogenic progenitors after the switch from neurogenesis to gliogenesis (Fig. 2). OPCs emerge from radial glia in distinct brain regions in a spatiotemporal gradient (*108*) and then migrate to their final locations where they continue to self-renew and differentiate into myelinating oligodendrocytes (*109*). Astrocytes are generated in two waves throughout the CNS and migrate primarily radially. The first wave is derived from proliferative glioblasts while the second is generated by direct differentiation of radial glia (*110*) (Fig. 2). In other amniotes, progenitors likely also switch to gliogenesis in later development (*107*), although this process is poorly understood, and given that parenchymal astrocytes are absent in most non-avian reptiles, gliogenesis has likely diverged across amniote lineages.

As development progresses, some radial glial cells transition into neural stem cells that persist into adulthood and retain the ability to generate new neurons throughout life. Adult neurogenesis is a well-studied process in amniotes, though its prevalence and functional significance vary across species. In mammals, adult neurogenesis is limited and predominantly occurs in two regions, the subventricular zone of the lateral ventricles, giving rise to neurons migrating into the olfactory bulb, and the dentate gyrus of the hippocampus (*111*). Among birds, songbirds exhibit an especially high rate of adult

neurogenesis compared to mammals, particularly in brain regions associated with vocal learning and memory (*112*, *113*), and considerable numbers of neural progenitor cells have also been described in the adult lizard and turtle pallium (*41*). These high levels of adult neurogenesis in sauropsids, as well as amphibians (*114*), indicate that adult neurogenesis is ancestral to tetrapods but was mostly lost in the mammalian lineage.

1.3.1 Development and organization of the avian pallium

The development of the avian pallium has been a subject of intense debate, particularly regarding the mechanisms that shape its regional organization. While multiple studies indicate that glutamatergic neuron migration in the avian pallium occurs predominantly in a radial fashion, with little to no evidence of tangential migration (*89*, *104*, *115–117*), the continuum hypothesis offers a contrasting view (Fig. 3). Based on the spatial expression of select marker genes and bulk RNA expression profiles from adult brains, this hypothesis proposes that the adult avian pallium exhibits a mirror-image arrangement of subdivisions (*37*, *48*). In this model, subdivisions with similar transcriptomic profiles and functions are situated above and below the lamina, which forms during development as the ventricle collapses due to the expansion of the brain parenchyma.

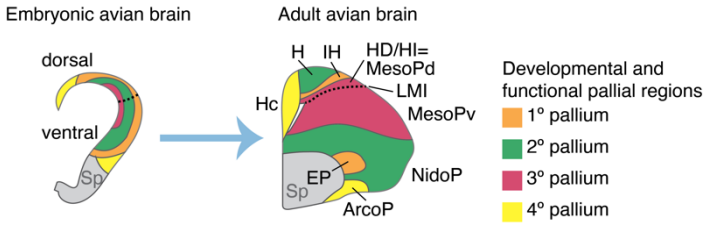

Figure 3 The continuum hypothesis of avian pallial regionalisation. Schematic representation of developmental regions in the avian embryo giving rise to adult structures above and below the Lamina mesopallialis intermediate (LMI) (dashed line) according to the continuum hypothesis colored according to their functional roles (1° pallium receives thalamic input, 2° and 3° process input, 4° sends output projections to brainstem). Under the continuum hypothesis, hyperpallial terminology differs slightly from the terminology used by other authors. H, hyperpallium; IH, intercalated hyperpallium; HD/HI, densocellular hyperpallium and intercalated hyperpallium; MesoPd/v; dorsal/ventral mesopallium; Sp, subpallium; Hc, hippocampal areas; NidoP, nidopallium; ArcoP, arcopallium; EP, entopallium. Adapted from (*1*).

In support of this model, the authors further identified “continuities” in spatial gene expression patterns of few selected marker genes during development, which they interpreted as linking mirrored subdivisions across the lamina (*47*). Based on these continuities they proposed a shared developmental origin of similar subdivisions above and below the mirror line, implying either massive tangential migration or an alternative, as-yet-unknown developmental mechanism that generates highly similar cell populations from progenitor pools in distinct topological locations. This interpretation challenges the traditional Cartesian-defined model of pallial organization.

Although the continuum hypothesis stimulates valuable discussion and encourages new investigations into avian brain development, it contradicts a substantial body of evidence

indicating that radial migration is the predominant mechanism in the avian pallium (*89*, *104*, *115–117*). Furthermore, it challenges the well-established role of signalling from early patterning centres in mediating medial-to-lateral and anterior-to-posterior morphogen gradients, which are thought to be critical for establishing distinct progenitor identities in the developing pallium (*17*).

1.4 Models of amniote pallium evolution

The evolution of the pallium has historically been studied through neuroanatomical comparisons, or *in situ* expression profiles of few chosen markers, which provided clear insights in mammals, e.g., the expansion of the isocortex and upper isocortical layers in primates (*118*), but led to substantial debates when extended to other amniote lineages with diverse pallial morphology. However, recent advances in single-cell multiomics have revolutionized our understanding of brain evolution, revealing both novel features within mammals, and allowing for more detailed and systematic identification of homologies in pallial structures and cell types across amniotes (*41*, *75*, *119*, *120*).

Especially the eutherian pallium has been extensively characterized, particularly in primates and rodents. These studies identified largely homologous cell types in the primate and mouse isocortex with only a few instances of potentially novel cell (sub-)types (*120–123*). Despite the general correspondences, these cell types exhibit varying degrees of conservation in their proportions, gene expression, DNA methylation, and chromatin states (*79*, *119*). GABAergic interneurons in the isocortex show a higher degree of conservation across species (*119*), although a human-specific cortical GABAergic interneuron subtype have been identified (*122*). In contrast, glutamatergic cell types display less conservation, particularly in the upper cortical layers, which are notably more divergent in primate-to-mouse comparisons, correlating with the expansion of these layers in primates (*79*, *119*, *124*).

Before the emergence of single-cell studies, the discourse on evolution of the amniote pallium was primarily shaped by two competing frameworks – the equivalent circuit hypothesis and development-based models (Fig. 4). The equivalent circuit hypothesis proposes homology for cell types with similar roles in an ancestral sensory-motor circuit, suggesting that neurons in the mammalian isocortex are homologous to those in the cortex or hyperpallium and DVR of sauropsids (Fig. 4B). This hypothesis is mostly based on similarities in axonal projections and physiological functions in the adult amniote pallium (*115*, *125*, *126*). In contrast, other models emphasize comparative embryonic development and topology and suggest that homologous developmental territories give rise to homologous adult structures (*127–129*) (Fig. 4A). This framework aligns with the well-established concept that developmental stages are more conserved across vertebrates than adult stages, due to stronger evolutionary constraints imposed by widespread pleiotropy during development (*130–132*). The most widely discussed development-based evolutionary model is the ‘tetrapartite pallium’ model (Fig. 4A),

suggesting the existence of four distinct pallial domains homologous across amniotes (*128*, *129*). However, alternative views propose varying numbers and positions of distinct progenitor domains, leading to diverse proposed homologies between mammals and sauropsids (*47*, *133*). Nevertheless, most of these development-based models agree that the sauropsid DVR and mammalian isocortex are not homologous, given that they arise from different embryonic domains, and thus suggest that the shared circuitry and functions (Fig. 1B) of these regions arose convergently during amniote evolution.

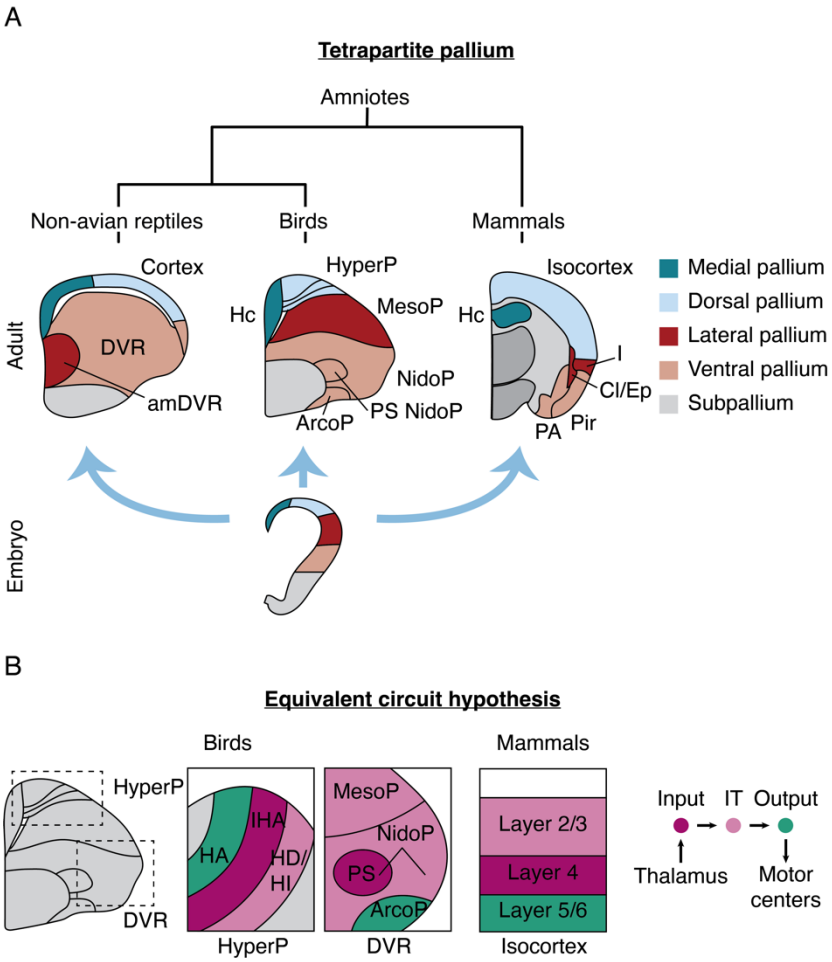

Figure 4 Theories of pallial evolution. (A) Schematic representation of coronal sections of the telencephalon in lizard (left), chicken (middle), and mouse (right) or amniote embryo (bottom). Brightly colored areas represent the pallium divided into developmental, homologous sectors according to the tetrapartite pallium model (*128*). **(B)** Schematic representation of regions constituting sensory-motor circuits in the pallium of birds (left) and mammals (right), colored according to their role in the canonical circuit (illustrated on the far right). Colored areas indicate regions that are homologous according to the equivalent circuit hypothesis, given their comparable circuit functions across birds and mammals. DVR, dorsal ventricular ridge; amDVR; anterior medial DVR; Hc, hippocampal area (chicken) / hippocampus (mouse); HyperP, hyperpallium; MesoP, mesopallium; NidoP, nidopallium; PS, primary sensory; ArcoP, arcopallium; Cl, claustrum; Ep, endopiriform nucleus; I, insular cortex; Pir, piriform cortex; PA, pallial amygdala; HA, apical hyperpallium; IHA, interstitial apical hyperpallium; HD/HI, densocellular and intercalated hyperpallium; IT, intra-telencephalic. Adapted from (*1*).

A limited number of single-cell studies on non-mammalian pallia has provided valuable insights into the evolution of the amniote pallium (*41*, *42*, *72*, *75*, *83*). These studies

revealed that at the gene expression level GABAergic neurons are more conserved across amniotes compared to glutamatergic neurons. Consequently, the investigation of glutamatergic neurons is especially crucial for evaluating contentious regional pallial homologies. This finding also aligns with the fact that GABAergic neurons originate in the more evolutionarily conserved subpallium, while glutamatergic neurons are generated locally in the morphologically less conserved pallium.

Despite the high conservation of gene expression in GABAergic neurons, a notable difference was observed in the distribution of LGE-derived neurons, which are widespread throughout the finch pallium but are mainly restricted to the olfactory bulb and specific amygdalar nuclei in the eutherian pallium (*75*, *123*). Comparative analyses of glutamatergic neurons across species indicate that cell types in the medial cortex of non-avian reptiles are homologous to eutherian hippocampal cell types (*41*). This supports the idea of embryonic regional homology, as both structures originate from medial pallial areas.

In these same comparisons, based on all expressed genes, neurons in the sauropsid DVR exhibit high similarity to neurons in the mammalian isocortex, seemingly supporting circuit-based homology models. However, when the analysis is restricted to transcription factors, whose cell type specificity has been suggested to be more conserved across species compared to function-related "effector" genes (*134*), DVR neurons show greater similarity to mammalian ventral pallial structures, such as the amygdala and piriform cortex, thus reinforcing development-based homology models. The only region suggested to be homologous to the mammalian isocortex, based on transcription factor expression profiles, is the anterior dorsal cortex in turtles. In this region, two populations of neurons were identified that share similarities with either deep layer or upper layer isocortical neurons, suggesting a diversification of these potentially ancestral neuron identities in the mammalian isocortex (*41*).

1.5 Aims

While these recent studies have significantly advanced our understanding of pallial evolution in amniotes, several critical gaps remain. Until recently, there was no single-cell data available for ventral pallial structures in mammals, like the amygdala or piriform cortex, forcing researchers to rely on other data types such as microarray or *in situ* hybridization data (*41*, *75*). The reliance on these disparate types of data introduces the potential for technical artifacts, and, even within single-cell studies, there is considerable variability in techniques and datasets, which complicates direct comparisons. Moreover, most studies have focused on two lineages of amniotes at a time, although evaluating a broader range of species across different lineages can facilitate the identification of robust cell type homologies and is crucial to distinguish ancestral from lineage-specific traits. Additionally, prior to this study, data for large portions of the avian pallium, including the

hyperpallium—suggested to be homologous to the reptilian dorsal cortex and mammalian isocortex according to developmental models (Fig. 4A)—were not available.

Additionally, although much is known about the eutherian pallium, the conservation of its features across all mammalian lineages remains largely unexamined. A comprehensive evaluation of cell types in the non-eutherian mammalian pallium could provide critical insights into which traits are conserved across mammals, thereby facilitating broader comparisons across amniotes.

Finally, despite the acknowledged significance of development for evolutionary comparisons, single-cell resolution studies of pallial development have been limited, even in eutherians. Many studies have focused on the isocortex (*71*, *135–137*) or the entire brain (*80*), leading to insufficient coverage of other pallial structures. In sauropsids, pallial development had not been explored at single-cell resolution at all prior to this study, leaving a substantial gap in our understanding of how diverse cell types and structures develop and evolve across amniotes.

This dissertation thus aims to advance our understanding of the evolution of the amniote pallium through the following specific objectives:

- Systematically identify and classify cell types within the pallium of selected species representing major amniote lineages.

- Characterize the cellular composition of distinct pallial structures across different amniote species.

- Investigate the developmental origins of cell types, particularly glutamatergic neurons, and their associated structures within the avian pallium.

- Identify and characterize conserved and divergent gene expression patterns in pallial cell types across amniote lineages to understand their evolutionary trajectories.

- Elucidate the evolutionary history of pallial structures by examining the evolution of their constituent cell types across amniotes

2 RESULTS

2.1 CELLULAR EVOLUTION OF THE MAMMALIAN ISOCORTEX

To elucidate the evolution of cell types in the amniote pallium, it is essential to study multiple representatives from all amniote lineages, enabling the distinction between species-specific and lineage-shared characteristics. While the current understanding of cell types in the sauropsid pallium is limited, extensive research has been conducted on the mammalian pallium. However, most of this knowledge is derived from studies on eutherians, with relatively little attention given to other mammalian lineages, marsupials and monotremes, although these lineages underwent ~160 and ~180 million years of independent evolution, respectively (Fig. S1) (*6*). In this first part of my thesis, I aimed to identify pan-mammalian and lineage-specific features of the mammalian pallium by investigating cell types in the isocortex of representatives from all three major mammalian lineages. Using single-nucleus RNA sequencing (snRNA-seq), I profiled the isocortex of the adult gray short-tailed opossum (*Monodelphis domestica*), a marsupial, and the adult short-beaked echidna (*Tachyglossus aculeatus*), a monotreme, and compared this data to a neuron-enriched external single-cell RNA-seq dataset covering the whole mouse brain (*76*), which became available only recently. Single-nucleus RNA-sequencing has been shown to yield comparable results to single-cell RNA sequencing (*138*, *139*), while enabling the analysis of frozen tissues, thus making it a valuable method to study cell types in non-model species. The following results are still preliminary, as these mammalian analyses were not the primary focus of my PhD work.

2.1.1 CELL TYPE ATLAS OF THE OPOSSUM FRONTAL ISOCORTEX

The resulting dataset covering the opossum frontal isocortex comprises 12,830 high-quality nuclear transcriptomes (median UMIs/genes: 3222/1768) from two adult individuals, one male and one female (Fig. 5A). We initially focused on the frontal cortex, as it has been proposed to play a key role in the evolution of advanced cognitive abilities in mammals (*140*). However, with the growing body of literature on eutherian isocortical cell types in early stages of this project, we shifted our focus to the broader amniote pallium, as described in the introduction. Although this dataset only covers the frontal isocortex, which limits a comprehensive comparison of all isocortical cell types across mammalian lineages, we believe it still provides valuable insights. Transcriptomic variability between cell types in different isocortical layers was shown to be greater than the variability between neurons within the same layer across isocortical regions in mice (*82*). At the evolutionary distances being examined, such regional differences are likely less significant than in comparisons within eutherians.

In this dataset I identified all major pallial cell types according to the expression of known marker genes i.e., glutamatergic excitatory neurons (*SYT1*+, *SLC17A7*+, *SLC17A6*+), GABAergic inhibitory neurons (*SYT1*+, *GAD1*+, *GAD2*+), immune cells likely corresponding to microglia (*SALL3*+), vasculature-associated cell types (*VWF*+), astrocytes (*GFAP*+),

oligodendrocyte progenitor cells (OPCs, *PDGFRA*+), and oligodendrocytes (*PLP1*+; Fig. 5B-C). Glutamatergic neurons, oligodendrocytes and GABAergic neurons represent the most abundant populations, in line with previous observations in the murine cortex (*141*). However, cell type proportions in single-cell or single-nucleus RNA-seq data may not accurately represent true tissue composition, as particularly cell-isolation protocols were shown to introduce biases (*142*, *143*).

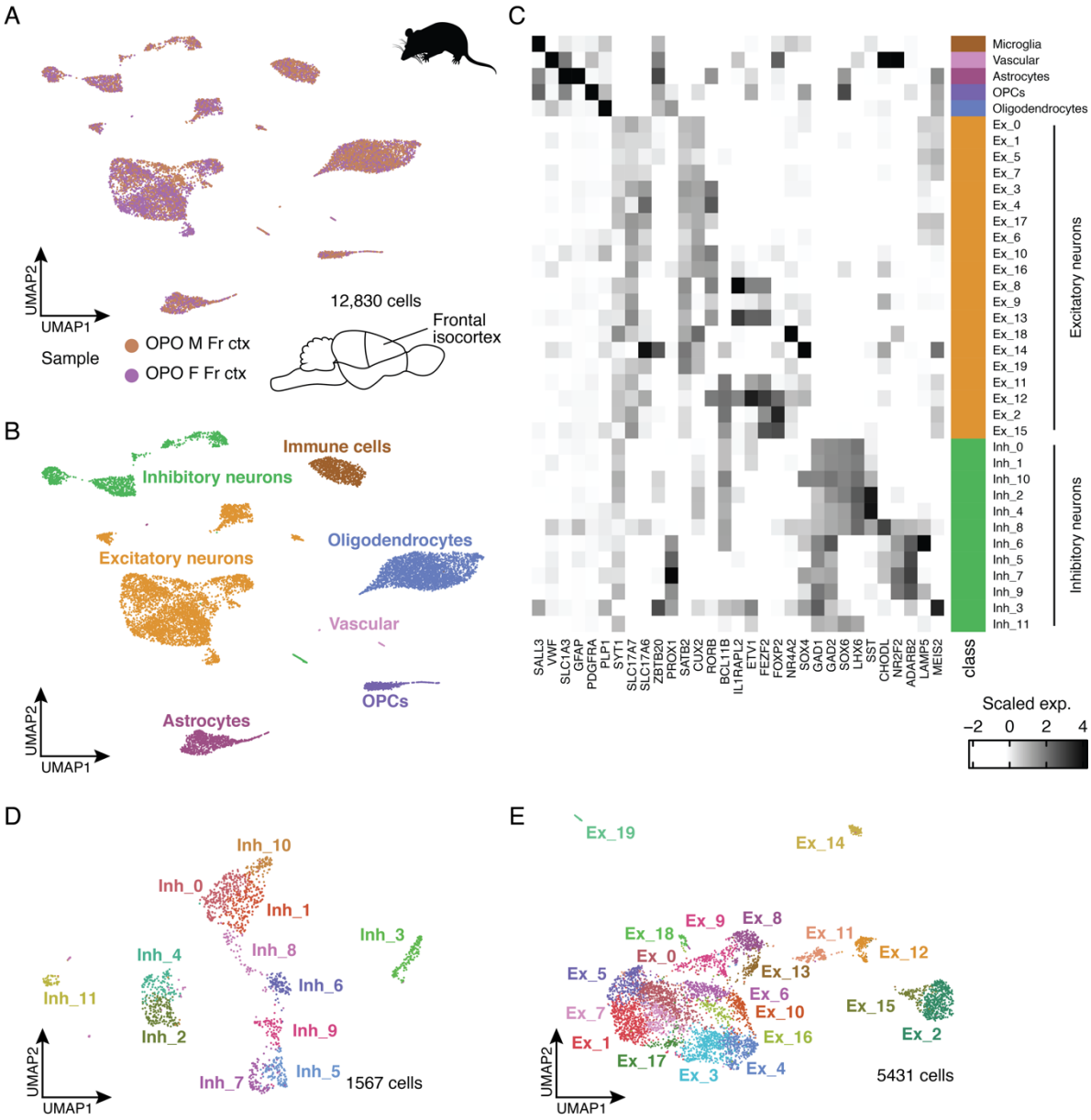

Figure 5 Cell type atlas of the adult opossum frontal isocortex. Uniform manifold approximation and projection (UMAP) of opossum frontal isocortex snRNA-seq atlas colored by sampled individual **(A)** and cell class **(B)**. **(C)** Heatmap of selected marker gene expression across non-neuronal cell populations and neuronal clusters. Exp., expression. UMAP of GABAergic inhibitory neurons **(D)** and glutamatergic excitatory neurons **(E)** colored by and labelled with cluster annotation.

In order to identify potential different neuronal cell types, I analyzed and clustered inhibitory and excitatory neurons separately, identifying 12 inhibitory and 20 excitatory clusters. Groups of inhibitory clusters exhibited specific expression of marker genes known to reflect embryonic origins in different ganglionic eminences in eutherians (*SOX6*, *LHX6* – MGE; *NR2F2*, *ADARB2* – CGE; *MEIS2* – LGE (*71*)), in line with the suggested conservation of gene expression in pallial inhibitory neurons across tetrapods (*19*, *41*).

Some excitatory clusters showed distinct expression of marker genes associated with neurons from specific isocortical layers (L1-L6) and their characteristic projections in eutherians, such as *CUX2* (L2-3; (*144*)), *RORB* (L4-5; (*145*)), or *FEZF2* (extra-telencephalic projecting neurons in L5/6; (*146*)). I also identified one excitatory neuron cluster (Ex_14) specifically expressing *SOX4,* likely representing immature neurons and indicating ongoing adult neurogenesis. Adult neurogenesis in mice predominantly occurs in the dentate gyrus of the hippocampus (*111*), thus this observation suggests that parts of the hippocampus were unintentionally co-dissected, which seems unlikely given its distinctive morphology and the fact that no other clusters specifically expressed hippocampal marker *ZBTB20* (*147*) or the post-mitotic dentate gyrus marker *PROX1* (Fig. 5C) (*148*). Alternatively, it suggests that adult neurogenesis is more widespread in the opossum compared to mouse.

2.1.2 Cell type atlas of the echidna isocortex

Extant monotremes include the platypus and four species of echidna. To generate the first single-cell resolution data for the monotreme brain, I profiled samples from multiple regions of the short-beaked echidna cortex, using three adult male individuals (Fig. 6A-B). Although coverage of the entire cortex was not feasible due to limited sample availability, this dataset provides valuable insights into the cellular composition of the monotreme cortex. It comprises 58,217 high-quality nuclear transcriptomes (median UMIs/genes: 2154/1430) from four anatomically distinct cortical regions. In the absence of a detailed echidna brain atlas at the time of sampling, these regions were labelled using human cortical terminology—frontal, parietal, occipital, and temporal—although functional areas located in these topological regions likely differ between humans and echidnas (*35*).

As in the opossum dataset, I identified major pallial cell types in the echidna cortex based on the expression of established marker genes. These include glutamatergic excitatory neurons (*SYT1*+, *RBFOX3*+, *SLC17A7*+, *SLC17A*6+), GABAergic inhibitory neurons (*SYT1*+, *GAD1*+, *GAD2*+), microglia-like immune cells (*TMEM119*+), vasculature-associated cells (*FLT*1+), astrocytes (*SLC1A3*+, *AQP4*+), oligodendrocyte progenitor cells (OPCs, *PDGFRA*+), and oligodendrocytes (*PLP1*+; Fig. 6C-D). While histological studies had hypothesized the existence of distinct glial types in monotremes compared to eutherians and marsupials (*149*), no obvious transcriptomic differences were observed in this dataset.

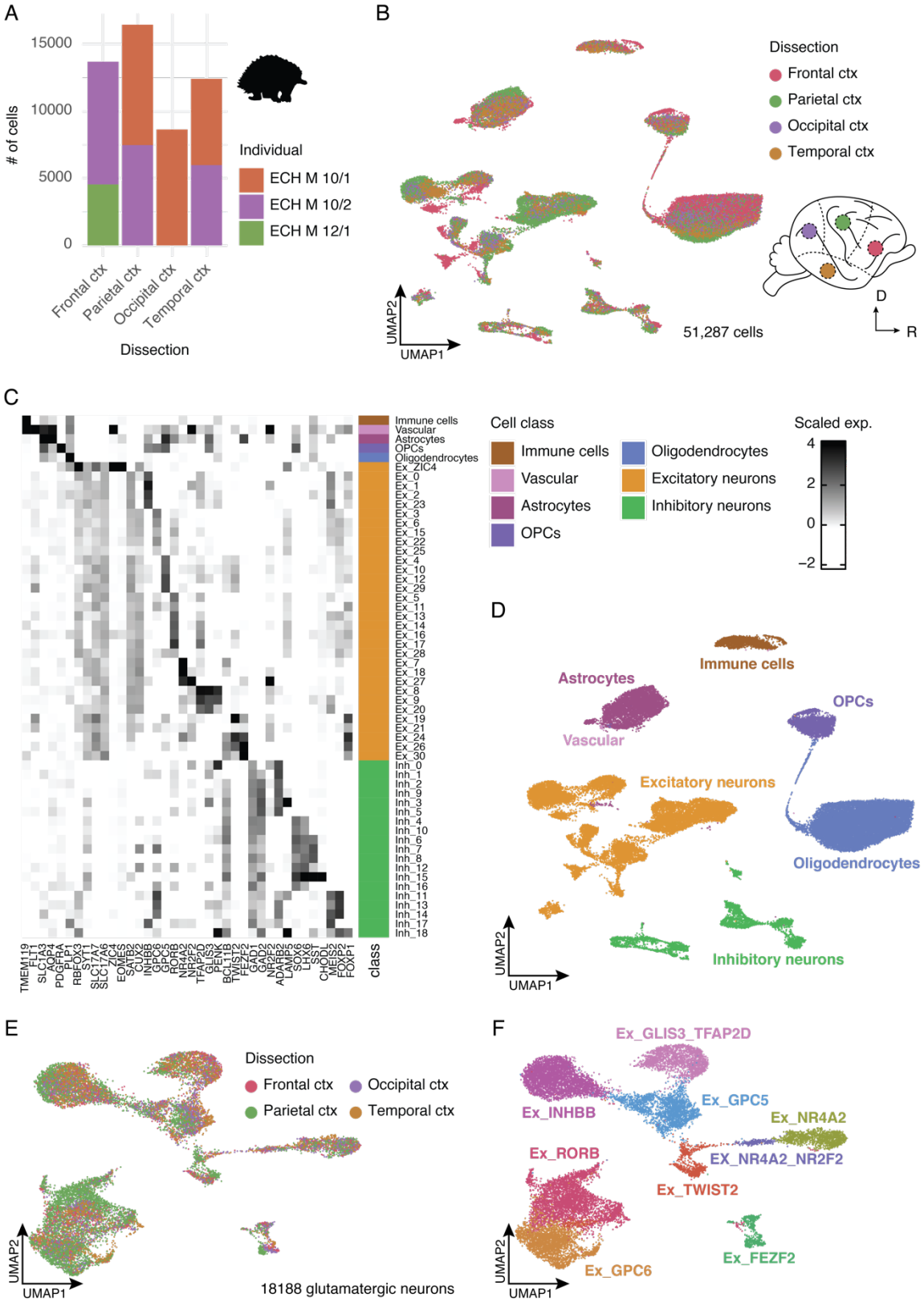

Figure 6 Cell type atlas of the adult echidna cortex. (A) Barplots of cell numbers per sampled region colored by sampled individual. **(B)** UMAP of echidna cortex snRNA-seq atlas colored by sampled region. **(C)** Heatmap of selected marker gene expression across non-neuronal cell populations and neuronal clusters. **(D)** UMAP of echidna cortex snRNA-seq atlas colored by cell class. UMAP of glutamatergic excitatory neurons **(E)** colored by dissected region and **(F)** colored by and labeled with major excitatory population annotation. Ctx, cortex; D, dorsal; R, rostral; Exp., expression.

To investigate neuronal diversity, I clustered inhibitory (4,877 cells) and excitatory neurons (18,188 cells) separately, resulting in the identification of 19 inhibitory and 31 excitatory clusters. Inhibitory neuron clusters expressed markers consistent with embryonic origins in various ganglionic eminences (Fig. 6C). Unlike in the opossum isocortex, I detected several clusters likely originating from the LGE (*MEIS2*+, *FOXP2*+), likely due to the broader regional sampling in the echidna cortex.

Excitatory neuron clusters were grouped into nine major populations based on their distinct marker genes. Although excitatory neurons show greater regional transcriptomic and projection variability in the pallium compared to inhibitory neurons (*82*), samples from different cortical regions contributed to all or most of these major populations. This suggests that the sampled regions may not correspond to distinct functional areas, and/or that regional heterogeneity could only be detected at finer resolution. While some populations were characterized by eutherian markers of specific isocortical layers (Ex_RORB, *RORB*+ (*145*)), projection identities (Ex_FEZF2, *FEZF2*+; (*146*)), or other pallial regions (Ex_NR4A2, NR4A2+, marker of subplate and claustral neurons (*150*)) several populations could not be readily annotated using known eutherian marker genes alone.

2.1.3 Comparison of isocortical glutamatergic neurons across mammalian lineages

To identify potentially homologous or lineage-specific excitatory cell types in the mammalian cortex, I compared the datasets covering the opossum frontal isocortex and different regions of the echidna cortex to a subset of a single-cell RNA-seq dataset for the entire mouse brain (*76*). This comparison was performed using an established integration method (*151*) based on all expressed one-to-one orthologous genes. These comparisons identify transcriptomic similarities, which can result from either shared ancestry (homology) or convergent evolution of cell types. Given the well-documented morphological conservation of the cortex across mammals, it is likely that the observed transcriptomic similarities primarily reflect homology. However, convergent evolution cannot be entirely ruled out without further functional and developmental validation.

Although the mouse-opossum comparison is based on fewer genes than the mouse-echidna comparison —likely due to the smaller size of the opossum dataset resulting in detection of fewer expressed genes— similarities between murine and opossum excitatory neuron types are overall higher than between mouse and echidna cell populations (Fig. 7). This observation aligns with the shorter evolutionary divergence time between eutherians and marsupials than between eutherians and monotremes.

All opossum excitatory clusters show predominant similarity to one murine excitatory subclass, suggesting a likely spatial location and projection identity for each cluster (Fig. 7A). High similarities are observed between deep-layer populations with distinct projection identities, such as L6 cortico-thalamic neurons (L6 CT CTX), L5 extra-telencephalic projecting neurons (L5 ET CTX), and L5 near-projecting neurons (L5 NP CTX).

In contrast, similarities among L2-5 intra-telencephalic (IT) neurons are lower, except for neurons in L2/3 of the retrosplenial area (L2/3 IT RSP). This could indicate greater transcriptomic divergence among these cell types or may be due to technical factors such as differences in clustering resolution between species, as multiple opossum clusters correspond to L2-5 IT neurons, while single clusters represent other types.

Some opossum clusters show greatest similarity to largely non-isocortical murine neurons. For instance, cluster Ex_18 corresponds to murine Car3 neurons, which are predominantly found in the claustrum, dorsal endopiriform nucleus, and in layer 6 of lateral cortical areas (*78*). Given the close anatomical proximity of the claustrum and endopiriform nucleus to the lateral isocortex, it is likely that portions of these regions were unintentionally co-dissected, accounting for the proportionately high abundance of Car3-like neurons in the opossum dataset. Cluster Ex_14, likely representing immature neurons, is most similar to murine immature neurons in the dentate gyrus (DG) and piriform cortex (DG-Pir Ex IMN). Accidental co-dissection of the hippocampus or piriform regions is unlikely given the distinctive morphology of the hippocampus, the likely absence of other hippocampal populations, and the absence of similarities to other murine piriform-related populations (IT AON-TT-DP, OB Eomes Ms4a15, L2/3 IT PIR-ENTl). Thus, this similarity suggests that adult neurogenesis may be more widespread in opossum compared to mouse, though further validation is needed.

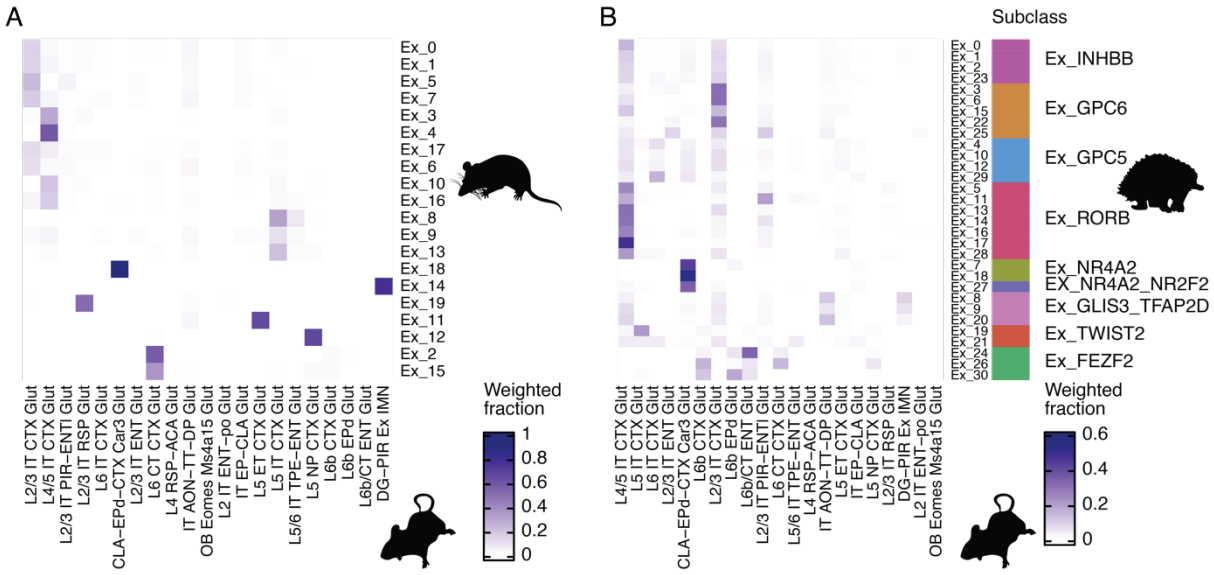

Figure 7 Comparison of adult excitatory neurons across mammalian lineages. (A) Comparison of opossum isocortical excitatory neuron clusters to mouse excitatory subclasses from (*76*) based on the expression of 11714 expressed one-to-one orthologous genes. **(B)** Comparison of echidna cortical excitatory neuron clusters to mouse excitatory subclasses from (*76*) based on the expression of 12955 expressed one-to-one orthologous genes. Color bar on the right represents major population labels shown in Fig. 6F. IT, intra-telencephalic projecting; CTX, isocortex; PIR, piriform cortex; ENT(l), (lateral) entorhinal cortex; RSP, retrosplenial area; CLA, claustrum; EP(d), (dorsal) endopiriform nucleus; CT, cortico-thalamic projecting; ACA, anterior cingulate area; AON, anterior olfactory nucleus; TT, taenia tecta; DP, dorsal peduncular area; Ob, olfactory bulb; ET, extra-telencephalic projecting; TPE, temporal association and perirhinal and ectorhinal area; NP, near-projecting; DG, dentate gyrus; IMN, immature neurons.

No opossum clusters show significant similarity to murine L6 IT or L6b neurons, indicating that these populations are either rare in the opossum frontal isocortex or exhibit greater similarity to other murine cell types.

Of the nine major excitatory neuron populations identified in the echidna cortex, only four show predominant similarity to specific murine excitatory subclasses (Fig. 7B). As seen in the opossum comparison, one of the greatest similarities is observed between murine Car3 neurons—found in the claustrum, endopiriform nucleus, and layer 6 of lateral isocortical areas—and two echidna populations expressing *NR4A2* (Fig. 6C). However, unlike the opossum, other echidna populations most similar to murine neurons primarily match L2-5 IT neurons. The remaining echidna populations display mixed similarities, with some clusters resembling multiple murine subclasses. For instance, the Ex_FEZF2 population in echidna resembles various L6 populations in both the isocortex and entorhinal cortex, also suggesting that the sampled regions encompass not only isocortical areas but also other cortical regions. Similarly, Ex_GLIS3_TFAP2D corresponds best to an olfactory-related population (IT AON-TT-DP), indicating that parts of these olfactory structures were also likely sampled. No echidna populations show significant similarities to isocortical L5 ET or NP neurons, although these were clearly distinguishable in the opossum, indicating that L5 ET or NP neurons may have been missed in the echidna.

Interestingly, two large echidna populations, specifically expressing *INHBB* and *GPC5*, exhibit only low levels of similarity to murine subclasses, though they most closely resemble L2-5 IT and L2-6 IT neurons, respectively. However, they are distinct from other echidna populations that also correspond to these murine neuron types, such as Ex_GPC6 and Ex_RORB. Notably, Ex_GPC5 is the only echidna population exhibiting some degree of similarity to murine L6 IT neurons, suggesting that it may represent a population of L6 IT neurons that has undergone divergence between monotremes and eutherians. In contrast, the identity of Ex_INHBB remains uncertain. Its similarity to various murine IT neuron types raises the possibility that it may represent an uncharacterized cell state rather than a distinct cell type. Alternatively, it could correspond to a unique IT neuron type specific to echidna or monotremes. This hypothesis aligns with monotremes' capacity for electroreception (*152*, *153*), a sensory modality that might require specialized neural circuits or cell types absent in most other mammals. However, further investigation is needed to validate the presence of Ex_INHBB *in situ* and elucidate its potential function.

In sum, my analyses of mammalian glutamatergic neurons revealed several key patterns of conservation and divergence. Car3(-like) neuron populations are highly similar across all mammalian lineages, highlighting a likely shared ancestral trait. Deep-layer neuron types, particularly those involved in corticofugal projections, show high similarity between mouse and opossum, indicating transcriptomic conservation among therians. In contrast, upper-layer IT neuron types seem to have diverged more significantly. Comparisons between eutherians and monotremes suggest greater similarity in upper-layer neurons

compared to deep layer types, although this may be due to limited sampling in the echidna. Additionally, I identified a potential monotreme-specific IT neuron type, suggesting lineage-specific adaptations.

2.2 Evolution of cell types and structures in the amniote pallium

To elucidate the evolution of cell types in the amniote pallium, I generated and analyzed snRNA-seq and spatial transcriptomics data for the pallium of three species representing all major amniote lineages: the mouse (*Mus musculus*), the green anole lizard (*Anolis carolinensis*), and the chicken (*Gallus gallus*). I focused on the chicken, as no single cell data was available for the avian pallium prior to the start of this work. Additionally, the avian pallium is of special interest due to the advanced cognitive abilities of birds and the presence of neural circuits analogous to the ones in the mammalian isocortex, as described in the introduction. While external datasets for the murine (*67*) and sauropsid pallium (specifically turtle and lizard (*41*)) were available, differences in covered regions and single-cell profiling techniques, as well as low cell numbers, limited their direct comparability. Nevertheless, I used some of these and newly available external datasets (*72*, *76*) to validate and strengthen my findings. The following results constitute the main part of my PhD work and were published a preprint (*1*).

2.2.1 Cell type atlas of the murine pallium

2.2.1.1 Cell type atlas of the adult murine pallium

To construct a comprehensive eutherian cell type atlas covering all regions of the pallium I generated snRNA-seq data for the murine frontal isocortex (including the anterior cingulate, prelimbic, orbital, infralimbic, primary and secondary motor, and frontal agranular insular areas) and ventral and lateral regions of the pallium (VLP; including insular cortex, claustrum, endopiriform nucleus, piriform cortex and amygdala; Fig. 8A). The resulting dataset comprises 22,505 high-quality nuclear transcriptomes (median UMIs/genes: 6,035/2,883; Fig. S2), including major pallial cell classes according to the expression of known marker genes, i.e., glutamatergic neurons (*Rbfox3*+, *Slc17a7*+, *Slc17a6*+), GABAergic neurons (*Rbfox3*+, *Gad1*+, *Gad2*+), microglia (*Tmem119*+), vasculature-associated cell types (*Flt1*+) and different types of glia, including astrocytes (*Gfap*+), OPCs (*Pdgfra*+) and oligodendrocytes (*Plp1*+) (Fig. 8B-C).

Non-neuronal cell types were only broadly annotated without further sub-clustering, as the focus of this project was on neuronal populations. Neuronal classes were isolated, re-clustered at higher resolution, and annotated in detail using various publicly available single-cell datasets and *in situ* hybridization data for specific pallial regions (*82*, *154*, *155*). I categorized neuronal populations into subclasses and supertypes, following a previously established grouping and naming scheme (Fig. 8D) (*82*). Both dissections contributed to all major neuronal and non-neuronal cell classes (Fig. 8C, Fig. S2B-C), though several neuron types were predominantly derived from one dissection, such as excitatory neurons from the piriform cortex (Ex_Pir) or isocortical IT neurons (Ex_CTX_IT; Fig. 8C-D).

This is consistent with the regional restriction of specific neuronal types, particularly excitatory neurons, to distinct pallial regions.

To ensure comprehensive coverage of murine pallial cell types, I supplemented this dataset with existing single-cell RNA-seq data encompassing neurons from the entire murine isocortex and hippocampal formation (Fig. 8E-F) (*82*). Both datasets contributed to neuronal types derived from shared dissected regions, such as Ex_CTX_IT in the isocortex, while certain cell types, like excitatory neurons in the piriform cortex or amygdala, were unique to our dataset. Conversely, hippocampal neurons were only present in the external dataset (Fig. 8E-F, Fig. S2B-C).

Together, these datasets provide comprehensive coverage of neuronal types across all pallial regions in mouse, establishing a solid foundation for comparative analyses of neuronal populations across amniotes.

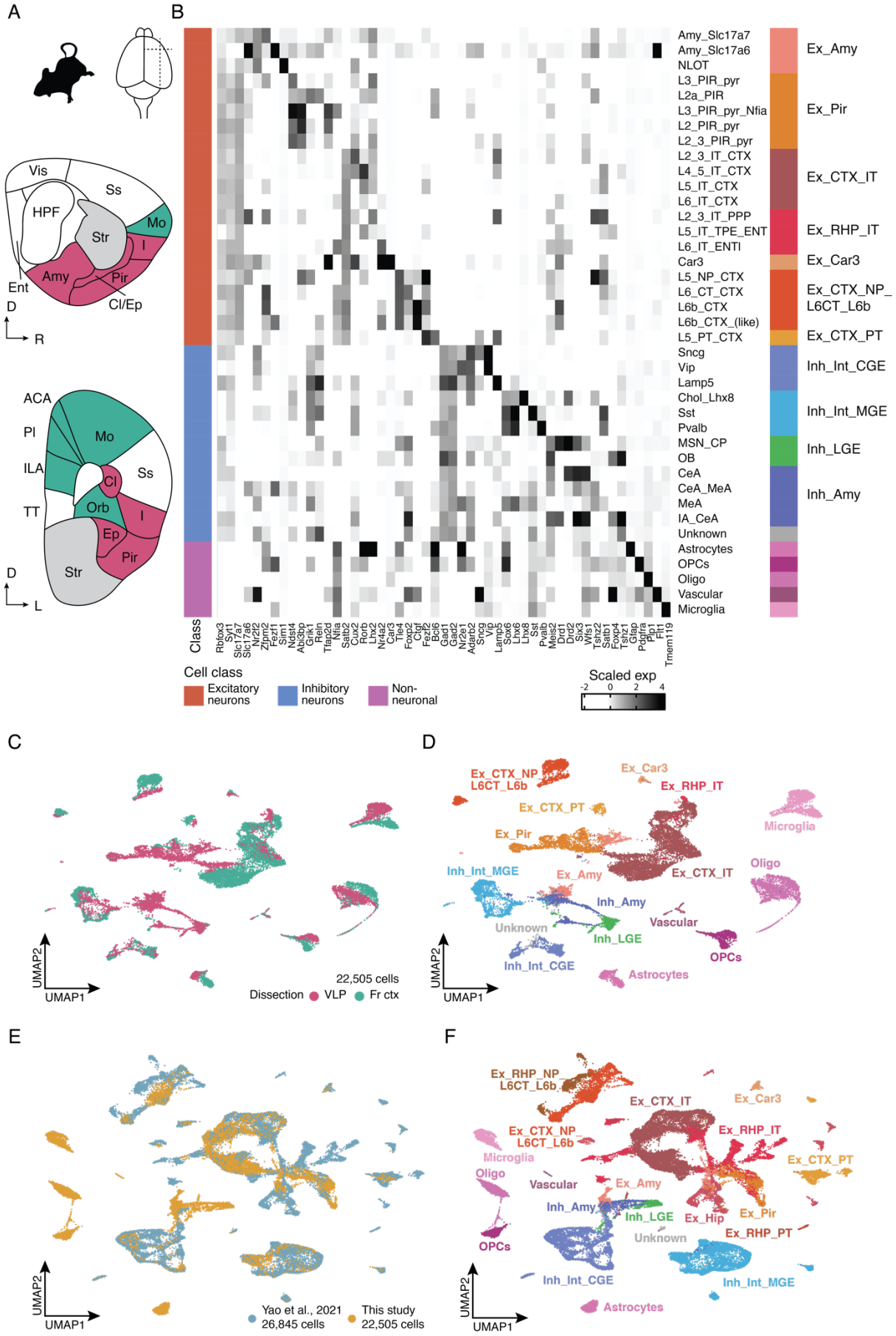
A
B
Vis
Ss
HPF
Mo
Str
I
Amy
Pir
Ent
Cl/Ep
D
R
ACA
Pl
Mo
ILA
Cl
Ss
TT
Orb
I
Ep
Pir
Str
D
L
Class
Amy_Slc17a7
Amy_Slc17a6
NLOT
L3_PIR_pyr
L2a_PIR
L3_PIR_pyr_Nfia
L2_PIR_pyr
L2_3_PIR_pyr
L2_3_IT_CTX
L4_5_IT_CTX
L5_IT_CTX
L6_IT_CTX
L2_3_IT_PPP
L5_IT_TPE_ENT
L6_IT_ENTl
Car3
L5_NP_CTX
L6_CT_CTX
L6b_CTX
L6b_CTX_(like)
L5_PT_CTX
Sncg
Vip
Lamp5
Chol_Lhx8
Sst
Pvalb
MSN_CP
OB
CeA
CeA_MeA
MeA
IA_CeA
Unknown
Astrocytes
OPCs
Oligo
Vascular
Microglia
Ex_Amy
Ex_Pir
Ex_CTX_IT
Ex_RHP_IT
Ex_Car3
Ex_CTX_NP_
L6CT_L6b
Ex_CTX_PT
Inh_Int_CGE
Inh_Int_MGE
Inh_LGE
Inh_Amy
Rbfox3
Syt1
Slc17a7
Slc17a6
Nr2f2
Zfpm2
Ebf1
Sim1
Ndst4
Abi3bp
Grik1
Reln
Tfap2b
Nfib
Satb2
Cux2
Rorb
Lhx2
Nr4a2
Car3
Tle4
Foxp2
Ctgf
Fezf2
Bcl6
Gad1
Gad2
Nr2e1
Adarb2
Sncg
Vip
Lamp5
Sox6
Lhx6
Lhx8
Sst
Pvalb
Meis2
Drd1
Drd2
Six3
Wfs1
Tshz2
Satb1
Foxp1
Tshz1
Glap
Pdgfra
Plp1
Flt1
Tmem119
Cell class
Excitatory neurons
Inhibitory neurons
Non-neuronal
Scaled exp
-2
0
2
4
C
UMAP2
UMAP1
22,505 cells
Dissection
VLP
Fr ctx
D
Ex_CTX_NP
L6CT_L6b
Ex_Car3
Ex_RHP_IT
Ex_CTX_PT
Ex_Pir
Microglia
Inh_Int_MGE
Ex_Amy
Ex_CTX_IT
Oligo
Inh_Amy
Unknown
Vascular
Inh_LGE
OPCs
Inh_Int_CGE
Astrocytes
UMAP2
UMAP1
E
UMAP2
UMAP1
Yao et al., 2021
26,845 cells
This study
22,505 cells
F
Ex_RHP_NP
L6CT_L6b
Ex_CTX_IT
Ex_Car3
Ex_CTX_NP_
L6CT_L6b
Ex_RHP_IT
Microglia
Ex_CTX_PT
Oligo
Vascular
Ex_Amy
Inh_Amy
Inh_LGE
Ex_Hip
Ex_Pir
Unknown
Ex_RHP_PT
OPCs
Inh_Int_CGE
Inh_Int_MGE
Astrocytes
UMAP2
UMAP1

Figure 8 Cell type atlas of the adult murine pallium. (A) Schematic illustration of sampled regions in an exemplary sagittal (top) and coronal (bottom) section according to the Allen Mouse Brain Atlas. **(B)** Heatmap of selected marker gene expression across murine cell subclasses. Coloured bar and text on the right represent broad "neighbourhood" labels adapted from (*82*). UMAP of murine dataset generated for this study **(C)** coloured by dissection and **(D)** broad neighbourhood labels as annotated in (B). UMAP of final murine pallium dataset used for cross-species comparisons including data from this study and (*82*), **(E)** coloured by data origin and **(F)** coloured by and labelled with broad neighbourhood labels. D, dorsal; R, rostral; L, lateral; Exp, expression; VLP, ventro-lateral pallium; Fr ctx, frontal isocortex. For abbreviations of murine cell populations and brain regions see List of abbreviations. Partially adapted from (*1*).

2.2.1.2 Refined annotation of cell types in the developing murine pallium

In order to enable comparisons of excitatory cell types across developing amniote pallia (see chapter 2.2.5.2.2) I refined the annotation of a subset from existing single-cell RNA-seq data that captures mouse brain development from embryonic day 7 (e7) to e18 (*80*).

To ensure a robust representation of all pallial lineages, I used data from embryonic day 9 through 17 (e09-e17), with the onset of neurogenesis around e10 (*88*). This developmental window was chosen because pre-neurogenesis stages are not covered in the chicken dataset (see chapter 2.2.4), and by later stages, murine forebrain samples predominantly consist of cells from the isocortex and non-pallial structures, with very limited representation of other pallial regions. Focusing on the e09–e17 period thus allowed for the most balanced sampling of pallial cell types, while maintaining comparability to the developmental timeframe of the chicken dataset (*132*). From the profiled forebrain dissections, I isolated pallial progenitors and excitatory neurons (Fig. 9A-B), which I identified based on specific marker gene expression (Fig. 8D). I further subclustered and annotated the 21,221 neurons in the subset to define distinct excitatory neuronal subtypes (Fig. 9C-D), using known marker genes largely derived from adult single-cell studies (*67*, *76*, *82*) and available *in situ* hybridization data of identified marker genes (*155*). This approach enabled a high-resolution annotation of excitatory neuronal types, while radial glia and intermediate progenitor cells (IPCs) were left at a broader classification level, as the primary focus was to resolve excitatory neuronal lineages.

Nevertheless, cells in certain pallial structures, such as the piriform and entorhinal cortices, could not be confidently separated into distinct populations, likely due to limited cell counts and the lack of marker genes distinguishing cells in these structures reported in literature, underscoring the need for further cellular lineage validation across non-isocortical regions in eutherians. Despite these limitations, this analysis provides the most refined view of early excitatory neuron development in the mouse pallium achievable with the current data, creating a solid framework for cross-species comparisons with cell populations in the developing avian pallium.

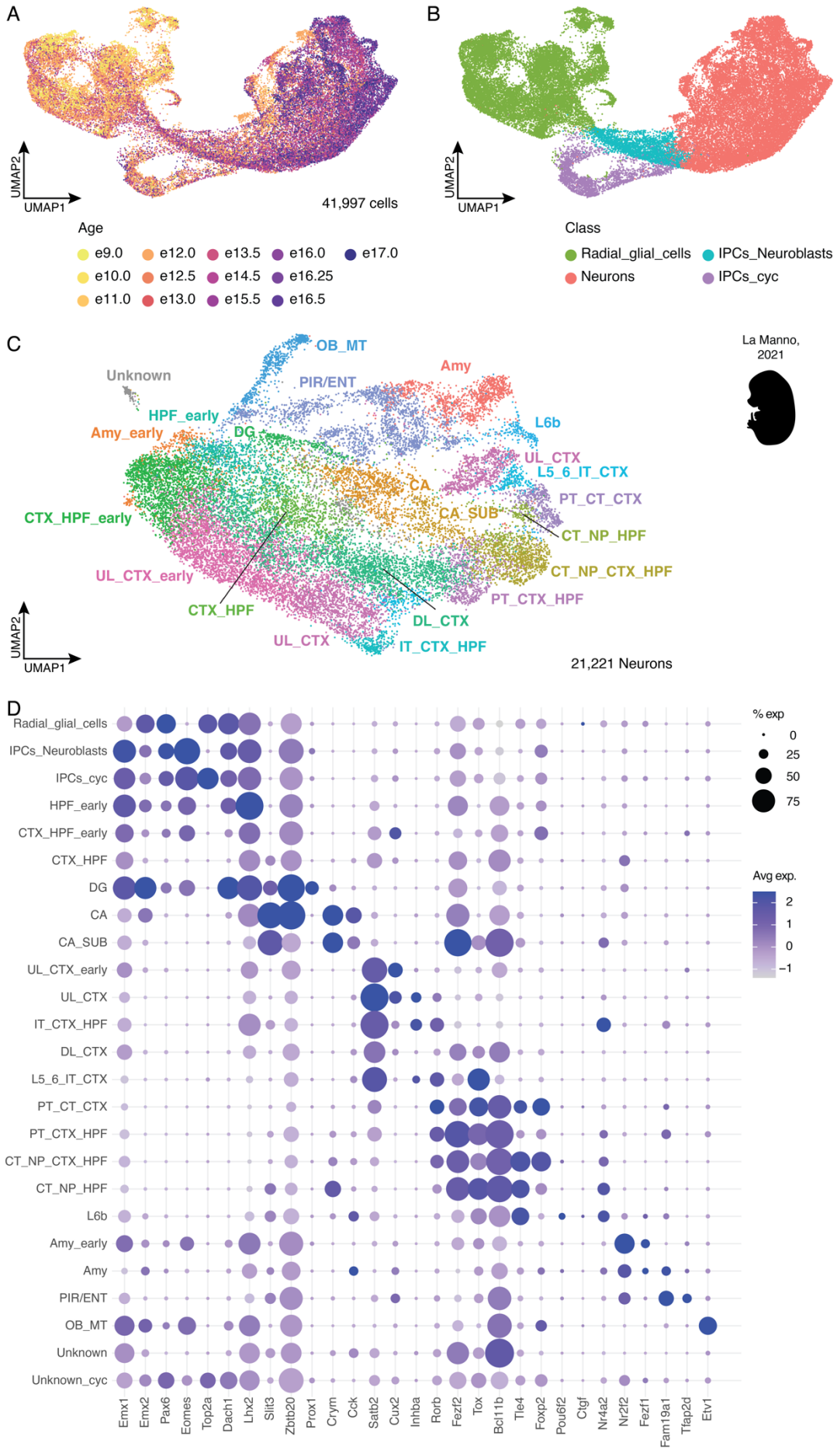
A
UMAP2
UMAP1
41,997 cells
Age
e9.0
e10.0
e11.0
e12.0
e12.5
e13.0
e13.5
e14.5
e15.5
e16.0
e16.25
e16.5
e17.0
B
UMAP2
UMAP1
Class
Radial_glial_cells
Neurons
IPCs_Neuroblasts
IPCs_cyc
C
OB_MT
Unknown
PIR/ENT
Amy
HPF_early
Amy_early
DG
L6b
UL_CTX
L5_6_IT_CTX
CA
PT_CT_CTX
CA_SUB
CTX_HPF_early
CT_NP_HPF
CT_NP_CTX_HPF
UL_CTX_early
PT_CTX_HPF
CTX_HPF
DL_CTX
UL_CTX
IT_CTX_HPF
UMAP2
UMAP1
21,221 Neurons
La Manno, 2021
D
Radial_glial_cells
IPCs_Neuroblasts
IPCs_cyc
HPF_early
CTX_HPF_early
CTX_HPF
DG
CA
CA_SUB
UL_CTX_early
UL_CTX
IT_CTX_HPF
DL_CTX
L5_6_IT_CTX
PT_CT_CTX
PT_CTX_HPF
CT_NP_CTX_HPF
CT_NP_HPF
L6b
Amy_early
Amy
PIR/ENT
OB_MT
Unknown
Unknown_cyc
Emx1
Emx2
Pax6
Eomes
Top2a
Dach1
Lhx2
Slit3
Zbtb20
Prox1
Crym
Cck
Satb2
Cux2
Inhba
Rorb
Fezf2
Tox
Bcl11b
Tle4
Foxp2
Pou6f2
Ctgf
Nr4a2
Nr2f2
Fezf1
Fam19a1
Tfap2d
Etv1
% exp
0
25
50
75
Avg exp.
2
1
0
−1

Figure 9 Annotation of cell populations in the developing murine pallium. UMAP of the pallial excitatory cell lineage taken from (*80*) **(A)** coloured by developmental age and **(B)** cell class. **(C)** UMAP of only excitatory neurons coloured by and labelled with more detailed cell population labels. **(D)** Gene expression dot plot of selected marker genes across cell populations shown in (C). Adapted from (*1*).

2.2.2 CELL TYPE ATLAS OF THE ADULT LIZARD PALLIUM

To survey cell types in the pallium of non-avian reptiles, I generated snRNA-seq data for the complete pallium of the green anole lizard (*Anolis carolinensis*; excluding olfactory bulbs). The green anole lizard belongs to the clade of squamates, including snakes and lizards, which represents a major clade within sauropsids and split from the lineage giving rise to extant turtles, crocodilians and birds ~ 280 million years ago (*6*). The resulting dataset comprises 21,424 cells (median UMIs/genes: 2,269/1,447; Fig. 10B, Fig. S3A-B) from distinct dissections of the DVR and cortex, which were profiled separately.

As in mammals, major cell classes in the lizard pallium were identified by the expression of known marker genes, including excitatory neurons (*SLC17A7*+), inhibitory neurons (*GAD1*+, *GAD2*+), astroglia (*GFAP*+), oligodendrocyte precursor cells (*PDGFRA*+), and oligodendrocytes (*PLP1*+) (Fig. 10A). Notably, I could not detect any immune cell populations, despite their identification in previous studies of other lizard species (*41*, *72*), suggesting that these cells may have been missed in our sampling.

Following a similar approach to the mouse dataset, I only broadly annotated non-neuronal populations, while neuronal populations were iteratively clustered to capture neuronal diversity (Fig. S3C-D). Inhibitory neuron clusters were grouped into five major categories based on the expression of known marker genes (Fig. 10A), reflecting their developmental origins in different ganglionic eminences (*SOX6*, *LHX6* – MGE; *NR2E1*, *ADARB2* – CGE; *MEIS2* – LGE; (*71*)), likely location in different pallial regions (*FOXP2*, *TSHZ1* – lizard amygdala-equivalent; (*41*, *156*), or neurotransmitter identities (*LHX8* – cholinergic neurons; (*157*). MGE- and CGE-derived neurons were found in both the DVR and cortex dissections, whereas LGE-derived neurons, including those from the putative lizard amygdala-equivalent region (Inh_Amy), mostly came from DVR dissections (Fig. 10B-C, Fig. S3B). This spatial distribution is similar to the organization seen in mammals, where MGE- and CGE-derived neurons are distributed across the pallium, but LGE-derived neurons are predominantly found in the olfactory bulbs and certain amygdalar nuclei (*67*, *154*).

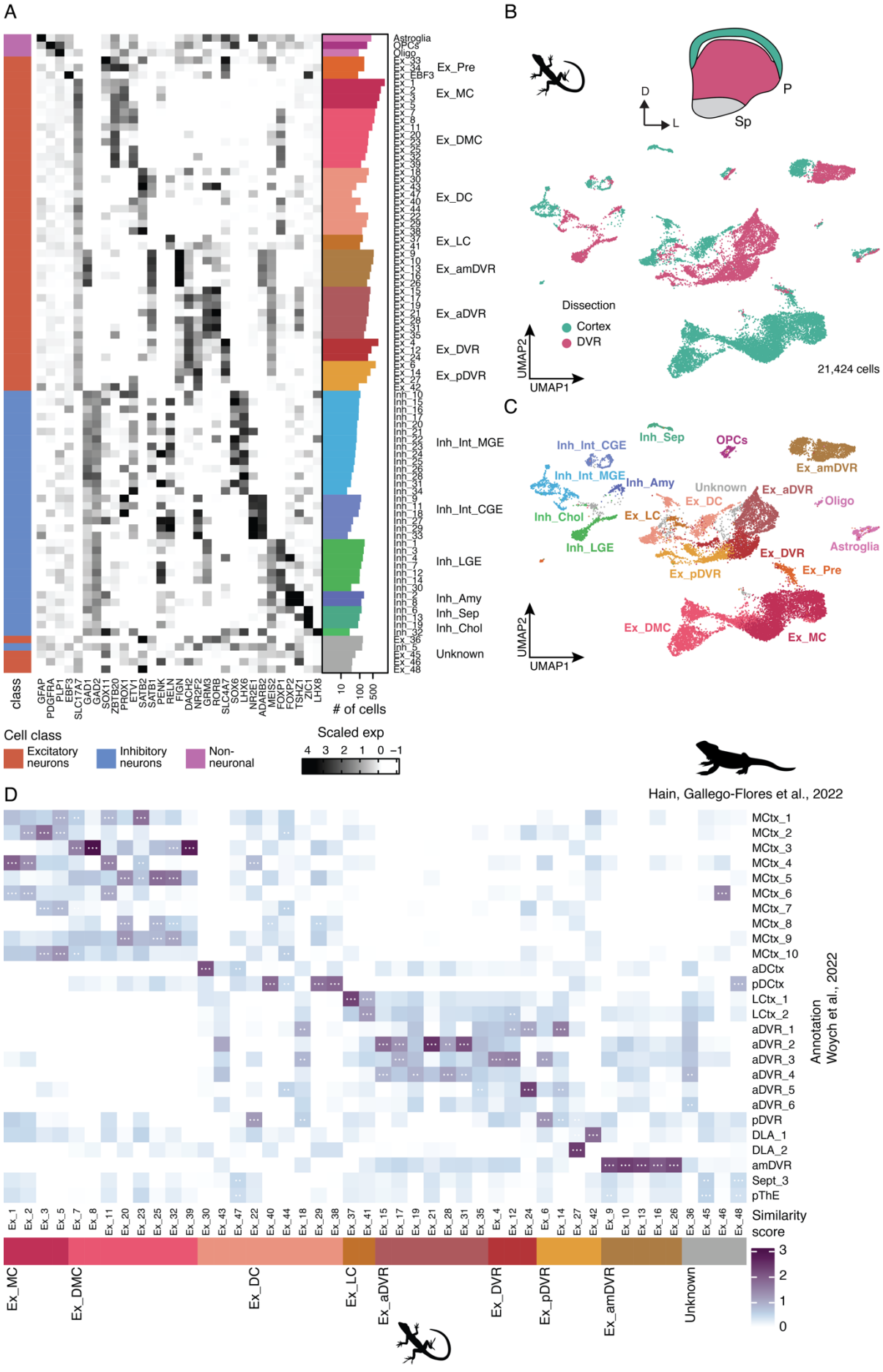
A
B
C
D
Astroglia
OPCs
Oligo
Ex_Pre
Ex_MC
Ex_DMC
Ex_DC
Ex_LC
Ex_amDVR
Ex_aDVR
Ex_DVR
Ex_pDVR
Inh_Int_MGE
Inh_Int_CGE
Inh_LGE
Inh_Amy
Inh_Sep
Inh_Chol
Unknown
class
GFAP
PDGFRA
PLP1
EBF3
SLC17A7
GAD1
GAD2
SOX11
ZBTB20
PROX1
ETV1
SATB2
SATB1
RELN
FEZF2
FIGN
DACH2
NR2F2
GRM3
RORB
SLC4A7
SOX6
LHX6
NR2E1
ADARB2
MEIS2
FOXP1
FOXP2
TSHZ1
ZIC1
LHX8
10
100
500
# of cells
Cell class
Excitatory neurons
Inhibitory neurons
Non-neuronal
Scaled exp
4 3 2 1 0 −1
D
P
Sp
L
Dissection
Cortex
DVR
UMAP2
UMAP1
21,424 cells
Inh_Sep
OPCs
Inh_Int_CGE
Ex_amDVR
Inh_Int_MGE
Inh_Amy
Unknown
Ex_aDVR
Ex_DC
Oligo
Inh_Chol
Ex_LC
Inh_LGE
Astroglia
Ex_DVR
Ex_pDVR
Ex_Pre
Ex_DMC
Ex_MC
Hain, Gallego-Flores et al., 2022
MCtx_1
MCtx_2
MCtx_3
MCtx_4
MCtx_5
MCtx_6
MCtx_7
MCtx_8
MCtx_9
MCtx_10
aDCtx
pDCtx
LCtx_1
LCtx_2
aDVR_1
aDVR_2
aDVR_3
aDVR_4
aDVR_5
aDVR_6
pDVR
DLA_1
DLA_2
amDVR
Sept_3
pThE
Annotation
Woych et al., 2022
Similarity score
3
2
1
0
Ex_MC
Ex_DMC
Ex_DC
Ex_LC
Ex_aDVR
Ex_DVR
Ex_pDVR
Ex_amDVR
Unknown

Figure 10 Cell type atlas of the adult lizard pallium. (A) Heatmap of selected marker gene expression across 86 clusters in snRNA-seq-based lizard pallium atlas. Barplots of cell numbers per cluster on the right are coloured by broader regional annotation as indicated by text labels. **(B)** UMAP of all cells (bottom) coloured by dissection, as illustrated in exemplary coronal section (top), and **(C)** coloured by and labelled with broad regional annotation. **(D)** Comparison between *Anolis carolinensis* excitatory clusters and *Pogona vitticeps* single cell data from (*72*) as annotated by (*19*) using three methods. Scores were scaled between 0 and 1 per method and summed across all methods to represent the similarity score. White dots in tiles are shown when populations are among the top reciprocal matches according to two or all three methods. D, dorsal; L, lateral; P, pallium; Sp, subpallium; MC, medial cortex; DMC, dorsal medial cortex; DC, dorsal cortex; LC, lateral cortex; amDVR, anterior medial DVR; aDVR, anterior DVR; pDVR, posterior DVR; Int, interneurons; Amy, amygdala; Sep, septum; Chol, cholinergic; Oligo, Oligodendrocytes; MCtx, medial cortex; aDCtx, anterior dorsal cortex; pDCtx, posterior dorsal cortex; LCtx, lateral cortex; DLA, dorsal lateral amygdala; Sept, septum; pThE, pre-thalamic eminence. Adapted from (*1*).

Among excitatory neurons, two clusters of immature neurons (*SOX11*+; Fig. 10A), mostly from the cortex dissections (Fig. S3B), expressed the mammalian hippocampal transcription factor *ZBTB20* (*147*), indicating ongoing neurogenesis in the hippocampal-like lizard medial cortex (*41*). Some DVR-derived cells also contributed to these clusters, suggesting either imprecise dissections or the presence of additional immature neuron populations in the DVR which might be uncovered with deeper sampling. Additionally, I identified a distinct excitatory cluster (Ex_EBF3, EBF3+, ZIC1+) likely originating from the prethalamic eminence, which is known to generate Cajal-Retzius cells in mammals (*97*), implying that either parts of this structure were unintentionally sampled, or that prethalamic neurons migrate into the pallium in lizards as observed in mammals.

Mature excitatory neurons were annotated using reference single-cell transcriptomics data from another lizard (*41*, *72*) and turtle species (*41*) (Fig. 10D; fig. S4). For this comparison, and for all other following cell type comparisons among adult amniotes, I employed three complementary comparative methods to investigate cell population similarities across species based on different gene sets (one-to-one orthologous genes or all orthologous genes) and algorithms, further discussed in chapter 2.2.5. Excitatory neurons from different dissected regions (i.e., DVR and cortex) mostly segregated into distinct populations (Fig. 10B-C, Fig. S3B-C), confirming the regional specificity of excitatory neurons in the lizard pallium as seen in mammals (*82*). Most excitatory clusters from the cortex dissections were mapped to likely spatial locations within the medial, dorsomedial, dorsal, or lateral cortex, based on the comparison to reference data (Fig. 10D). However, I could not unambiguously identify clusters from the anterior dorsal cortex, a region suggested to contain neurons homologous to mammalian isocortical neurons in turtles (*41*), which is comparatively smaller in lizards than in turtles (*41*).

DVR excitatory neurons were primarily categorized into three groups, representing neurons in the anterior DVR (Ex_aDVR), posterior DVR (Ex_pDVR), and likely intermediate DVR (Ex_DVR). Interestingly, both the DVR and cortex dissections contributed to a population resembling neurons of the anterior medial DVR (amDVR; Fig. S3B), previously

proposed to be homologous to the mammalian claustrum based on gene expression and functional characteristics (*42*). This suggests either unintended co-dissection of the anterior medial DVR with cortical regions or the possibility that claustrum-like neurons, originally described in the amDVR of the bearded dragon *Pogona vitticeps*, might also be present in cortical regions of the green anole lizard, which shared a last common ancestor with the bearded dragon ~ 146 million years ago.

Overall, the generated dataset offers a comprehensive map of neuronal diversity in the lizard pallium. Combined with existing datasets from other non-avian reptiles, it provides a robust foundation for comparative analyses across multiple amniote lineages.

2.2.3 CELL TYPES IN THE ADULT AVIAN PALLIUM

To construct the first comprehensive cell type atlas of the avian pallium, we profiled the pallium of the chicken (*Gallus gallus*), chosen due to its widespread use as a model organism and the comparatively extensive body of existing research. Using snRNA-seq, I profiled the pallium from four individuals in three broad rostral-to-caudal sections (excluding the olfactory bulbs), and the pallium from a fifth individual, specifically dissected into four anatomical regions: hippocampal area, hyperpallium, anterior DVR, posterior DVR (excluding the arcopallium), and arcopallium (Fig. 11A). The resulting dataset comprises 91,829 high-quality cells (median UMIs/genes: 4,808/2,057; Fig. S5-6).

To investigate the spatial distribution of cell types within the chicken pallium, I utilized In Situ Sequencing (ISS; (*158*)) to map the expression of 50 selected marker genes (Fig. S7, Table S1). Since this gene set did not include specific markers for all annotated cell populations, I employed Tangram (*159*) to infer the spatial distribution of these populations (Fig. S7). Tangram allowed me to integrate the collective in situ expression profiles of the 50 mapped genes with single-nucleus RNA sequencing (snRNA-seq) data to predict the locations of cell populations. To complement the high-resolution, targeted spatial data from ISS, we incorporated lower-resolution, whole-transcriptome spatial data obtained using the Visium platform (10x Genomics; Fig. S8). CCA-based integration of the Visium spatial data with snRNA-seq profiles provided additional insights into cell population distributions and served as an independent validation of the ISS results.

I classified cells in the snRNA-seq dataset into three primary cell type classes using known marker gene expression: inhibitory (GABAergic) neurons (*SYT1*+, *GAD67*+, *GAD*2+), excitatory (glutamatergic) neurons (*SYT1*+, *SLC17A6*+), and non-neuronal cells. The non-neuronal cell class includes oligodendrocyte progenitor cells (*SOX6*+, *PDGFRA*+), mature oligodendrocytes (*PLP1*+), astrocytes (*SLC1A3*+, *GFAP*+), immune cells (*TMEM119*+), and a heterogeneous group of vasculature-associated cells (*VWF*+; Fig. 11B-C). Given their relatively low abundance, limited heterogeneity, and the primary neuronal focus of this project, I did not further sub-cluster non-neuronal cells.

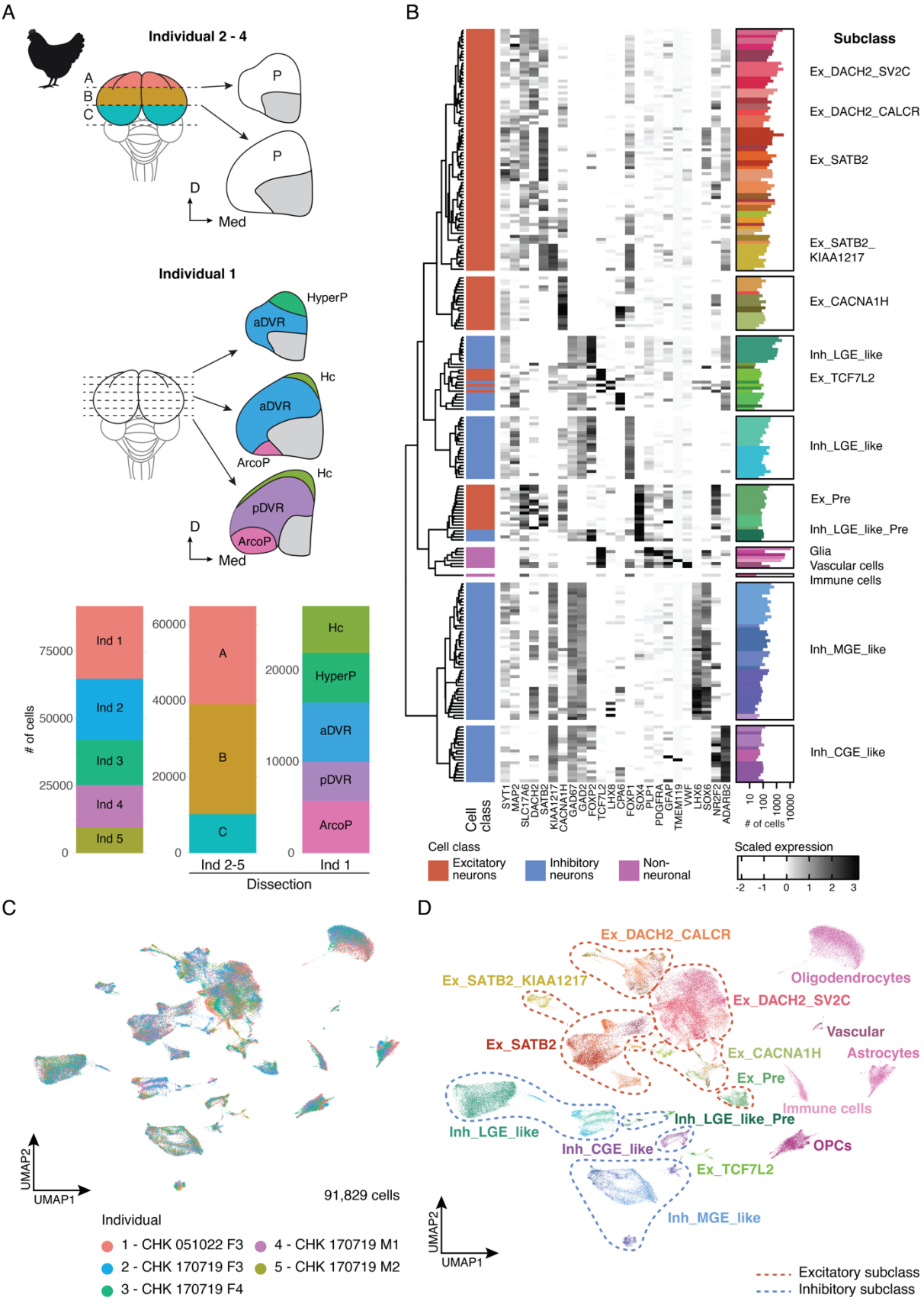

Figure 11 Cell type atlas of the adult chicken pallium. (A) Dissection scheme of adult chicken individuals (top) and barplots of cell numbers per individual and dissection (bottom). **(B)** Heatmap of selected marker gene expression across 237 clusters, ordered by independently constructed cluster dendrogram. Barplots

of cell numbers per cluster on the right are coloured by supertype annotation, text labels indicate subclass labels. UMAP of all cells **(C)** coloured by individual and **(D)** coloured by supertype annotation. Dotted lines and text labels represent subclass annotations. D, dorsal; Med, medial; P, pallium; HyperP, hyperpallium; aDVR, anterior DVR including nido- and mesopallium; Hc, hippocampal areas; ArcoP, arcopallium; pDVR, posterior DVR including nido- and mesopallium; Ind, individual. Adapted from (*1*).

For neurons, I organized cells into hierarchical categories across four levels: classes (excitatory or inhibitory neurons), subclasses, supertypes, and clusters. Using a bottom-up approach, I iteratively clustered inhibitory (23,848 cells) and excitatory neurons (45,425 cells), ultimately identifying 109 inhibitory and 120 excitatory clusters (Fig. S6). I then performed hierarchical clustering of the dataset based on average gene expression profiles per cluster (or for broad non-neuronal populations) to construct a dendrogram. Based on this dendrogram and low-resolution Louvain clustering, I grouped neuronal clusters into supertypes and subclasses (Fig. 11B-C), naming each group according to its most distinct marker genes.

In total, I annotated 46 supertypes representing mature and immature neurons, which were further consolidated into 11 subclasses. In the resulting hierarchical dendrogram, non-neuronal cells, inhibitory neurons, and excitatory neurons generally segregated, with the exception of likely immature neurons (*SOX4*+) from the pallium and a small subclass (*TCF7L2*+) likely representing cells co-dissected from the neighbouring thalamus (*160*) (Fig. 11B).

2.2.3.1 GABAergic inhibitory cell types in the adult avian pallium

Hierarchical clustering of inhibitory neuron clusters in the chicken pallium identified three major groups that likely reflect distinct developmental origins in the MGE, CGE or LGE. These origins were inferred based on the expression of marker genes known from eutherian mammals, such as *SOX6* and *LHX6* for MGE, *NR2E1* and *ADARB2* for CGE, and *MEIS2*, *FOXP1*, and *FOXP2* for LGE ((*71*); Fig. 12A). Most identified inhibitory neurons exhibit MGE- or LGE-like profiles, while CGE-derived neurons are comparably rare. This contrasts with the mammalian pallium, where CGE-derived neurons are more abundant than LGE-derived neurons across most pallial regions, with the exception of the olfactory bulbs (*67*, *71*). In total, I identified eight MGE-like, three CGE-like, and six LGE-like inhibitory supertypes.

Most MGE- and CGE-like supertypes were reliably mapped across the pallium using ISS and Visium data, showing an interspersed distribution across regions (Fig. 12D-E). This distribution aligns with their likely role as interneurons modulating various circuits, similar to the broad distribution of MGE- and CGE-derived interneurons in the mammalian pallium.

Among the LGE-derived clusters, I identified two small supertypes that express marker genes associated with olfactory bulb neurons (*CPA6*, *SCGN;* (*161*, *162*)) and spatially mapped to the olfactory bulbs (Fig. 12G). This suggests that either parts of the olfactory

bulbs were inadvertently included in the dissections or that these cells represent a newly generated population migrating from the ventricular wall to the olfactory bulbs (*113*).

The remaining LGE-derived clusters form two major groups distinguished by *FOXP2* and *FOXP1* expression. The *FOXP2*+ group consists of a large, relatively homogenous supertype (Inh_LGE_like_FOXP2) and a smaller supertype representing immature neurons (*SOX4*+; Inh_LGE_like_Pre) that may differentiate into the Inh_LGE_like_FOXP2 population based on shared marker gene expression (Fig. 12A). Notably, the Inh_LGE_like_FOXP2 supertype is abundant and distributed broadly across both the pallium and subpallium according to ISS and Visium data (Fig. 12F), in line with its origin from all dissected pallial regions (Fig. S6A). A similarly widespread LGE-derived population was recently identified in the zebra finch (*75*), suggesting that this characteristic is shared across avian species. In contrast, LGE-derived neurons in the mammalian pallium are primarily confined to the amygdala and olfactory bulbs (*67*, *71*). Furthermore, studies in a turtle and a lizard species show a distribution of LGE-derived neurons across the pallium similar to that observed in mammals (*41*). These findings thus underscore a lineage-specific divergence in the distribution patterns and abundance of LGE-derived neurons within the avian lineage.

The FOXP1+ group separated into two distinct supertypes, differentiated by the expression of *SGCG* and *DGKH*, both of which mapped to subpallial regions (Fig. 12H), indicating that portions of the subpallium were likely inadvertently co-dissected with the pallial dissections. However, the *DGKH*+ supertype was also reliably mapped to specific regions within the arcopallium (Fig. 12H-I), corroborating previous studies showing that the avian arcopallium encompasses functionally distinct regions, likely containing unique cell types (*163*). Both *FOXP1*+ supertypes include clusters expressing markers characteristic of mammalian medium spiny neurons, found in the striatum, as well as of transcriptomically similar neurons within the central amygdala, such as *MEIS2*, *PRKCD*, and *PENK* (Fig. 12A). These findings align with recent studies indicating a central amygdala (CA)-like structure in chickens (*83*), and suggest that medium spiny neuron-related cell types, found in both the mammalian striatum and the amygdala, may be shared across amniotes.

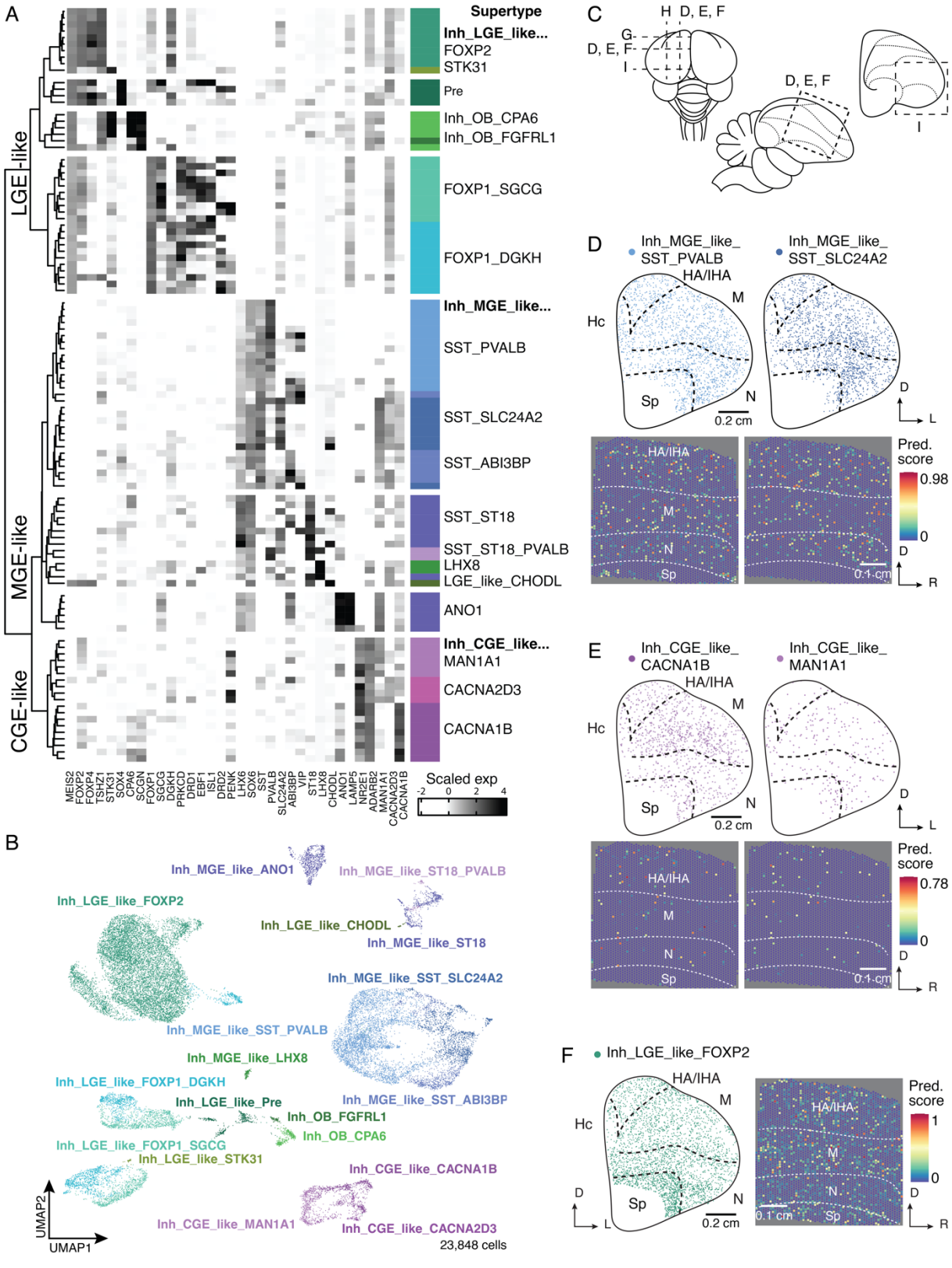
A
Supertype
Inh_LGE_like...
FOXP2
STK31
Pre
Inh_OB_CPA6
Inh_OB_FGFRL1
FOXP1_SGCG
FOXP1_DGKH
Inh_MGE_like...
SST_PVALB
SST_SLC24A2
SST_ABI3BP
SST_ST18
SST_ST18_PVALB
LHX8
LGE_like_CHODL
ANO1
Inh_CGE_like...
MAN1A1
CACNA2D3
CACNA1B
LGE-like
MGE-like
CGE-like
MEIS2 FOXP2 FOXP4 TSHZ1 STK31 SOX4 CPA6 SCGN FOXP1 SGCG DGKH PRKCD DRD1 EBF1 ISL1 DRD2 PENK LHX6 SOX6 SST PVALB SLC24A2 ABI3BP NTS ST18 LHX8 CHODL ANO1 LAMP5 NR2E1 ADARB2 MAN1A1 CACNA2D3 CACNA1B
Scaled exp
-2 0 2 4
B
Inh_MGE_like_ANO1
Inh_MGE_like_ST18_PVALB
Inh_LGE_like_FOXP2
Inh_LGE_like_CHODL
Inh_MGE_like_ST18
Inh_MGE_like_SST_SLC24A2
Inh_MGE_like_SST_PVALB
Inh_MGE_like_LHX8
Inh_LGE_like_FOXP1_DGKH
Inh_LGE_like_Pre
Inh_OB_FGFRL1
Inh_OB_CPA6
Inh_LGE_like_FOXP1_SGCG
Inh_LGE_like_STK31
Inh_CGE_like_CACNA1B
Inh_CGE_like_MAN1A1
Inh_CGE_like_CACNA2D3
Inh_MGE_like_SST_ABI3BP
UMAP2
UMAP1
23,848 cells
C
H D, E, F
G
D, E, F
I
D, E, F
I
D
Inh_MGE_like_ SST_PVALB
Inh_MGE_like_ SST_SLC24A2
HA/IHA
Hc
M
N
Sp
0.2 cm
D
L
HA/IHA
M
N
Sp
0.1 cm
Pred. score
0.98
0
D
R
E
Inh_CGE_like_ CACNA1B
Inh_CGE_like_ MAN1A1
HA/IHA
Hc
M
N
Sp
0.2 cm
D
L
HA/IHA
M
N
Sp
0.1 cm
Pred. score
0.78
0
D
R
F
Inh_LGE_like_FOXP2
HA/IHA
Hc
M
D
L
Sp
N
0.2 cm
HA/IHA
M
N
0.1 cm
Sp
Pred. score
1
0
D
R
G
Inh_OB_CPA6
Inh_OB_FGFRL1
Mapping prob.
High
Low
D
L
0.1 cm
OB
H
Inh_LGE_like_FOXP1_ SGCG
Inh_LGE_like_FOXP1_ DGKH
Mapping prob.
High
Low
D
R
ArcoP
Sp
0.25 cm
I
Inh_LGE_like_FOXP1_DGKH
0.1 cm
AD
AI
AMV
Med
D
Pred. score
0.63
0

Figure 12 GABAergic inhibitory neurons in the adult chicken pallium. (**A)** Heatmap of selected marker gene expression across 109 clusters of inhibitory neurons in the chicken pallium ordered according to cluster dendrogram. Colour bar and text labels on the right indicate supertype annotation. **(B)** UMAP of inhibitory cells coloured by and labelled with supertype annotation. **(C)** Schematics of the chicken brain viewed from the top (left), a mid-sagittal (middle), and a posterior coronal (right) section, illustrating positions of tissue sections shown in (D-I). Dashed lines represent sections, thin dotted lines represent borders between pallial brain regions. Spatial location of **(D)** the two most abundant MGE-like supertypes, **(E)** the two most abundant CGE-like supertypes, and **(F)** the most abundant LGE-like supertype according to in situ sequencing (ISS; top) and Visium data (bottom). For ISS, only segmented cells with confidently assigned identity are shown. For Visium, high prediction (Pred.) scores indicate high probability that cells with the respective identity were present within the spot's area. **(G)** Spatial location probabilities of two LGE-like supertypes according to ISS. **(H)** Spatial location probabilities of both *FOXP1*+ LGE-derived supertypes according to ISS. **(I)** Spatial location of one *FOXP1*+ LGE-derived supertypes according to Visium. High prediction (Pred.) scores indicate high probability that cells with the respective identity were present within the spot's area. HA/IHA, apical and interstitial apical hyperpallium; M, Mesopallium; N, Nidopallium; Sp, subpallium; D, dorsal; L, lateral; R, rostral; Hc, hippocampal areas; OB, olfactory bulbs; ArcoP, arcopallium; AMV, medial ventral arcopallium; AI, intermediate arcopallium; AD, dorsal arcopallium; Med, medial. Adapted from (*1*).

2.2.3.2 Glutamatergic excitatory cell types in the adult avian pallium

One of the primary goals of this project was to investigate excitatory neuron diversity in the avian pallium, a cell class crucial for understanding amniote pallium evolution. Based on hierarchical and low-resolution Louvain-clustering, I identified and annotated 7 excitatory subclasses, which further divided into 28 supertypes (Fig. 13A-B).

The most distinct subclass, Ex_Pre, likely represents immature neurons based on its specific expression of *SOX4* (*164*). Within this subclass, clusters were further divided into two supertypes, Ex_Pre_SATB2 and Ex_Pre_KCNH7, which share marker gene expression with different excitatory subclasses. This suggests that multiple types of excitatory neurons continue to be generated in the adult chicken brain. These supertypes could not be reliably mapped to the tissue using the spatial data (not shown) but predominantly stemmed from hippocampal and arcopallial dissections (Fig. S6B) consistent with these structures sharing relatively large borders with the lateral ventricle, as new neurons likely arise in the ventricular zone (*113*).

2.2.3.2.1 Excitatory cell types in the adult avian hippocampal areas and arcopallium

The most distinct mature excitatory subclass, Ex_CACNA1H, specifically expresses markers associated with the mammalian hippocampal and retrohippocampal areas, such as *LHX2* and *ZBTB20* (Fig. 13A) (*147*, *165*). Regions homologous to the mammalian hippocampus, including subfields like the dentate gyrus (DG) and Cornu Ammonis regions (CA3 and CA1), have previously been identified in non-avian reptiles (*41*). However, whether these regions and their constituent cell types are also found in birds has been unclear. In this study, I identified one supertype expressing *ZBTB20* and the DG-specific marker *PROX1* (*148*), which localizes to the medial-most area of the chicken's putative hippocampus, aligning with the DG's anatomical position in mammals (Fig. 13A, D). Additionally, two other supertypes within the Ex_CACNA1H subclass, Ex_CACNA1H_CPA6 and Ex_CACNA1H_KIT, map to distinct areas within the putative chicken hippocampal region

(Fig. 13D), indicating the presence of subfields defined by unique cell types within this area. These identified subfields generally correspond to previously characterized regions with distinct functional roles (*166*), though functional heterogeneity appears broader than the diversity observed at the cell type level.

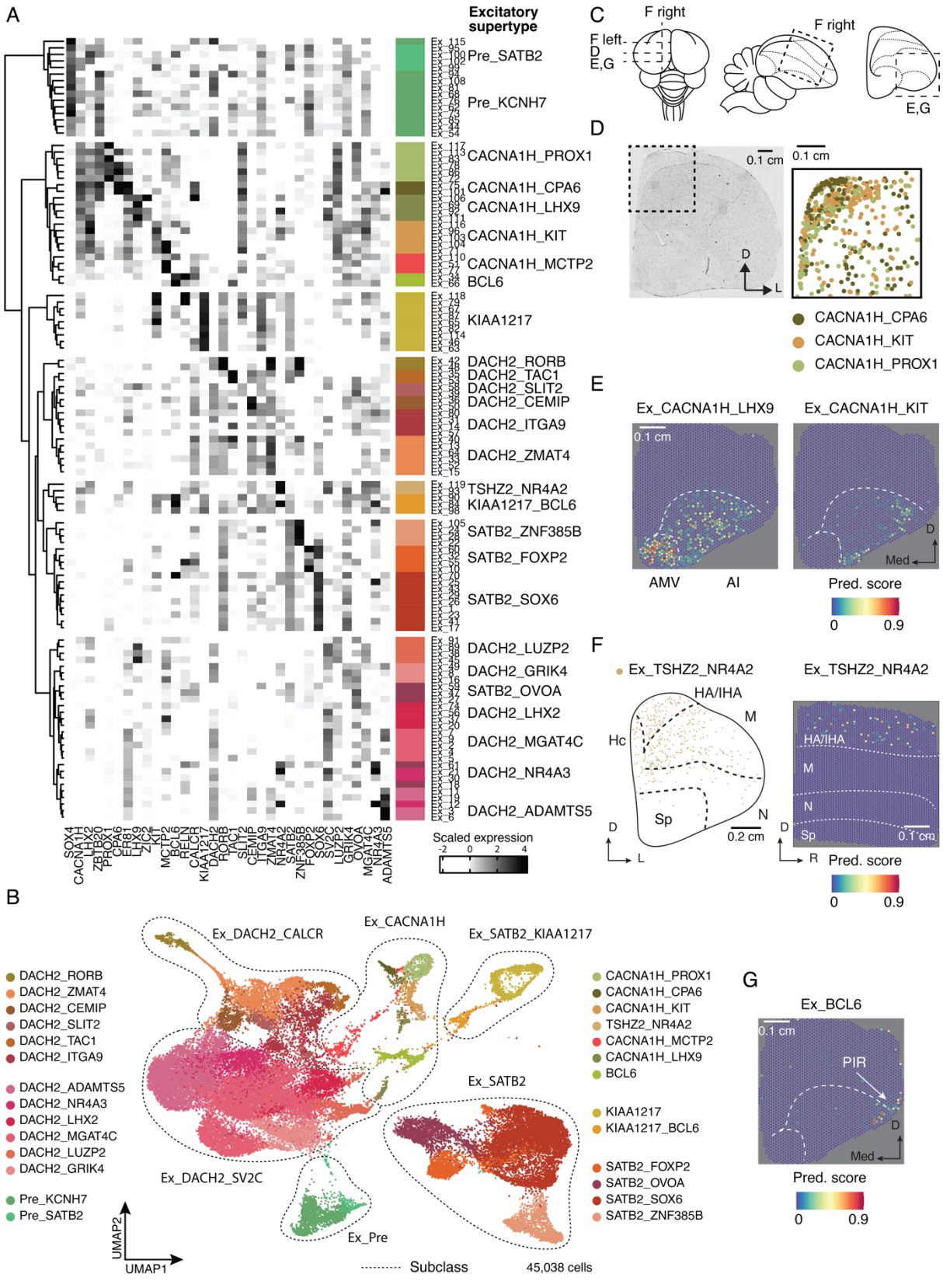

Figure 13 Glutamatergic excitatory neurons in the adult chicken pallium. (A) Heatmap of selected marker gene expression across 120 clusters of excitatory neurons in the chicken pallium ordered according to cluster dendrogram. Colour bar and text labels on the right indicate supertype annotation. (**B**) UMAP of pallial excitatory cells coloured by supertype annotation. Text labels represent subclass annotation. (**C**) Schematics of the chicken brain viewed from the top (left), a mid-sagittal (middle), and a posterior coronal (right) section, illustrating positions of tissue sections shown in (D-G). Dashed lines represent sections, thin dotted lines represent borders between pallial brain regions. (**D**) Spatial location of hippocampal supertypes according to ISS. **(E)** Spatial location of selected supertypes of the Ex_CACNA1H subclass according to Visium data. **(F)** Spatial location of a supertype related to the Ex_CACNA1H subclass according to ISS (Left) and Visium (right). **(G)** Spatial location of a supertype related to the Ex_CACNA1H subclass according to Visium. For ISS, only segmented cells with confidently assigned identity are shown. For Visium, high prediction (Pred.) scores indicate high probability that cells with the respective identity were present within the spot's area. D, dorsal; L, lateral; AMV, medial ventral arcopallium; AI, intermediate arcopallium; PIR, piriform area; HA/IHA, apical and interstitial apical hyperpallium; M, mesopallium; N, nidopallium; Sp, subpallium; Med, medial; R, rostral; PIR, piriform area. Adapted from (*1*).

In line with studies observing gene expression similarities between hippocampal regions and the arcopallium in the zebra finch (*37*, *48*), two supertypes of the Ex_CACNA1H subclass, Ex_CACNA1H_KIT and Ex_CACNA1H_LHX9, also mapped to the arcopallium (Fig. 13E). Ex_CACNA1H_LHX9 specifically is exclusive to the arcopallium, where it is enriched in a specific arcopallial subregion, consistent with previous suggestions that the arcopallium comprises various functionally distinct subfields (*44*, *163*). However, the comparatively low numbers of cells in the Ex_CACNA1H subclass likely limited my ability to capture the full extent of cellular heterogeneity in both the hippocampal region and the arcopallium. Therefore, while these findings reveal cell type-based regionalization in these areas, further sampling may uncover additional cell type diversity and allow finer alignment with previously observed heterogeneity on the functional and gene expression level.

One supertype within the Ex_CACNA1H subclass, Ex_CACNA1H_MCTP2, could not be confidently localized using adult ISS and Visium data (data not shown). However, observations from the developing chicken pallium suggest this may result from an absence of tissue sections capturing the relevant area (see chapter 2.2.4.1).

The supertype Ex_BCL6 clusters with the Ex_CACNA1H subclass in the cluster dendrogram (Fig. 13A) but exhibits distinct gene expression (low *CACNA1H*, *BCL6*+, *RELN*+). This supertype is situated in a superficial region near the arcopallium and posterior hippocampal area (Fig. 13G), which is known to receive projections from the olfactory bulbs (*167*). Consistent with its potential role as an olfactory input-receiving population, *RELN* is a marker for neurons that receive olfactory input in the mammalian piriform cortex, a related cell type in the entorhinal cortex, and neurons in the olfactory input-associated lateral cortex of lizards (*168*).

The small supertype Ex_TSHZ2_NR4A2 does not cluster with the Ex_CACNA1H subclass in the excitatory cluster dendrogram, yet it exhibits moderate expression of associated

markers such as *LHX2* and *ER81* (Fig. 13A). Notably, *NR4A2*, a specific marker for this supertype, is an immediate early response gene linked to neuronal activity. However, apart from the paralogous *NR3A4* gene, it does not specifically express other immediate early genes (Fig. S6D). Spatial analysis indicates that Ex_TSHZ2_NR4A2 is sparsely distributed primarily in the apical hyperpallium (HA; Fig. 13F), which borders hippocampal areas. This aligns with previous observations of sparse *NR4A2* expression in animals under quiet, dark conditions (*169*). These findings suggest that, despite the expression of two activity-related genes, Ex_TSHZ2_NR4A2 likely represents a distinct cell type rather than a transient active state, a notion further supported by evidence from the developing chicken pallium (see chapter 2.2.4.2). Additionally, these observations indicate that the HA contains a cell type with gene expression profiles similar to those found in the chicken hippocampal region.

2.2.3.2.2 Excitatory cell types in the adult avian mesopallium

Two excitatory subclasses within the avian pallium, Ex_SATB2 and Ex_SATB2_KIAA1217, are characterized by the specific expression of the mesopallial marker *SATB2* (*115*) and predominantly localize to the mesopallium, which constitutes a significant portion of the DVR (Fig. 14).

As mentioned before, the boundary between the avian hyperpallium and mesopallium has been a topic of considerable debate. While most authors and functional studies designate the region commonly annotated as HD/HI (Fig. 1A) as part of the hyperpallium (*43*, *129*), some researchers argue that this area corresponds to the dorsal mesopallium (*37*, *47*, *48*). In response to this proposal, it has been suggested that there are actually two valleculae —grooves on the brain's surface — rather than a single one previously thought to delineate the hyperpallium-mesopallium boundary. The more medial of these supposedly duplicated landmarks still marks the boundary between hyper- and mesopallium, while the other more lateral one separates the ventral and dorsal mesopallium. If one is mistaken for the other, this might lead to conflicting annotations of the HD/HI region. According to this proposal the medial vallecula is more prominent in anterior coronal sections of the chicken brain, while the lateral vallecula becomes more prominent in posterior sections (*44*).

In contrast to this proposal, I identified only a single, distinct vallecula in each spatially profiled section, though my dataset included only a limited number of coronal sections. Even in the most anterior tissue section of the ISS dataset, *SATB2* expression, along with cells belonging to the mesopallial subclasses Ex_SATB2 and Ex_SATB2_KIAA1217, extends dorsally beyond the presumed medial vallecula (Fig. 14B). Additionally, mesopallial cell types expressing *SATB2* are consistently located directly adjacent to a cell type marked by high *TAC1* expression, a known marker of the IHA (*44*), across various anterior-to-posterior levels (Fig. 14B). This close proximity effectively rules out the existence of an additional, distinct region between these areas that could correspond to the HD/HI.

Altogether, these findings support the reinterpretation of the HD/HI as containing mesopallial rather than hyperpallial cell types. Nevertheless, cell types in this region retain functional differences from the ones in the mesopallium, as they participate in the sensory-motor circuits of the hyperpallium rather than the DVR (*38*). In line with these functional distinctions and to remain consistent with common nomenclature I will continue to refer to the HD/HI region as part of the hyperpallium for the rest of this thesis.

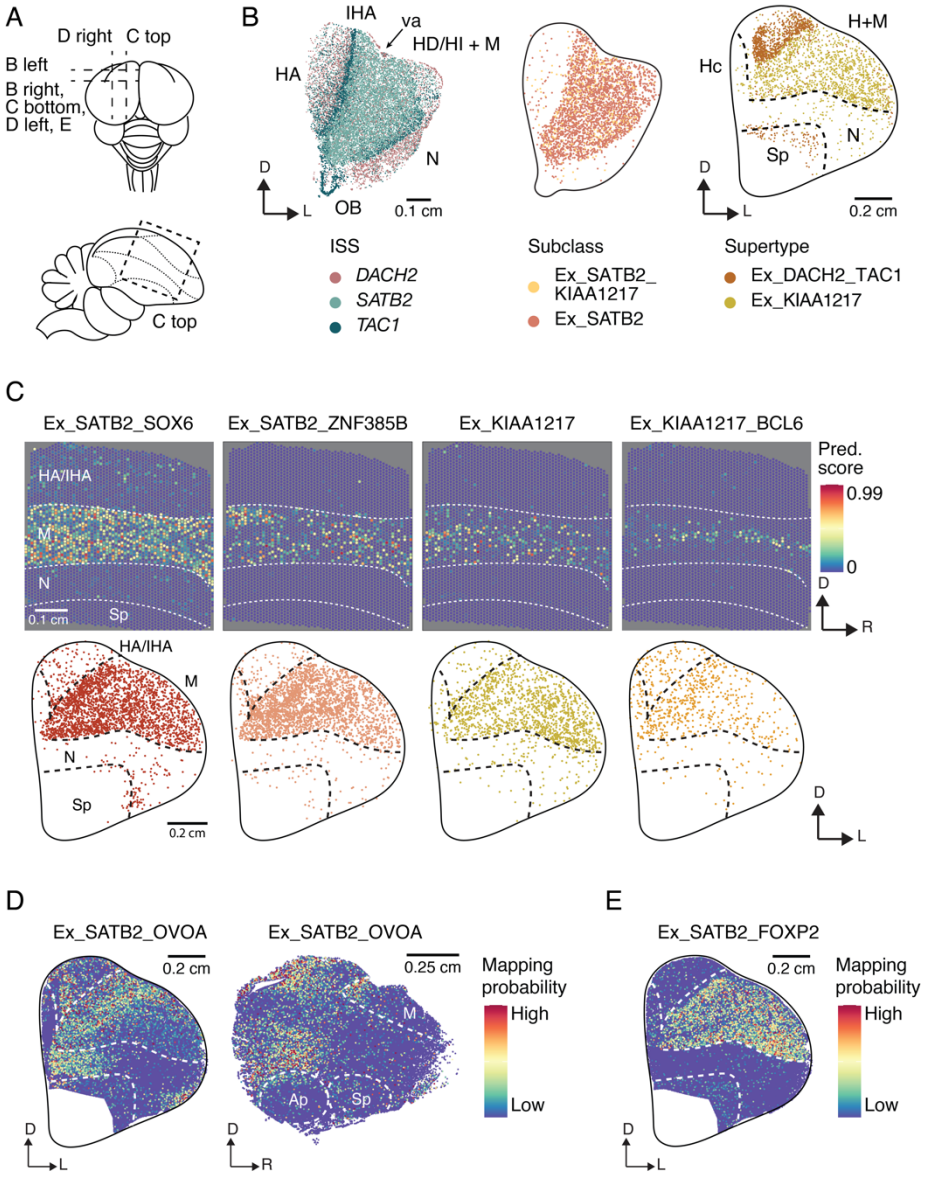

Figure 14 Cell populations in the adult avian mesopallium. (A) Schematics of the chicken brain viewed from the top (left), and a mid-sagittal section (bottom) illustrating positions of tissue sections shown in (B-E). Dashed lines represent sections, thin dotted lines represent borders between pallial brain regions. **(B)** Border between mesopallial and hyperpallial cell populations. Left: spatial expression of three representative marker genes as profiled by ISS, marking the apical hyperpallium (HA) and nidopallium (N), the interstitial apical hyperpallium (IHA), and the densocellular hyperpallium, intercalated hyperpallium, and mesopallium (HD/HI + M). Middle: area populated by mesopallial subclasses as predicted based on collective ISS profile. Right: Spatial location of a hyperpallial and a mesopallial supertype in a more posterior section according to ISS. **(C)** Spatial location of mesopallial supertypes. In Visium sections (top) high prediction (Pred.) scores indicate high probability that cells with the respective identity were present within the spot's area. In ISS sections (bottom) only segmented cells with confidently assigned identity are shown.

(D) Spatial location probabilities of supertype Ex_SATB2_OVOA according to ISS. **(E)** Spatial location probability of a mesopallial supertype according to ISS. Va, vallecula; Hc, hippocampal areas; Sp, subpallium; D, dorsal; L, lateral; R, rostral. Adapted from (*1*).

In exploring the heterogeneity within the now-extended mesopallium, I identified four supertypes within the Ex_SATB2 subclass. Three of these—Ex_SATB2_SOX6, Ex_SATB2_ZNF385B, and Ex_SATB2_FOXP2—exhibit a relatively homogeneous distribution throughout the mesopallium (Fig. 14C and E). In contrast, Ex_SATB2_OVOA appears more widely distributed across various pallial regions, although the mapping on different tissue sections remains inconclusive (Fig. 14D). Notably, while Ex_SATB2_OVOA shares specific expression of *SATB2* and lacks expression of other subclass markers, it clusters with supertypes from different subclasses in the hierarchical clustering dendrogram (Fig. 13A).

The Ex_SATB2_KIAA1217 subclass consists of two supertypes: Ex_KIAA1217 and Ex_KIAA1217_BCL6. The former also displays a relatively homogeneous distribution across the mesopallium, whereas the latter may be enriched in a specific dorsal to central region (Fig. 14C). Although the mesopallium has been proposed to contain several distinct subregions (*38*, *44*, *45*), my analysis did not reveal significant variations in cell type distribution. This suggests either a limitation in the spatial data to differentiate between similar cell types in these subclasses or that the previously observed regional heterogeneity, primarily inferred from functional studies and histological differences, may arise from factors other than distinct cell types. Evidence from the developing chicken pallium indicates a combination of both factors (see chapter 2.2.4.1)

2.2.3.2.3 Glutamatergic excitatory cell types in the adult avian hyperpallium and nidopallium

The nidopallium constitutes the ventral DVR and comprises functionally diverse regions, such as primary sensory areas, as well as highly associative areas. The avian-specific hyperpallium also consists of functionally diverse subregions (*37*, *38*, *49*). Despite their distinct topological locations in the ventral and dorsal areas of the pallium respectively, bulk tissue studies have found great gene expression similarities between these regions in adults (*37*, *48*).

In line with this observation, excitatory neurons of both, the avian nido- and hyperpallium, predominantly belong to the same two subclasses: Ex_DACH2_CALCR and Ex_DACH2_SV2C (Fig. 13A-B, Fig. S6B). The Ex_DACH2_CALCR subclass is divided into six supertypes, several of which appear to be closely linked with sensory processing due to their specific localization in regions associated with sensory input. For example, the Ex_DACH2_RORB supertype localizes to primary sensory input areas in the nidopallium (Entopallium -E, auditory Field L2 -L2, nucleus basorostralis -Bas; Fig 15A-C), while the Ex_DACH2_TAC1 and Ex_DACH2_ITGA9 supertypes are mostly concentrated within the primary sensory region of the hyperpallium (IHA; Fig 15A-D). The Ex_DACH2_CEMIP supertype primarily localizes to the intermediate nidopallium (Fig. 15B-C), which likely

represents a predominantly visual association area (*38*). The Ex_DACH2_SLIT2 supertype, though not clearly mapped to a specific location in the spatial data (not shown), appears to primarily reside in the posterior DVR based on dissection data, likely in a region not captured in the adult brain sections as results in the developing chicken pallium suggest (see chapter 2.2.4.1). Interestingly, one supertype of the Ex_DACH2_CALCR subclass, Ex_DACH2_ZMAT4, demonstrates strong signal in both the nidopallium, near primary sensory regions, and in the hyperpallium, including and surrounding the IHA (Fig. 15B-C).

The largest subclass, Ex_DACH2_SV2C, includes six supertypes, most of which demonstrate an even greater degree of regional intermixing, with cells originating from various dissected regions (Fig. S6B). Additionally, all but two small supertypes, Ex_DACH2_LHX2 and Ex_DACH2_LUZP2, which could not be reliably mapped to the tissue (not shown), exhibit a broad spatial distribution across both the nidopallium and hyperpallium (Fig. 15E). In some supertypes, such as Ex_DACH2_MGAT4C, individual clusters still predominantly originate from either the anterior dorsal or posterior ventral dissections, suggesting limited mixing at the cluster level. However, in other supertypes, including Ex_DACH2_NR4A3, Ex_DACH2_GRIK4, and Ex_DACH2_ADAMTS5, this regional mixing persists even within individual clusters. This extensive overlap of regional identities—often evident even within single clusters—highlights a striking similarity between the nidopallium and hyperpallium despite their distinct anatomical locations.

Previous studies indicate that radial migration is the predominant migratory pattern in the avian pallium, with a lack of tangential migration between the hyperpallium and nidopallium, at least before embryonic day E14 (*115*, *116*). Therefore, the observed regional overlap likely reflects shared functional roles within analogous neural circuits across these regions. Additionally, Ex_DACH2_NR4A3, a supertype within the Ex_DACH2_SV2C subclass, specifically expresses multiple activity-related genes (Fig. S6D), suggesting that the similarity between cell populations across these areas may arise not only from functional parallels but also from shared cellular states.

To further examine the remarkable transcriptome similarity between the nidopallium and hyperpallium, I performed single-nucleus multiome ATAC and RNA sequencing on samples from a second individual, dissecting the hyperpallium (including HA, IHA and HD/HI) and the DVR (covering nido- and mesopallium) separately. From these samples, I recovered high-quality nuclei for 8,119 cells, including 4,801 glutamatergic cells, which were confidently assigned to previously defined supertypes (Fig. S9). Hierarchical clustering of transcriptome pseudobulks for all excitatory supertypes in the hyper-, meso- and nidopallium, split by dissection, reveals that cells of the same supertype from different dissections always exhibit greater similarity to each other than to other cell type populations from the same dissection (Fig. 15F). This was anticipated for supertypes within the Ex_SATB2 and Ex_SATB2_KIAA1217 subclasses, given that the dissections split the continuous region of HD/HI and the mesopallium where these supertypes are

distributed (Fig. 14B). However, this clustering pattern also applies to supertypes within the Ex_DACH2_CALCR and Ex_DACH2_SV2C subclasses, despite cells from the hyperpallium and nidopallium being separated by these dissections. This suggests that mature cell type identity may outweigh potential differences in gene expression due to developmental origins in distinct areas of the pallium.

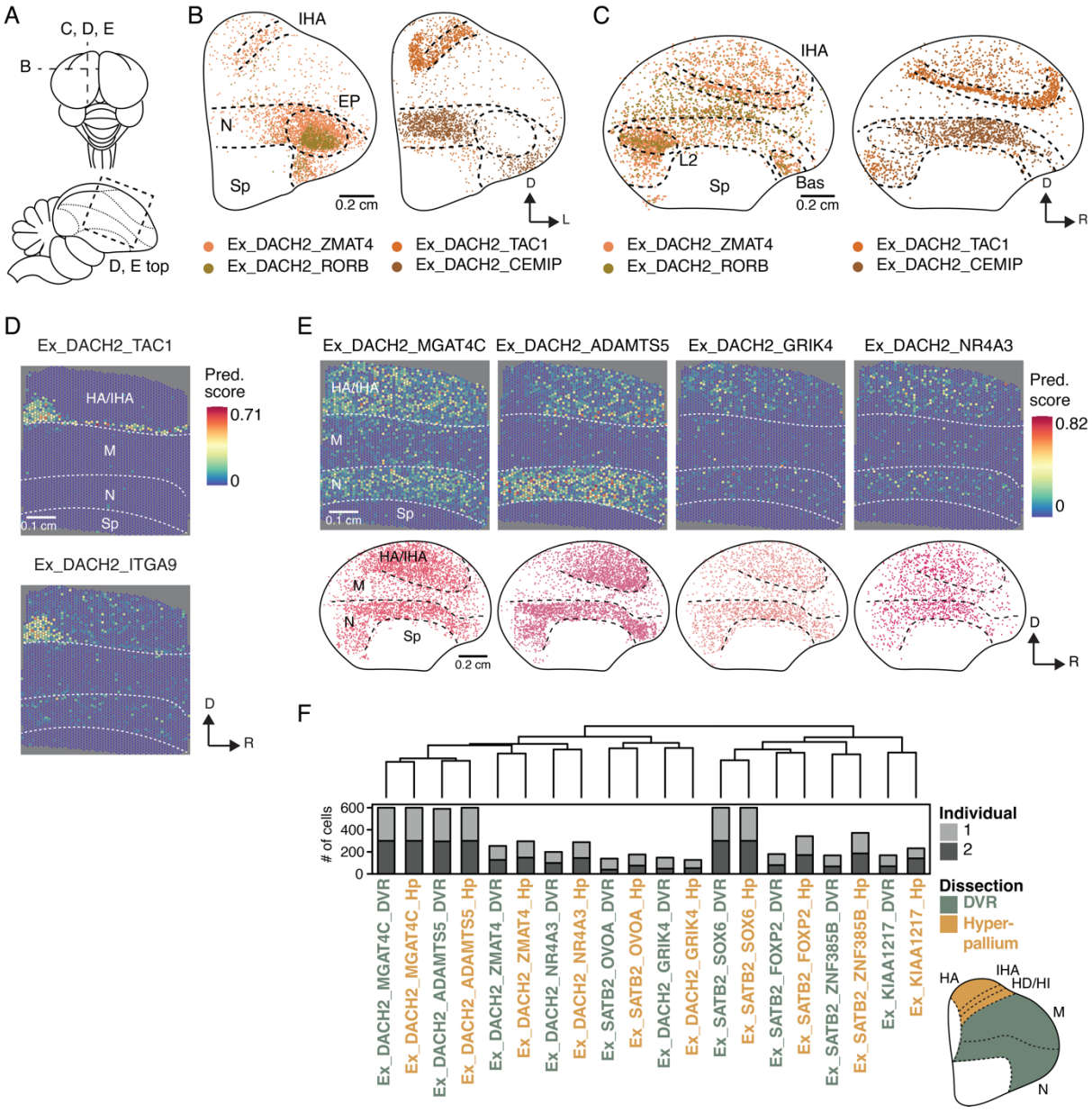

Figure 15 Cell populations in the adult avian hyperpallium and nidopallium. (A) Schematics of the chicken brain viewed from the top (left), and a mid-sagittal section (bottom) illustrating positions of tissue sections shown in (B-E). Dashed lines represent sections, thin dotted lines represent borders between pallial brain regions. **(B)** and **(C)** Spatial location of supertypes of the Ex_DACH2_CALCR subclass mostly in and around sensory input receiving areas in the hyperpallium/nidopallium based on ISS. **(D)** Spatial location of hyperpallial Ex_DACH2_CALCR supertypes according to Visium. **(E)** Spatial location of the most abundant supertypes of the EX_DACH2_SV2C subclass in the hyperpallium/nidopallium according to Visium (top) and ISS (bottom). In Visium sections (top) high prediction (Pred.) scores indicate high probability that cells with the respective identity were present within the spot's area. In ISS sections (bottom) only segmented cells with confidently assigned identity are shown. **(F)** Correlation dendrogram of pseudobulk expression profiles per supertype and dissection (at least 20 cells each). Bootstrap support (n = 1000) was above 80% for all

nodes. Schematic bottom right: illustration of borders between dissections. DVR dissections include the nido- and mesopallium, but not the arcopallium. IHA, interstitial apical hyperpallium; EP, entopallium (visual nidopallial nucleus); N, nidopallium; Sp, subpallium; L2, auditory L2 field; Bas, (somatosensory) basorostral nidopallial nucleus; D, dorsal; L, lateral; R, rostral; HA, apical hyperpallium; HD/HI, densocellular and intercalated hyperpallium; M, mesopallium. Adapted from (*1*).

To further characterize transcriptional differences between the hyperpallium and nidopallium, I investigated differentially expressed genes within shared supertypes. In the Ex_DACH2_CALCR subclass, the Ex_DACH2_ZMAT4 supertype is the only one prominently represented in both regions. Within Ex_DACH2_ZMAT4, I identified 24 genes with significant differential expression between hyperpallium and DVR dissections. Notable among these are *NR2F2*, a known nidopallium-specific transcription factor (*47*, *48*), and GABRG3, the top hyperpallium-specific gene, despite low cell numbers for Ex_DACH2_ZMAT4 in in the second individual limiting the power to detect differential gene expression. These findings suggest that with deeper sampling, cells from the hyper- or nidopallium may be differentiated reliably within this supertype. For the Ex_DACH2_SV2C subclass, supertypes from different dissections generally displayed less pronounced differential expression. Only the most abundant supertype, Ex_DACH2_MGAT4C, showed significant differential expression, with 15 DVR-specific genes identified. Even though higher cell counts were available in supertypes of the Ex_DACH2_SV2C subclass, than Ex_DACH2_ZMAT4, fewer or no differentially expressed genes were detected across most supertypes within this subclass.

To assess whether the distinct developmental origins of supertypes shared between the adult hyperpallium and nidopallium are reflected at the gene regulatory level, Dr. Ioannis Sarropoulos analysed chromatin accessibility differences between DVR- and hyperpallium-derived cells within each supertype using single-nucleus ATAC-seq data from the profiled individual. This analysis did not reveal any robust differences, though it may be limited by low cell numbers and the absence of an snATAC-seq replicate. Pseudobulk correlation analysis across regions confirmed that supertypes shared between dissections generally displayed higher similarity to each other than to other supertypes from the same dissection (Fig. S9). While he identified 12,595 differentially accessible regions across all cell types, and 3,932 across excitatory neuron supertypes (at FDR <5%), no significant differentially accessible regions were found between corresponding supertypes from the hyperpallium and DVR dissections.

Overall, these findings indicate that the molecular profiles defining cell identity in shared supertypes across the hyperpallium and nidopallium —especially within the Ex_DACH2_SV2C subclass— display extensive similarity, with adult gene regulatory and transcriptional programs prevailing over any potential differences due to distinct developmental origins.

2.2.4 *CELL TYPES IN THE DEVELOPING AVIAN PALLIUM*

Given the substantial transcriptomic similarity observed between the hyperpallium and nidopallium at the bulk tissue level, previous studies have proposed that the cell populations in these regions share a common developmental origin (*37*, *48*). This hypothesis was further supported by *in situ* expression patterns of few selected marker genes during development (*47*). However, this interpretation contrasts with other research indicating a lack of tangential migration between the hyper- and nidopallium and the predominance of radial migration, which restricts excitatory neuronal lineages to distinct regions within the pallium (*115*, *116*).

To investigate the developing avian pallium, I generated snRNA-seq data for the chicken pallium across eight developmental stages, ranging from early/mid-neurogenesis (embryonic day 6, E6) to late in ovo development (E19). Starting from stage E8, the pallium of at least one individual was dissected into dorsal and ventral halves (by Dr. Fernando García-Moreno and Rodrigo Senovilla-Ganzo), effectively splitting the prospective mesopallium and HD/HI region along the mirror line suggested by the continuum hypothesis (Fig. 16A, Fig. 3). Each dissection was then profiled separately. This approach yielded high-quality snRNA-seq data for a total of 142,429 cells (Fig. 16B, Fig. S10). I integrated the data from all developmental stages which revealed a smooth, continuous developmental progression from early to later stages (Fig. 16D), suggesting that our sampling spans all critical phases within this developmental period, without major gaps or abrupt transcriptional shifts. I chose not to directly integrate this developmental data with adult data, as the transition to adulthood likely entails additional, unprofiled stages. Such integration may obscure the detailed developmental trajectories that emerge within the densely sampled pre-hatching period.

To annotate major cell classes, I used the expression patterns of established marker genes from eutherians (Fig. 16C and E). This analysis identified several distinct progenitor cell populations likely giving rise to specific mature cell types. For instance, ependymal progenitors (Ependymal_PCs; *ZIC5*+; (*170*)) likely differentiate into ependymal cells (*FOXJ*+; (*55*)), while pallial progenitors (Ex_PC; *PAX6*+; (*171*, *172*)) give rise to excitatory neurons (Ex_neurons), and presumptive subpallial progenitors (In_PCs; *VAX1*+; (*173*)) generate inhibitory neurons (In_neurons). The presence of proliferative inhibitory progenitor cells (*TOP2A*+; (*174*)) indicates potential partial co-dissection of the subpallium, as these progenitors typically originate in the subpallium and migrate to the pallium once post-mitotic (*175*). Alternatively, it suggests that inhibitory progenitors may also exist within the pallium, though this would require further validation.).

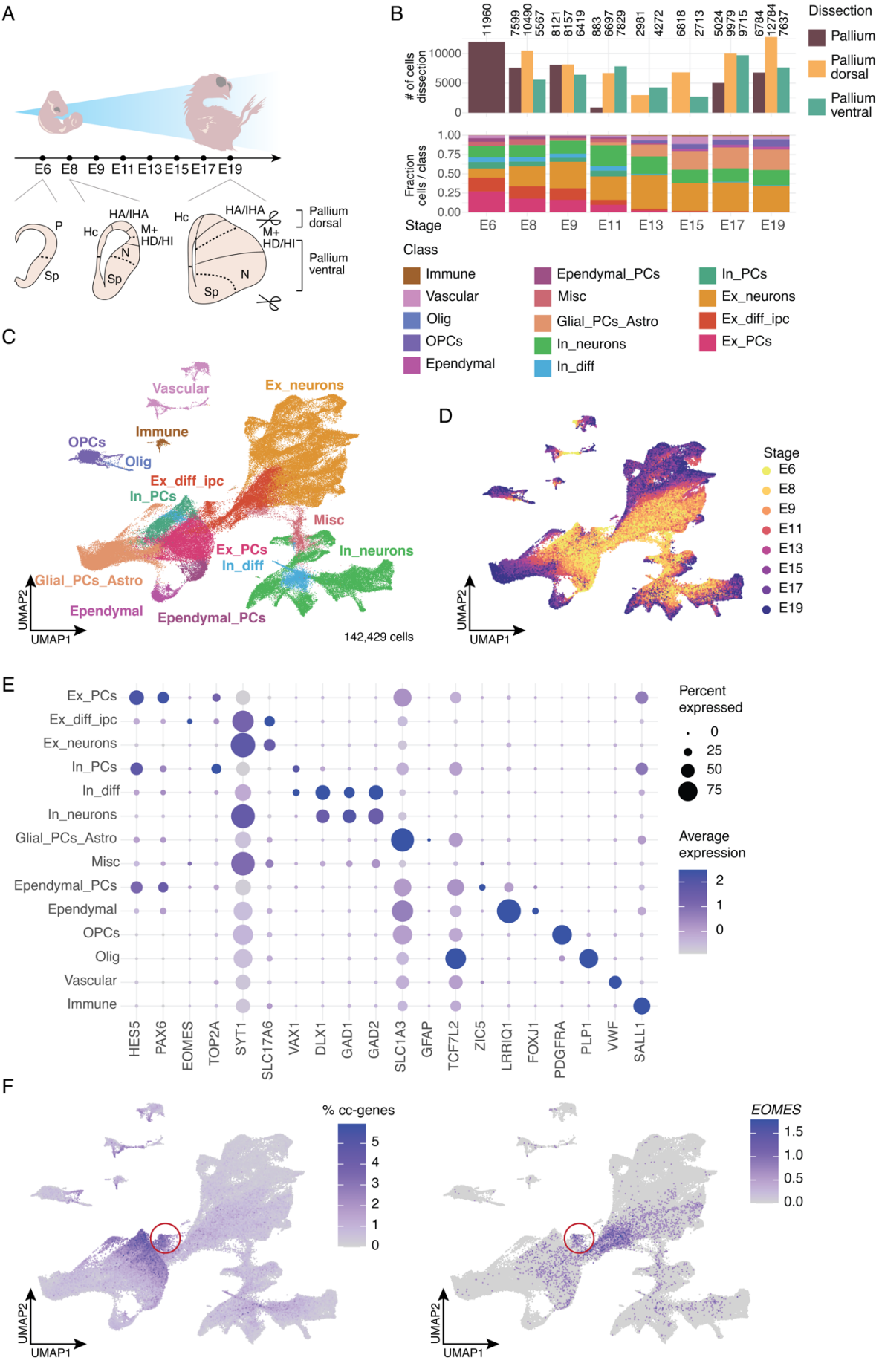
A
E6 E8 E9 E11 E13 E15 E17 E19
P
Sp
Hc
HA/IHA
M+
HD/HI
N
Pallium dorsal
Pallium ventral
B
11960 7599 10490 5567 8121 8157 6419 883 6697 7829 2981 4272 6818 2713 5024 9979 9715 6784 12784 7637
# of cells dissection
Fraction cells / class
Stage
Dissection
Pallium
Pallium dorsal
Pallium ventral
Class
Immune
Vascular
Olig
OPCs
Ependymal
Ependymal_PCs
Misc
Glial_PCs_Astro
In_neurons
In_diff
In_PCs
Ex_neurons
Ex_diff_ipc
Ex_PCs
C
142,429 cells
UMAP1
UMAP2
D
Stage
E6
E8
E9
E11
E13
E15
E17
E19
E
Percent expressed
Average expression
HES5 PAX6 EOMES TOP2A SYT1 SLC17A6 VAX1 DLX1 GAD1 GAD2 SLC1A3 GFAP TCF7L2 ZIC5 LRRIQ1 FOXJ1 PDGFRA PLP1 VWF SALL1
F
% cc-genes
EOMES

Figure 16 Cellular development of the chicken pallium. (A) Illustration of sampling strategy across pallial development in the chick. Samples were taken on eight different days of *in ovo* (E) development. At E6 the pallium (P) was collected as a whole, from E8 onwards the pallium was dissected into two halves for at least one individual per stage. **(B)** Number of cells per developmental stage and dissected region (top) and fraction of cells per developmental stage belonging to different cell populations (bottom). UMAP of pallial cells **(C)** colored by and labeled with class annotation and (**D**) colored by developmental stage. **(E)** Gene expression dotplot of selected marker genes across annotated cell classes. **(F)** UMAP of pallial cells colored by percentage of UMIs stemming from cell cycle (cc) related genes (left) and coloured by expression of *Eomes* (right). Red circle highlights population of cycling *EOMES*+ cells likely representing intermediate progenitors. P, pallium; Sp, subpallium; Hc, hippocampal areas; HA/IHA, apical and interstitial apical hyperpallium; M+HD/HI, mesopallium plus densocellular and intercalated hyperpallium; N, nidopallium; Ex_neurons, excitatory neurons; OPCs, oligodendrocyte progenitor cells; Olig, oligodendrocytes; Ex_diff_ipc, excitatory intermediate progenitors and differentiating neurons; In_PCs, inhibitory progenitors; In_diff, inhibitory differentiating neurons; In_neurons, inhibitory neurons; Glial_PCs_Astro, late radial glia and astrocytes; Ex_PCs, early radial glia (likely neurogenic); Ependymal_PCs, ependymal progenitor cells; Misc, miscellaneous. Partially adapted from (*1*).

Potential gliogenic progenitors (*HES5*+, *SLC1A3*+) could not be reliably distinguished from astrocytes (*GFAP*+), whereas oligodendrocyte progenitor cells (OPCs; *PDGFRA*+) were clearly identifiable. Notably, I observed a population of *EOMES*+ pallial progenitors, including a subset of cycling cells, suggesting the presence of intermediate progenitor cells (IPCs; Fig. 16F). IPCs are a secondary class of neural progenitors found in eutherians (*172*), and their presence in avian species has been debated (*95*). However, the relatively low proportion of cycling IPCs compared to cycling primary progenitors (Ex_PCs) indicates that, in chickens, IPCs may not proliferate to the extent observed in mammals, consistent with previous findings (*94*, *95*).

Cells expressing a mix of diverse marker genes, possibly representing varied cell types from outside the pallium, were grouped into a “miscellaneous” class.

The proportions of various cell classes across developmental stages align with previous findings. For example, the sharp decline in neural progenitor cells around E11 (Fig. 16B) supports the notion that neurogenesis in chickens is largely completed by E10 (*89*, *104*, *117*). Ependymal progenitors are detected from the earliest sampled stage, while other gliogenic progenitors, including potential astrocyte progenitors (Glial_PCs_Astro) and oligodendrocyte progenitor cells (OPCs), appear later, consistent with the suggested sequence of emergence of glial cell types in amniotes (*54*, *107*).

2.2.4.1 A cell type atlas of the developing chicken pallium at *in ovo* day 19

To further refine and validate our cell type atlas for the chicken pallium, I utilized data from the final developmental stage profiled, E19 (Fig. 17A). At this stage, populations of mature neurons show strong transcriptional similarity to the adult-defined supertypes and subclasses, as confirmed by CCA integration and label transfer (Fig. 17B). This suggests that most subclasses and supertypes observed in the adult are already present at E19. While the morphology of the brain at E19 closely resembles the adult form, the smaller

size at this stage enables broader spatial resolution. I therefore conducted spatial transcriptomic profiling on three E19 pallium sections using the Visium platform. This mapping largely corroborated our adult observations while providing enhanced resolution in some regions (Fig. 17F-K).

For instance, mesopallial supertypes at E19 displayed more distinct spatial distributions than in the adult (Fig. 17F and I, Fig. 14C), suggesting greater regional heterogeneity within the mesopallium than previously inferred or that some mesopallial cell types may disperse post-E19. The Ex_KIAA1217 supertype was localized to the putative HD/HI region, bordering the IHA, and a superficial intermediate mesopallial area, while Ex_SATB2_ZNF385B mapped to a superficial dorsal mesopallial region. Notably, Ex_SATB2_FOXP2 was found in a specific ventral mesopallial nucleus (Fig. 17F), which likely corresponds to a region involved in the visual tectofugal pathway (*45*). Additionally, Ex_SATB2_OVOA, the only Ex_SATB2 subclass supertype with spatial presence outside the mesopallium in the adult, predominantly mapped to the caudal hyperpallium at E19, with additional mapping to superficial meso- and nidopallial regions (Fig. 17I).

The E19 data also revealed additional heterogeneity within the nidopallial sensory input-receiving populations, where subtypes appear to correspond to distinct sensory inputs (Fig. 17G). This heterogeneity likely went undetected in the adult dataset due to the small relative size of these regions, resulting in fewer recovered cells of the Ex_DACH2_RORB sensory-input-receiving supertype.

Furthermore, E19 profiling revealed distinct segmentation of the hippocampus by cell type and enabled clear mapping of the Ex_CACNA1H_MCTP2 supertype to the anterior hippocampus. This supertype's position could not be determined in the adult dataset, likely due to the absence of this region in sampled sections.

Similarly, E19 data allowed for the localization of the Ex_DACH2_SLIT2 supertype, part of the predominantly sensory input-related Ex_DACH2_CALCR subclass, to a specific region in the caudal nidopallium, not clearly associated with any known functional subdivision (Fig. 17J).

Lastly, the olfactory-related Ex_BCL6 supertype mapped to a similar region as in the adult (Fig. 17K, Fig. 13G), but at E19 it appears separated from the nidopallium by the ventricle. This supports a developmental origin in the hippocampal area, aligning it more closely with *RELN*+ cells of the mammalian entorhinal cortex (retro-hippocampal areas) rather than the piriform cortex (ventral pallial areas) (*168*).

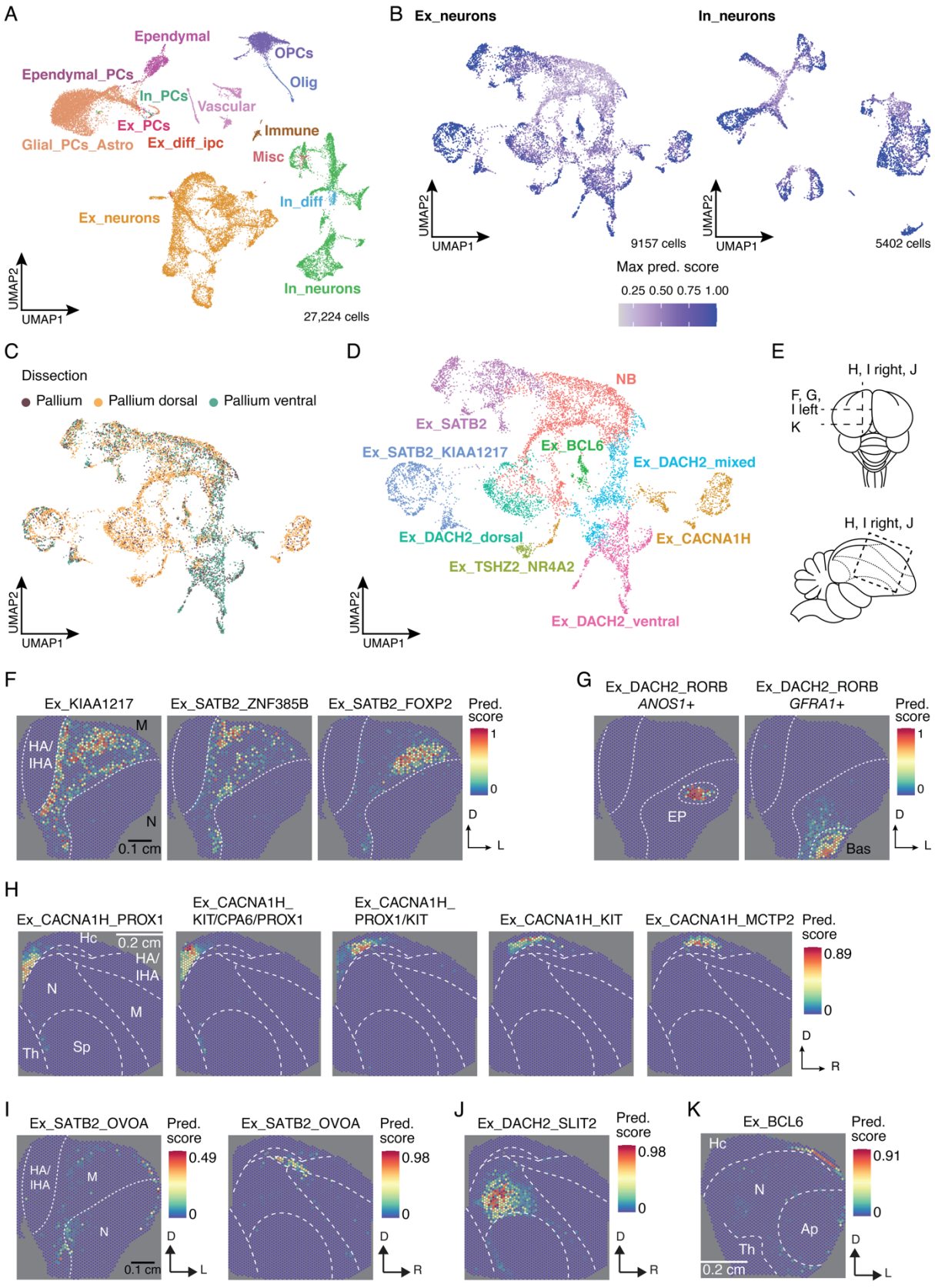

Figure 17 Cell type atlas of the developing chicken pallium at in ovo day 19. (A) UMAP of E19 snRNA-seq data coloured by cell class as annotated in complete dataset. **(B)** UMAP of excitatory neurons (left) and inhibitory neurons (right) coloured by maximum prediction score for any adult supertype after CCA label transfer. UMAP of excitatory neurons **(C)** coloured by dissection and **(D)** coloured by and labelled with annotation of broad populations roughly equivalent to adult subclasses, based on transferred supertype

labels form adult. **(E)** Schematics of the E19 chicken brain viewed from the top (top) and a mid-sagittal (bottom) section, illustrating positions of tissue sections shown in (F-K). **(F -K)** Spatial location of E19 excitatory supertypes, named after adult supertypes predicted with label transfer, according to Visium. High prediction (Pred.) scores indicate high probability that cells with the respective identity were present within the spot's area. Ex_neurons, excitatory neurons; OPCs, oligodendrocyte progenitor cells; Olig, oligodendrocytes; Ex_diff_ipc, excitatory intermediate progenitors and differentiating neurons; In_PCs, inhibitory progenitors; In_diff, inhibitory differentiating neurons; In_neurons, inhibitory neurons; Glial_PCs_Astro, late radial glia and astrocytes; Ex_PCs, early radial glia (likely neurogenic); Ependymal_PCs, ependymal progenitor cells; Misc, miscellaneous; HA/IHA, apical and interstitial apical hyperpallium; M, mesopallium; N, nidopallium; D, dorsal; L, lateral; R, rostral; EP, entopallium (visual nidopallial nucleus); Bas, (somatosensory) basorostral nidopallial nucleus; Th, Thalamus; Hc, hippocampal areas; Ap, arcopallium. Adapted from (*1*).

2.2.4.2 Developmental origins of glutamatergic excitatory avian pallial neurons

To trace the developmental origins of transcriptional similarities observed between glutamatergic populations in the adult nido- and hyperpallium (see chapter 2.2.3.2.3), I isolated cells from the glutamatergic lineage, including early and intermediate progenitors, differentiating cells, and excitatory neurons. Using pseudotime analysis (*176*, *177*), I established a continuous developmental trajectory that aligned with the integration of sampled stages (Fig 18A-C).

To approximate different developmental lineages of excitatory neurons across stages, I initially identified clusters of neurons within each developmental stage and integrated each stage sequentially with its adjacent stages to generate shared embeddings. Using a k-nearest-neighbour heuristic, as described in (*178*), I constructed and subsequently clustered a weighted graph of these cluster relationships. These analyses revealed four major clusters encompassing a large fraction of the intermediate to most mature neurons in the dataset (clusters 4-6 and 9; Fig. 18E), with significant differences to the cluster assignment generated by a standard clustering procedure (Fig. 18D). Some populations of the earliest and most mature neurons form separate clusters (Fig. 18E) likely because these are highly similar across few stages and are connected to later or previous stages with lower confidence. To integrate these largely disconnected populations into the four major groups, I identified marker genes uniquely expressed in each of the four major groups at various points along their pseudotime trajectories. Using these markers, I was able to classify the majority of the previously unassigned neuron populations into one of the four primary trajectories (Fig. 18I).

The four principal trajectories identified likely correspond to the hippocampal/arcopallial, mesopallial (encompassing cells in the mesopallium and HD/HI), hyperpallial (encompassing cells in HA and IHA), and nidopallial lineages (Fig. 18I). I annotated each trajectory based on several criteria: its stage-specific proportions of dorsal or ventral pallial dissections (Fog. 18F), characteristic marker gene expression, and label transfer results from the adult data (Fig. 18G-H), which provided insight into their potential subclass and supertype identities in the mature pallium.

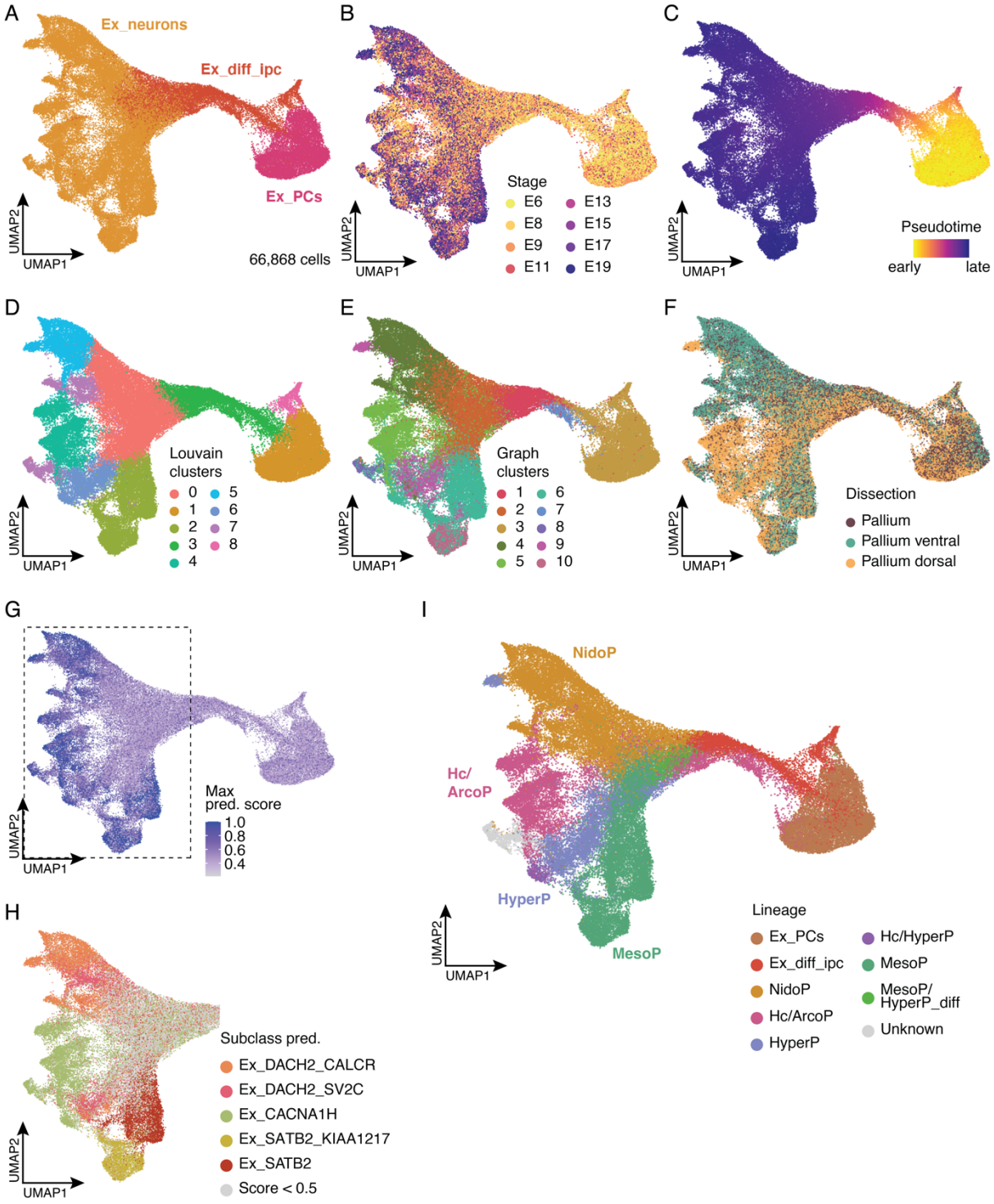

Figure 18 Development of excitatory neurons in the chicken pallium. UMAP of the excitatory neuron lineage (A) coloured by and labelled with cell class annotation, (B) coloured by developmental stage, (C) coloured by diffusion pseudotime, (D) coloured by low-resolution clusters identified based on standard clustering procedure, (E) coloured by clusters resulting from clustering of a weighted graph constructed from clustering and integration of data from individual developmental stages, (F) coloured by dissection, and (G) coloured by maximum prediction score for any adult excitatory subclass after CCA label transfer. (H) Zoom into UMAP shown in (A – G) to show only early neurons coloured by adult subclass prediction if prediction score (G) was above 0.5. (F) UMAP of excitatory neuron lineage coloured by and labelled with developmental lineage annotation. Four major early neuron lineages are labelled in the UMAP, progenitor populations or early neuron populations with ambiguous lineage identity are indicated in the legend. Ex_neurons, excitatory neurons; Ex_diff_ipc, excitatory intermediate progenitors and differentiating

neurons; Ex_PCs, early radial glia (likely neurogenic); NidoP, nidopallial lineage; Hc/ArcoP, hippocampal and arcopallial lineage; HyperP, hyperpallial lineage; MesoP, mesopallial lineage; Hc/HyperP, between hippocampal and hyperpallial lineage; MesoP/HyperP_diff, early differentiating cells of mesopallial or hyperpallial lineage. Adapted from (*1*).

Cells within the hippocampal/arcopallial lineage are characterized by specific expression of *LHX2* and are predominantly predicted to belong to the Ex_CACNA1H subclass (Fig. 19A), which maps to the hippocampus and arcopallium in the adult (Fig. 13). While most cells from this lineage originate from dorsal pallial dissections, the subset corresponding most closely to the arcopallial supertype Ex_CACNA1H_LHX9 consists of cells from ventral dissections, aligning with the arcopallium's caudoventral location in the adult pallium (Fig. 18F). The inability to clearly separate cells of these two structures, the hippocampus and the arcopallium, into distinct lineages, despite differential expression of markers such as *NRP2* and *LHX9*, highlights their similarity during development—a parallel to the transcriptional similarity observed in the adult.

The population predicted to belong to the Ex_BCL6 supertype (Fig. 19B), which is closely associated with the Ex_CACNA1H subclass in the adult, forms its own cluster in the graph clustering and stems from dorsal and ventral pallial dissections, in line with this supertype's location at the border of the hippocampal regions and the arcopallium (Fig. 17K). It also expresses both hippocampal and nidopallial markers (Fig. 19A, Fig. 21A). Due to this ambiguity, I did not assign this population to any of the four major lineages.

Similarly, the population predicted to belong to the Ex_TSHZ2_NR4A2 supertype exhibits features of the hippocampal/arcopallial lineage (Fig. 19), as well as the hyperpallial lineage (Fig. 21B) and was thus not assigned to either of those lineages. As noted before, this supertype specifically expresses the neuronal activity-related receptors *NR4A2* and *NR4A3* (*169*), but no other known activity related genes (Fig. S6D). Its presence in the embryonic pallium further argues against the notion that this population might represent a transient active cell state, since neurons only exhibit significant activity in late development (*179*). In line with this interpretation, hardly any cells in the developmental dataset were predicted to belong to the Ex_DACH2_NR4A3 supertype, which likely consists of neurons in an active state in the adult (Fig. 21D, Fig. S6D).

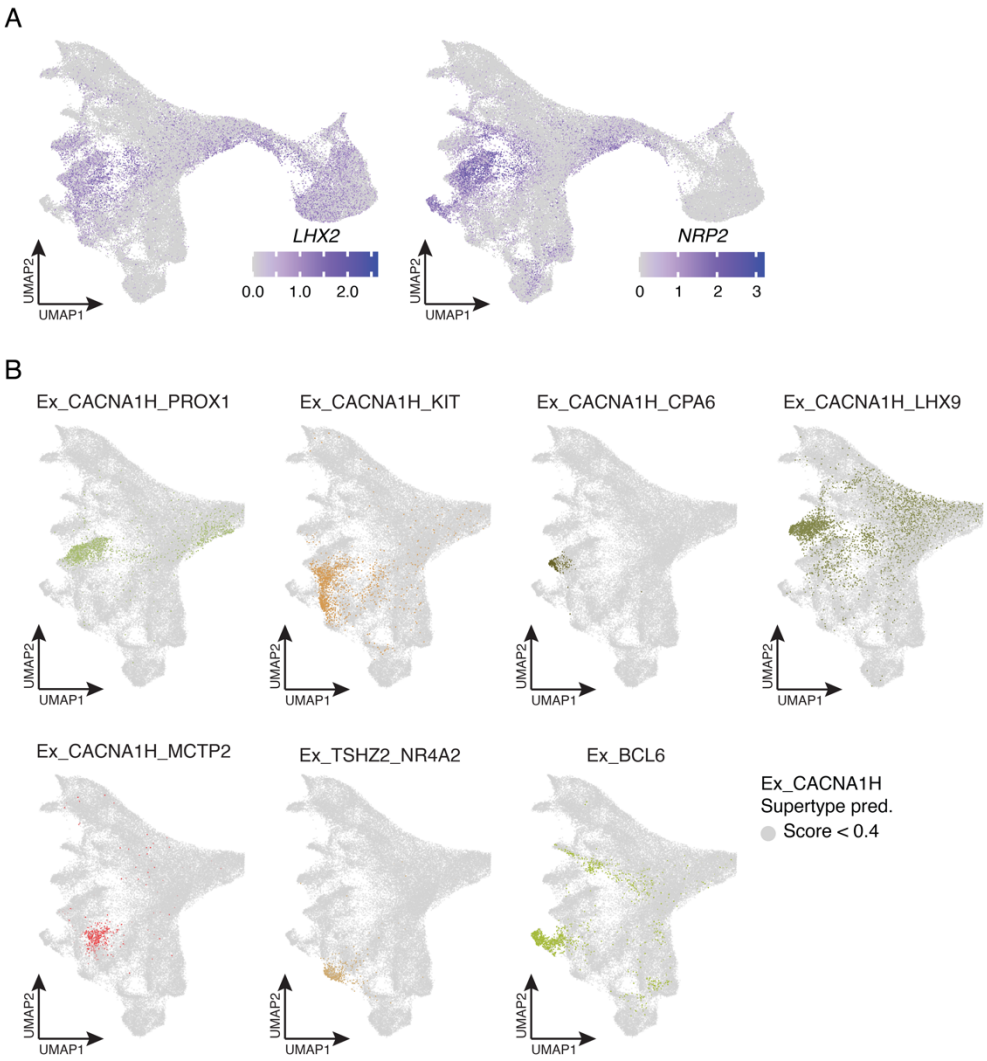

Figure 19 Development of excitatory neurons in the chicken hippocampus and arcopallium. (A) UMAP of the excitatory neuron lineage coloured by expression of selected markers of the hippocampal/arcopallial lineage. **(B)** Zoom into UMAP shown in (A) to show only early neurons coloured by prediction for adult supertypes of the adult Ex_CACNA1H subclass. Coloured cells had a prediction score of > 0.4 based on CCA label transfer. Zoomed area of UMAP is highlighted in Fig. 18G. Adapted from (*1*).

Cells in the mesopallial lineage display high expression of markers like *SATB2* and *FOXP1*, partially also expressed by cells in the hyperpallial lineage (Fig. 20A). The mesopallial lineage includes cells from both dorsal and ventral dissections in roughly equal proportions (Fig. 18F), consistent with the dissection strategy and adult observations, which indicate that parts of the prospective hyperpallium, specifically HD/HI, contain mesopallial cell types. The most mature neurons along this trajectory are predicted to belong to the Ex_SATB2 and Ex_SATB2_KIAA1217 subclasses, aligning with their adult mesopallial localization (Fig. 18H). All supertypes within these subclasses could also be identified within the developmental dataset (Fig. 20B-C).

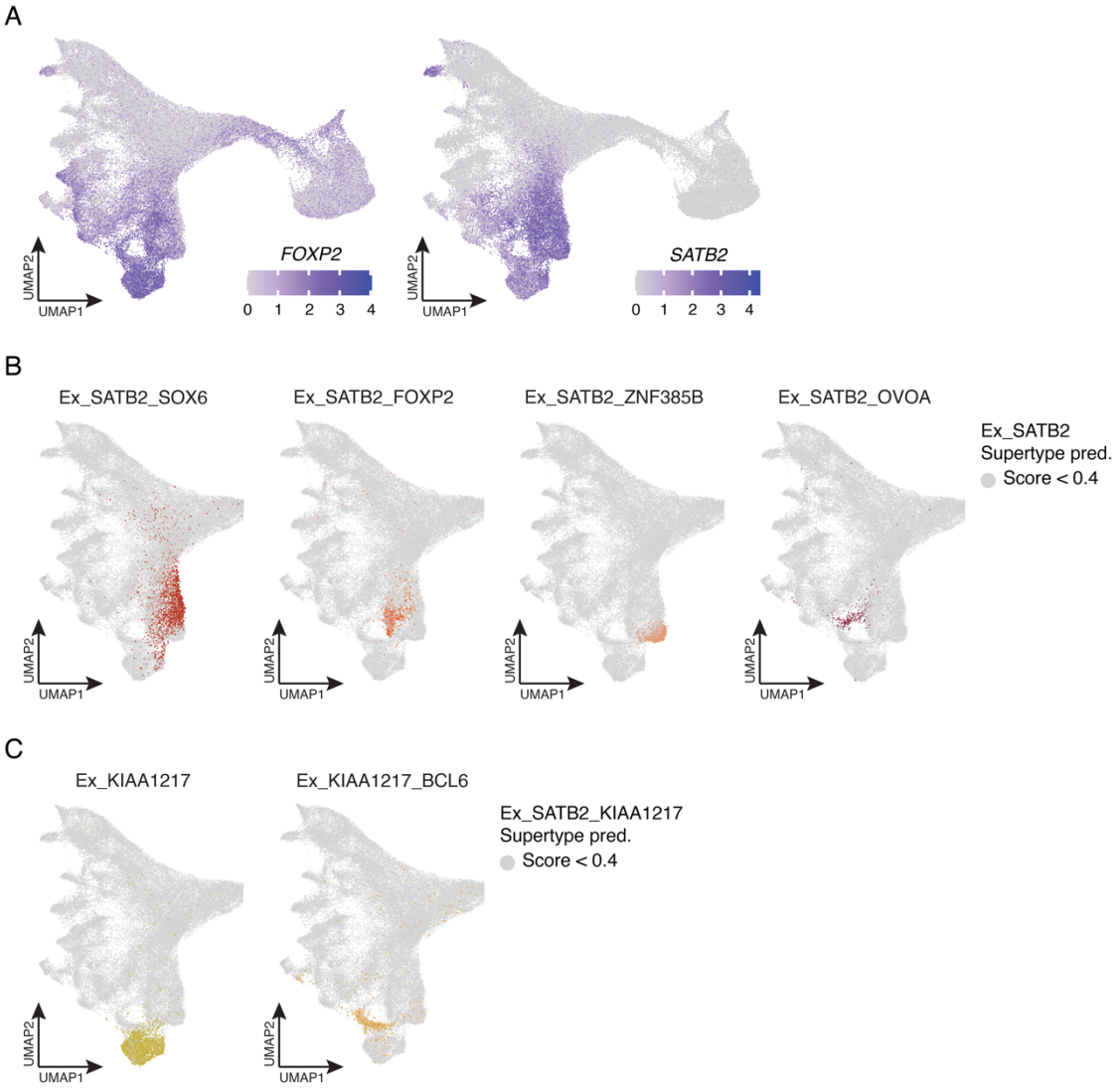

Figure 20 Development of excitatory neurons in the chicken mesopallium. (A) UMAP of the excitatory neuron lineage coloured by expression of selected markers of the mesopallial lineage. Zoom into UMAP shown in (A) to show only early neurons **(B)** coloured by prediction for adult supertypes of the adult Ex_SATB2 subclass or **(C)** for adult supertypes of the adult Ex_KIAA1217 subclass. Coloured cells had a prediction score of > 0.4 based on CCA label transfer. Zoomed area of UMAP is highlighted in Fig. 17G. Adapted from (*1*).

Cells in the hyperpallial and nidopallial lineages were predominantly assigned to two major subclasses encompassing cell types found in both the hyperpallium and nidopallium in the adult, Ex_DACH2_CALCR and Ex_DACH2_SV2C (Fig. 18H). However, unlike in the adult data, there is minimal intermixing of cells from dorsal and ventral dissections between these two lineages in development (Fig. 18F), with each lineage exhibiting differential expression of several marker genes. These include the established nidopallium-specific transcription factor *NR2F2* and a newly identified hyperpallium-specific marker, *IKZF2* (Fig. 21A-B). When I transferred adult supertype labels, cells in the nidopallial and hyperpallial lineages largely matched supertypes that are exclusive to their respective regions in the adult pallium (Fig. 21C-D). For example, the most mature neurons in the hyperpallial lineage predominantly correspond to the Ex_DACH2_TAC1 and

Ex_DACH2_ITGA9 supertypes (Fig. 21C), both localized to the IHA in adults (Fig. 15B-D). Conversely, the nidopallial lineage gave rise to cells associated with the nidopallium-specific supertypes Ex_DACH2_RORB, Ex_DACH2_CEMIP, and Ex_DACH2_SLIT2 (Fig. 21C).

The Ex_DACH2_ZMAT4 supertype, part of the mostly sensory-input-associated subclass Ex_DACH2_CALCR, which shows a mixed regional origin in adults, appeared predominantly in the nidopallial lineage but also showed limited representation within the hyperpallial lineage (Fig. 21C). Another example of partial overlap was found in the Ex_DACH2_GRIK4 supertype within the Ex_DACH2_SV2C subclass, which was distributed between both lineages (Fig. 21D). Notably, other supertypes within Ex_DACH2_SV2C that exhibit substantial mixing in the adult, such as Ex_DACH2_MGAT4C and Ex_DACH2_ADAMTS5, were only sparsely represented in the developmental dataset, despite their high abundance in adulthood (Fig. 21D). Together, these observations suggest that hyperpallial and nidopallial cells, while extensively similar in the adult, arise from distinct developmental lineages and are transcriptomically distinct until at least E19.

Despite the distinct origins of the hyper- and nidopallial cells, there are signs of emerging transcriptomic similarity in later developmental stages. A small subset of mature hyperpallial neurons, predicted to belong to the Ex_DACH2_TAC1 supertype, which localizes to the IHA in adults, is located near the nidopallial lineage on the UMAP (Fig. 21C, Fig. 18I) and clusters with mature nidopallial neurons in lower-resolution Louvain clustering (Fig. 18D). Additionally, the most mature neurons within the hyperpallial lineage begin expressing the transcription factor *DACH2*, a marker of nidopallial neurons from early developmental stages onward (Fig. 21A).

To examine how transcriptomic similarity between the hyperpallial and nidopallial lineages changes, I divided cells from each of the four major lineages into pseudotime bins and conducted a correlation analysis across developmental time. This analysis showed that while overall similarity between the hyperpallial and nidopallial lineages is lower than that observed with other lineages, it gradually increases with development (Fig. 21E). Notably, the correlation between the hyperpallial and hippocampal/arcopallial lineage is low at the earliest pseudotime points, likely reflecting the distinctiveness of early hippocampal cells compared to other lineages at this stage.

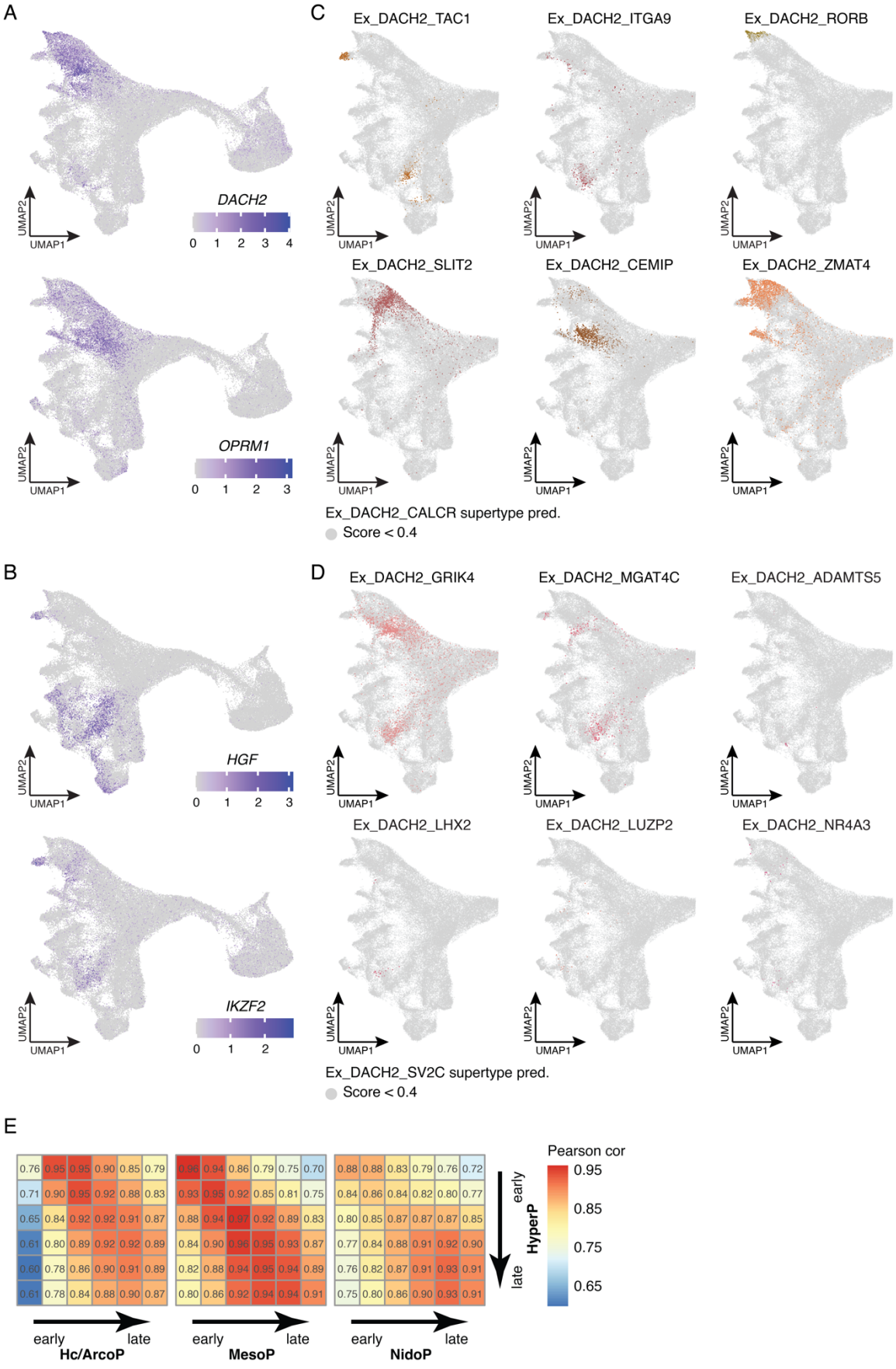

Figure 21 Development of excitatory neurons in the chicken nidoallium and hyperpallium. UMAP of the excitatory neuron lineage coloured by **(A)** expression of selected markers of the nidopallial lineage or **(B)**

expression of selected markers of the hyperpallial lineage. Zoom into UMAP shown in (A-B) to show only early neurons **(C)** coloured by prediction for adult supertypes of the adult Ex_DACH2_CALCR subclass or **(D)** for adult supertypes of the adult Ex_DACH2_SV2C subclass. Coloured cells had a prediction score of > 0.4 based on CCA label transfer. Zoomed area of UMAP is highlighted in Fig. 17G. **(E)** Heatmap of Pearson correlation between the hyperpallial and other excitatory neuron lineages. Each lineage was split into six bins according to pseudotime, each represented by one tile in the correlation heatmap. Values in tiles represent correlation values. NidoP, nidopallial trajectory; Hc/ArcoP, hippocampal and arcopallial trajectory; HyperP, hyperpallial trajectory; MesoP, mesopallial trajectory. Adapted from (*1*).

In sum, these findings suggest a gradual convergence between hyperpallial and nidopallial lineages that is still incomplete at E19. Supporting this trend, two concurrent studies by Rueda-Alaña et al. (*104*) and Hecker et al. (*180*) observed partial cell type overlaps between the hyper- and nidopallium at E15 and a pronounced similarity at post-hatch day 15, respectively. These findings suggest that the transcriptomic similarity between these lineages, which begins in late embryonic stages, continues into early post-hatch development, reaching completion by latest day 15 post-hatching.

2.2.5 COMPARISON OF NEURONS ACROSS AMNIOTES

To investigate the evolution of cell types within the amniote pallium, I conducted pairwise comparisons across representative species from different amniote lineages using three complementary methods: gene-cell type specificity index correlation (*41*), label transfer via canonical correlation analysis (*151*), and SAMap (*181*). Each method identifies cross-species cell population similarities based on distinct gene sets (either one-to-one orthologous genes or all orthologous genes) and uses unique algorithms, allowing me to mitigate the potential limitations of any single approach. Pairwise comparisons maximize the number of orthologous genes used for each species pair, while multiple pairwise analyses across different species enable independent tests of potential cell type relationships.

Observed similarities across amniote lineages can support one of two evolutionary scenarios: (1) homology, where cell types share a common ancestral origin, or (2) convergent evolution, where cell types evolve independently to perform similar functions. Homology is strongly suggested when transcriptomically similar cell types are consistently identified across mammals, birds, and non-avian reptiles, implying that these cell types may have originated from a common cell type in the last common amniote ancestor. This scenario is particularly plausible when similar cell types share similar developmental origins, despite potential functional divergence in the adult, based on the evolutionary conservation of embryonic stages. By contrast, convergence is more likely if cell type similarities are inconsistent across lineages or if these types do not share developmental origins.

2.2.5.1 Inhibitory neurons are transcriptomically conserved across amniotes

As described in the introduction, GABAergic inhibitory neurons in amniotes originate from the subpallium, a region that is more morphologically and transcriptomically conserved across species compared to the pallium (*15*, *16*, *41*, *74*, *75*). Most major inhibitory cell

types have been identified in various amniote species, strongly suggesting that these populations were already established in the last common amniote ancestor (*41*, *72*, *75*). Consistent with this hypothesis, I observed that nearly all adult chicken inhibitory supertypes exhibit strong correspondences to adult murine and lizard GABAergic populations, with high similarity scores and agreement across all three comparative methods (Fig. 22, Fig. S11). Additionally, the comparison of chicken supertypes with mouse subclasses of known developmental origin supports previous hypotheses that chicken supertypes arise from distinct ganglionic eminences, as indicated by their marker gene expression. Although some chicken inhibitory supertypes correspond to multiple murine inhibitory subclasses, this relationship largely reverses when comparing datasets at finer resolution, suggesting that these patterns are primarily due to differences in annotation resolution rather than reflecting evolutionary diversification of these cell types.

The only chicken supertype that shows limited similarity to murine populations is an MGE-derived ST18+ supertype (Inh_MGE_like_ST18; Fig. 22A), which could not be reliably located within the tissue. This observation may indicate that the supertype represents a specific inhibitory cell state rather than a distinct cell type, although it closely resembles a lizard inhibitory cluster (Inh_10), which in turn shows high similarity to the murine Pvalb population.

In line with marker gene expression, the LGE-derived supertypes Inh_LGE_like_FOXP1_SGCG and Inh_LGE_like_FOXP1_DGKH include clusters that align with either the murine striatal medium spiny neuron D1 or D2 type, also consistent with this supertype's spatial mapping to the chicken striatum (Fig. S12). However, Inh_LGE_like_FOXP1_DGKH also contains two clusters best matching cells of the murine central amygdala-like nucleus (Fig. S12), in line with its presence in the chicken arcopallium, which has been suggested to be homologous to the mammalian amygdala (*128*, *133*). Notably, the widespread Inh_LGE_like_FOXP2 supertype closely resembles cells of the murine intercalated amygdala nucleus, as already indicated by shared transcription factor markers (Fig. 12). Consistently, both populations also best match a GABAergic population in the lizard (Fig. 22B, Fig. S13), likely located in a restricted amygdala-like region (*41*). However, I found no indication of Inh_LGE_like_FOXP2 enrichment in any particular region of the chicken pallium (Fig. 12F).

These findings highlight that while inhibitory neurons have retained highly conserved transcriptomic identities across all major amniote lineages, their spatial organization and relative abundance have diversified throughout evolution.

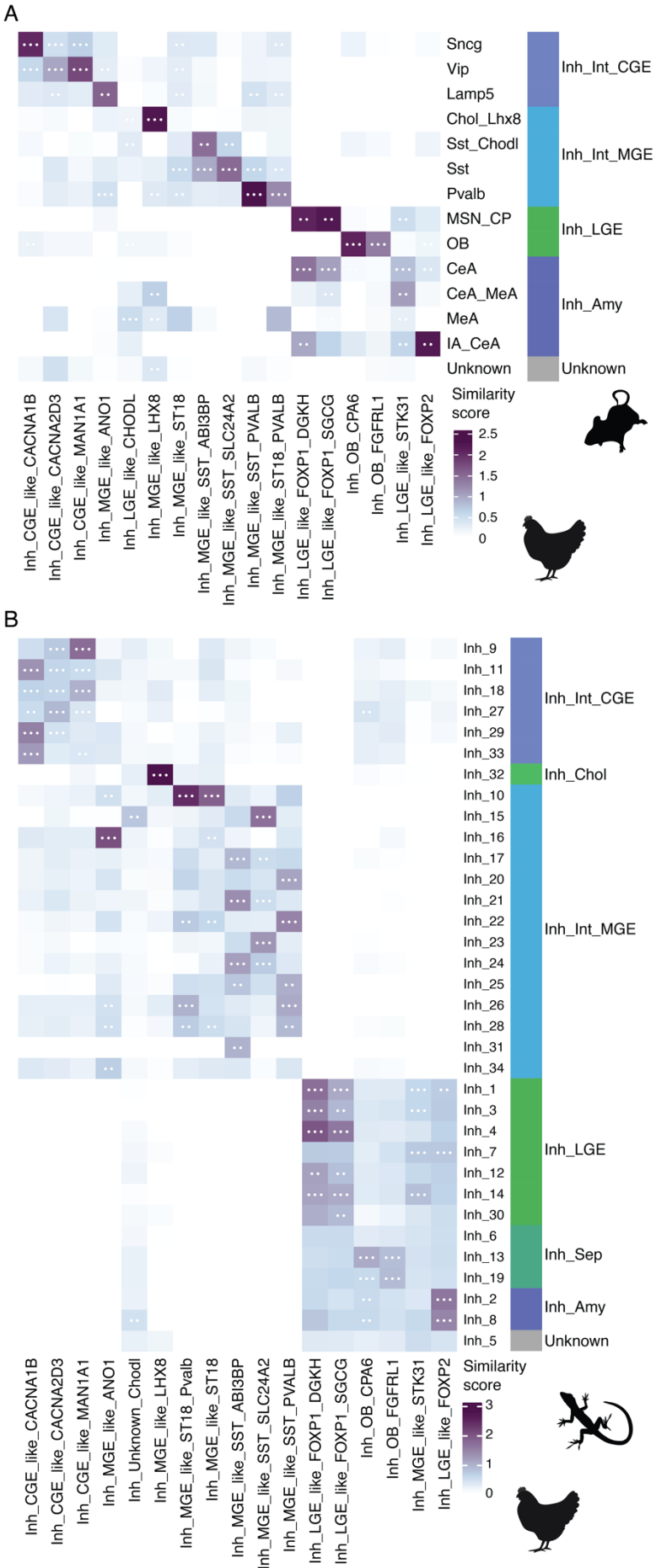
A
Sncg
Vip
Lamp5
Chol_Lhx8
Sst_Chodl
Sst
Pvalb
MSN_CP
OB
CeA
CeA_MeA
MeA
IA_CeA
Unknown
Inh_Int_CGE
Inh_Int_MGE
Inh_LGE
Inh_Amy
Unknown
Inh_CGE_like_CACNA1B
Inh_CGE_like_CACNA2D3
Inh_CGE_like_MAN1A1
Inh_MGE_like_ANO1
Inh_LGE_like_CHODL
Inh_MGE_like_LHX8
Inh_MGE_like_ST18
Inh_MGE_like_SST_ABI3BP
Inh_MGE_like_SST_SLC24A2
Inh_MGE_like_SST_PVALB
Inh_MGE_like_ST18_PVALB
Inh_LGE_like_FOXP1_DGKH
Inh_LGE_like_FOXP1_SGCG
Inh_OB_CPA6
Inh_OB_FGFRL1
Inh_LGE_like_STK31
Inh_LGE_like_FOXP2
Similarity score
2.5
2
1.5
1
0.5
0
B
Inh_9
Inh_11
Inh_18
Inh_27
Inh_29
Inh_33
Inh_32
Inh_10
Inh_15
Inh_16
Inh_17
Inh_20
Inh_21
Inh_22
Inh_23
Inh_24
Inh_25
Inh_26
Inh_28
Inh_31
Inh_34
Inh_1
Inh_3
Inh_4
Inh_7
Inh_12
Inh_14
Inh_30
Inh_6
Inh_13
Inh_19
Inh_2
Inh_8
Inh_5
Inh_Int_CGE
Inh_Chol
Inh_Int_MGE
Inh_LGE
Inh_Sep
Inh_Amy
Unknown
Inh_CGE_like_CACNA1B
Inh_CGE_like_CACNA2D3
Inh_CGE_like_MAN1A1
Inh_MGE_like_ANO1
Inh_Unknown_Chodl
Inh_MGE_like_LHX8
Inh_MGE_like_ST18_Pvalb
Inh_MGE_like_ST18
Inh_MGE_like_SST_ABI3BP
Inh_MGE_like_SST_SLC24A2
Inh_MGE_like_SST_PVALB
Inh_LGE_like_FOXP1_DGKH
Inh_LGE_like_FOXP1_SGCG
Inh_OB_CPA6
Inh_OB_FGFRL1
Inh_MGE_like_STK31
Inh_LGE_like_FOXP2
Similarity score
3
2
1
0

Figure 22 Comparison of adult GABAergic inhibiotry neurons across amniotes. (A) Comparison between chicken supertypes and mouse inhibitory subclasses based on three different methods. **(B)** Comparison between chicken supertypes and lizard inhibitory clusters based on three different methods. Scores were scaled between 0 and 1 per method and summed across all methods to represent the similarity score. White dots in tiles are shown when populations are among the top reciprocal matches according to two or all three methods. Coloured bar on the right represents broader annotation. Chol, cholinergic; Amy, amygdala; MSN, medium spiny neurons; CP, caudate putamen; OB, olfactory bulbs; CeA, central amygdala; MeA, medial amygdala; IA, intercalated amygdala; Sep, septum. Adapted from (*1*).

2.2.5.2 Comparison of excitatory neurons across amniotes

Compared to GABAergic inhibitory neurons in the subpallium, glutamatergic excitatory neurons in the pallium are thought to have diverged more extensively during amniote evolution. While cell type similarities among inhibitory neurons likely indicate homology, similarities among excitatory neurons are often attributed to convergent evolution based on analyses using transcription factors versus effector genes (*41*, *75*, *134*). Therefore, multiple comparative methods, multiple species, and developmental context are essential for distinguishing homology from convergence.

2.2.5.2.1 Comparison of adult excitatory neurons across amniotes

2.2.5.2.1.1 Avian hippocampal and arcopallial neurons correspond to mammalian hippocampal and amygdalar neurons

Consistent with the greater conservation of inhibitory neurons, I found that similarity scores between murine and chicken excitatory neurons are generally lower than those of inhibitory neurons in comparisons across all neuronal supertypes (Fig. S14). Even within the subset of excitatory neurons, numerous chicken supertypes lack clear murine counterparts, only few display one-to-one correspondence (Fig. 23), and different methods do not always agree (Fig. S15). To avoid confounding effects, immature neuron populations were excluded from these analyses, as their inclusion would introduce developmental variation that could obscure evolutionary signals.

One of the strongest cross-species similarities among excitatory neurons in my data is observed between Ex_CACNA1H_PROX1 in chickens and neurons in the murine dentate gyrus (DG) of the hippocampus (Fig. 23A, Fig. S15A), aligning with their comparable medial pallial localization. Consistently, both populations also correspond to clusters in the lizard medial cortex (Fig. 24, Fig. 25, Fig. S17, Fig. S18). The closely related supertype, Ex_CACNA1H_CPA6, best matches murine CA3 neurons (Fig. 23) and lizard dorso-medial cortex clusters (Fig.24), strongly suggesting that the DG and CA3 subfields, along with their characteristic cell types, are conserved across amniotes. The comparison to an external mouse dataset (Fig. 23B) reveals similar correspondences, however murine DG neurons are not represented as a separate population in this dataset.

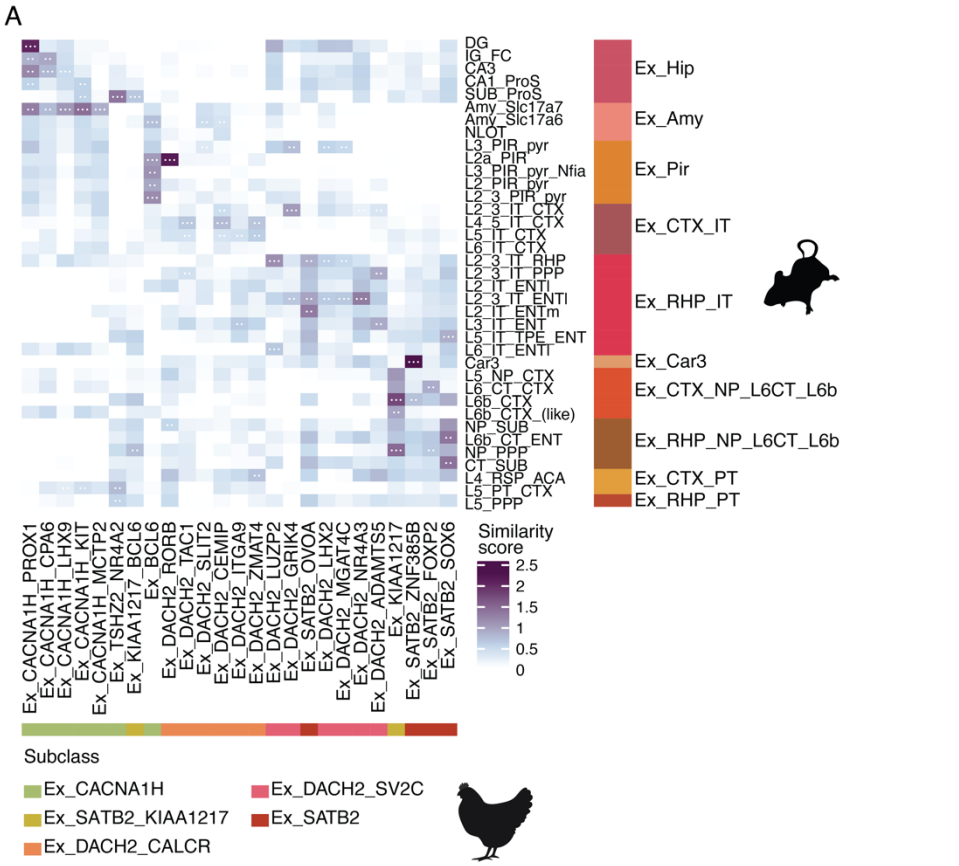
A
DG
IG_FC
CA3
CA1_ProS
SUB_ProS
Amy_Slc17a7
Amy_Slc17a6
NLOT
L3_PIR_pyr
L2a_PIR
L3_PIR_pyr_Nfia
L2_PIR_pyr
L2_3_PIR_pyr
L2_3_IT_CTX
L4_5_IT_CTX
L5_IT_CTX
L6_IT_CTX
L2_3_IT_RHP
L2_3_IT_PPP
L2_IT_ENTl
L2_3_IT_ENTl
L2_IT_ENTm
L3_IT_ENT
L5_IT_TPE_ENT
L6_IT_ENTl
Car3
L5_NP_CTX
L6_CT_CTX
L6b_CTX
L6b_CTX_(like)
NP_SUB
L6b_CT_ENT
NP_PPP
CT_SUB
L4_RSP_ACA
L5_PT_CTX
L5_PPP
Ex_Hip
Ex_Amy
Ex_Pir
Ex_CTX_IT
Ex_RHP_IT
Ex_Car3
Ex_CTX_NP_L6CT_L6b
Ex_RHP_NP_L6CT_L6b
Ex_CTX_PT
Ex_RHP_PT
Ex_CACNA1H_PROX1
Ex_CACNA1H_CPA6
Ex_CACNA1H_LHX9
Ex_CACNA1H_KIT
Ex_CACNA1H_MCTP2
Ex_TSHZ2_NR4A2
Ex_KIAA1217_BCL6
Ex_BCL6
Ex_DACH2_RORB
Ex_DACH2_TAC1
Ex_DACH2_SLIT2
Ex_DACH2_CEMIP
Ex_DACH2_ITGA9
Ex_DACH2_ZMAT4
Ex_DACH2_LUZP2
Ex_DACH2_GRIK4
Ex_SATB2_OVOA
Ex_DACH2_LHX2
Ex_DACH2_MGAT4C
Ex_DACH2_NR4A3
Ex_DACH2_ADAMTS5
Ex_KIAA1217
Ex_SATB2_ZNF385B
Ex_SATB2_FOXP2
Ex_SATB2_SOX6
Similarity score
2.5
2
1.5
1
0.5
0
Subclass
Ex_CACNA1H
Ex_SATB2_KIAA1217
Ex_DACH2_CALCR
Ex_DACH2_SV2C
Ex_SATB2

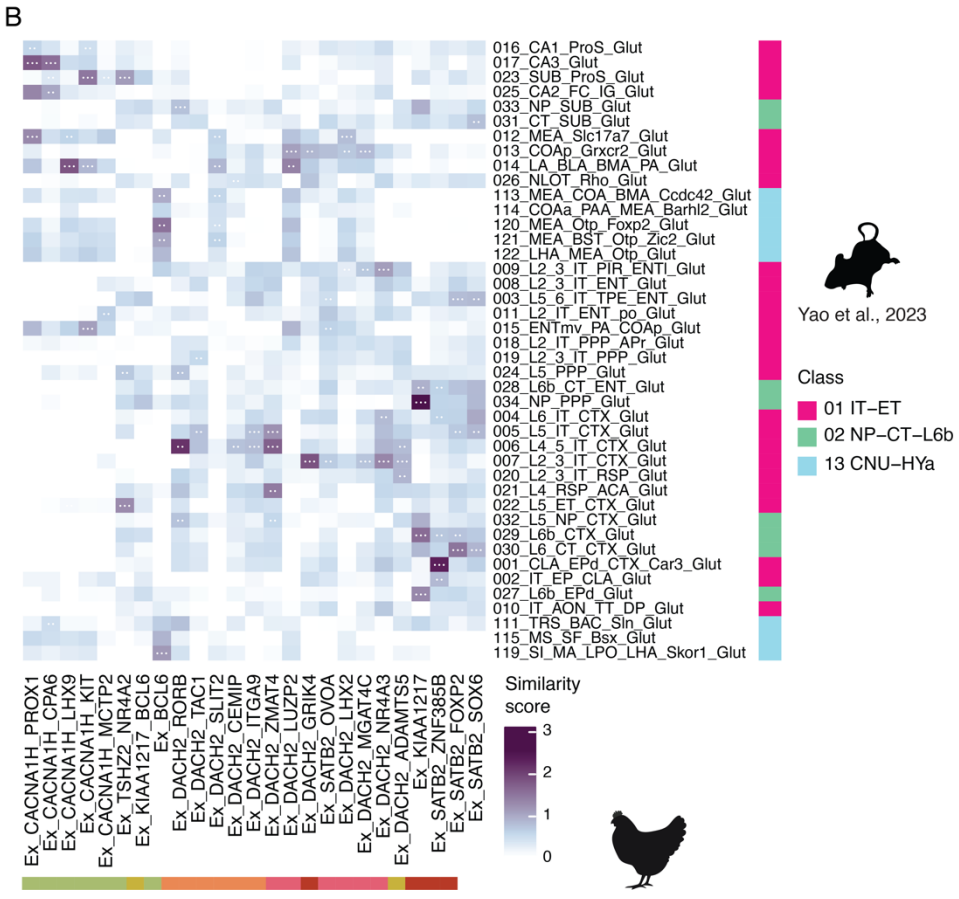
B
016_CA1_ProS_Glut
017_CA3_Glut
023_SUB_ProS_Glut
025_CA2_FC_IG_Glut
033_NP_SUB_Glut
031_CT_SUB_Glut
012_MEA_Slc17a7_Glut
013_COAp_Grxcr2_Glut
014_LA_BLA_BMA_PA_Glut
026_NLOT_Rho_Glut
113_MEA_COA_BMA_Ccdc42_Glut
114_COAa_PAA_MEA_Barhl2_Glut
120_MEA_Otp_Foxp2_Glut
121_MEA_BST_Otp_Zic2_Glut
122_LHA_MEA_Otp_Glut
009_L2_3_IT_PIR_ENTl_Glut
008_L2_3_IT_ENT_Glut
003_L5_6_IT_TPE_ENT_Glut
011_L2_IT_ENT_po_Glut
015_ENTmv_PA_COAp_Glut
018_L2_IT_PPP_APr_Glut
019_L2_3_IT_PPP_Glut
024_L5_PPP_Glut
028_L6b_CT_ENT_Glut
034_NP_PPP_Glut
004_L6_IT_CTX_Glut
005_L5_IT_CTX_Glut
006_L4_5_IT_CTX_Glut
007_L2_3_IT_CTX_Glut
020_L2_3_IT_RSP_Glut
021_L4_RSP_ACA_Glut
022_L5_ET_CTX_Glut
032_L5_NP_CTX_Glut
029_L6b_CTX_Glut
030_L6_CT_CTX_Glut
001_CLA_EPd_CTX_Car3_Glut
002_IT_EP_CLA_Glut
027_L6b_EPd_Glut
010_IT_AON_TT_DP_Glut
111_TRS_BAC_Sln_Glut
115_MS_SF_Bsx_Glut
119_SI_MA_LPO_LHA_Skor1_Glut
Yao et al., 2023
Class
01 IT–ET
02 NP–CT–L6b
13 CNU–HYa
Ex_CACNA1H_PROX1
Ex_CACNA1H_CPA6
Ex_CACNA1H_LHX9
Ex_CACNA1H_KIT
Ex_CACNA1H_MCTP2
Ex_TSHZ2_NR4A2
Ex_KIAA1217_BCL6
Ex_BCL6
Ex_DACH2_RORB
Ex_DACH2_TAC1
Ex_DACH2_SLIT2
Ex_DACH2_CEMIP
Ex_DACH2_ITGA9
Ex_DACH2_ZMAT4
Ex_DACH2_LUZP2
Ex_DACH2_GRIK4
Ex_SATB2_OVOA
Ex_DACH2_LHX2
Ex_DACH2_MGAT4C
Ex_DACH2_NR4A3
Ex_DACH2_ADAMTS5
Ex_KIAA1217
Ex_SATB2_ZNF385B
Ex_SATB2_FOXP2
Ex_SATB2_SOX6
Similarity score
3
2
1
0

Figure 23 Comparison of adult glutamatergic excitatory neurons between chicken and mouse. (A) Comparison between chicken supertypes and murine excitatory subclasses from this study (presented in chapter "Cell type atlas of the adult murine pallium") based on three different methods. Coloured bar on the right represents broader annotation. **(B)** Comparison of excitatory supertypes in the chicken pallium to mouse excitatory subclasses from (*76*) based on three methods. Scores were scaled between 0 and 1 per method and summed across all methods to represent the similarity score. White dots in tiles are shown when populations are among the top reciprocal matches according to two or all three methods. For cell population abbreviations in mouse see List of abbreviations. Adapted from (*1*).

The extent to which other chicken hippocampal supertypes correspond to known mammalian hippocampal subfields and cell types is less certain. Ex_CACNA1H_KIT shows some resemblance to murine CA1 neurons (Fig. 23A) and retrohippocampal cell types (Fig. 23B), consistent with its hippocampal localization, but aligns most closely with Slc17a7+ populations in the murine amygdala (Fig. 23A). In lizard, Ex_CACNA1H_KIT matches neurons in the dorsal cortex, which, in turn, correspond to murine CA1 neurons as well as to cells in retro-hippocampal regions like the subiculum and entorhinal cortex. These varied alignments, along with the relatively low numbers of Ex_CACNA1H neurons, suggest that further sampling of the chicken hippocampal areas could reveal additional heterogeneity and potentially uncover other hippocampal subfields

The Ex_CACNA1H_LHX9 supertype, located in the chicken arcopallium, closely resembles neurons in both the murine and lizard amygdala (Fig. 23A, 24). Comparisons with an external mouse dataset confirm its similarity to populations in the lateral, basolateral, basomedial, and posterior amygdalar nuclei (Fig. 23B), supporting previous findings that suggest homology between certain arcopallial and amygdalar populations across amniotes (*41*, *75*). These observations also align with the hypothesis that the arcopallium and amygdala share a developmental origin in the ventral-caudal regions of the pallium, suggesting they could be field-homologous (*128*). However, these structures differ significantly in anatomy and function: in birds, the arcopallium serves as the principal output structure of the pallium (*37*, *38*), while in mammals, this function is primarily carried out by layer 5 pyramidal tract (L5 PT) neurons in the isocortex (*182*). The observed transcriptomic similarity between Ex_CACNA1H_LHX9 and L5 PT neurons suggests that Ex_CACNA1H_LHX9 likely represents the primary output neurons within the arcopallium, reflecting a degree of functional convergence with L5 PT neurons as output populations in the pallial circuits of birds and mammals, respectively.

The Ex_TSHZ2_NR4A2 supertype, which shares some marker gene expression with Ex_CACNA1H supertypes and is sparsely distributed in the HA, exhibits a strong transcriptomic similarity to the murine subiculum and limited similarity to extratelencephalic-projecting neurons in the isocortex and retrohippocampal regions (L5_PT_CTX, L5_PPP, L5_ET_CTX; Fig. 23). Given that the subiculum is the primary output structure of the hippocampus (*183*), these findings suggest that Ex_TSHZ2_NR4A2 corresponds to the outward-projecting neurons of the hyperpallium, known to be located within the HA (*38*, *49*). Consistently, comparisons to the lizard indicate a close alignment

of Ex_TSHZ2_NR4A2 with clusters in the posterior dorsal cortex (Fig. 24, Fig. S17), which in turn correspond to the mammalian subiculum (Fig. 25, Fig. S18). Together, these observations suggest that this hyperpallial subregion may share greater similarity with the mammalian retrohippocampal area than with the isocortex, despite development-based homology hypotheses proposing a field-homology between the entire hyperpallium and the isocortex (Fig. 4A) (*128*, *133*).

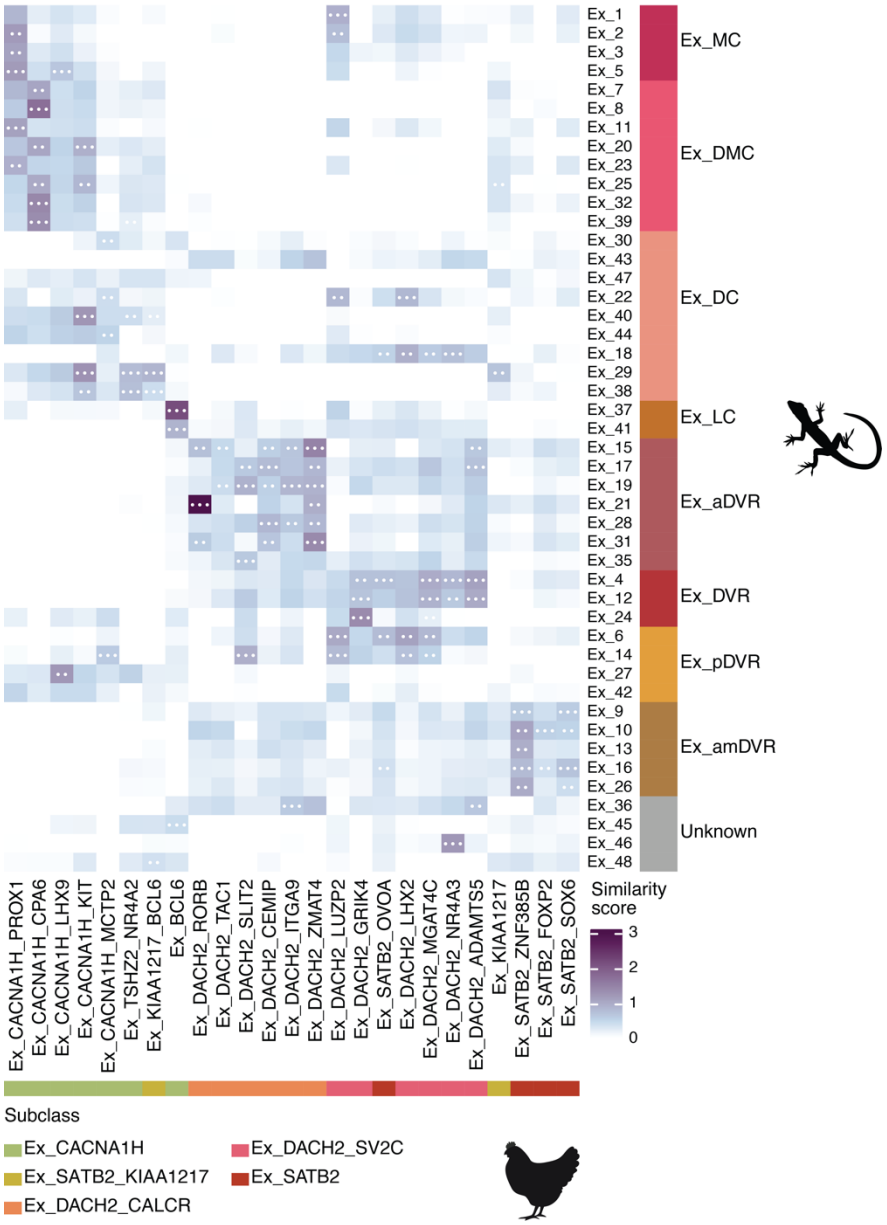

Figure 24 Comparison of adult glutamatergic excitatory neurons between chicken and lizard. Comparison between chicken supertypes and lizard excitatory clusters based on three different methods. Coloured bar on the right represents broader reginal annotation as presented in chapter "Cell type atlas of the adult lizard pallium". Scores were scaled between 0 and 1 per method and summed across all methods to represent the similarity score. White dots in tiles are shown when populations are among the top reciprocal matches according to two or all three methods. MC, medial cortex; DMC, dorso-medial cortex; DC, dorsal cortex; LC, lateral cortex; aDVR, anterior DVR; pDVR, posterior DVR; amDVR, anterior medial DVR. Adapted from (*1*).

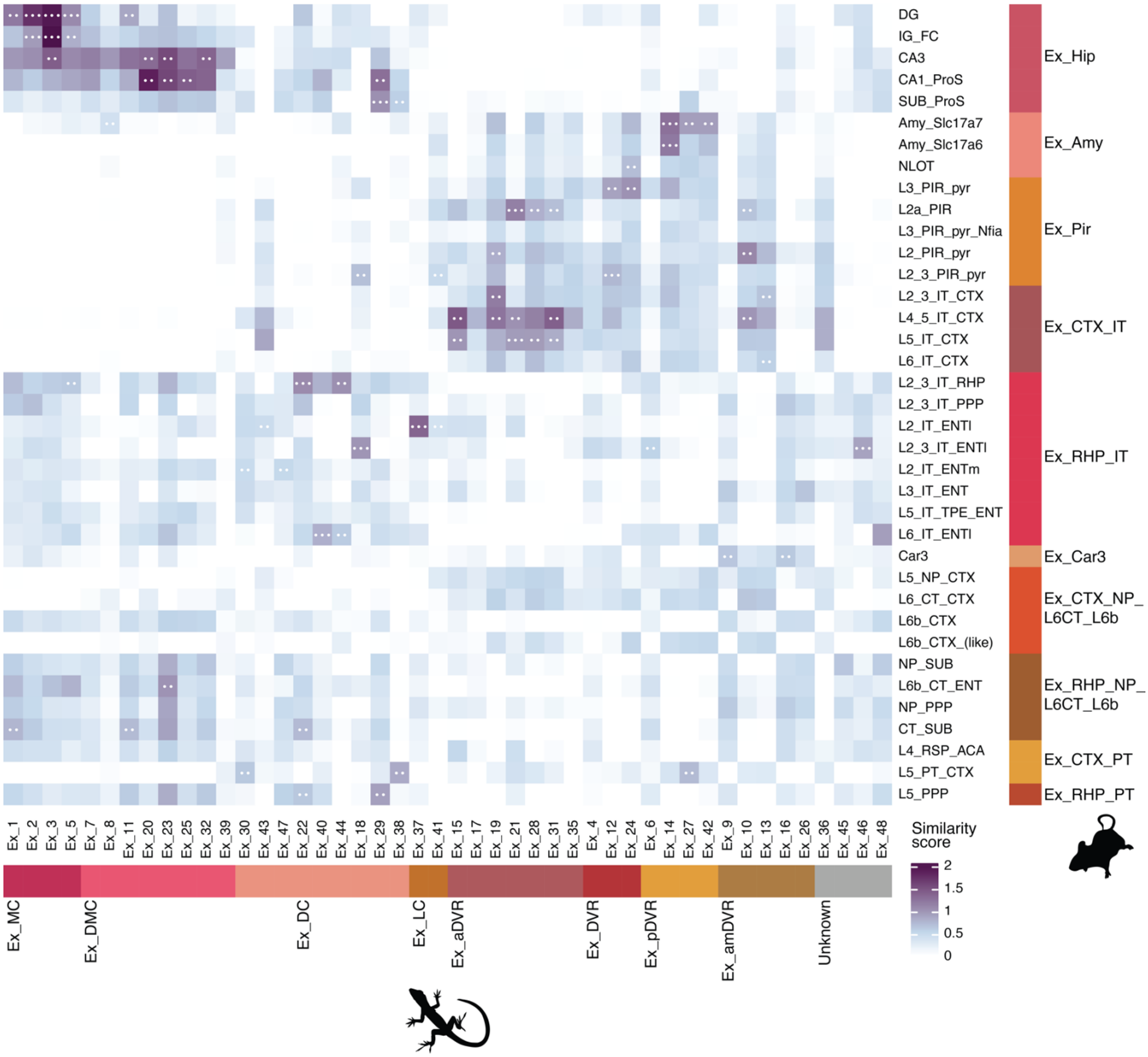

Figure 25 Comparison of adult glutamatergic excitatory neurons between mouse and lizard. Comparison between murine excitatory subclasses from this study and lizard excitatory clusters based on three different methods. Coloured bars represent broader annotations as presented in chapters "Cell type atlas of the murine pallium" and "Cell type atlas of the adult lizard pallium". Scores were scaled between 0 and 1 per method and summed across all methods to represent the similarity score. White dots in tiles are shown when populations are among the top reciprocal matches according to two or all three methods. MC, medial cortex; DMC, dorso-medial cortex; DC, dorsal cortex; LC, lateral cortex; aDVR, anterior DVR; pDVR, posterior DVR; amDVR, anterior medial DVR. For cell population abbreviations in mouse see List of abbreviations. Adapted from (*1*).

Ex_BCL6, which is associated with the Ex_CACNA1H subclass and situated in an olfactory-input-receiving area (Fig. 13G), shows great similarity to neurons in the murine piriform cortex (Fig. 23A, Fig. S15A) and lizard lateral cortex (Fig. 24), also associated with olfactory input processing (*24*, *168*). However, these lizard lateral cortex neurons more closely match a population in the murine entorhinal cortex rather than the piriform cortex (Fig. 25, Fig. S18). Additional comparisons with a different mouse dataset reveal a predominant

similarity of Ex_BCL6 to cells in the murine medial extended amygdala (Fig. 23B, Fig.S15B), another region implicated in olfactory processing (*184*). Despite these cross-dataset and cross-species inconsistencies, these findings suggest that Ex_BCL6 likely represents a conserved olfactory-input-related neuronal population. Expanding the sampling of olfactory-associated populations across amniotes may clarify these correspondences further.

2.2.5.2.1.2 Avian mesopallial neurons correspond to neurons in the mammalian claustrum and deep cortical layers

Mesopallial Ex_SATB2_ZNF385B supertype exhibits strong similarity to cells in the lizard anterior medial DVR and the murine Car3 population (Fig. 23A), a result corroborated by comparisons to an external mouse dataset (Fig. 23B). The Car3 population represents the primary cell type of the murine claustrum and potentially the dorsal endopiriform nucleus, though it is also sparsely distributed in deep cortical layers (*76*, *78*). The lizard anterior medial DVR has been proposed as the reptilian homolog of the mammalian claustrum based on transcriptomic and functional parallels (*42*), with my comparisons also showing some similarity between neurons in this region and murine Car3 cells (Fig. 25, Fig. S18). Together, these findings reveal a distinct correspondence of this cell population across all major amniote lineages, suggesting its presence in the last common amniote ancestor. Based on the great transcriptomic similarity, this cell type appears to have been comparatively conserved throughout amniote evolution unlike many other glutamatergic populations, potentially suggesting an essential function.

The similarity between the avian mesopallium and the mammalian claustrum aligns with several developmental homology models that propose the existence of distinct pallial sectors (*128*, *133*). According to the tetrapartite pallium hypothesis, specifically, the lateral pallial sector gives rise to the claustrum, endopiriform nucleus, and insular cortex in mammals, as well as the mesopallium in birds (Fig. 4A) (*128*). Conversely, circuit-based homology models posit that the mesopallium is homologous to upper cortical layers due to their shared predominant associative functions and intra-telencephalic connectivity (Fig. 4B) (*115*, *126*).

Two other mesopallial supertypes, Ex_SATB2_SOX6 and Ex_SATB2_FOXP2, exhibit weaker transcriptomic similarities with both lizard and mouse cell populations. The closest match for these supertypes in lizards is also neurons of the anterior medial DVR (Fig. 24), while in mouse they resemble corticothalamic (CT) projecting neurons (Fig. 23). If the resemblance to lizard amDVR cells reflects homology, this may indicate that Ex_SATB2_SOX6 and Ex_SATB2_FOXP2 diverged from a Car3-like cell populations within the avian lineage. However, this interpretation would necessitate a convergent evolution of transcriptomic features with murine CT neurons, despite their differing functional roles. If instead the similarities to murine CT populations are indicative of homology, this

suggests an evolutionary divergence in connectivity patterns, given that mesopallial neurons primarily establish intra-telencephalic connections, whereas CT neurons project to the thalamus. Such findings would also pose challenges to the tetrapartite hypothesis, which suggests that avian mesopallial and murine CT neurons originate from distinct pallial regions (Fig. 4A) (*128*).

The remaining supertype within the Ex_SATB2 subclass, Ex_SATB2_OVOA, exhibits low transcriptomic similarities to various populations in both mouse and lizard (Fig. 23, Fig. 24), rendering the evolutionary origin of this cell type non-conclusive and suggesting multiple potential scenarios. For example, Ex_SATB2_OVOA may represent a new chicken-specific cell type; alternatively, corresponding cell types may have been lost in mammals and lizards. It is also possible that this supertype has diverged to such an extent from other homologous cell types that homology is not detectable anymore in these transcriptomic comparisons.

Within the Ex_SATB2_KIAA1217 subclass, the Ex_KIAA1217_BCL6 supertype shows only limited similarity to mammalian populations, while Ex_KIAA1217 aligns closely with murine layer 6b (L6b) neurons and near-projecting neurons of the subiculum (NP PPP) (Fig. 23). The similarity to mammalian L6b cells is further corroborated by an independent study that compared mammalian and chicken cell types based on enhancer codes (*180*), supporting the resemblance between Ex_KIAA1217 and deep-layer cortical neurons.

Given the strong similarity between Ex_KIAA1217 and murine populations but limited similarity to lizard clusters (Fig. 24), I extended the analysis to available turtle pallial data (Fig. 26, Fig. S19), which includes a larger representation of neurons from the anterior dorsal cortex, a region comparably larger in turtles than in lizards (*41*). This analysis uncovered a three-way correspondence between Ex_KIAA1217, murine L6b cells, and turtle neurons in layer 2a of the anterior dorsal cortex (e08; Fig. 26, Fig. 27). This population in turtle has been proposed to be homologous to deep-layer isocortical neurons (*41*). These observations strengthen the notion that L6b-like neurons, which constitute the deepest layer of the mammalian cortex and arise from the subplate, a largely transient developmental structure (*185*), may derive from ancestral subplate-like neurons in the last common amniote ancestor, although reptiles lack a defined subplate structure (*186*).

These findings indicate that the avian mesopallium may share homology with regions of the mammalian isocortex beyond the insular cortex alone. This broader similarity contrasts with the tetrapartite pallium hypothesis, which limits homology of the mesopallium to the insular cortex (Fig. 4A) (*128*). Although a more recent version of the hypothesis proposes tangential migration from early claustral cells into the mammalian subplate (*129*), which could explain the observed similarities, this migration remains unconfirmed, and one tracing study, while not exhaustive, provides no support for this migration (*150*).

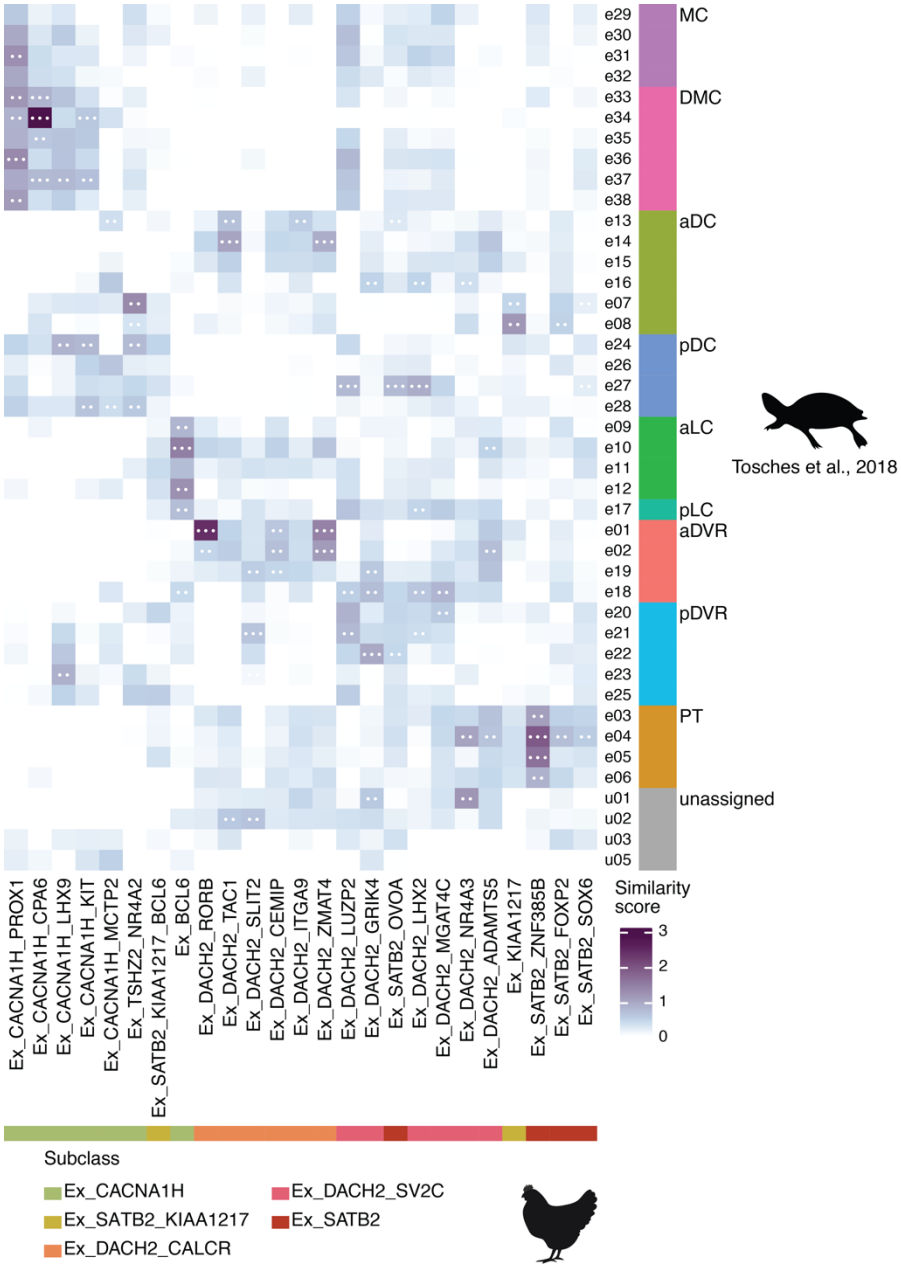

Figure 26 Comparison of adult glutamatergic excitatory neurons between chicken and turtle. Comparison between chicken supertypes and turtle excitatory clusters from (*41*) based on three different methods. Coloured bar on the right represents broader regional annotation from (*41*). Scores were scaled between 0 and 1 per method and summed across all methods to represent the similarity score. White dots in tiles are shown when populations are among the top reciprocal matches according to two or all three methods. MC, medial cortex; DMC, dorso-medial cortex; aDC, anterior dorsal cortex; pDC, posterior dorsal cortex; aLC, anterior lateral cortex; pLC, posterior lateral cortex; aDVR, anterior DVR; pDVR, posterior DVR; PT, pallial thickening. Adapted from (*1*).

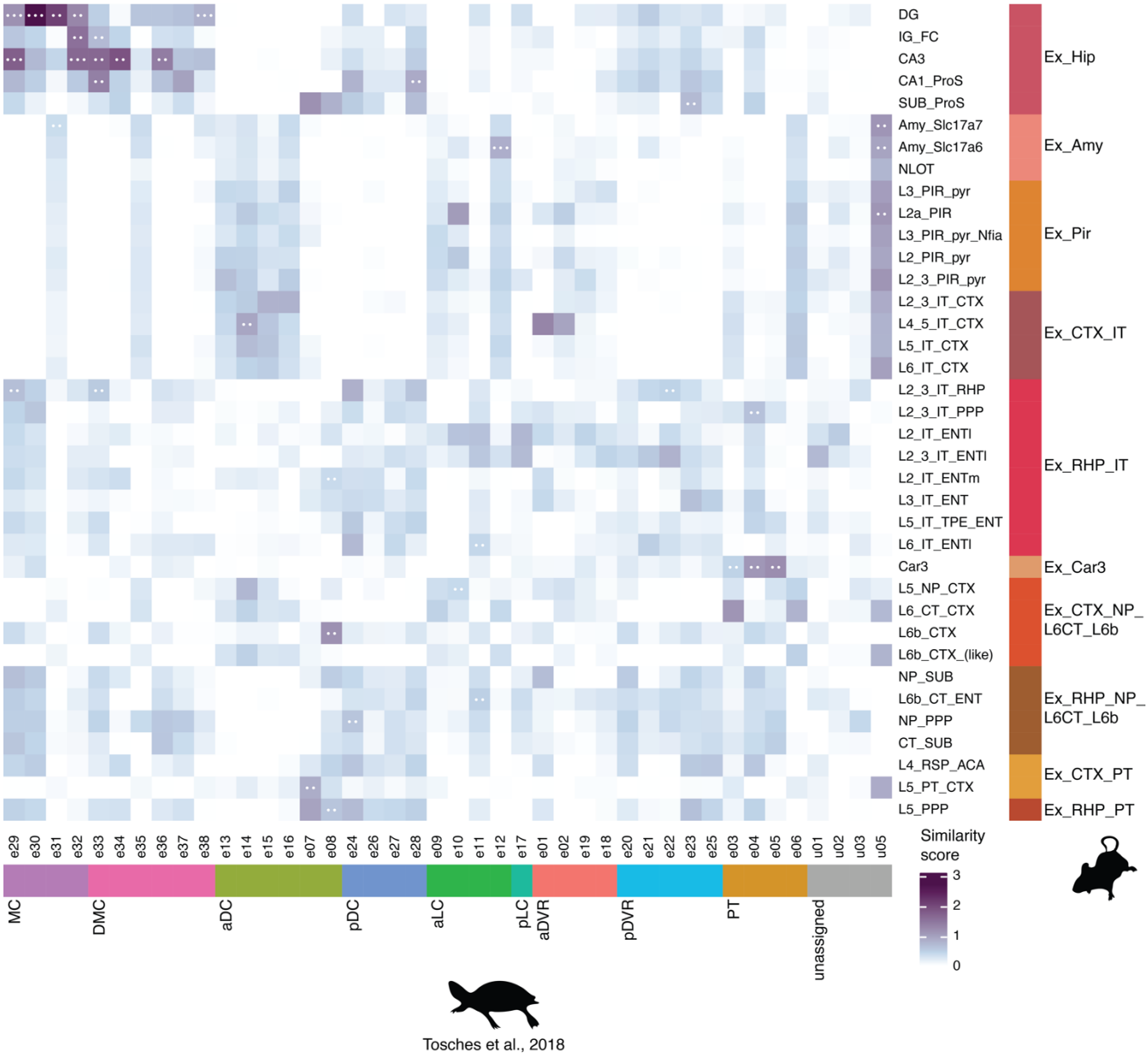

Figure 27 Comparison of adult glutamatergic excitatory neurons between turtle and mouse. Comparison between turtle excitatory clusters from (*41*) and murine excitatory subclasses from this study based on three different methods. Coloured bars represent broader regional annotation taken from (*41*) or as presented in chapter "Cell type atlas of the murine pallium". Scores were scaled between 0 and 1 per method and summed across all methods to represent the similarity score. White dots in tiles are shown when populations are among the top reciprocal matches according to two or all three methods. MC, medial cortex; DMC, dorso-medial cortex; aDC, anterior dorsal cortex; pDC, posterior dorsal cortex; aLC, anterior lateral cortex; pLC, posterior lateral cortex; aDVR, anterior DVR; pDVR, posterior DVR; PT, pallial thickening. For cell population abbreviations in mouse see List of abbreviations. Adapted from (*1*).

2.2.5.2.1.3 Avian hyperpallial and nidopallial neurons and corresponding mammalian neuron populations diverged

Supertypes belonging to the hyperpallial an nidopallial subclasses, Ex_DACH2_CALCR and Ex_DACH2_SV2C, align primarily with populations in the lizard DVR rather than in the dorsal or medial cortex, despite their partly dual regional origins (Fig. 24, Fig. S17). Most

Ex_DACH2_CALCR supertypes, including the mixed supertype Ex_DACH2_ZMAT4, show a stronger similarity to the sensory-recipient anterior DVR in lizards. However, when compared to turtle, where the anterior dorsal cortex is more extensive, predominantly hyperpallial supertypes (Ex_DACH2_TAC1 and Ex_DACH2_ITGA9) correspond more closely to clusters in the anterior dorsal cortex (Fig. 26, Fig. S19). Consistently, Ex_DACH2_ZMAT4 exhibits similarities to both the turtle's anterior DVR and anterior dorsal cortex, reflecting its dual regional identity.

In assessing Ex_DACH2_CALCR supertypes—predominantly located within sensory-processing regions of the nidopallium and hyperpallium—against the mouse dataset, I predominantly observed weak similarities to populations in isocortical layers 4 and 5 (Fig. 23, Fig. S15). Circuit-based homology models have proposed that sensory-recipient neurons in the avian nidopallium may be homologous to those in layer 4 of the mammalian isocortex. However, my findings show that the Ex_DACH2_RORB supertype, situated centrally within these sensory-input regions, very closely resembles neurons in layer 2a of the murine piriform cortex rather than isocortical populations (Fig. 23A, Fig. S15A). In support of this correspondence, I identified a three-way correspondence between Ex_DACH2_RORB, a lizard anterior DVR cluster (Ex_21; Fig. 24, Fig. S17), and murine piriform cortex cells (Fig. 25, Fig. S18). Comparisons with an external mouse dataset shows predominant similarity of this supertype to layer four isocortical neurons (Fig. 23B, Fig. S15B), but a comparison to the same dataset at a more finely resolved annotation level additionally confirms the resemblance to a murine piriform cortex population (Fig. S16).

Neurons in layer 2a of the piriform cortex arise from ventral pallial regions (*187*, *188*) and function as the primary recipients of olfactory bulb input in mice (*189*). This alignment suggests that nidopallial sensory-input neurons, which also originate from ventral pallial regions, employ gene expression programs similar to those of isocortical neurons but may have evolved from ventral pallial sensory-input-processing neurons. Whether these ventral pallial sensory-input neurons in the last common ancestor of amniotes processed olfactory or other sensory modalities remains unclear.

The Ex_DACH2_SV2C supertypes most closely resemble clusters in the posterior DVR of lizards (Fig. 24, Fig. S17), despite being distributed across diverse regions in the chicken brain. Even highly regionally mixed Ex_DACH2_SV2C supertypes, such as Ex_DACH2_MGAT4C and Ex_DACH2_ADAMTS5, align more closely with turtle DVR populations than with dorsal cortex clusters, though similarity scores are generally low (Fig. 26, Fig. S19). In comparisons with mouse populations, Ex_DACH2_SV2C supertypes show weak similarity to neurons in retrohippocampal regions, the posterior cortical amygdala, and parts of the isocortex (Fig. 23, Fig. S15). However, these similarities lack corroboration from three-way matches with lizard or turtle clusters (Fig. 25, Fig. 27), suggesting that low similarity scores in these cases do not reliably indicate homology.

These findings imply that neuron types within the sauropsid DVR—particularly in the avian nidopallium, and to some extent the hyperpallium—and their potential mammalian homologs have undergone significant transcriptomic divergence. Consequently, the evolutionary origins of Ex_DACH2_CALCR and especially Ex_DACH2_SV2C remain elusive.

2.2.5.2.2 Comparison of excitatory neurons in the developing pallium between birds and mammals reveals broad homologies

Given the distinct glutamatergic developmental trajectories in the developing chick pallium (Fig. 18I) and higher conservation of gene expression across species during development compared to adults (*132*), I reasoned that a comparison based on developmental data may reveal broader but more robust homologies between avian and mammalian pallial cell populations which might not be obvious in adult comparisons. I thus compared the chicken developmental data for the glutamatergic lineage to corresponding mouse data (*60*) where I refined the annotation of the pallial glutamatergic lineage (see chapter 2.2.1.2).

Given the continuous nature of the developmental datasets for the chicken and murine pallium and the absence of clearly identifiable cellular lineages in the murine data (in contrast to the chicken pallium), I chose not to subsample cell type populations for this comparison. Gene specificity index (GSI) correlation relies on average gene expression per population and is thus particularly sensitive to variations in cell numbers between populations. This sensitivity, along with other potential factors such as differences in gene selection between comparative methods, likely contributed to the observed GSI correlation being more strongly influenced by developmental stage than by lineage identity (Fig. S22). To better capture lineage relationships, I therefore only used Seurat's CCA-based integration with label transfer and SAMap for this comparison; these approaches use different gene sets—one-to-one orthologs and all orthologs, respectively—and distinct algorithms.

The comparison revealed that the two types of progenitor cells (radial glial cells, RGCs; intermediate progenitor cells, IPCs) exhibit the highest inter-species similarity, suggesting that pallial radial glia are very highly similar between birds and mammals and the identified proposed IPCs in chicken are indeed homologous to mammalian IPCs (Fig. 28, Fig. S21).

The inter-species comparison of early neuronal trajectories mostly supports my adult findings and reveals additional relationships not discernible in adults. Hippocampal neurons also show conservation during development, but the avian hippocampal/arcopallial trajectory hardly resembles the mammalian amygdala, although the main avian arcopallial cell population (Ex_CACNA1H_LHX9) clearly resembled mammalian amygdalar cells in adult comparisons (Fig. 23). This discrepancy may arise from challenges in distinguishing early arcopallial and hippocampal glutamatergic neurons

in the chicken dataset, or cells from different amygdalar nuclei in the mouse developmental dataset. More refined comparisons, with deeper sampling of the chicken hippocampal/arcopallial lineage and the mouse amygdalar lineage, may provide further insights into these developmental relationships.

The mesopallial trajectory closely resembles both early and mature deep-layer cortical neurons, consistent with trends observed in adult analyses, where several mesopallial supertypes resemble neurons in murine isocortical layer 6. However, the avian Ex_SATB2_ZNF385D population strongly resembles a claustral population in adults (Fig. 23). Due to the claustrum's small size and consequently limited sampling in the developing mouse brain dataset, no distinct claustral population was identifiable in this developmental dataset to corroborate this correspondence.

The hyperpallial trajectory, which likely generates cells in the hyperpallial subregions IHA and HA, aligns most closely with upper and deep cortical layer neurons during development. This matches findings in adults, where the primary IHA cell population (Ex_DACH2_TAC1) shows similarities to neurons in mammalian isocortical layers 4/5 (Fig. 23). However, HA cell populations displayed a convergent transcriptomic profile with nidopallial populations in adults and did not clearly correspond to any mammalian cell types in adult comparisons.

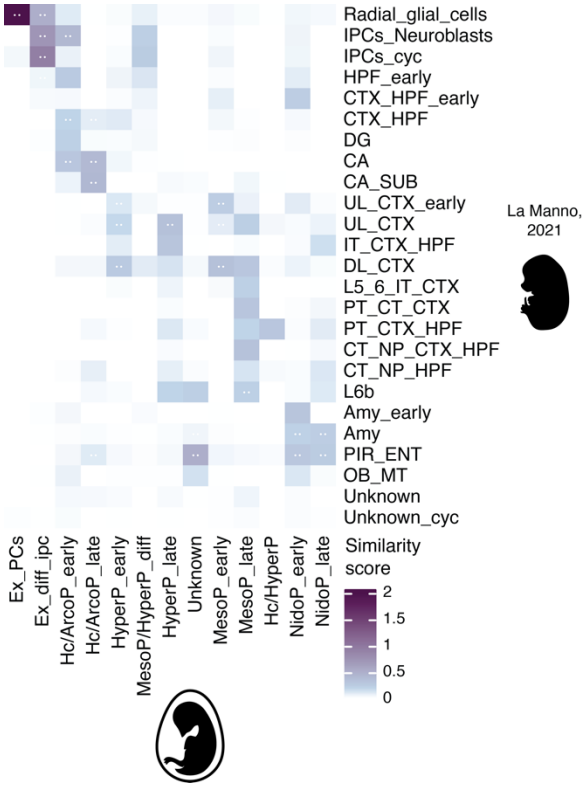

Figure 28 Comparison of developing glutamatergic excitatory neurons between chicken and mouse. Comparison between chicken pallial lineages as presented in chapter "Developmental origins of glutamatergic excitatory avian pallial " and populations in the developing murine pallium from (*80*) as presented in chapter "Refined annotation of cell types in the developing murine pallium". Lineages

comprising many cells in chick were split into early and late according to pseudotime (Fig. 17C). Comparison is based on two methods. Scores were scaled between 0 and 1 per method and summed across both methods to represent the similarity score. White dots in tiles are shown when populations are among the top reciprocal matches according to both methods. IPCs, intermediate progenitor cells; cyc, cycling; HPF, hippocampal formation; DG, dentate gyrus; CA, Cornu Ammonis; SUB, subiculum; UL, upper cortical layers; CTX, cortex; IT, intra-telencephalic; DL, deep cortical layers; PT, pyramidal-tract-projecting; NP, near-projecting; CT, corticothalamic-projecting; Amy, amygdala; PIR, piriform cortex; ENT, entorhinal cortex; OB_MT, olfactory bulb mitral tufted cells; Ex_PCs, early radial glia (likely neurogenic); Ex_diff_ipc, excitatory intermediate progenitors and differentiating neurons; NidoP, nidopallial lineage; Hc/ArcoP, hippocampal and arcopallial lineage; HyperP, hyperpallial lineage; MesoP, mesopallial lineage; Hc/HyperP, between hippocampal and hyperpallial lineage; MesoP/HyperP_diff, early differentiating cells of mesopallial or hyperpallial lineage. Adapted from (*1*).

Notably, the nidopallial trajectory closely resembles the developing amygdala, piriform, and entorhinal cortex — a correspondence not fully evident in adult comparisons. In adults, only one population located in the sensory-input-receiving areas of the nidopallium (Ex_DACH2_RORB) exhibited clear similarity to piriform cortex cells (Fig. 23, Fig. S16), while others showed low or inconclusive similarities to mammalian populations. Although these developmental correspondences remain broad, likely largely due to the underrepresentation of non-isocortical lineages in the murine dataset, they provide a valuable framework for refining cell population homologies. Together, these developmental comparisons also underscore that avian hyperpallial and nidopallial populations, despite their convergent transcriptomic profiles in adults, likely have distinct developmental (see chapter 2.2.4.2) and also evolutionary origins.

Together, these findings suggest that pallial intermediate progenitor cells (IPCs) were already present in the last common amniote ancestor. Moreover, unlike their adult counterparts, early neurons in the avian pallium retain transcriptomic signatures that reflect their developmental origins, enabling the identification of broad homologies between mammalian and avian cell populations.

3 DISCUSSION

In my dissertation, I investigated the evolution of cell types in the amniote pallium, a forebrain region critical for integrating sensory information, for cognition, memory, and complex behaviours (*7*, *25*, *27*, *38*). In amniotes (mammals, birds, and non-avian reptiles), the pallium has undergone remarkable morphological diversification (*17*), with its cell types forming the basis for the distinctive structural and functional features observed in these lineages. The evolutionary relationships of amniote pallia are arguably one of the most controversial topics in comparative neuroscience (*48*, *129*, *133*), which I addressed by generating and investigating crucial datasets including unprecedentedly thorough cross-species comparisons.

A central component of this work was the generation of the first comprehensive, spatially resolved cell type atlas of the chicken pallium, capturing the diversity and regional specificity of cell populations across both adult and *in ovo* developmental stages. By comparing this avian pallial atlas to various pallial datasets from mice and non-avian reptiles, I traced the evolution of pallial cell types and structures across amniotes.

3.1 EVOLUTION OF GABAERGIC INHIBITORY NEURONS IN THE AMNIOTE PALLIUM

Consistent with a previous study (*75*) I showed that in the adult avian pallium, as in mammals, the transcriptomic profiles of GABAergic inhibitory neurons reflect their developmental origins in distinct subpallial regions, specifically the lateral, medial, and caudal ganglionic eminences. Most inhibitory neuron populations are broadly distributed across the pallium, suggesting they function as interneurons, while a few populations are regionally confined to areas in the olfactory bulbs and arcopallium, which likely represent GABAergic projection neurons. These potential projection populations are derived from the lateral ganglionic eminence (LGE), consistent with distributions in the mammalian pallium (*15*, *71*). As previously shown (*41*, *75*), cross-species comparisons reveal strong transcriptomic conservation of inhibitory neuron types across amniotes.

Notably, despite this overall conservation, an LGE-derived cell population which is localized in the intercalated amygdala in mammals (*154*) and in a specific caudal pallial region in lizards (*41*), has become widely distributed and highly abundant throughout the chicken pallium, matching a population previously characterized in finches. This finding is significant because the avian pallium has been shown to harbour sensory-motor circuits similar to those in the mammalian isocortex (*37*, *38*), suggesting that these circuits in birds may incorporate an entirely different type of interneuron that lacks a counterpart in the mammalian isocortex. This difference suggests functional adaptations within avian pallial circuits.

3.2 Regional organization and development of glutamatergic excitatory neurons in the avian pallium

I demonstrated that glutamatergic excitatory neuron populations in the avian pallium exhibit a more spatially restricted distribution compared to inhibitory interneurons, a pattern also observed in mammals (*68*, *76*, *82*). Their transcriptomic profiles reflect both their functional roles and their confinement to specific regions, likely influenced by their developmental origins in distinct pallial domains. To disentangle signals related to adult functional roles from those tied to developmental origins, I traced the developmental lineages that give rise to these excitatory populations during *in ovo* development.

One adult excitatory neuron subclass (Ex_CACNA1H) harboured populations located in the chicken hippocampal regions and the arcopallium, a structure in the caudal ventral pallium, serving as the primary output structure of the DVR (*36*, *38*). I showed that neurons in this subclass also likely arise from a shared developmental cellular lineage. These findings challenge several previous hypotheses regarding the organization of the avian pallium, including the tetrapartite pallium theory, that define distinct pallial sectors along the medial-to-lateral and rostral-to-caudal axes (*128*, *133*). According to these hypotheses hippocampal and arcopallial neurons arise from distinct pallial sectors, which should be mirrored in their transcriptome. Although hippocampal and arcopallial excitatory neurons show some unique marker gene expression, my observations indicate the existence of a continuous region around the caudal pole of the developing avian telencephalon rather than distinct germinative sectors, as previously suggested by the continuum hypothesis (Fig. 3).

Additionally, according to the tetrapartite and related development-based hypotheses, cells in all hyperpallial subregions share a common developmental origin in the dorsal pallial sector (Fig. 4A). However, I observed that excitatory cells in different hyperpallial subregions arise from two to three distinct cellular lineages. Specifically, cells in the densocellular and intermediate hyperpallium (HD/HI) form a homogeneous territory together with cells in the adjacent mesopallium and arise from the same lineage during development, as previously suggested by the continuum hypothesis (*47*, *48*). The apical hyperpallium (HA), located adjacent to the hippocampal regions, contains a cell population that resembles both, cells in the hippocampal and hyperpallial lineage in gene expression (Ex_TSHZ2_NR4A2). Only the remaining cells in the apical hyperpallium (HA) and cells in the interstitial apical hyperpallium (IHA) clearly originate from the distinct hyperpallial developmental lineage. These findings suggest significant medial to lateral variation in cellular transcriptomes in the chicken hyperpallium instead of a singular transcriptomic identity.

I observed pronounced transcriptomic and gene regulatory similarities between cell populations in the (interstitial) apical hyperpallium (HA+IHA) and nidopallium, consistent with bulk transcriptome analyses of the adult zebra finch pallium (*48*) and evident in two-

week old chicks in a parallel study (*180*). Based on these adult similarities and *in situ* expression profiles of few selected genes during development (*47*), the continuum hypothesis suggests that neurons in the apical hyperpallium and associative nidopallium, as well as those in the interstitial apical hyperpallium and sensory-input receiving areas of the nidopallium, respectively, arise from shared embryonic regions. Contrary to this hypothesis, I identified distinct cellular trajectories in the hyper- and nidopallium during *in ovo* development, likely giving rise to both associative and sensory input-related cell types in each structure. These observations better align with the tetrapartite pallium and related hypotheses, which suggest that hyperpallial and nidopallial neurons do not share a common developmental origin given they arise from topologically separated pallial domains (*128*, *133*).

The identified hyperpallial and nidopallial lineages exhibit only base-level similarity at mid-neurogenesis stages - similar to the level of similarity observed between the hyperpallial and other lineages. This limited similarity also aligns with my observation that shared cell populations in adults are partially absent at embryonic day 19. Although tangential migration from the nidopallium to the hyperpallium or vice versa could explain the similarity, a previous tracing study (*116*) and my data show no evidence for it. Specifically, this study showed that tangential migration from ventral to dorsal pallial areas (and vice versa) is absent before E14. Consistently, I observe only minimal contribution from dorsal pallial dissections to the nidopallial developmental lineage, and minimal contribution of ventral pallial dissections to the hyperpallial developmental lineage until E19. However, these in silico observations warrant further validation with true lineage tracing techniques. Extensive tangential migration after E19, which would be required to explain the strong similarity between the hyper- and nidopallium in adults and on post-hatch day 15 (*180*), seems unlikely. By E19, the brain morphologically already closely resembles its adult form, and upon certain stimuli chicks at this stage show metabolic activity across the entire brain similar to that observed in awake postnatal chicks (*179*), indicating that the brain is nearing its full functional activity by this stage.

Thus, while I cannot formally exclude tangential migration after E19, I propose that the remarkable similarity between avian hyperpallial and nidopallial cell populations — both of which perform analogous roles in different sensory circuits — is fully established by post-hatch day 15 in chicks (*180*) due to substantial gene expression convergence. This convergence may be driven by the dramatically increased sensory input experienced post-hatching, consistent with studies indicating that early postnatal development in both mammals and birds represents a period of significant transcriptional change in brain development (*132*). One study in mammals further links early postnatal neuronal activity to the formation of new gene regulatory elements, which drive the expression of neuron-subtype-specific genes and shape mature neuronal identity (*190*).

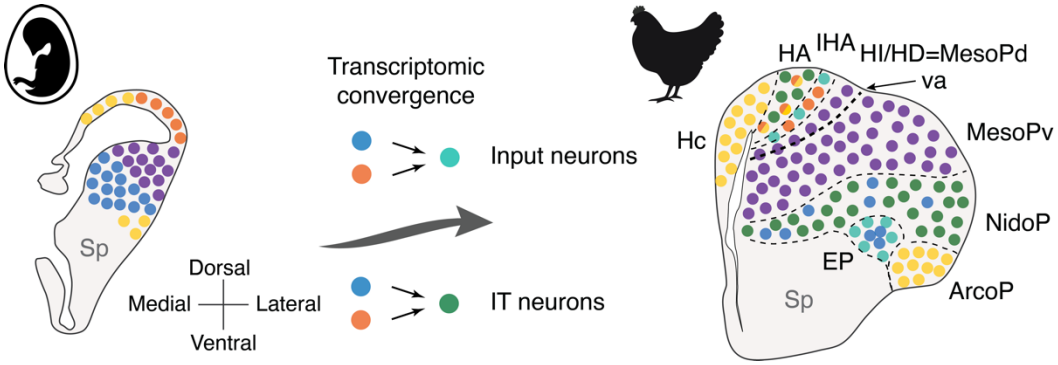

Figure 29 Proposed model of cellular development in the chicken pallium. Schematic representation of coronal sections of the telencephalon in the developing chick (left) and adult chicken (right). Differently colored dots correspond to transcriptomically distinct glutamatergic cell populations, largely corresponding to early neuron lineages in the developing, and subclass and supertype annotations in the adult pallium. I propose that, during development, neuron populations from dorsal (orange) and ventral (blue) pallial regions progressively converge to similar transcriptomic profiles. These converged populations represent input (cyan) and intra-telencephalic-projecting (IT) neurons (dark green) in the hyperpallium and nidopallium in the adult. Few populations do not converge and can clearly be linked to their ontogenetic origin from distinct embryonic territories. These populations are represented by remaining dorsal (orange) and ventral (blue) dots in the interstitial apical hyperpallium (IHA) and nidopallium (NidoP), respectively. Half orange, half yellow dots represent the Ex_TSHZ2_NR4A2 population, for which it is not clear if it originates from the hippocampal (yellow) or hyperpallial (orange) lineage. Sp, subpallium; Hc, hippocampal areas; HA, apical hyperpallium; HI/HD, intercalated and densocellular hyperpallium; va, vallecula; MesoPd, dorsal mesopallium; MesoPv, ventral mesopallium; NidoP, nidopallium; EP, entopallium (visual nidopallial nucleus); ArcoP, Arcopallium.

Overall, I could classify pallial glutamatergic cell types into four major developmental lineages in chicken with likely distinct spatial origins, supporting the existence of distinct pallial developmental sectors in birds (Fig. 29). However, the extent and position of these sectors does not entirely match any single previously proposed model. Although I confirm certain aspects of the continuum model (*37*, *47*, *48*), my findings deviate from it in key conclusions regarding the hyperpallium and nidopallium. My findings also differ from the tetrapartite pallium model in the exact extent of the four sectors (*128*), although one could argue that the differences are minor. However, the tetrapartite pallium hypothesis suggests the existence of the same sectors across amniote species, which remains to be validated (further discussed below), and implies that developmental territories confer strong regional identity in the adult. However, I observed an extensive developmental convergence of gene expression programs between excitatory cell populations from the hyperpallium and nidopallium during late developmental stages (Fig. 29), suggesting that the topological location within the embryonic pallium is not always a determinant factor for gene expression programs defining functions in adults, at least in birds.

3.3 Evolution of glutamatergic excitatory cell populations in the amniote pallium

The evolutionary relationships of pallial regions and cell types across amniotes have long been debated. My analyses validated previously proposed relationships but also uncovered unexpected potential homologies (Fig. 30, Fig. S23).

My findings that homologs of excitatory neurons in the mammalian hippocampus are present in corresponding regions of the chicken pallium, together with data for non-avian reptiles (*41*) and amphibians (*19*), indicate that key hippocampal regions and cell types were present in the last common tetrapod ancestor and have been preserved across amniotes. This suggests an essential function of hippocampal cell types, potentially related to its fundamental role in spatial memory and navigation (*26*).

The principal glutamatergic population in the avian arcopallium (Ex_CACNA1H_LHX9) closely resembles certain mammalian amygdalar cells, suggesting their homology.

These correspondences were previously proposed by development-based homology models on the basis of assumed common developmental origins of mammalian and avian hippocampal neurons in a medial pallial sector, and amygdalar and arcopallial neurons in a ventral sector (*128*, *133*). However, as mentioned above, I find that in chicken, excitatory cell types in the hippocampus and arcopallium likely arise from a shared developmental lineage, in line with observations in zebra finch (*48*), suggesting that at least in birds the previously defined medial sector extends into caudal ventral pallial areas. According to my knowledge a similar scenario has never been proposed for mammals, i.e., that cells in any amygdalar nuclei share high similarity with (retro-) hippocampal cells during development. However, the similarity of lineages giving rise to different pallial excitatory cell types in different pallial regions during development has also never been evaluated in detail in the mammalian pallium. Still, these observations suggest that pallial subdivisions may not be conserved across amniotes.

Further, I identified notable divergence between the avian nidopallium and its proposed mammalian counterparts. Circuitry-based hypotheses suggest homology between the avian nidopallium and various mammalian isocortical layers (Fig. 4B) (*115*, *126*). While I detected some transcriptomic similarities between nidopallial sensory-input-related populations and neurons in mammalian isocortical layers 4 and 5, these similarities are overall low, and nidopallial neurons also exhibit some similarity to populations in the mammalian entorhinal cortex and cortical amygdala. None of these similarities was corroborated by comparisons across multiple amniote lineages. Only one distinct cell type in the sensory-input-receiving regions of the nidopallium (Ex_DACH2_RORB) clearly resembles neurons in the mammalian piriform cortex.

Consistently, my developmental analyses revealed homology between the avian nidopallial lineage and neurons in the developing mammalian amygdala, piriform cortex, and entorhinal cortex—structures that, like the avian nidopallium, predominantly arise from ventral regions of the pallium (*99*, *187*, *188*). These findings suggest that excitatory neurons in the avian nidopallium are homologous to at least some cell types in these mammalian structures, although their gene expression patterns have diverged significantly (Fig. 30). Further investigations, including more comprehensive sampling of

these regions during mammalian pallial development, are essential to clarify these potential homologies.

Neurons in distinct subregions of the avian hyperpallium, previously proposed to be field-homologous to the entire mammalian isocortex (*128*, *133*), do not uniformly correspond to neurons within a single mammalian structure. This aligns with their diverse transcriptomic profiles and developmental origins, as discussed above. For instance, one cell type in the apical hyperpallium (Ex_TSHZ2_NR4A2) shows similarities to neurons in mammalian retrohippocampal structures and the posterior dorsal cortex of other reptiles, which in turn was proposed to resemble mammalian retro-hippocampal structures (*41*). In contrast, cells in the densocellular and intercalated hyperpallium (HD/HI) resemble mesopallial cell types, which are similar to mammalian claustral and deep cortical layer neurons. Despite notable transcriptomic similarity between nidopallial and hyperpallial sensory-input-receiving populations, my analysis suggests homology only between cells in the interstitial apical hyperpallium (Ex_DACH2_TAC1) and mammalian isocortical layers 4 and 5. Specifically, while both, nidopallial and hyperpallial sensory-input-receiving populations, show some similarities to neurons in mammalian isocortical layers 4 and 5, only the latter correspondence is corroborated by developmental. This is consistent with these populations' shared roles as sensory-input-receiving neurons in the pallium (*38*, *49*). Together, these findings partially support development-based hypotheses of field homology between the hyperpallium and isocortex (*128*, *133*) but do not fully align with circuit-based hypotheses suggesting homology between all sensory input-receiving neurons in the avian pallium and neurons in mammalian isocortical layers 4 and 5 (*126*).

Neurons in the avian mesopallium resemble those in the mammalian claustrum and deep layers (L6b, L6 CT) of the isocortex and retrohippocampal areas. This completely contrasts with correspondences suggested by circuit-based models proposing homology of mesopallial populations to neurons in upper isocortical layers due to their shared integrative functions (*115*, *126*). One mesopallial population (Ex_SATB2_ZNF385B) strongly resembles the main murine claustral population (Car3) and neurons in the lizard anterior medial DVR. I also observed high similarity of Car3-corresponding populations among all mammalian lineages. This close transcriptomic similarity, along with proven functional resemblance in lizards (*42*), suggests homology, high transcriptomic, and at least partial functional conservation of this cell type across all amniote and mammalian lineages. Notably, an equivalent cell type was not identified in the salamander nor different teleost species (*73*, *74*, *191*), indicating that this cell type may have originated within amniotes, potentially evolving essential functions that contributed to its retention and conservation within this clade.

The correspondence of Car3-like populations aligns with development-based hypotheses suggesting that both the mammalian claustrum and avian mesopallium emerge from a lateral pallial sector (*128*, *133*). However, I also identified a population in the avian

mesopallium (Ex_KIAA1217) and turtle anterior dorsal cortex resembling mammalian subplate-derived layer 6b neurons. These layer 6b neurons are present across different pallial sectors, as defined by those development-based hypotheses. Additionally, other adult mesopallial cell populations transcriptomically resemble mammalian cortico-thalamic (CT) projecting neurons in isocortical L6 and retrohippocampal areas, rather than neurons is the proposed mammalian lateral pallium, encompassing the claustrum, endopiriform nucleus and insular cortex (Fig. 4A). My developmental comparisons and a study comparing amniote enhancer codes (*180*) further support the similarity of the mesopallial lineage to deep layers of the isocortex and hippocampal formation. These findings challenge the tetrapartite and other development-based hypotheses and again suggest that pallial subdivisions are not conserved across amniotes.

Altogether, my cross-amniote comparisons reveal general correspondences among populations in the medial and ventral pallial areas, though the latter is evident only during development. These findings align more closely with development-based hypotheses than circuit-based ones. However, while some cell populations are conserved across amniotes in proposed dorsal and lateral pallial sectors, my results do not support a strict one-to-one regional homology. This challenges the notion of amniote-shared pallial territories, particularly in dorsal and lateral regions, as proposed by several development-based homology models (*128*, *133*). Nevertheless, a dorsoventral organization is evident in the developing chicken pallium, consistent with conserved early brain patterning likely inherited from a common tetrapod ancestor (*17*). This suggests a conserved gradient-based topological organization, though pallial subdivisions or lineages may have evolved largely independently across different tetrapod lineages (*192*).

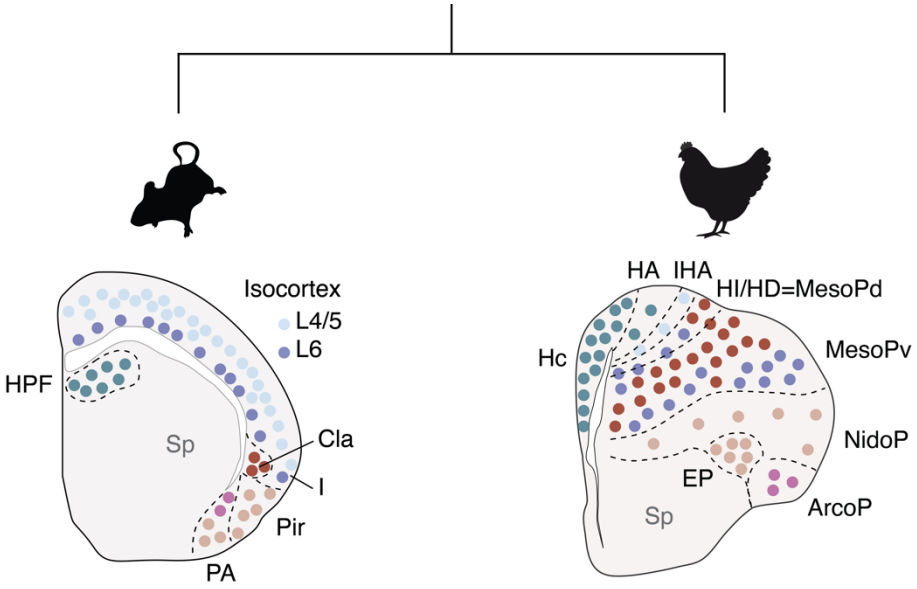

Figure 30 Proposed homologies of excitatory neuron populations between birds and mammals. Schematic representation of coronal sections of the telencephalon in the adult mouse (left) and chicken (right). Differently coloured dots represent transcriptomically distinct glutamatergic excitatory neuron populations, likely homologous across species. Dotted lines in the mouse separate distinct pallial territories as suggested

by the tetrapartite hypothesis (*128*). In selected avian pallial regions, many dots indicate high transcriptomic similarity of most cell types in this region to murine populations, while fewer dots suggest lower similarity or that only a few avian populations resemble murine populations. HPF, hippocampal formation; L4/5; isocortical layer four and five; L6, isocortical layer six; Cla, claustrum; I, insular cortex; Pir, piriform cortex; PA, pallial amygdala.

Despite differences in projection patterns and regional localization, mammalian cell types corresponding to avian mesopallial populations—claustral Car3, layer 6b, and layer 6 corticothalamic (CT) neurons—share a defining characteristic: they all originate early in development from the murine cortical neuroepithelium (*185*), reflected in their shared transcriptomic profiles. For example, claustrum and layer 6b neurons exhibit numerous shared developmental markers (*150*), though the neurons in the adult mammalian claustrum ultimately adopt a distinct transcriptomic identity (*78*, *82*). Additionally, single-cell RNA sequencing reveals numerous shared marker genes between layer 6b and 6 CT neurons (*82*). In contrast, upper-layer cortical neurons originate at later stages in development (*137*).

Although avian mesopallial neurons are generated at intermediate stages of neurogenesis (*104*), my comparisons therefore suggest potential homology with early-born neurons in the lateral, dorsal, and medial regions of the mammalian pallium. Furthermore, neurons in the avian interstitial apical hyperpallium (IHA) may be homologous to mammalian layer 4 and 5 neurons and are produced after most mesopallial neurons (*104*). A previous study comparing turtle and mouse pallial excitatory neurons similarly identified neurons in the turtle anterior dorsal cortex that share characteristics with neurons in either deep or upper cortical layers, with deep-layer-like neurons in the turtle cortex emerging first during development (*41*). Consistent with these findings, my own cross-species comparisons also reveal evidence of deep-layer and layer 4-like programs in the turtle anterior dorsal cortex. These findings suggest that sequential development of cells with deep- to higher-layer-like transcriptomic programs may represent an ancestral trait among amniotes. However, cells resembling mammalian layer 2 and 3 neurons appear absent in both chicken and turtle. This absence suggests that upper-layer neuron types, particularly layer 2 and 3, may represent a mammalian-specific innovation.

Together, these findings indicate a conserved deep-layer-like program present in the last common ancestor of amniotes. In mammals, this program appears to have diversified independently, ultimately giving rise to the distinct upper-layer neuron types in the isocortex. This diversification may have been influenced by factors such as an extended neurogenic period in early mammals compared to early sauropsids or the emergence of new neuronal progenitor cell types in the pallium (*90*). These changes could have allowed neurons specified during later developmental stages or derived from novel progenitors to acquire unique transcriptomic and functional profiles.

3.4 Implications for the evolution of advanced cognitive abilities in birds and mammals

Arguably, natural selection acts on behaviour, which is the output of neural circuit activity. To elucidate the evolution of cognitive capabilities across amniotes it is thus crucial to understand the evolution of the underlying neural circuits. While previous studies have shown that circuitry in the mammalian and avian pallium is remarkably similar (*38*), the findings of this dissertation underscore the dual evolutionary pattern shaping the cells constituting these circuits in the amniote pallium.

Inhibitory interneurons show high transcriptomic conservation, suggesting that they serve as a stable element within pallial circuits across amniotes. This conserved inhibitory framework may be crucial for core functions like feedforward and feedback inhibition, oscillatory activity, spike timing, and to maintain circuit stability (*193*). Despite this conservation, some functional divergence remains possible as evidenced by birds incorporating a unique interneuron type not observed in the mammalian isocortex, which may contribute to circuit specialization.

In contrast to inhibitory interneurons, my results make clear that most excitatory neurons supporting similar circuits in the mammalian isocortex and avian pallium have evolved convergently, rather than through a shared ancestry. These neurons differ in relative time and topological location of origin during development, gene expression patterns and specification mechanisms. For example, cells forming the microcircuit of the avian hyperpallium appear specified by spatial origin, with a medial-to-lateral transcriptomic gradient, while in the mammalian isocortex, excitatory neurons populating different layers are specified temporally during development. Overall, this dual evolutionary pattern might suggest that conserved inhibitory mechanisms support essential network requirements, while allowing excitatory circuitry to adapt and evolve to meet the demands of higher cognitive functions. However, the factors underlying the remarkable evolutionary flexibility of principal excitatory projection neurons in contrast to inhibitory interneurons, despite the presence of conserved circuits, remain unclear and warrant further investigation.

3.5 Outlook

Overall, this dissertation provides valuable novel insights and clarifies key aspects of the evolution of neuronal cell types in the amniote pallium. It also highlights the limitations of current hypotheses on pallial evolution and motivates further research into the cellular evolution and development of the pallium across species.

The generated datasets lay the foundation for the investigation of several other evolutionary questions, which were not the focus of this study. For instance, a comparison of glial cell expression patterns across species may offer insights into glial diversity in amniotes, as glia play critical roles in neural function and cognition. Additionally, the data

for the developing avian pallium can be leveraged to identify genes involved in the neurogenesis-to-gliogenesis transition. Such investigations could reveal how these transitions are timed and modified across different amniote lineages.

This study did not specifically target the subpallium, which would be necessary to fully characterize the diversity of subpallial progenitor populations generating GABAergic neurons. However, further analysis of GABAergic neuron development using the existing data could already illuminate the mechanisms driving the high abundance and broad distribution of LGE-derived interneurons in the avian pallium and elucidate how evolutionarily conserved gene expression programs are modified to result in a major phenotypic change. Tracing the differentiation pathways of these interneurons may reveal avian-specific features underlying their extensive proliferation and migration.

To better understand the proposed convergence between cell types in the avian hyperpallium and nidopallium, developmental profiling across additional pre-hatch and post-hatch stages is essential. Coupling this with chromatin accessibility data would help identify shared or distinct gene regulatory networks and clarify how and when convergent gene expression arises in these regions. This approach could reveal which molecular mechanisms drive parallel transcriptomes in different avian brain areas.

Expanding comparative datasets across a broader range of species—both for adults and development—will be crucial to advancing our understanding of pallial cell type evolution. A pan-mammalian cell type atlas covering eutherians, marsupials, and monotremes that spans all pallial regions, not just the isocortex as presented in this dissertation, would be instrumental in reconstructing the ancestral cell type composition of the mammalian pallium. Alongside equivalent pan-avian or potentially pan-sauropsid atlases, these resources would enhance our ability to distinguish lineage-specific changes from core features retained across larger clades, revealing more incremental steps in the evolution of diverse cellular profiles within the amniote pallium. Developmental data for the chicken pallium was foundational in this study, as more conserved developmental stages offer valuable insights into cell population homologies across species. Comparable datasets for mammals and other sauropsids would significantly improve our ability to identify homologous and convergent cell types and clarify whether the cellular developmental lineages identified in chicken represent shared amniote lineages or evolved independently. Although mammalian data exist, targeted dissections and spatially resolved analyses beyond the isocortex are needed to achieve a truly comprehensive perspective on pallial evolution across amniotes.

Lastly, this study used the chicken as the primary avian model. While chickens provide many advantages for developmental studies, they do not represent the peak of avian cognitive abilities. Advanced cognitive capabilities are observed in birds like corvids and parrots, which have higher neuron counts and extended neurogenic periods compared to chicken (*194*). Examining these species, alongside mammalian models, will be crucial to

understanding the evolutionary pathways that give rise to complex cognitive functions. Future studies of these more cognitively advanced avian species will further clarify how developmental timing, cell type diversity, and network complexity interact to produce advanced cognitive traits across amniotes.

4 METHODS

4.1 SAMPLE COLLECTION

Mice (*Mus musculus*, RjOrl:SWISS) were housed under a 12h/12h dark/light cycle in a temperature (20-24 °C) and humidity (40-65%) controlled room with ad libitum access to food and water. Mice were sacrificed by cervical dislocation on post-natal day 56. Dissections of the frontal isocortex include the anterior cingulate area, the prelimbic area, the orbital area, the infralimbic area, primary and secondary motor areas and the agranular insular area up to the start of the corpus callosum. Dissections of the ventral and lateral pallial derived structures include the insular cortex, the claustrum, the endopiriform nucleus, the piriform cortex and the amygdala. The positions of these regions were determined according to the Allen Mouse Brain Reference Atlas (2004). All animal procedures were performed in compliance with national and international ethical guidelines for the care and use of laboratory animals, and were approved by the local animal welfare authorities: Heidelberg University Interfaculty Biomedical Research Facility (T-23/19, T-28/21).

Gray short-tailed opossums (*Monodelphis domestica*) were bred in a colony in Museum für Naturkunde Berlin, Leibniz Institute for Evolution and Biodiversity Science (Germany). The animals were housed under a 12h/12h light/dark cycle in a temperature (24-26 °C) and humidity (60-65%) controlled environment with ad libitum access to food and water. Animals were sacrificed by isoflurane overdose. All animal procedures were performed in compliance with national and international ethical guidelines for the care and use of laboratory animals, and were approved by the local animal welfare authority Berlin State Office of Health and Social Affairs, LAGeSo (T0198/13, ZH104).

The collection of samples from wild short-beaked echidnas (*Tachyglossus aculeatus*) was approved by the Australian Animal Ethics Committee and carried out according to local guidelines.

Most samples from adult chickens (*Gallus gallus*, aged 1-2 years, breed: red junglefowl) were received from Linköping university. The study was approved by the Linköping Council for Ethical Licensing of Animal Experiments, license number 288-2019. The animals were kept in pens under a 12:12 h dark:light schedule and provided with food and water ad libitum. In addition, we were provided with heads of healthy domestic chickens (*Gallus gallus*, aged ca. 2 years, breed: Lohmann white) by a local farm. Brains were extracted and either dissected in ice-cold PBS and snap frozen in liquid nitrogen, or embedded in OCT sectioning medium and frozen on dry ice to preserve for cryosectioning. The brains of two individuals were dissected into four anatomical regions, meso- and nidopallium combined, arcopallium, hyperpallium and hippocampal region. Our dissection of the hyperpallium does not include most of the proposed caudal hyperpallium , which was previously annotated as the dorsolateral corticoid area (CDL) (*43*, *195*). This

area was mostly dissected as part of the hippocampal region.

Fertilized chicken eggs (*Gallus gallus*) were purchased from Granja Santa Isabel and incubated at 37.5 °C in a humidified atmosphere until the required developmental stage. The day when eggs were incubated was considered embryonic day (E)0. All animal experiments were approved by a local ethical review committee and conducted in accordance with personal and project licenses in compliance with the current normative standards of the European Union (Directive 2010/63/EU) and the Spanish Government (Royal Decrees 1201/2005 and 53/2013, Law 32/107).

Wild lizards (*Anolis carolinensis*) were obtained from a commercial supplier (Interaquaristik.de) and were kept in temporary cages before they were anesthetized by intraperitoneal injection of Narcoren (16 g/100 ml Sodium – Pentobarbital, Boehringer Ingelheim; 200 mg/kg body weight) and subsequently decapitated. Brains were extracted and dissected in ice-cold PBS. All animal procedures were performed in compliance with national and international ethical guidelines for the use of laboratory animals, and were approved by the local animal welfare authorities: Heidelberg University Interfaculty Biomedical Research Facility (T-04/21).

4.2 SINGLE-NUCLEUS RNA-SEQUENCING

4.2.1 NUCLEI PREPARATION

Nuclei were isolated from fresh frozen tissue according to a protocol adapted from (*196*). Briefly, the tissue was homogenized by trituration on ice in 250 mM sucrose, 25 mM KCl, 5 mM $MgCl_2$, 10 mM Tris HCl (pH 8), 0.1 % IGEPAL, 1 µM DTT, 0.4 U/µl, Murine RNase Inhibitor (New England Biolabs), 0.2 U/µl SUPERas-In (Thermo Fisher) and Hoechst DNA dye. After 5 min of incubation, remaining unlysed tissue was pelleted and removed by centrifugation at 100 g for 1 min. Nuclei in the collected supernatant were pelleted at 400 g for 5 min. Then, nuclei were washed once in homogenization buffer before they were resuspended in 1x PBS and filtered using Flowmi cell filters (pore size 40 µm; Merck). For adult samples used in single nuclei RNA experiments, fluorescence activated cell sorting (BD FACSAria ii, 85 µm nozzle, BD Biosciences) was used to separate single nuclei from remaining debris and aggregates according to forward and sideward scatter properties, as well as DNA content based on Hoechst signal. Due to the limited volume allowed as input, samples used for single nuclei multiome experiments were not sorted to keep a high concentration of nuclei in the solution. Following sorting or final resuspension, nuclei were counted on Countess II FL Automated Cell Counter (Thermo Fisher). 17 000 nuclei were employed for single nuclei RNA and multiome sequencing experiments.

4.2.2 LIBRARY PREPARATION AND SEQUENCING

Single nuclei RNA and multiome sequencing experiments were performed using the 10x Chromium Single Cell 3’ v3 and v3.1 Gene Expression Kit (10x Genomics) and the 10x Chromium single cell multiome ATAC + gene expression kit (v1), respectively, following

the manufacturer's instructions. Quantification and quality control of libraries was performed using a Qubit Fluorometer and the High Sensitivity NGS Fragment Kit for Agilent's Fragment Analyzer (Agilent, Santa Clara, CA, USA). V3 and v3.1 gene expression libraries were sequenced on an Illumina NextSeq 500/550 (Illumina) using the High Output Kit v2.5 (75 Cycles; Illumina) with paired end sequencing and 28 cycles for Read 1, 56 cycles for Read 2 and 8 cycles for i7 index to a depth of ca. 200 million reads.

Multiome libraries were sequenced on NextSeq 500/550 using the High Output Kit v2.5 (150 Cycles; Illumina) with paired end sequencing. A custom recipe, provided by Illumina, was used to sequence the multiome ATAC libraries to specify 8 dark cycles at i5 index. Multiome RNA libraries were sequenced with 28 cycles for Read 1, 90 cycles for Read 2 and 10 cycles for both indices to a depth of ca. 200 million reads. For Multiome ATAC libraries the read lengths were 50 cycles for Read 1 (DNA), 8 cycles for i7 index (sample index), 8 dark cycles followed by 16 cycles for i5 index (Barcode), and 50 cycles for Read 2 (DNA).

4.2.3 GENOME ANNOTATION AND ALIGNMENT

For mouse samples I used the ensembl reference genome (release 91). For opossum samples I used assembly monDom5 with a custom annotation provided by Dr. Evgeny Leushkin, for which RNA-seq data form the opossum brain was used to extend the annotation provided by ensembl release 91 as described in (*197*). For echidna samples, assembly mTacAcu1 was used with the RefSeq NCBI annotation (released 2020). For chicken samples, I used genome assembly galGal5 and a custom annotation. The custom annotation, generated by Dr. Evgeny Leushkin, is based on the reference genome annotation from Ensembl release 87, which was extended using chicken brain 3'-RNA-sequencing data as previously described in (*197*). Assembly AnoCar2.0 and the ensembl reference genome annotation (release 104) was used for green anole samples. I used STAR aligner (v 2.7.10a) to produce references for all species and used the STARsolo mode (--soloType CB_UMI_Simple) to align reads to references (--clipAdapterType CellRanger4; --outFilterScoreMin 20; --soloCBmatchWLtype 1MM_multi_Nbase_pseudocounts; --soloUMIfiltering MultiGeneUMI_CR; --soloUMIdedup 1MM_CR; --soloMultiMappers EM) (*198*, *199*).

4.3 ANALYSIS OF SINGLE-NUCLEUS RNA-SEQUENCING

4.3.1 DATA QUALITY CONTROL

Nuclei-containing barcodes were identified based on the number of UMIs and the fraction of intronic reads. Doublets were identified and removed in each library using ScDblFinder (v 1.12; settings: dbr = 0.1; dbr.sd = 1) (*69*). Subsequently, barcodes with a high fraction of mitochondrial reads (chicken adult > 0.03, developmental chicken > 0.1, mouse > 0.05, green anole > 0.2, opossum > 0.05) were removed. Mitochondrial genes were not annotated in the echidna genome. Each library was then clustered and any low-quality

clusters (lower average number of UMIs, higher average fraction of mitochondrial reads, lower average fraction of intronic reads, few differentially expressed genes and spread appearance on the UMAP) were removed.

4.3.2 Integration of replicates per species

Whole datasets, as well as subsets, were integrated as follows. Each library was individually normalized and highly variable genes were identified using the SCTransform function implemented in Seurat (v 4.3.0) (*200*) with residual variance cutoff (variable.features.rv.th) set to 1.4. The fraction of mitochondrial reads was regressed out during normalization (except for echidna datasets). Subsequently, libraries were merged using Seurat's merge function. For chicken datasets, where I had profiled multiple individuals, I chose the union of variable genes, which were called variable in at least two individuals, as the set of variable genes for the merged dataset. Genes whose expression could not be detected in all individuals but were part of the set of variable genes, were set to 0 scaled expression in all libraries, in which expression could not be detected, so they were not lost in the merged object.

For mouse, green anole, opossum and echidna datasets I called variable genes independently for each dissection, if they were variable in at least one individual and were expressed in the other individual (detected in at least 5 cells). I then used the union of these dissection-specific variable genes as the set of variable genes for the whole dataset. As described above, genes, whose expression could not be detected in all individuals, i.e., across dissections, were set to 0 scaled expression.

For the echidna and opossum datasets, and the glutamatergic lineage in the developing chick pallium I used batch integration to achieve a better integration across individuals or developmental stages, respectively. Specifically, I performed Harmony integration (v 0.1.1) (*201*) based on 40 principal components that were computed on the whole dataset or neuronal subsets (echidna) or on glutamatergic lineage dataset (chick), which were merged as described above, before I generated the UMAP projections shown in Fig. 6 and Fig. 18-21 and ran diffusion pseudotime on the chick dataset (see below).

4.3.3 Clustering and annotation

4.3.3.1 Clustering

In all merged datasets, I identified cell classes according to the expression of major known marker genes. Cell populations in the non-neuronal class were only broadly annotated and not clustered further. In the adult chicken dataset, neuronal cell classes were subset and again split into broad groups, which roughly correspond to the annotated subclasses, although the exact subclass annotation was determined post-hoc. These groups were merged, renormalized and integrated as described above, and subsequently clustered using Louvain clustering at different resolutions. The highest resolution was chosen so the dataset was clearly overclustered. The cluster identity of cells at different resolutions was then used to construct a dendrogram using MRtree, which allows to build cluster

hierarchy based on flat clustering obtained for multiple resolutions (*202*). Differentially expressed genes were called between clusters representing nodes of the dendrogram using Seurat's FindMarkers function (min.pct = 0.3; logfc.threshold = 0.2) to decide whether these clusters should be merged. Clusters were merged if we could not identify robust differential expression of any transcription factors or genes related to neuronal function. The green anole and adult mouse datasets were clustered similarly, only that neuronal cell classes were not further split into groups due to overall lower cell numbers. The developing chick dataset was only broadly clustered to define major cell populations shown in Fig. 16C.

Opossum and echidna neuronal subsets were clustered to a resolution which I selected guided by the extent to which populations appeared distinct in the UMAP and exhibited variation in the expression of key marker genes. Echidna excitatory clusters were grouped into broader populations based on lower resolution clustering and shared marker gene expression.

4.3.3.2 Identification of supertypes and subclasses in the adult chicken pallium

Supertype and subclass identity of individual clusters was determined according to their position in a cluster dendrogram, which was constructed for the complete dataset or for neuronal cell classes, and according to low resolution Louvain clustering. To construct cluster dendrograms, I calculated the average expression per cluster of the union of the top 5000 expressed genes per cluster in the dataset or cell class, respectively, using Seurat's AverageExpression function. Gene expression was correlated across clusters using Spearman correlation and the resulting correlation matrix was used as an input for hierarchical clustering using pvclust (method.hclust = "ward.D2", nboot = 1000) (*203*). For the dendrogram of excitatory neuron clusters I excluded clusters, which likely contained cells inadvertently dissected from the thalamus (*TCF7L2*+) (*160*).

4.3.3.3 Annotation of adult mouse data

Since I expected little overlap between cell populations from different dissections (frontal isocortex or ventro-lateral pallial regions, see Fig. 8A, I analyzed dissections separately. Libraries from each dissection were integrated and clustered as detailed above. Subsequently I used CCA-based integration and label transfer implemented in Seurat (*151*) to transfer labels from different subsets of external datasets to our data to aid with annotation (see below). Specifically, I used subsets of (*82*) to annotate our data for the frontal isocortex, since dissections overlap between the two datasets. To aid with annotation of our data for ventro-lateral pallial derivatives, I used different datasets which partly covered the regions we dissected (*82*, *83*, *154*). Especially cell populations of the piriform cortex were annotated using available in situ hybridization data (*155*) of identified marker genes, since this region was not covered in any external dataset at the time. I named overlapping populations according to the supertype and subclass nomenclature introduced in (*82*) and only introduced new names for non-overlapping

populations. To create the final adult mouse pallium dataset, I subsampled 300 cells per neuronal supertype from all profiled regions in (*82*) and integrated this subset with our datasets from both dissections.

4.3.3.4 Annotation of lizard data

Libraries from all dissections (cortex and DVR) were integrated and clustered as detailed above. Clusters were assigned a probable regional identity according to the expression of marker genes, whose *in situ* expression is known in other reptiles, and according to comparisons to available scRNA-seq data from the pallium of one turtle and another lizard species (*41*, *42*, *72*). For details on comparisons across species see below.

4.3.3.5 Annotation of developing mouse pallium

Data from (*80*) was subset as described in chapter 2.2.1.2. The subset was integrated as described under data integration, followed by batch integration using Harmony (*201*) to produce the UMAPs shown in Fig. 9. In order to annotate early neurons in more detail, I subset late intermediate progenitor cells and neurons and ran the same integration procedure before clustering to a high resolution. Clusters of early neurons were annotated based on the expression of known marker genes and spatial expression of identified marker genes in available *in situ* hybridization data (*204*). Radial glia and intermediate progenitor cells (IPCs) were not annotated in more detail.

4.3.4 Supertypes shared across regions – dendrogram and differential gene expression

I used snRNA-seq data from two individuals (one profiled using 10x Chromium Single Cell 3' v3.1 Gene Expression Kit, the other using 10x Chromium single cell multiome ATAC + gene expression kit) for which the pallium was dissected into anatomical regions, to construct a dendrogram of supertypes split by dissection. For one individual I pooled the "anterior DVR" and "posterior DVR" samples *in silico* to represent the DVR. I identified "shared" excitatory supertypes as supertypes with at least 35 cells from both DVR and hyperpallium dissections in both individuals. The datasets were subset to shared supertypes and cells were subsampled for roughly equal contribution from both individuals per supertype, with a maximum of 300 cells per supertype and dissection. If one individual had fewer than 100 cells per supertype and dissection, the other individual was subsampled to contain 100 cells. Subsequently, data from both individuals was merged and I calculated average gene expression per supertype and dissection across all expressed genes using Seurat's AverageExpression function. Average gene expression of supertypes per dissection were correlated using Spearman correlation, and the resulting correlation matrix was hierarchically clustered using pvclust (method.hclust = "ward.D2", nboot = 1000) (*203*).

To identify differentially expressed genes between supertypes shared across regions, I used the same dataset as described above, but did not subsample cells before merging data from both individuals. Counts were aggregated per dissection and supertype using

Seurat's AggregateExpression function and significantly (adjusted p-value <= 0.05) differentially expressed genes were identified using DESeq2 (v 1.38.3) (*205*) according to the standard workflow.

4.4 COMPARISON ACROSS SPECIES

4.4.1 COMPARISONS ACROSS MAMMALIAN LINEAGES

For CCA-based label transfer from the murine to opossum and echidna isocortex datasets, 1:1 orthologous genes were identified using OrthoFinder (v 2.5.4) (*206*). The species and genomes used for OrthoFinder are listed in Table 1.

Table 1 Species and genomes used for OrthoFinder to determine orthologous genes across mammals.

Species	Genome assembly
Mus musculus	GRCm38
Callithrix jacchus	mCalJac1.pat.X
Homo sapiens	GRCh38
Loxodonta Africana	LoxAfr3
Vombatus ursinus	bare-nosed_wombat_genome_assembly
Monodelphis domestica	ASM229v1
Tachyglossus aculeatus	mTacAcu1
Ornithorhynchus anatinus	mOrnAna1.p.v1
Sarciphilus harrisii	mSarHar1.11

For label transfer I identified all 1:1 orthologs, which could be detected in both species. I then subset each dataset to the chosen set of genes and ran the standard Seurat pipeline (v 4.3.0) to map and annotate query datasets, using canonical correlation analysis (CCA) as the reduction method (*151*). To calculate the weighted fraction shown in Fig.7, I first calculated the fraction of cell type populations in one species predicted to belong to cell type populations in the other species. I then weighted this fraction by the average prediction score for each prediction.

4.4.2 COMPARISONS ACROSS AMNIOTE LINEAGES

For adult cross-amniote comparisons I used three different methods to compare adult cell type populations across species, namely gene specificity index (GSI) correlation as described in (*41*), Seurat's CCA-based integration with label transfer (*151*) and SAMap (v1.0.7) (*181*). To calculate the similarity score, scores resulting from each method were scaled from 0 to 1 and added, meaning the similarity score can range from 0 to 3 for all adult comparisons. I excluded immature neuron populations from these comparisons, as these were not detected in all species, and to avoid adding the extra dimensionality of development. For each method and comparison, I determined the top reciprocal matches per cell type population by finding the overlap between the top five most similar populations for each cell type population as viewed from one species and the top five

most similar populations as viewed from the other species.

For GSI correlation and CCA-based label transfer, 1:1 orthologous genes were identified using OrthoFinder (v 2.5.4) (*206*). The species and genomes used for OrthoFinder are listed in Table 2. The standard SAMap workflow includes a BLAST-based approach to identify orthologous genes.

Table 2 Species and genomes used for OrthoFinder to determine orthologous genes across amniotes.

Species	Genome assembly
Mus musculus	GRCm38
Homo sapiens	GRCh38
Monodelphis domestica	ASM229v1
Chrysemys picta bellii	Chrysemys_picta_BioNano-3.0.4
Chelydra serpentina	Celydra_serpentina-1.0
Pogona vitticeps	pvi1.1
Anolis carolinensis	AnoCar2.0v2
Crocodylus porosus	CroPor_comp1
Taeniopygia guttata	bTaeGut1_v1
Gallus gallus	Gallus_gallus-5.0

To mitigate any differences in power to identify shared gene expression across species between different cell type populations within one species, I subsampled cells and UMIs within each species. Specifically, for label transfer and SAMap, cell populations containing more than the median cell number were subsampled to the median cell number. For GSI correlation, I additionally subsampled UMI counts per cell in large cell type populations (cell number > median cell number) because I saw that this approach is especially sensitive to differences in power, as large populations on average always showed higher correlations. The mouse datasets were subsampled so that cells from our own dataset were preferred over cells from (*82*) in shared populations. For the comparison to the entirely external mouse dataset (*76*) the dataset was subset to glutamatergic neurons from pallial regions (excluding neuroblasts) before subsampling 300 cells per supertype identity, which were then used in the comparison.

Seurat CCA-based label transfer: For label transfer I identified all 1:1 orthologs, which could be detected in both species. I then subset each dataset to the chosen set of genes and ran the standard Seurat pipeline (v 4.3.0) to map and annotate query datasets, using canonical correlation analysis (CCA) as the reduction method (*151*). To calculate one third of the overall similarity score, I first calculated the fraction of cell type populations in one species predicted to belong to cell type populations in the other species. I then weighted this fraction by the average prediction score for each prediction. Values from one comparison (two species, glutamatergic and/or GABAergic neurons) were then scaled between 0 and 1.

GSI correlation: For GSI correlation, I first calculated the average expression of all genes per cell type population in the subsampled datasets of each species. I then subset the expression matrix to genes, which were robustly expressed in both species i.e. genes which showed an average expression of at least 5 UMIs summed across all cell type populations, and which were expressed by at least 2% of cells of at least one cell type population in both species in the complete dataset (not subsampled). I then calculated the gene specificity indices according to (*41*) and correlated cell type populations based on the calculated indices using spearman correlation. I scaled the resulting correlation between 0 and 1.

SAMap: I used datasets subsampled as detailed above to run the standard SAMap workflow (*181*). When constructing the SAMap object, I set "keys" to the highest resolution defined in the dataset, which was usually clusters. When running the SAMap algorithm I set "neigh_from_keys" to the levels of annotation I wanted to compare. Resulting cell type mapping scores were scaled from 0 to 1.

Comparison of developmental mouse and chicken datasets: As explained in the results section I did not subsample cell type populations for the comparison. Since GSI correlation is particularly sensitive to differences in cell number and number of detected genes, I decided to only use SAMap and Seurat CCA label transfer for this comparison, meaning the maximum similarity score is 2.

4.4.3 Identification of excitatory neuron lineages in the developing chicken pallium

To identify different lineages of early excitatory neurons in the developing chicken pallium, I adapted an approach previously established to identify cellular lineages in mouse embryogenesis (*178*). Therefore, cells of the excitatory lineage were subset and split by developmental stage. Data for each stage was normalized and integrated separately as described in chapter 4.3.2 with minor adaptations. The residual variance cutoff was set to 1.3 and variable genes of the merged object encompassed all variable genes which were called variable in at least one individual and detected in at least two individuals. Integrated datasets per stage were clustered to high resolutions and subsequently integrated with the previous and following stages using Harmony integration (*201*) to calculate a shared UMAP embedding. I then used a k-nearest-neighbor (k-NN) heuristic on the shared embeddings, as described in (*178*), to connect "pseudoancestor" and "pseudodescendant" populations across stages with weighted edges resulting in a weighted graph. Because the weighted graph was too complex to examine visually, I filtered out edges with a weight below 0.1 and applied leiden clustering implemented in igraph (v 1.4.2) with different resolution parameters (n_iterations = 4, objective_function = 'modularity') (*207*) to identify potential lineages of early neurons. I identified four major lineages which encompassed most neurons in the dataset. Some populations of the earliest and most mature neurons formed separate leiden

communities at higher resolutions likely because these are highly similar across few stages and are connected to later or previous stages, respectively, by low weight edges only. To assign these largely disconnected populations to lineages, I identified marker genes of the four major identified lineages using Seurat's FindMarkers function and different subsets of cells per lineage with high or low pseudotime values and evaluated the expression of these genes in populations with unidentified lineage identity. I could assign a clear lineage identity to most cell populations, although some could not be unambiguously assigned and remained "unknown" or were named after their two most closely related lineages.

4.4.4 PSEUDOTIME

I calculated diffusion-based pseudotime (*177*) implemented in scanpy (v 1.9.3) for the excitatory neuron lineage in the developing chicken pallium as described in (*176*). Briefly, I used Harmony-corrected components to construct a graph based on the 20 k-nearest neighbors of each cell. A diffusion map was computed based on the neighborhood graph and was used as input for pseudotime estimated with zero branchings. The root of the pseudotime was specified as a random cell belonging to the earliest developmental stage (E6) and to a cluster of non-cycling radial glia (Ex_PCs).

4.4.5 CORRELATION OF EARLY NEURON LINEAGES

The four major lineages of early neurons identified in the developing chicken pallium (HyperP, medial/ArcoP, MesoP and NidoP) were split into six bins according to pseudotime. Pseudotime - lineage bins were correlated using Pearson correlation of average expression across variable genes identified in the whole excitatory lineage as described in chapter 4.3.2.

4.5 IN SITU SEQUENCING (ISS)

Samples embedded in OCT mounting medium were cryosectioned into 10 µm sections and stored at −80 °C until further use. Sections were processed for ISS using the High Sensitivity Library Preparation Kit from CARTANA AB (now 10x Genomics) (*208*). After fixation in 3.7% (v/v) paraformaldehyde in UltraPure distilled water for 10 min, sections were processed in SecureSeal hybridization chambers (Grace Bio-Labs) following the manufacturer's protocol. The mounted sections were shipped to CARTANA's facility (Solna, Sweden) for ISS. The 50 chosen profiled genes (Table S1) represent marker genes with medium expression levels identified from the chicken adult dataset, as well as known markers from mammals. In order to assign identities to cells in the sections, segmentation of cells is needed. Therefore, I first segmented cells based on the DAPI image (Fig. S7A) only, using an approach provided by CARTANA which is based on intensity thresholding and a watershed segmentation (*209*). I then used this segmentation as a prior distribution for baysor (v 0.5.1) (*210*), which allows to incorporate information from gene molecule positions as well as the DAPI image. Baysor was run with the following specifications: scale = 12, scale_std = 3, prior-segmentation-confidence = 0.2, min_molecules_per_cell = 3. The segmentation output of baysor was evaluated visually (Fig. S7B).

Following segmentation, I used Tangram (v1.0.4) (*159*) to map snRNA-seq data to tissue sections. As spatial data input to Tangram, I subset baysor output to cells mostly located in the pallium in order to mimic the dissections used for snRNA-seq and make the spatial and snRNA-seq data most comparable, since Tangram also takes abundances of populations into account. I then integrated the chosen subsets of cells in each section with the complete snRNA-seq dataset from the adult chicken using the cluster mode and all 50 spatially profiled genes, resulting in a matrix containing mapping probabilities for each cell in the section to each identity in the snRNA-seq dataset. I separately mapped class as well as supertype labels to all cells in the sections. Cells were confidently assigned a supertype identity if cell class as well as supertype label assignment were in agreement (e.g., a cell with supertype identity Ex_CACNA1H_PROX1 should also be identified as an excitatory neuron), and the cell belonged to the top 75% of cells with the highest probability for this supertype.

To assess the robustness of my cell type mappings, I calculated the Spearman correlation of expression profiles across all 50 genes profiled by ISS between supertypes identified in the snRNA-seq data and those in the ISS data (Fig. S7B). Specifically, I used Seurat's AverageExpression function to compute the mean expression of the 50 profiled genes for each supertype in the snRNA-seq dataset. For the ISS data, I calculated the mean expression of these genes per section and supertype by averaging the molecule counts (produced by baysor) across cells that were confidently assigned to a supertype. These analyses reveal that cells sharing the same supertype labels in the snRNA-seq and ISS datasets exhibit the highest correlation within at least one of the profiled tissue sections, while also identifying mappings that require further validation using Visium.

4.6 VISIUM

Samples embedded in OCT mounting medium were cryosectioned into 10 µm sections and collected on Visium Spatial Gene Expression slides (10x Genomics). Dr. Bianka Berki fixed the slides in methanol and stained them using Hematoxylin & Eosin staining as suggested by 10x genomics. She took images images with an Olympus VS200 Slide Scanner (20X magnification; Fig. S8) before she processed the slides using the Visium Spatial Gene Expression Reagent Kit (10x) according to the manufacturer's instructions. Sections from adult samples were permeabilized for 18 min, embryonic day 19 sections for 16 min. cDNA and library concentrations were quantified using the Qubit Fluorometer with the DNA High Sensitivity kit. cDNA quality was assessed on Bioanalyzer High Sensitivity DNA chips. Library quality was assessed using Agilent's TapeStation with the D1000 kit. Subsequent steps were carried out by me. Visium libraries were sequenced on an Illumina NextSeq500/550 using the High Output Kit v2.5 (75 Cycles) with paired end sequencing and 28 cycles for Read 1, 56 cycles for Read 2 and 8 cycles for i7 index to a depth of ca. 200 million reads. Reads were mapped to our custom annotation (see above) using Space Ranger (v2.0.1) with default settings.

4.7 Analysis of multiome data

The following analyses were conducted in collaboration with Dr. Ioannis Sarropoulos. He used our custom chicken genome annotation to create reference files for cellranger-arc (v2.0.1) and ArchR (v1.0.2). Single-nucleus multiome libraries were demultiplexed and aligned to the genome using cellranger-arc (v2.0.1).

4.7.1 Identification of High-Quality Cells

The following analyses were carried out by Dr. Ioannis Sarropoulos. Barcodes corresponding to high-quality cells were identified based on the following four metrics: Number of UMIs (for full-length transcripts), fraction of intronic reads, number of ATAC fragments and transcription start site (TSS) enrichment scores (estimated by ArchR).

Gaussian mixture models (v5.4.7) were applied to separate barcodes into two groups for each metric. Only barcodes in the higher-value group across all four metrics were considered. Additionally, barcodes were required to have at least 40% of the median number of UMIs for putative cells in the sample to be considered high-quality.

To filter doublets, we used scrublet (v0.2.3) for the gene expression modality and ArchR for the chromatin accessibility modality. Doublet scores were standardized within each modality as Z-scores, and a consensus doublet score was calculated as the mean of the two scores for each barcode. Barcodes ranking in the top 10% of the consensus doublet score or the top 5% in either modality were excluded.

4.7.2 Gene Expression Recalculation and Integration

The following analyses were carried out by me. For high-quality cells, gene expression counts were recalculated using STARsolo for consistency with other datasets. Multiome gene expression data were integrated with the full snRNA-seq dataset using Harmony (*201*), creating a unified embedding.

Unannotated cells were assigned cell type labels based on the 20 nearest annotated neighbours in the integrated embedding. The most frequent label among the 20 neighbours was assigned, and a confidence score was calculated as the fraction of neighbours with that label. Only cells with at least 15 (75%) consistent neighbours were retained. For glutamatergic neuron subtypes, the annotation procedure was repeated in a subsetted embedding containing only glutamatergic neurons. Cells retaining consistent labels in both rounds of annotation were kept for downstream analyses. This stringent annotation strategy yielded a total of 8,119 high-confidence cells.

4.7.3 Chromatin Accessibility Profiling

The following analyses were carried out by Dr. Ioannis Sarropoulos. Chromatin accessibility was quantified for these 8,119 cells across 500 bp genomic tiles using ArchR. Iterative latent semantic indexing (LSI) was applied over five iterations with increasing resolutions (0.1, 0.2, 0.4, 0.8) to project the data into 100 dimensions.

Fragment files were subsetted by cell type and brain region, then input into MACS (v2.1.2) for peak calling with the following parameters: -f BEDPE --nomodel --nolambda --extsize 150 --shift -75 --keep-dup all -q 0.05 --gsize 1.2e9 --call-summits.

Peak calling was performed at all three levels of hierarchical annotation (e.g., cell types, brain regions) to maximize granularity while retaining the ability to detect shared peaks. ArchR's peak merging procedure was then used to create a consensus peak set, resulting in 367,896 peaks. This peak set was imported into ArchR for downstream analyses using addPeakSet and addPeakMatrix.

4.7.4 Aggregated Chromatin Accessibility Profiles

The following analyses were carried out by Dr. Ioannis Sarropoulos. To assess cell type- and brain region-specific chromatin accessibility, peak counts were aggregated across groups with at least 40 cells. Spearman's correlations were calculated using peaks with a minimum of 10 CPM in at least one group. The resulting correlation matrix was hierarchically clustered to evaluate the relationships between cell types and brain regions.

4.7.5 Differentially Accessible Regions (DARs)

The following analyses were carried out by Dr. Ioannis Sarropoulos. ArchR's getMarkerFeatures function was used to identify differentially accessible regions (DARs) between cell types and brain regions. Analysis accounted for TSS enrichment bias, fragment counts per cell, and included groups with at least 40 cells. DARs were filtered for statistical significance (FDR < 5%) and a log2 fold-change of ≥ 1.25, resulting in 12,595 DARs across all cell types.

For visualization, the pseudobulk peak count matrix (cell type × brain region) was normalized for sequencing depth (counts per million, CPM) and scaled by each peak's maximum accessibility across pseudobulks.

5 LIST OF ABBREVIATIONS

Abbreviation	**Full name**
ACA	Anterior cingulate area
aDC	Anterior dorsal cortex
aDVR	Anterior DVR
AI	Intermediate arcopallium
aLC	Anterior dorsal cortex
amDVR	Anterior medial DVR
amDVR	Anterior medial DVR
AMV	Medial ventral arcopallium
Amy	Amygdala
Amy	Amygdala
AON	Anterior olfactory nucleus
APr	Area prostriata
aRGCs	Apical radial glial cells
Aud	Auditory
BAC	Bed nucleus of anterior commissure
BLA	Basolateral amygdala
BMA	Basomedial amygdala
BS	Brain stem
CA	Cornu Ammonis
Cb	Cerebellum
CGE	Caudal ganglionic eminence
Chol	Cholinergic
Cl	Claustrum
CNU	cerebral nuclei
COA	Cortical amygdala
COAa	Anterior cortical amygdala
COAp	Posterior cortical amygdala
CT	Cortico-thalamic projecting
CTX	Cortex
DC	Dorsal cortex
DG	Dentate gyrus
DLA	Dorso-lateral amygdala
DMC	Dorso-medial cortex
DP	Dorsal peduncular area
DVR	Dorsal ventricular ridge
ENTl	Lateral entorhinal cortex
ENTm	Medial entorhinal cortex
Ep	Endopirirform nucleus
EP	Entopallium

EP	Endopiriform nucleus
EPd	Dorsal endopiriform nucleus
ET	extra-telencephalic projecting
ET	Extratelencephalic-projecting
Ex	Excitatory
FC	Fasciola cinerea
GABA	gamma-aminobutyric acid releasing
H	Hyperpallium
HA	Apical hyperpallium
HD	Densocellular hyperpallium
HI	Intercalated hyperpallium
Hip	Hippocampus
HPF	Hippocampal formation
Hy	Hypothalamus
Hya	anterior hypothalamus
I	Insular cortex
IG	Indusium griseum
IHA	Interstitial apical hyperpallium
ILA	Infralimbic area
IMN	Immature neurons
Inh	Inhibitory
ISS	In situ sequencing
IT	Intra-telencephalic
L	Layer
LA	Lateral amygdala
LC	Lateral cortex
LGE	Lateral ganglionic eminence
LHA	Lateral hypothalamic area
LMI	Lamina mesopallialis intermediate
LPO	Lateral preoptic area
M	Mesopallium
MA	Magnocellular nucleus
Mb	Midbrain
MC	Medial cortex
MEA	Medial amygdala
MGE	Medial ganglionic eminence
Mo	Motor
MS	Medial septal nucleus
N	Nidopallium
NLOT	Nucleus of the lateral olfactory tract
NP	Near-projecting
OB	Olfactory bulbs

Oligo	Oligodendrocytes
OPCs	Oligodenrocyte progenitor cells
Orb	Orbital area
P	Pallium
PA	Pallial amygdala
PA	Posterior amygdala
pDC	Posterior dorsal cortex
pDVR	Posterior DVR
Pir	Piriform cortex/area
Pl	Prelimic area
pLC	Posterior lateral cortex
PPP	Parasubiculum, postsubiculum, presubiculum
ProS	Prosubiculum
PS	Primary sensory
PT	Pallial thickening
pTHE	Prethalamic eminence
pyr	Pyramidal
RGCs	Radial glial cells
RHP	Retrohippocampal area
RSP	Retrosplenial area
Sep	Septum
SF	Septofimbrial nucleus
SI	Substantia innominata
snRNA-seq	Single-nucleus RNA-sequencing
Sp	Subpallium
SS	Somato-sensory
Str	Striatum
SUB	Subiculum
SVZ	Subventricular zone
Th	Thalamus
TPE	Temporal association, perirhinal, ectorhinal areas
TRS	Triangular nucleus of septum
TT	Taenia tecta
TT	Taenia tecta
UMI	Unique molecular identifier
va	Vallecula
Vis	Visual
VZ	Ventricular zone

6 SUPPLEMENTARY FIGURES

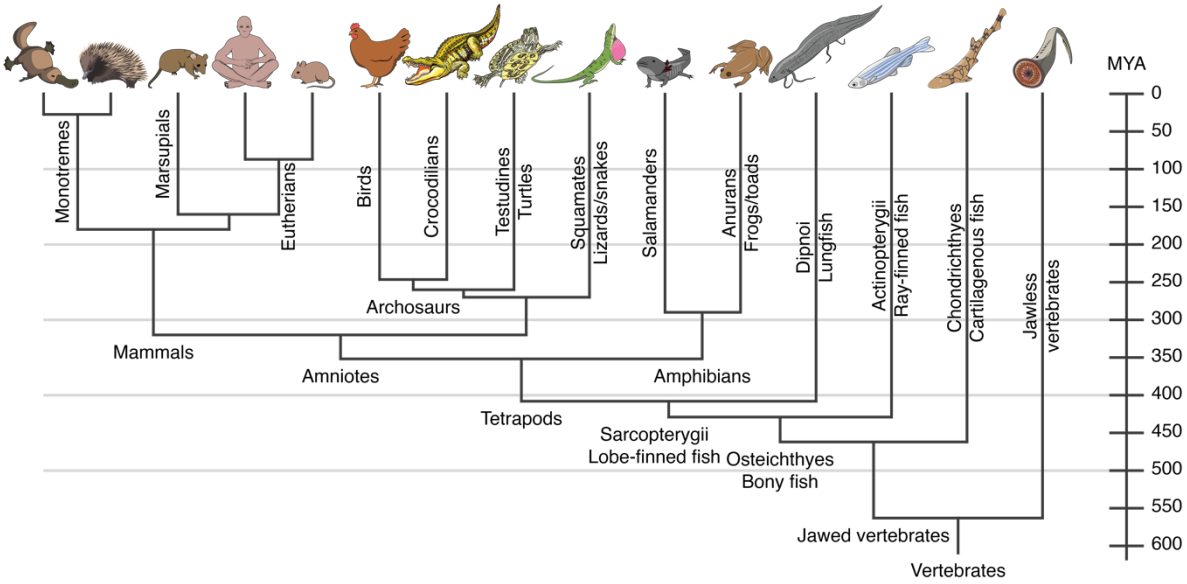

Supplementary figure 1 Vertebrate phylogeny. Phylogeny representing major vertebrate clades with representative species depicted on top. Divergence times were taken from TimeTree 5.0 (6). Species icons were mostly drawn by Nils Trost and Marta Sanchez-Delgado. MYA, million years ago.

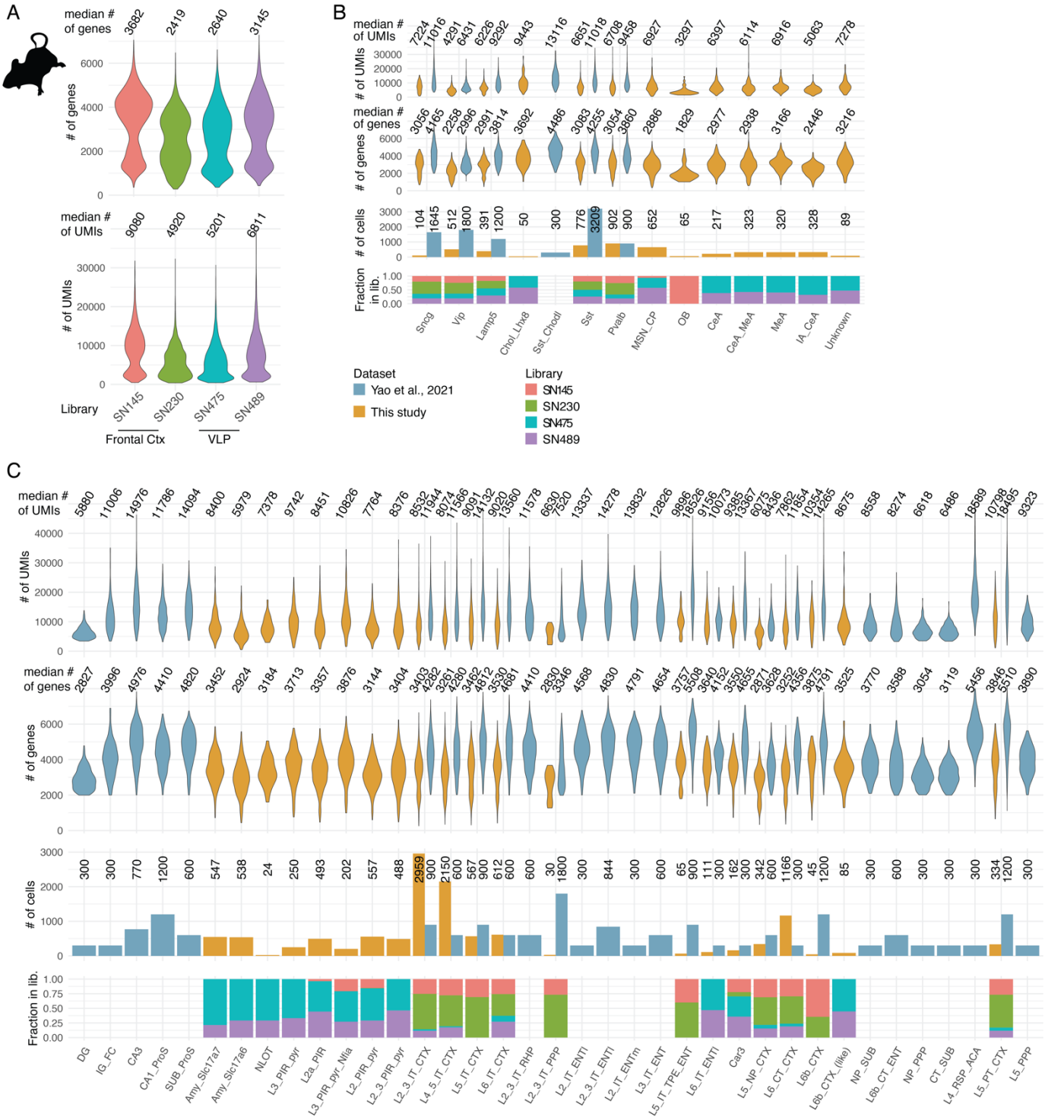

Supplementary figure 2 Adult mouse pallium dataset. (A) Number of UMI counts (bottom) and detected genes (top) per snRNA-seq library in my dataset after selection of high-quality cells coloured by library (each library sampled from a different individual). Ctx, cortex; VLP, structures derived from lateral and ventral pallial areas. Number of UMI counts and detected genes (top), number of cells (mid) per datasets and fraction of cells in our dataset stemming from different snRNA-seq libraries/individuals per inhibitory subclass (B) and excitatory subclass (C). For abbreviations see List of abbreviations.

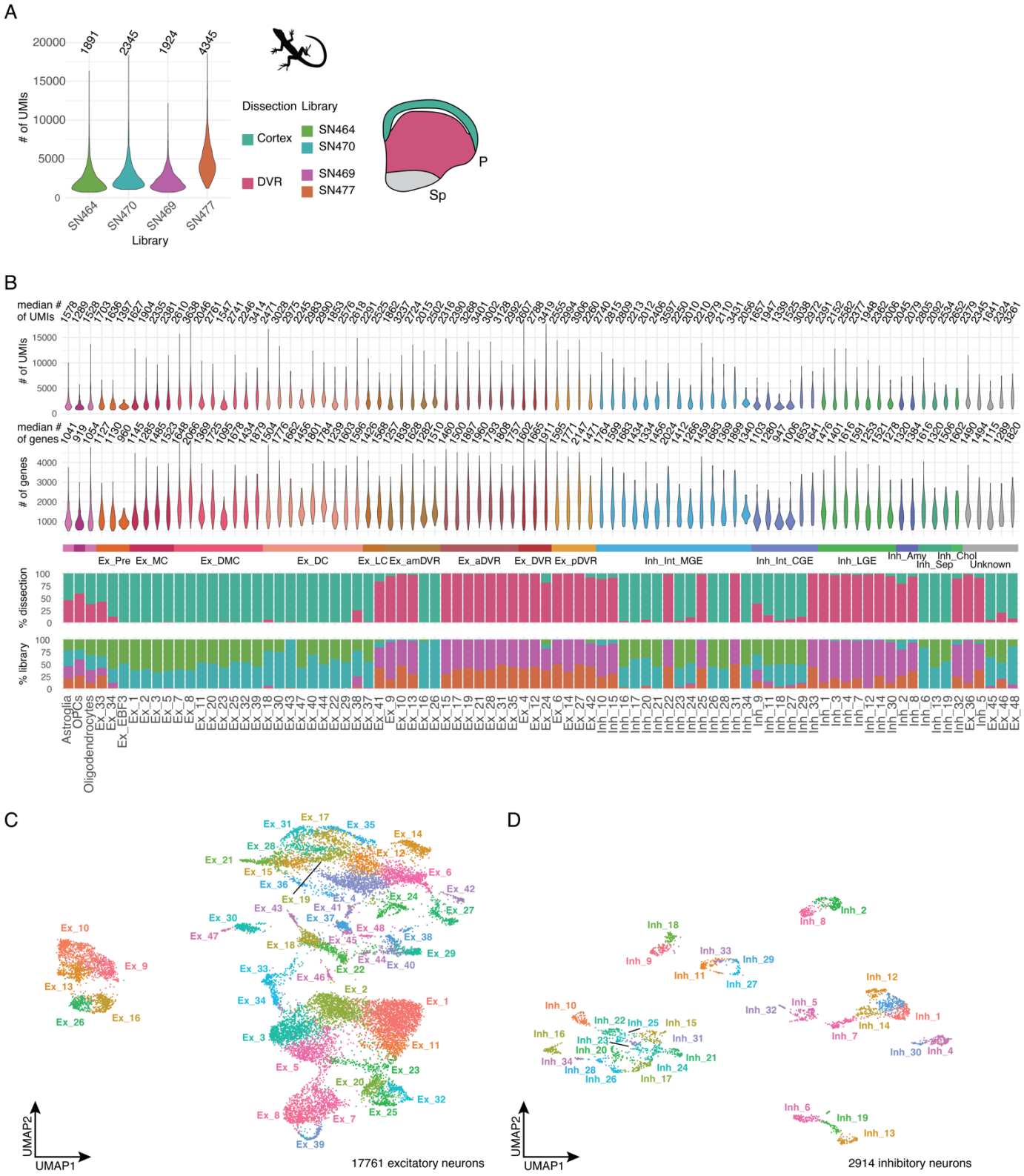

Supplementary figure 3 Lizard pallium single nucleus RNA-sequencing dataset. (A) (left) Number of UMI counts per snRNA-seq library in the *Anolis carolinensis* dataset after selection of high-quality cells coloured by library, together sampling the entire pallium of two individuals. (Right) Illustration of dissections and snRNA-seq libraries per dissection. (B) Number of UMI counts and detected genes (top) per cluster and fraction of cells per cluster stemming from different dissections and snRNA-seq libraries (bottom). UMAP of excitatory (C) and inhibitory (D) neurons coloured by and labelled with cluster annotation. (D) Illustration of dissections and snRNA-seq libraries per dissection.

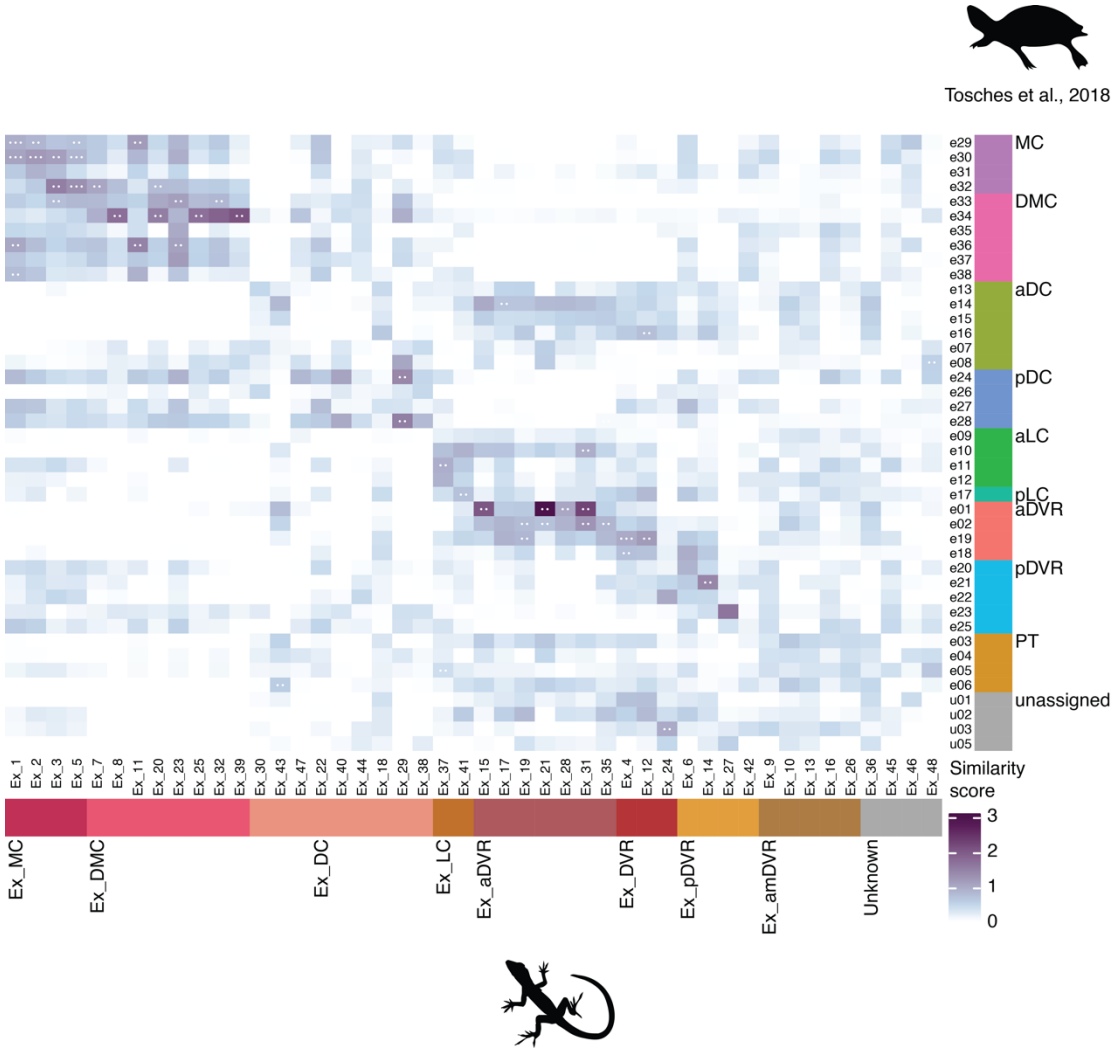

Supplementary figure 4 Comparison of excitatory neurons between lizard and available reptilian datasets. Comparison between *Anolis carolinensis* excitatory clusters and *Trachemys scripta elegans* data from (*41*) using three methods. Scores were scaled between 0 and 1 per method and summed across all methods to represent the similarity score. White dots in tiles are shown when populations are among the top reciprocal matches according to two or all three methods. MC, medial cortex; DMC, dorsal medial cortex; a/pDC, anterior/posterior dorsal cortex; a/pLC, anterior/posterior lateral cortex; a/pDVR, anterior/posterior DVR; PT, pallial thickening; amDVR, anterior medial DVR.

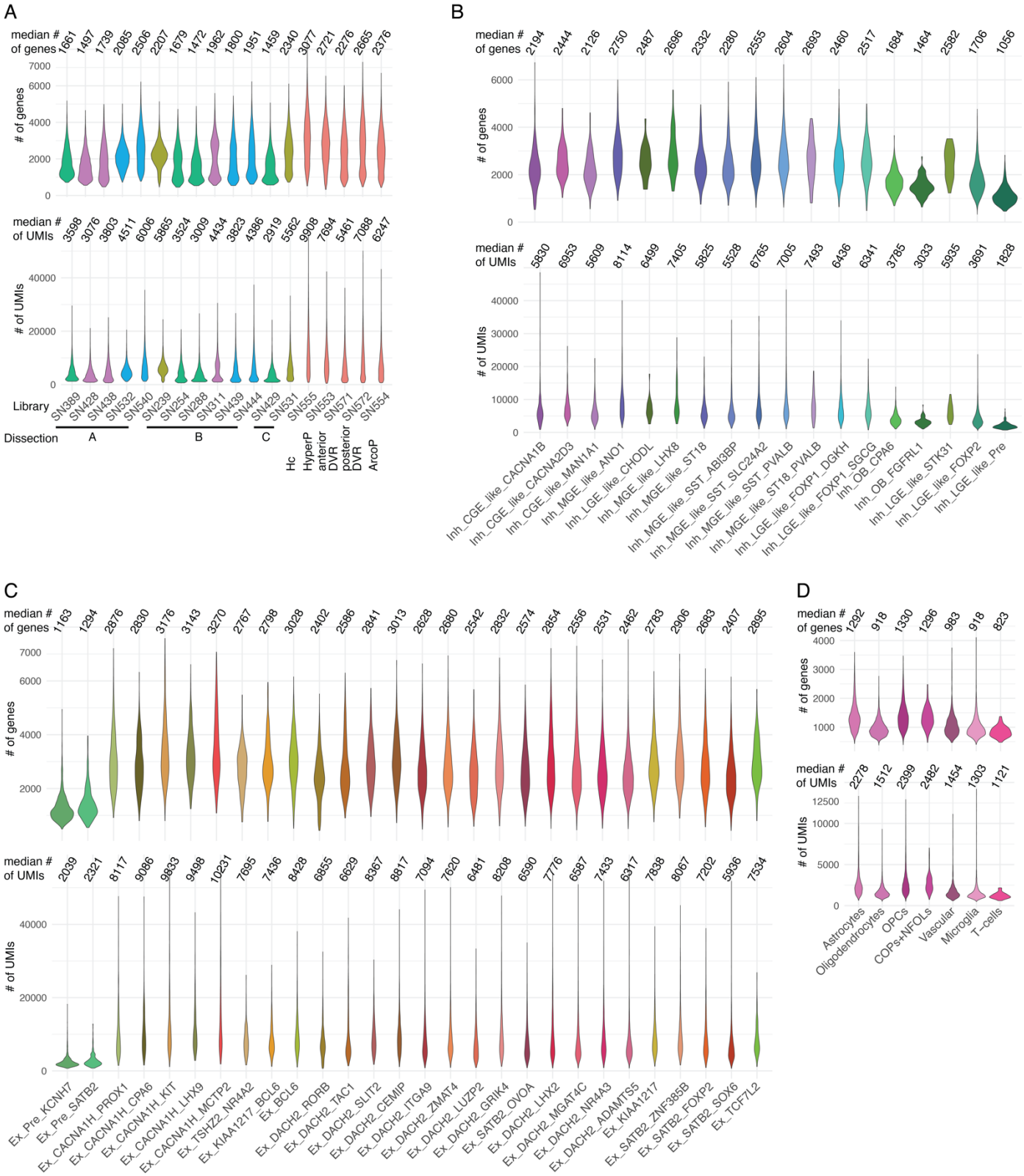

Supplementary figure 5 Adult chicken pallium single nucleus RNA-sequencing statistics. (A) Number of UMI counts (bottom) and detected genes (top) per snRNA-seq library after selection of high-quality cells coloured by sampled individuals. DVR dissections include the nidopallium, including its primary sensory areas like the entopallium, and mesopallium. Hyperpallial dissections include all subdivisions of the hyperpallium as defined by the Avian Nomenclature Forum, meaning apical hyperpallium (HA), interstitial apical hyperpallium (IHA) and densocellular and intercalated hyperpallium (HD/HI). Hc, hippocampal areas; HyperP, hyperpallium; ArcoP, arcopallium. (B) Number of UMI counts (bottom) and detected genes (top) per inhibitory supertype, (C) excitatory supertype, or (D) per cell population of non-neuronal class coloured by cell population/supertype.

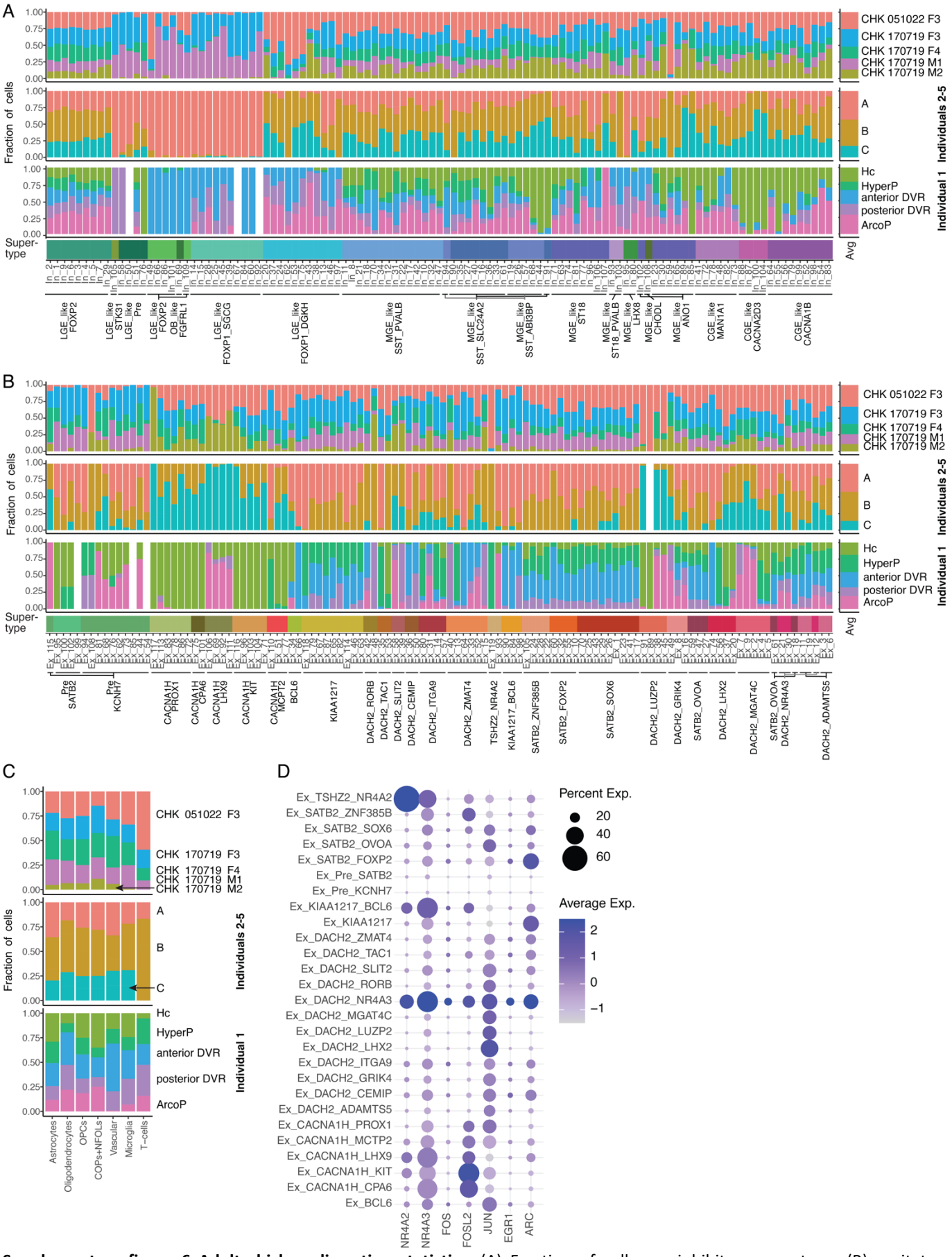

Supplementary figure 6 Adult chicken dissection statistics. (A) Fraction of cells per inhibitory supertype, (B) excitatory supertype, or (C) non-neuronal cell population stemming from sampled individuals (top), broad pallial dissections (individuals 2-5) (mid) or pallial dissections of anatomical regions (individual 1) (bottom). Dissections are illustrated in Fig. 11A. (D) Gene expression dotplot of activity related genes in excitatory supertypes. Hc, hippocampal area; ArcoP, arcopallium; Exp, expression.

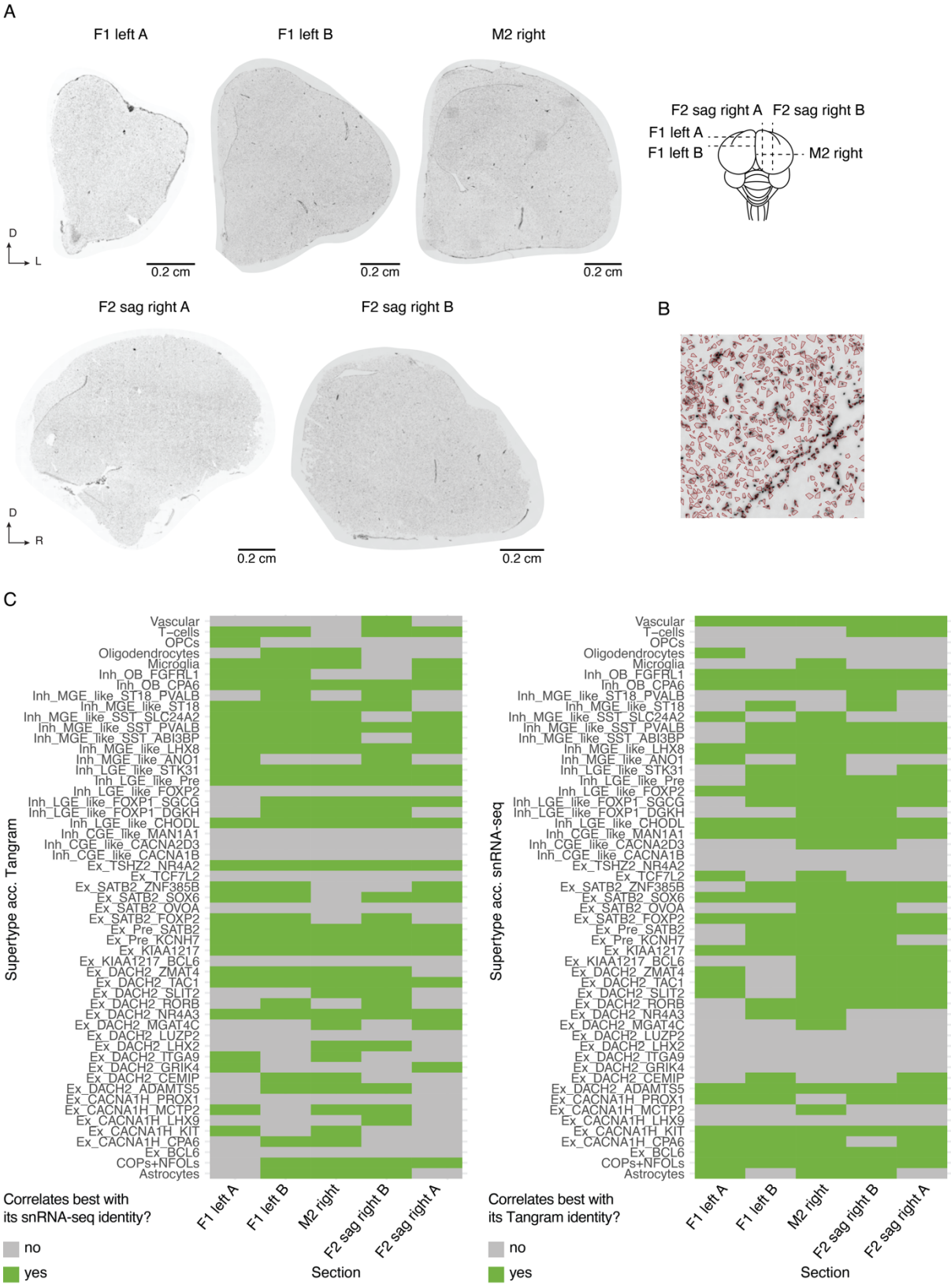

Supplementary figure 7 *In situ* sequencing (ISS). (A) DAPI images of section profiled with ISS titled with information about individual and hemisphere of origin (right). Schematic representation of adult brain viewed from the top to illustrate levels of sections. (B) Example for overlay of baysor output over corresponding DAPI image, where most peripheral detected RNA molecules assigned to each cell are connected. (C) Heatmaps showing if snRNA-seq supertypes correlate best with their spatial counterpart

(and vice versa) based on spearman corelation of gene expression profiles of 50 genes profiled by ISS. See chapter 4.5.

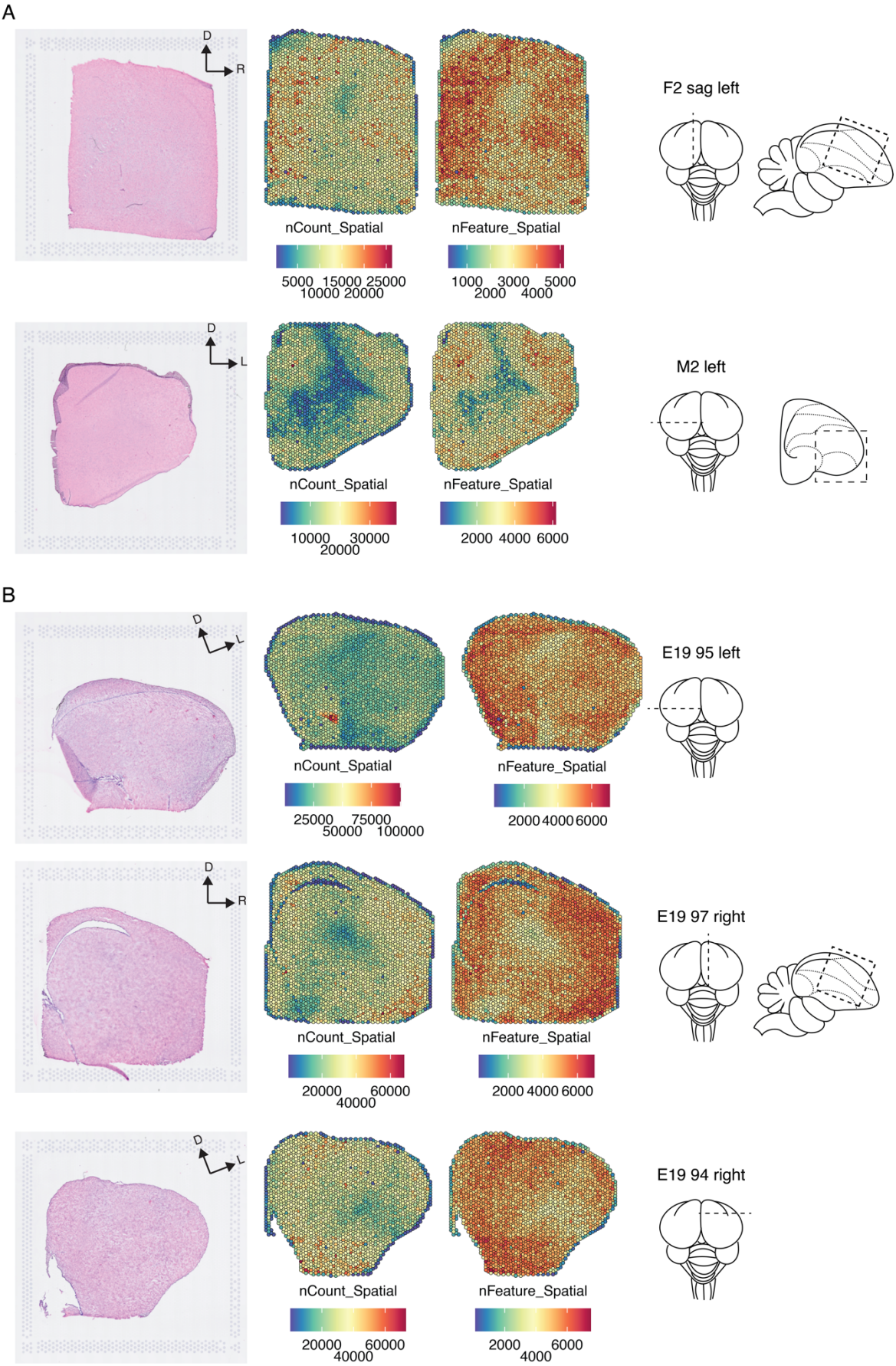
A
D
R
nCount_Spatial
5000 15000 25000
10000 20000
nFeature_Spatial
1000 3000 5000
2000 4000
F2 sag left
D
L
nCount_Spatial
10000 30000
20000
nFeature_Spatial
2000 4000 6000
M2 left
B
D
L
nCount_Spatial
25000 75000
50000 100000
nFeature_Spatial
2000 4000 6000
E19 95 left
D
R
nCount_Spatial
20000 60000
40000
nFeature_Spatial
2000 4000 6000
E19 97 right
D
L
nCount_Spatial
20000 60000
40000
nFeature_Spatial
2000 6000
4000
E19 94 right

Supplementary figure 8 Visium sections and quality metrics. (Sections of the (A) adult and (B) E19 brain profiled by Visium. (Left) Hematoxylin and Eosin stained sections, (middle) number of counts and features detected per dot, and (right) schematic representation of the brain as viewed from the top indicating the location of the sections. D, dorsal; L, lateral; R, rostral.

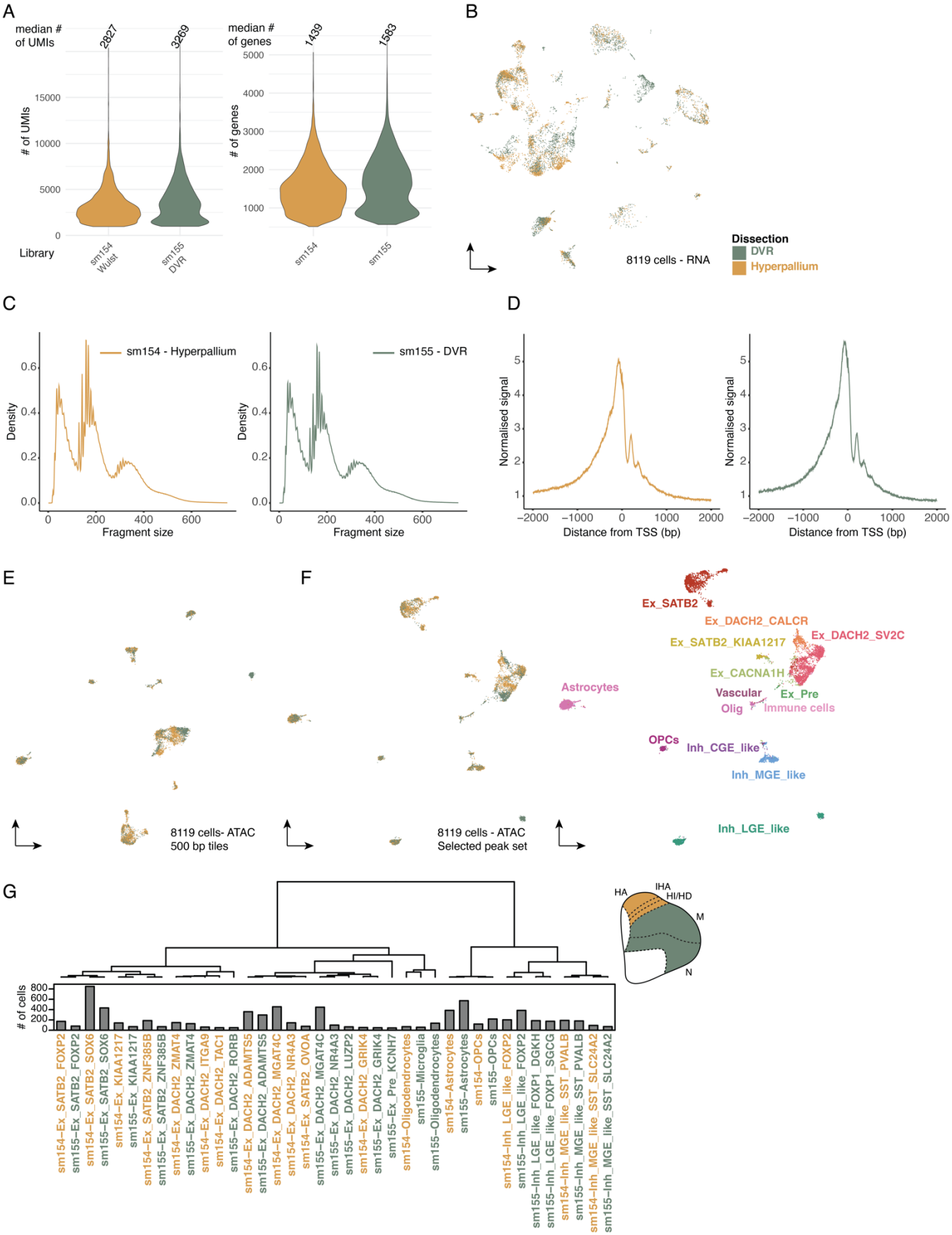
A
median # of UMIs
2827
3269
# of UMIs
15000
10000
5000
0
Library
sm154 Wulst
sm155 DVR
median # of genes
1439
1583
# of genes
5000
4000
3000
2000
1000
sm154
sm155
B
8119 cells - RNA
Dissection
DVR
Hyperpallium
C
sm154 - Hyperpallium
sm155 - DVR
Density
0.6
0.4
0.2
0.0
0
200
400
600
Fragment size
D
Normalised signal
5
4
3
2
1
−2000
−1000
0
1000
2000
Distance from TSS (bp)
E
8119 cells- ATAC
500 bp tiles
F
8119 cells - ATAC
Selected peak set
Ex_SATB2
Ex_DACH2_CALCR
Ex_SATB2_KIAA1217
Ex_DACH2_SV2C
Ex_CACNA1H
Vascular
Ex_Pre
Olig
Immune cells
Astrocytes
OPCs
Inh_CGE_like
Inh_MGE_like
Inh_LGE_like
G
HA
IHA
HI/HD
M
N
# of cells
800
600
400
200
0
sm154−Ex_SATB2_FOXP2
sm155−Ex_SATB2_FOXP2
sm154−Ex_SATB2_SOX6
sm155−Ex_SATB2_SOX6
sm154−Ex_KIAA1217
sm155−Ex_KIAA1217
sm154−Ex_SATB2_ZNF385B
sm155−Ex_SATB2_ZNF385B
sm154−Ex_DACH2_ZMAT4
sm155−Ex_DACH2_ZMAT4
sm154−Ex_DACH2_ITGA9
sm154−Ex_DACH2_TAC1
sm155−Ex_DACH2_RORB
sm154−Ex_DACH2_ADAMTS5
sm155−Ex_DACH2_ADAMTS5
sm154−Ex_DACH2_MGAT4C
sm154−Ex_DACH2_NR4A3
sm154−Ex_SATB2_OVOA
sm155−Ex_DACH2_MGAT4C
sm155−Ex_DACH2_NR4A3
sm155−Ex_DACH2_LUZP2
sm154−Ex_DACH2_GRIK4
sm155−Ex_DACH2_GRIK4
sm155−Ex_Pre_KCNH7
sm154−Oligodendrocytes
sm155−Microglia
sm155−Oligodendrocytes
sm154−Astrocytes
sm155−Astrocytes
sm154−OPCs
sm155−OPCs
sm154−Inh_LGE_like_FOXP2
sm155−Inh_LGE_like_FOXP2
sm155−Inh_LGE_like_FOXP1_DGKH
sm155−Inh_LGE_like_FOXP1_SGCG
sm154−Inh_MGE_like_SST_PVALB
sm155−Inh_MGE_like_SST_PVALB
sm154−Inh_MGE_like_SST_SLC24A2
sm155−Inh_MGE_like_SST_SLC24A2

Supplementary figure 9 SnRNA and ATAC multiome of the chicken pallium. (A) Number of UMI counts (left) and detected genes (right) per snRNA-seq library after selection of high-quality cells colored by library/sampled region. DVR dissections include the nido- and mesopallium. (B) UMAP of snRNA-seq data colored by library/dissection. (C) Fragment size distribution of ATAC libraries. (D) Transcription start site (TSS) enrichment scores of the snATAC-seq libraries. (E) UMAP of snATAC data, based on accessibility across 500bp tiles colored by library/sampled region. (F) UMAP of snATAC data, based on accessibility in selected peak set coloured by library/sampled region (left) and assigned subclass identity (right). (G) Correlation dendrogram of pseudobulk accessibility profiles per supertype and library/region (at least 40 cells). Schematic top right: illustration of borders between dissections. HA, apical hyperpallium; IHA, interstitial apical hyperpallium; HI/HD, intercalated and densocellular hyperpallium; M, mesopallium; N, nidopallium.

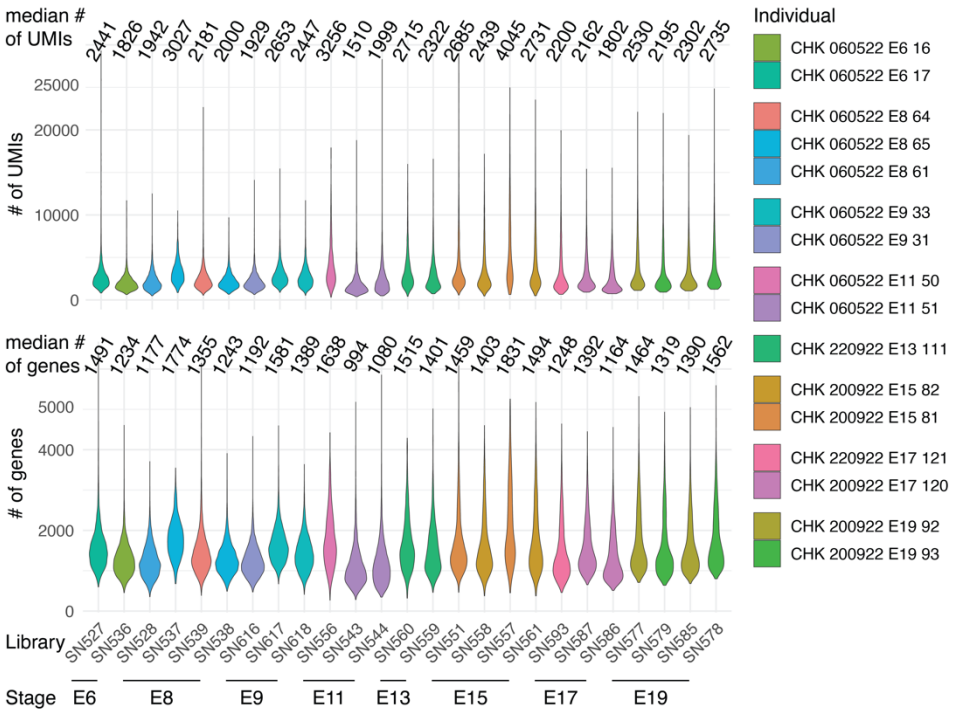

Supplementary figure 10 Developing chicken pallium single nucleus RNA-sequencing dataset. Number of UMI counts (top) and detected genes (bottom) per snRNA-seq library after selection of high-quality cells coloured by sampled individuals.

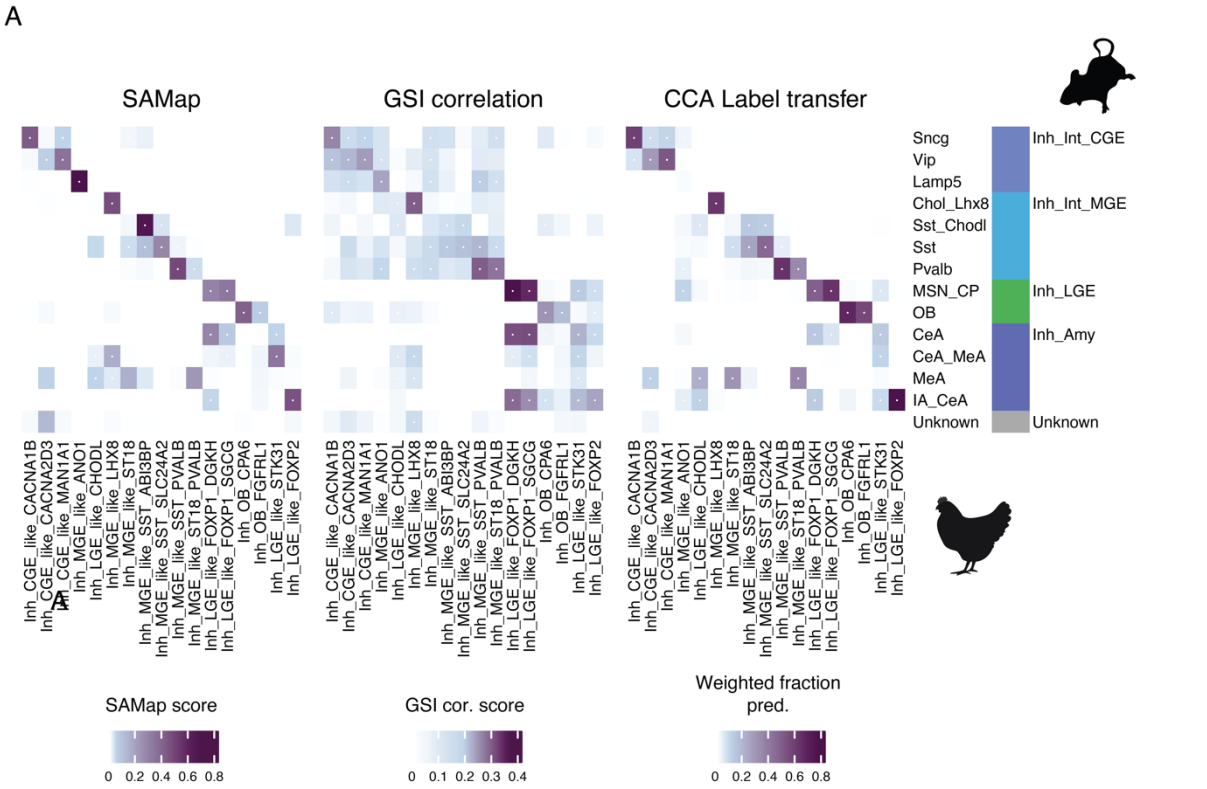
A
SAMap
GSI correlation
CCA Label transfer
Sncg
Vip
Lamp5
Chol_Lhx8
Sst_Chodl
Sst
Pvalb
MSN_CP
OB
CeA
CeA_MeA
MeA
IA_CeA
Unknown
Inh_Int_CGE
Inh_Int_MGE
Inh_LGE
Inh_Amy
Unknown
Inh_CGE_like_CACNA1B
Inh_CGE_like_CACNA2D3
Inh_CGE_like_MAN1A1
Inh_MGE_like_ANO1
Inh_LGE_like_CHODL
Inh_MGE_like_LHX8
Inh_MGE_like_ST18
Inh_MGE_like_SST_ABI3BP
Inh_MGE_like_SST_SLC24A2
Inh_MGE_like_SST_PVALB
Inh_LGE_like_FOXP1_DGKH
Inh_LGE_like_FOXP1_SGCG
Inh_OB_CPA6
Inh_OB_FGFRL1
Inh_LGE_like_STK31
Inh_LGE_like_FOXP2
SAMap score
0 0.2 0.4 0.6 0.8
GSI cor. score
0 0.1 0.2 0.3 0.4
Weighted fraction pred.
0 0.2 0.4 0.6 0.8

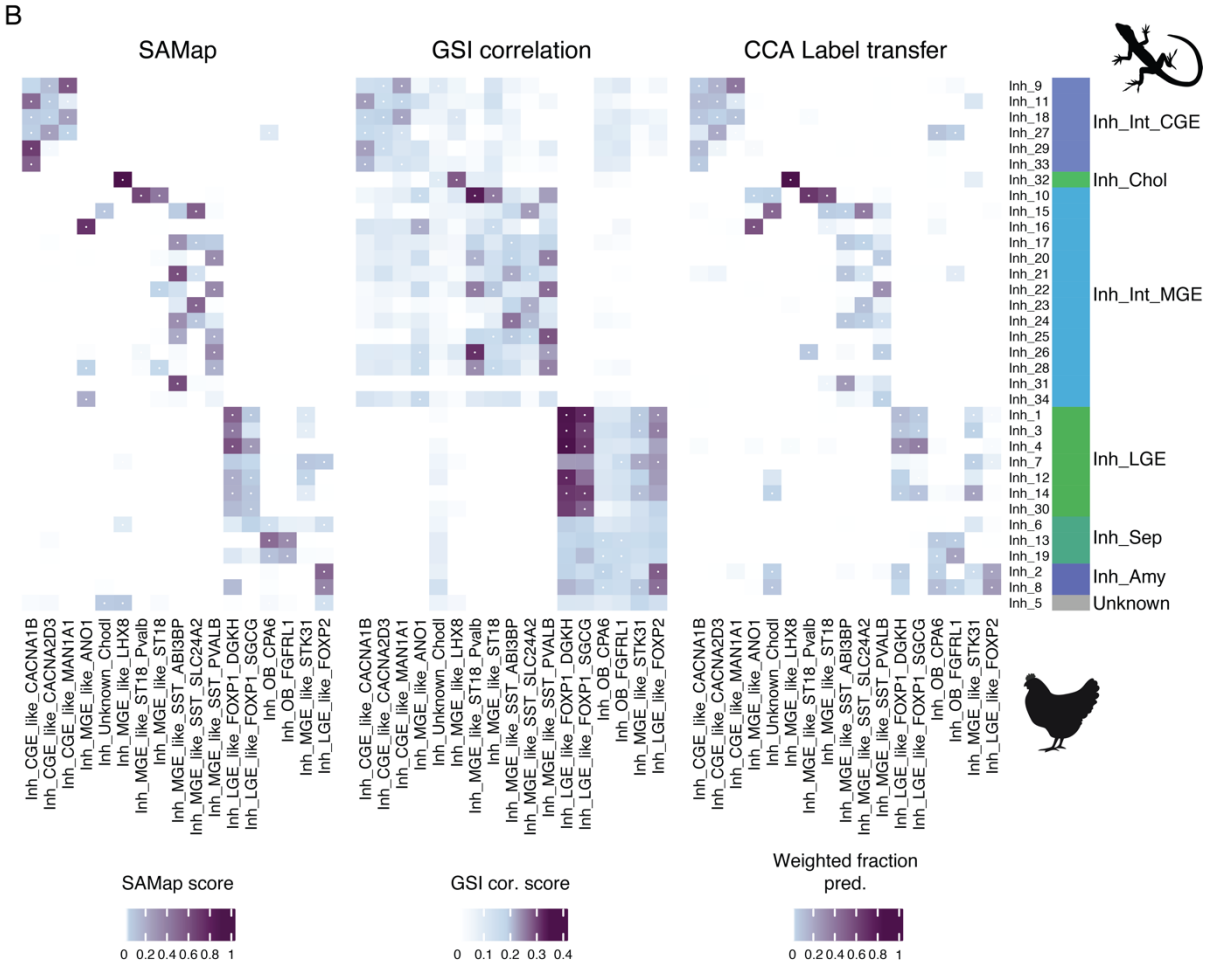
B
SAMap
GSI correlation
CCA Label transfer
Inh_Int_CGE
Inh_Chol
Inh_Int_MGE
Inh_LGE
Inh_Sep
Inh_Amy
Unknown
Inh_CGE_like_CACNA1B
Inh_CGE_like_CACNA2D3
Inh_CGE_like_MAN1A1
Inh_MGE_like_ANO1
Inh_Unknown_Chodl
Inh_MGE_like_LHX8
Inh_MGE_like_ST18_Pvalb
Inh_MGE_like_ST18
Inh_MGE_like_SST_ABI3BP
Inh_MGE_like_SST_SLC24A2
Inh_MGE_like_SST_PVALB
Inh_LGE_like_FOXP1_DGKH
Inh_LGE_like_FOXP1_SGCG
Inh_OB_CPA6
Inh_OB_FGFRL1
Inh_MGE_like_STK31
Inh_LGE_like_FOXP2
SAMap score
0 0.2 0.4 0.6 0.8 1
GSI cor. score
0 0.1 0.2 0.3 0.4
Weighted fraction pred.
0 0.2 0.4 0.6 0.8 1

Supplementary figure 11 Comparison of inhibitory neurons across amniotes (separate methods). Comparison of inhibitory supertypes in the chicken pallium to (A) mouse inhibitory subclasses, or (B) to clusters of inhibitory neurons in the lizard pallium based on three methods. White dots in tiles are shown when populations are among the top five reciprocal matches according to the chosen method.

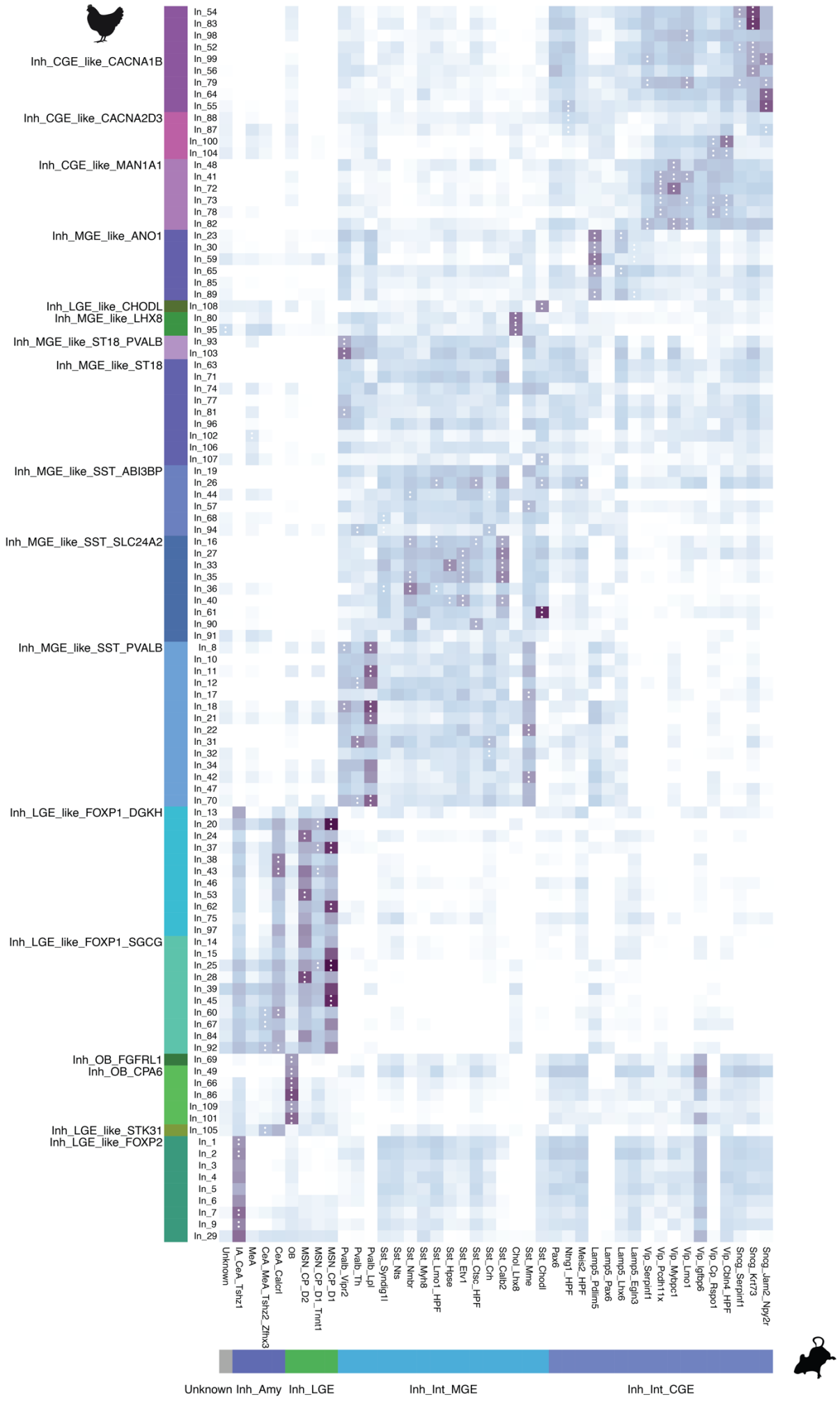
In_54
In_83
In_98
In_52
Inh_CGE_like_CACNA1B
In_99
In_56
In_79
In_64
In_55
Inh_CGE_like_CACNA2D3
In_88
In_87
In_100
In_104
Inh_CGE_like_MAN1A1
In_48
In_41
In_72
In_73
In_78
In_82
Inh_MGE_like_ANO1
In_23
In_30
In_59
In_65
In_85
In_89
Inh_LGE_like_CHODL
In_108
Inh_MGE_like_LHX8
In_80
In_95
Inh_MGE_like_ST18_PVALB
In_93
In_103
Inh_MGE_like_ST18
In_63
In_71
In_74
In_77
In_81
In_96
In_102
In_106
In_107
Inh_MGE_like_SST_ABI3BP
In_19
In_26
In_44
In_57
In_68
In_94
Inh_MGE_like_SST_SLC24A2
In_16
In_27
In_33
In_35
In_36
In_40
In_61
In_90
In_91
Inh_MGE_like_SST_PVALB
In_8
In_10
In_11
In_12
In_17
In_18
In_21
In_22
In_31
In_32
In_34
In_42
In_47
In_70
Inh_LGE_like_FOXP1_DGKH
In_13
In_20
In_24
In_37
In_38
In_43
In_46
In_53
In_62
In_75
In_97
Inh_LGE_like_FOXP1_SGCG
In_14
In_15
In_25
In_28
In_39
In_45
In_60
In_67
In_84
In_92
Inh_OB_FGFRL1
In_69
Inh_OB_CPA6
In_49
In_66
In_86
In_109
In_101
Inh_LGE_like_STK31
In_105
Inh_LGE_like_FOXP2
In_1
In_2
In_3
In_4
In_5
In_6
In_7
In_9
In_29
Unknown
IA_CeA_Tshz1
MeA
CeA_MeA_Tshz2_Zfhx3
CeA_Calcrl
OB
MSN_CP_D2
MSN_CP_D1_Tnnt1
MSN_CP_D1
Pvalb_Vipr2
Pvalb_Th
Pvalb_Lpl
Sst_Syndig1l
Sst_Nts
Sst_Nmbr
Sst_Myh8
Sst_Lmo1_HPF
Sst_Hpse
Sst_Etv1
Sst_Ctsc_HPF
Sst_Crh
Sst_Calb2
Chol_Lhx8
Sst_Mme
Sst_Chodl
Pax6
Ntng1_HPF
Meis2_HPF
Lamp5_Pdlim5
Lamp5_Pax6
Lamp5_Lhx6
Lamp5_Egln3
Vip_Serpinf1
Vip_Pcdh11x
Vip_Mybpc1
Vip_Lmo1
Vip_Igfbp6
Vip_Cp_Rspo1
Vip_Cbln4_HPF
Sncg_Serpinf1
Sncg_Krt73
Sncg_Jam2_Npy2r
Unknown
Inh_Amy
Inh_LGE
Inh_Int_MGE
Inh_Int_CGE

Supplementary figure 12 Cluster level comparison of inhibitory neurons between chicken and mouse pallium. Comparison between chicken clusters and mouse inhibitory supertypes based on three different methods. Scores were scaled between 0 and 1 per method and summed across all methods to represent the similarity score. White dots in tiles are shown when populations are among the top reciprocal matches according to two or all three methods. Amy, amygdala; MSN; medium spiny neuron; CP, caudate putamen; OB, olfactory bulb; CeA, central amygdala; MeA, medial amygdala; IA, intercalated amygdala.

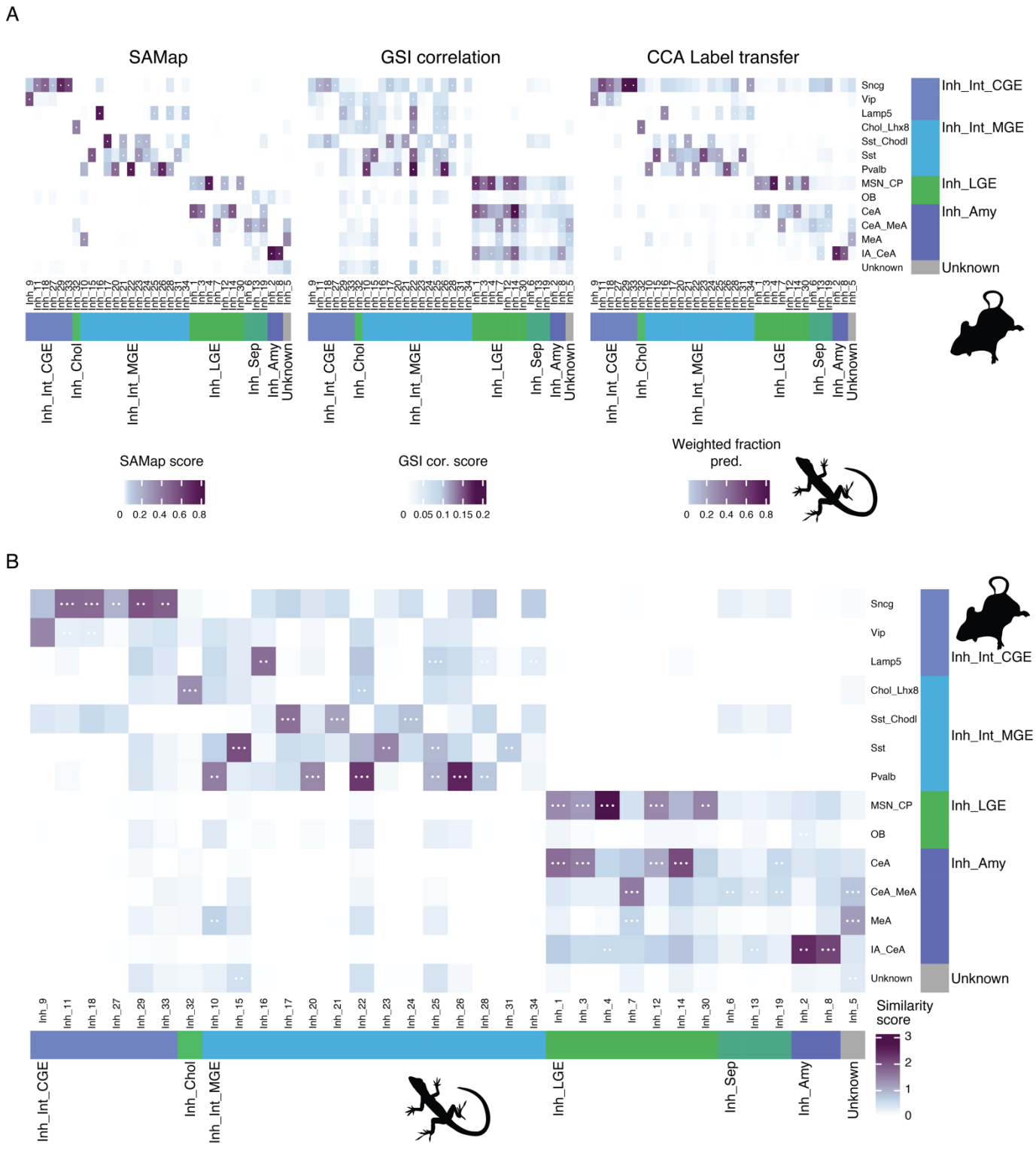

Supplementary figure 13 Comparison of inhibitory neurons between mouse and lizard pallium. (A) Comparison between inhibitory mouse subclasses and lizard clusters based on three methods. White dots in tiles are shown when populations are among the top five reciprocal matches according to the chosen method. (B) Aggregated results from all three comparative methods. Scores were scaled between 0 and 1 per method and summed across all methods to represent the similarity score. White dots in tiles are shown when populations are among the top five reciprocal matches according to the chosen method. Pred, prediction; CGE, caudal ganglionic eminence; MGE, medial ganglionic eminence; LGE, lateral ganglionic eminence; Chol, cholinergic; Sep, septum; Amy, amygdala; CeA, central amygdala; MeA, medial amygdala; IA, intercalated amygdala.

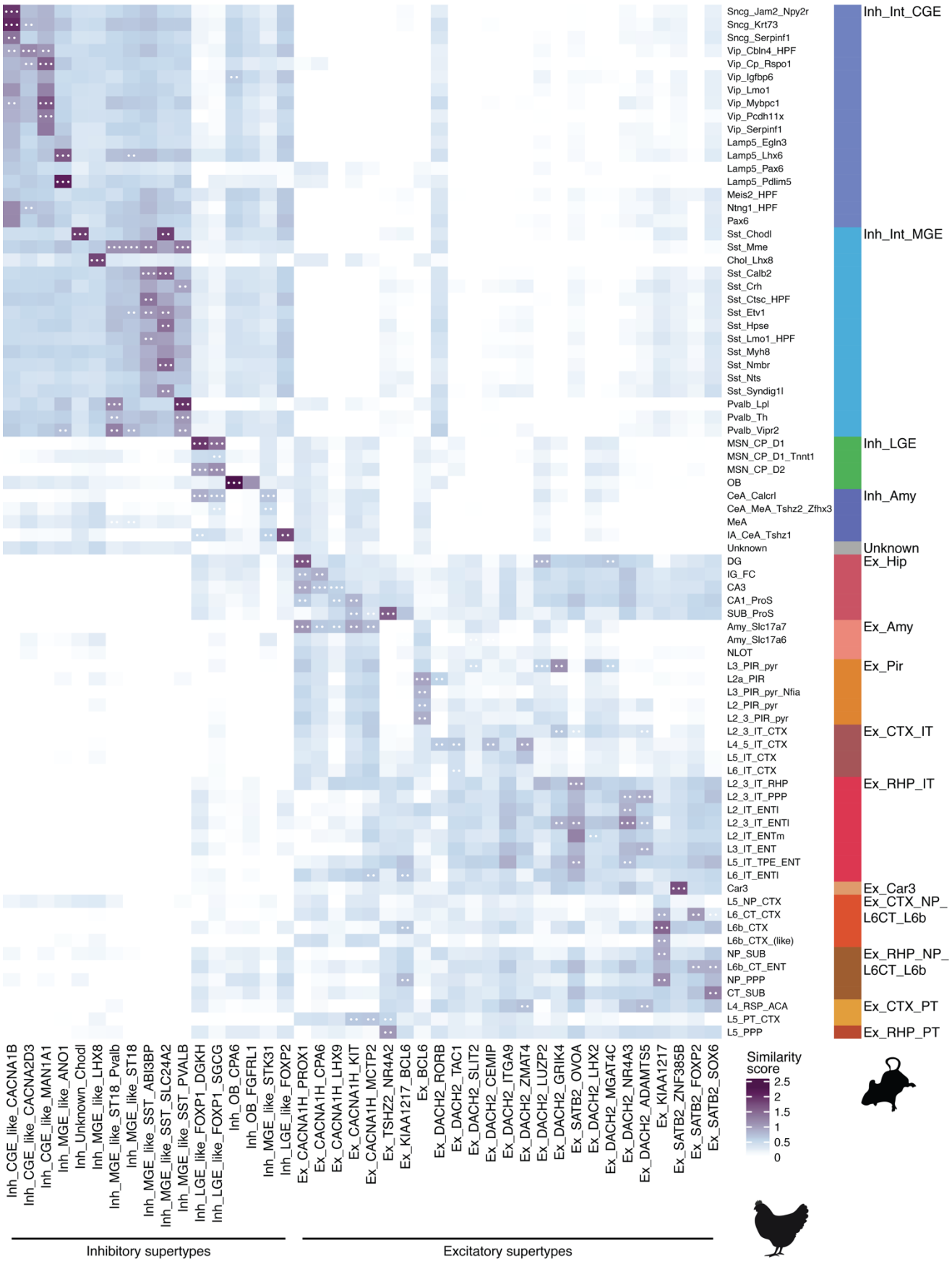
Sncg_Jam2_Npy2r
Sncg_Krt73
Sncg_Serpinf1
Vip_Cbln4_HPF
Vip_Cp_Rspo1
Vip_Igfbp6
Vip_Lmo1
Vip_Mybpc1
Vip_Pcdh11x
Vip_Serpinf1
Lamp5_Egln3
Lamp5_Lhx6
Lamp5_Pax6
Lamp5_Pdlim5
Meis2_HPF
Ntng1_HPF
Pax6
Sst_Chodl
Sst_Mme
Chol_Lhx8
Sst_Calb2
Sst_Crh
Sst_Ctsc_HPF
Sst_Etv1
Sst_Hpse
Sst_Lmo1_HPF
Sst_Myh8
Sst_Nmbr
Sst_Nts
Sst_Syndig1l
Pvalb_Lpl
Pvalb_Th
Pvalb_Vipr2
MSN_CP_D1
MSN_CP_D1_Tnnt1
MSN_CP_D2
OB
CeA_Calcrl
CeA_MeA_Tshz2_Zfhx3
MeA
IA_CeA_Tshz1
Unknown
DG
IG_FC
CA3
CA1_ProS
SUB_ProS
Amy_Slc17a7
Amy_Slc17a6
NLOT
L3_PIR_pyr
L2a_PIR
L3_PIR_pyr_Nfia
L2_PIR_pyr
L2_3_PIR_pyr
L2_3_IT_CTX
L4_5_IT_CTX
L5_IT_CTX
L6_IT_CTX
L2_3_IT_RHP
L2_3_IT_PPP
L2_IT_ENTl
L2_3_IT_ENTl
L2_IT_ENTm
L3_IT_ENT
L5_IT_TPE_ENT
L6_IT_ENTl
Car3
L5_NP_CTX
L6_CT_CTX
L6b_CTX
L6b_CTX_(like)
NP_SUB
L6b_CT_ENT
NP_PPP
CT_SUB
L4_RSP_ACA
L5_PT_CTX
L5_PPP
Inh_Int_CGE
Inh_Int_MGE
Inh_LGE
Inh_Amy
Unknown
Ex_Hip
Ex_Amy
Ex_Pir
Ex_CTX_IT
Ex_RHP_IT
Ex_Car3
Ex_CTX_NP_
L6CT_L6b
Ex_RHP_NP_
L6CT_L6b
Ex_CTX_PT
Ex_RHP_PT
Similarity
score
2.5
2
1.5
1
0.5
0
Inh_CGE_like_CACNA1B
Inh_CGE_like_CACNA2D3
Inh_CGE_like_MAN1A1
Inh_MGE_like_ANO1
Inh_Unknown_Chodl
Inh_MGE_like_LHX8
Inh_MGE_like_ST18_Pvalb
Inh_MGE_like_ST18
Inh_MGE_like_SST_ABI3BP
Inh_MGE_like_SST_SLC24A2
Inh_MGE_like_SST_PVALB
Inh_LGE_like_FOXP1_DGKH
Inh_LGE_like_FOXP1_SGCG
Inh_OB_CPA6
Inh_OB_FGFRL1
Inh_MGE_like_STK31
Inh_LGE_like_FOXP2
Ex_CACNA1H_PROX1
Ex_CACNA1H_CPA6
Ex_CACNA1H_LHX9
Ex_CACNA1H_KIT
Ex_CACNA1H_MCTP2
Ex_TSHZ2_NR4A2
Ex_KIAA1217_BCL6
Ex_BCL6
Ex_DACH2_RORB
Ex_DACH2_TAC1
Ex_DACH2_SLIT2
Ex_DACH2_CEMIP
Ex_DACH2_ITGA9
Ex_DACH2_ZMAT4
Ex_DACH2_LUZP2
Ex_DACH2_GRIK4
Ex_SATB2_OVOA
Ex_DACH2_LHX2
Ex_DACH2_MGAT4C
Ex_DACH2_NR4A3
Ex_DACH2_ADAMTS5
Ex_KIAA1217
Ex_SATB2_ZNF385B
Ex_SATB2_FOXP2
Ex_SATB2_SOX6
Inhibitory supertypes
Excitatory supertypes

Supplementary figure 14 Comparison of all neurons between chicken and mouse pallium. Comparison between neuronal chicken supertypes and mouse neuronal subclasses based on three different methods. Scores were scaled between 0 and 1 per method and summed across all methods to represent the similarity score. White dots in tiles are shown when populations are among the top reciprocal matches according to two or all three methods. For abbreviations see List of abbreviations.

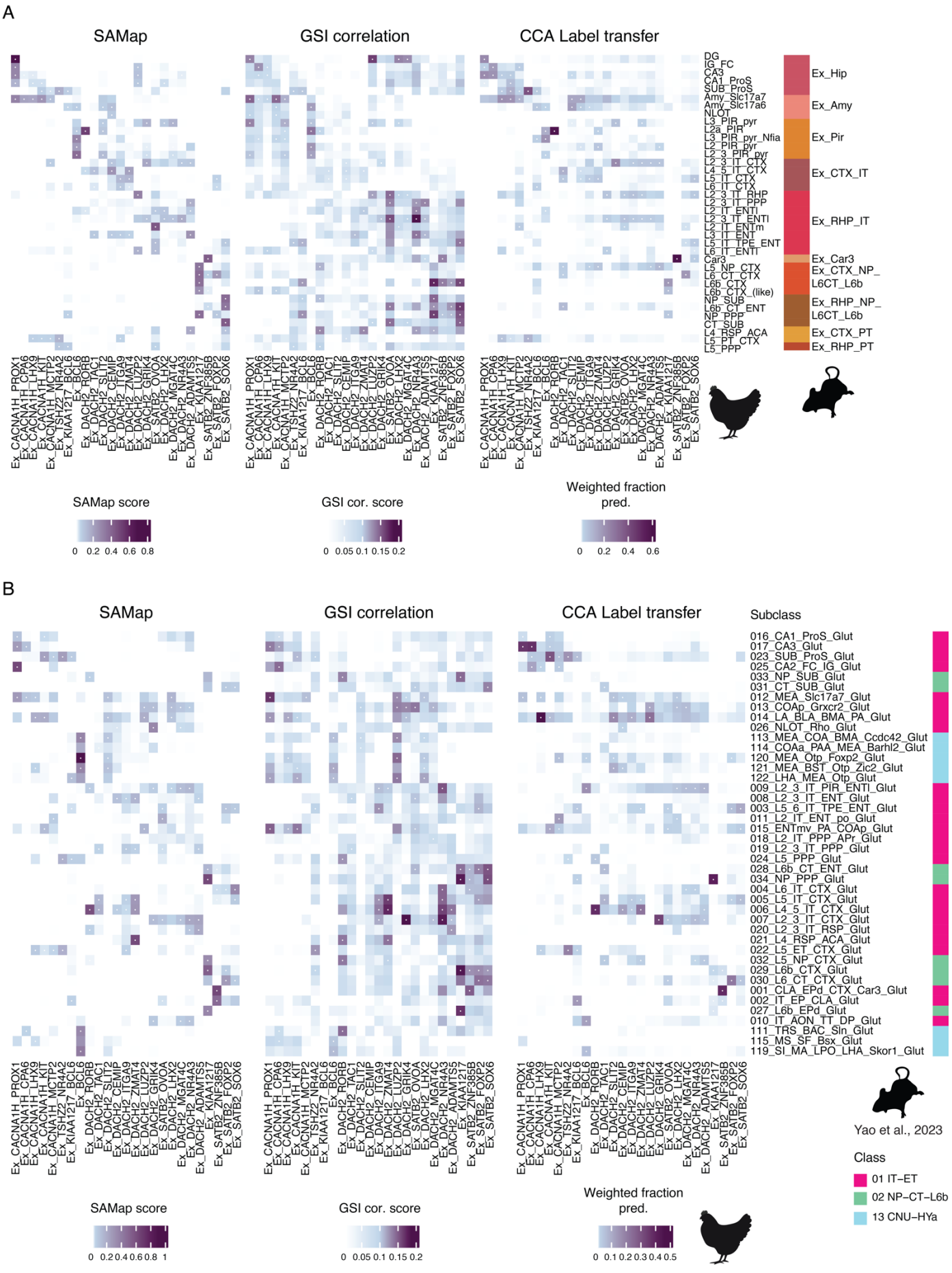
A
SAMap
GSI correlation
CCA Label transfer
DG
IG_FC
CA3
CA1_ProS
SUB_ProS
Amy_Slc17a7
Amy_Slc17a6
NLOT
L3_PIR_pyr
L2a_PIR
L3_PIR_pyr_Nfia
L2_PIR_pyr
L2_3_PIR_pyr
L2_3_IT_CTX
L4_5_IT_CTX
L5_IT_CTX
L6_IT_CTX
L2_3_IT_RHP
L2_3_IT_PPP
L2_IT_ENTl
L2_3_IT_ENTl
L2_IT_ENTm
L3_IT_ENT
L5_IT_TPE_ENT
L6_IT_ENTl
Car3
L5_NP_CTX
L6_CT_CTX
L6b_CTX
L6b_CTX_(like)
NP_SUB
L6b_CT_ENT
NP_PPP
CT_SUB
L4_RSP_ACA
L5_PT_CTX
L5_PPP
Ex_Hip
Ex_Amy
Ex_Pir
Ex_CTX_IT
Ex_RHP_IT
Ex_Car3
Ex_CTX_NP_
L6CT_L6b
Ex_RHP_NP_
L6CT_L6b
Ex_CTX_PT
Ex_RHP_PT
Ex_CACNA1H_PROX1
Ex_CACNA1H_CPA6
Ex_CACNA1H_LHX9
Ex_CACNA1H_KIT
Ex_CACNA1H_MCTP2
Ex_TSHZ2_NR4A2
Ex_KIAA1217_BCL6
Ex_RORB
Ex_DACH2_TAC1
Ex_DACH2_SLIT2
Ex_DACH2_CEMIP
Ex_DACH2_ITGA9
Ex_DACH2_ZMAT4
Ex_DACH2_LUZP2
Ex_DACH2_GRIK4
Ex_SATB2_OVOA
Ex_DACH2_LHX2
Ex_DACH2_MGAT4C
Ex_DACH2_NR4A3
Ex_DACH2_ADAMTS5
Ex_KIAA1217
Ex_SATB2_ZNF385B
Ex_SATB2_FOXP2
Ex_SATB2_SOX6
SAMap score
0 0.2 0.4 0.6 0.8
GSI cor. score
0 0.05 0.1 0.15 0.2
Weighted fraction pred.
0 0.2 0.4 0.6
B
SAMap
GSI correlation
CCA Label transfer
Subclass
016_CA1_ProS_Glut
017_CA3_Glut
023_SUB_ProS_Glut
025_CA2_FC_IG_Glut
033_NP_SUB_Glut
031_CT_SUB_Glut
012_MEA_Slc17a7_Glut
013_COAp_Grxcr2_Glut
014_LA_BLA_BMA_PA_Glut
026_NLOT_Rho_Glut
113_MEA_COA_BMA_Ccdc42_Glut
114_COAa_PAA_MEA_Barhl2_Glut
120_MEA_Otp_Foxp2_Glut
121_MEA_BST_Otp_Zic2_Glut
122_LHA_MEA_Otp_Glut
009_L2_3_IT_PIR_ENTl_Glut
008_L2_3_IT_ENT_Glut
003_L5_6_IT_TPE_ENT_Glut
011_L2_IT_ENT_po_Glut
015_ENTmv_PA_COAp_Glut
018_L2_IT_PPP_APr_Glut
019_L2_3_IT_PPP_Glut
024_L5_PPP_Glut
028_L6b_CT_ENT_Glut
034_NP_PPP_Glut
004_L6_IT_CTX_Glut
005_L5_IT_CTX_Glut
006_L4_5_IT_CTX_Glut
007_L2_3_IT_CTX_Glut
020_L2_3_IT_RSP_Glut
021_L4_RSP_ACA_Glut
022_L5_ET_CTX_Glut
032_L5_NP_CTX_Glut
029_L6b_CTX_Glut
030_L6_CT_CTX_Glut
001_CLA_EPd_CTX_Car3_Glut
002_IT_EP_CLA_Glut
027_L6b_EPd_Glut
010_IT_AON_TT_DP_Glut
111_TRS_BAC_Sln_Glut
115_MS_SF_Bsx_Glut
119_SI_MA_LPO_LHA_Skor1_Glut
Yao et al., 2023
Class
01 IT–ET
02 NP–CT–L6b
13 CNU–HYa
SAMap score
0 0.2 0.4 0.6 0.8 1
GSI cor. score
0 0.05 0.1 0.15 0.2
Weighted fraction pred.
0 0.1 0.2 0.3 0.4 0.5

Supplementary figure 15 Comparison of excitatory neurons between chicken and mouse pallium (separate methods). Comparison of chicken supertypes (A) to mouse subclasses in my dataset, or (B) to mouse excitatory subclasses from (*76*) based on three methods. White dots in tiles are shown when populations are among the top five reciprocal matches according to the chosen method. Pred, prediction. For more mouse abbreviations see List of abbreviations.

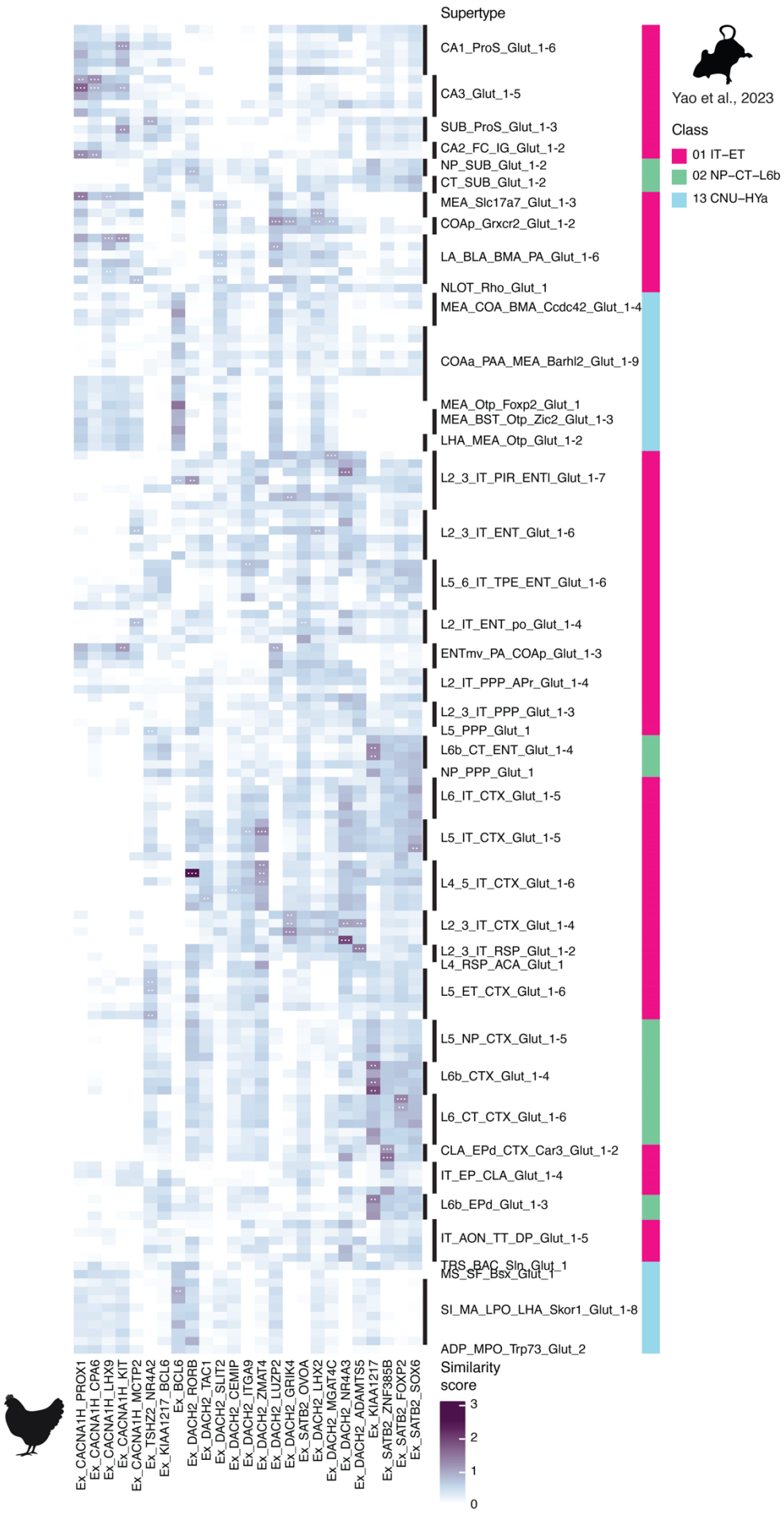
Supertype
CA1_ProS_Glut_1-6
CA3_Glut_1-5
SUB_ProS_Glut_1-3
CA2_FC_IG_Glut_1-2
NP_SUB_Glut_1-2
CT_SUB_Glut_1-2
MEA_Slc17a7_Glut_1-3
COAp_Grxcr2_Glut_1-2
LA_BLA_BMA_PA_Glut_1-6
NLOT_Rho_Glut_1
MEA_COA_BMA_Ccdc42_Glut_1-4
COAa_PAA_MEA_Barhl2_Glut_1-9
MEA_Otp_Foxp2_Glut_1
MEA_BST_Otp_Zic2_Glut_1-3
LHA_MEA_Otp_Glut_1-2
L2_3_IT_PIR_ENTl_Glut_1-7
L2_3_IT_ENT_Glut_1-6
L5_6_IT_TPE_ENT_Glut_1-6
L2_IT_ENT_po_Glut_1-4
ENTmv_PA_COAp_Glut_1-3
L2_IT_PPP_APr_Glut_1-4
L2_3_IT_PPP_Glut_1-3
L5_PPP_Glut_1
L6b_CT_ENT_Glut_1-4
NP_PPP_Glut_1
L6_IT_CTX_Glut_1-5
L5_IT_CTX_Glut_1-5
L4_5_IT_CTX_Glut_1-6
L2_3_IT_CTX_Glut_1-4
L2_3_IT_RSP_Glut_1-2
L4_RSP_ACA_Glut_1
L5_ET_CTX_Glut_1-6
L5_NP_CTX_Glut_1-5
L6b_CTX_Glut_1-4
L6_CT_CTX_Glut_1-6
CLA_EPd_CTX_Car3_Glut_1-2
IT_EP_CLA_Glut_1-4
L6b_EPd_Glut_1-3
IT_AON_TT_DP_Glut_1-5
TRS_BAC_Sln_Glut_1
MS_SF_Bsx_Glut_1
SI_MA_LPO_LHA_Skor1_Glut_1-8
ADP_MPO_Trp73_Glut_2
Yao et al., 2023
Class
01 IT–ET
02 NP–CT–L6b
13 CNU–HYa
Ex_CACNA1H_PROX1
Ex_CACNA1H_CPA6
Ex_CACNA1H_LHX9
Ex_CACNA1H_KIT
Ex_CACNA1H_MCTP2
Ex_TSHZ2_NR4A2
Ex_KIAA1217_BCL6
Ex_BCL6
Ex_DACH2_RORB
Ex_DACH2_TAC1
Ex_DACH2_SLIT2
Ex_DACH2_CEMIP
Ex_DACH2_ITGA9
Ex_DACH2_ZMAT4
Ex_DACH2_LUZP2
Ex_DACH2_GRIK4
Ex_SATB2_OVOA
Ex_DACH2_LHX2
Ex_DACH2_MGAT4C
Ex_DACH2_NR4A3
Ex_DACH2_ADAMTS5
Ex_KIAA1217
Ex_SATB2_ZNF385B
Ex_SATB2_FOXP2
Ex_SATB2_SOX6
Similarity score
3
2
1
0

Supplementary figure 16 Comparison of excitatory neurons between chicken and external mouse pallium dataset at supertype level. (A) Comparison of excitatory supertypes in the chicken pallium to supertypes of excitatory neurons in the mouse pallium from (*76*) based on three methods. Scores were scaled between 0 and 1 per method and summed across all methods to represent the similarity score. White dots in tiles are shown when populations are among the top reciprocal matches according to two or all three methods. IT, intratelencephalic; ET, extratelencephalic; NP, near-projecting; CT, corticothalamic; CNU, cerebral nuclei; HYa, anterior hypothalamic. For more mouse abbreviations see List of abbreviations.

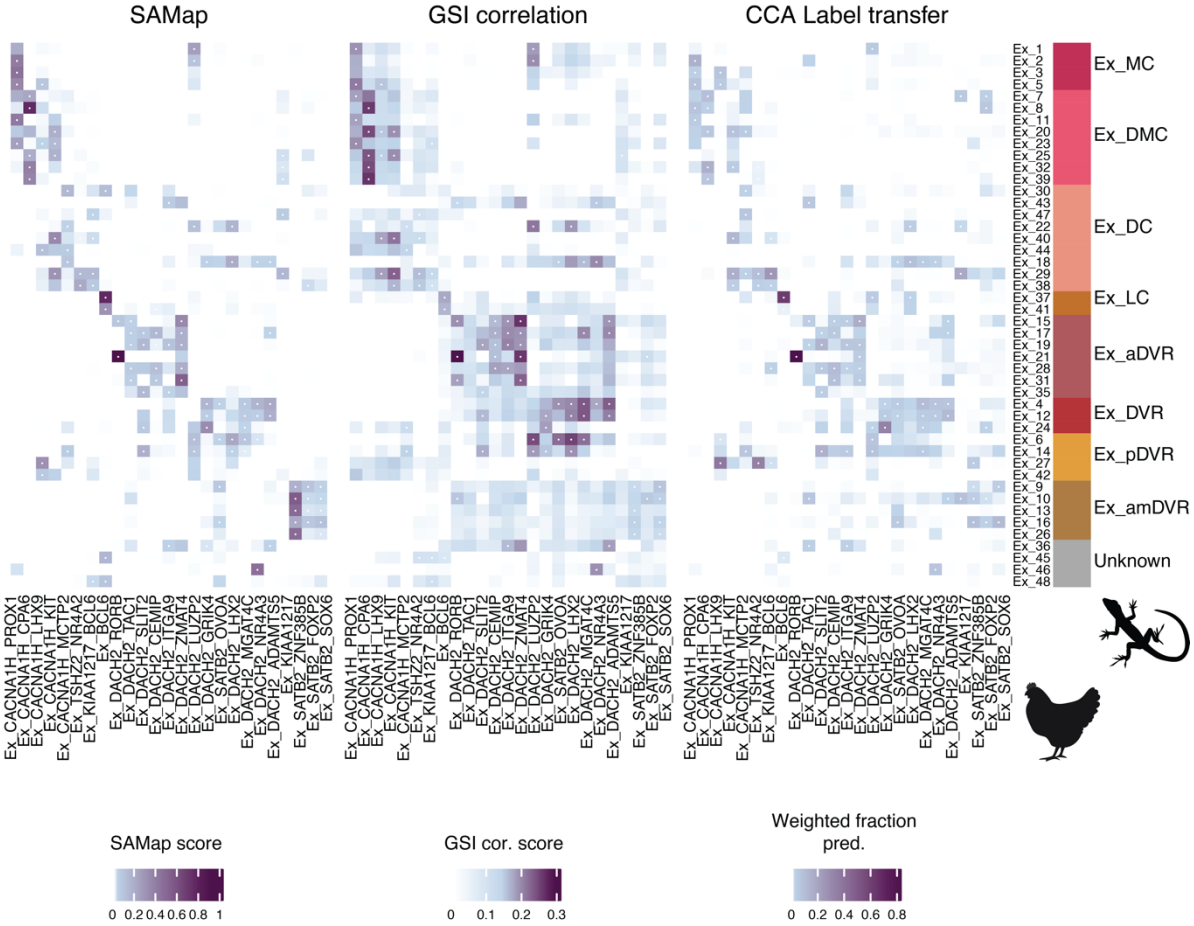

Supplementary figure 17 Comparison of excitatory neurons between chicken and lizard pallium (separate methods). Comparison of excitatory supertypes in the chicken pallium to clusters of excitatory neurons in the lizard pallium based on three methods. White dots in tiles are shown when populations are among the top five reciprocal matches according to the chosen method. Pred, prediction; MC, medial cortex; DMC, dorsal medial cortex; DC, dorsal cortex; LC, lateral cortex; aDVR, anterior DVR; pDVR, posterior DVR; amDVR, anterior medial DVR.

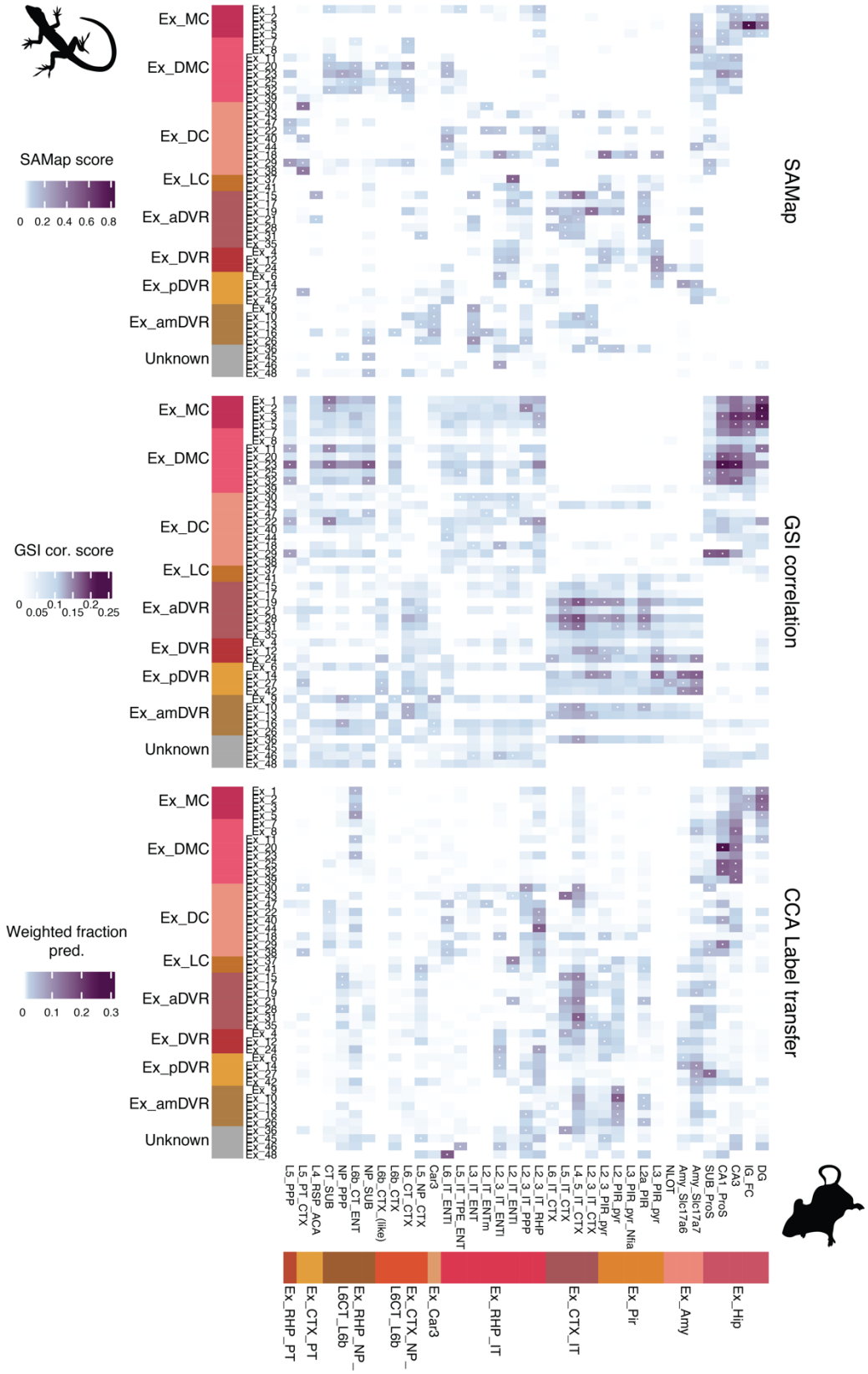

Supplementary figure 18 Comparison of excitatory neurons between mouse and lizard pallium (separate methods). Comparison between excitatory mouse subclasses and lizard clusters based on three methods. White dots in tiles are shown when populations are among the top five reciprocal matches according to the

chosen method. Pred, prediction; MC, medial cortex; DMC, dorsal medial cortex; DC, dorsal cortex; LC, lateral cortex; aDVR, anterior DVR; pDVR, posterior DVR; amDVR, anterior medial DVR. For more mouse abbreviations see List of abbreviations.

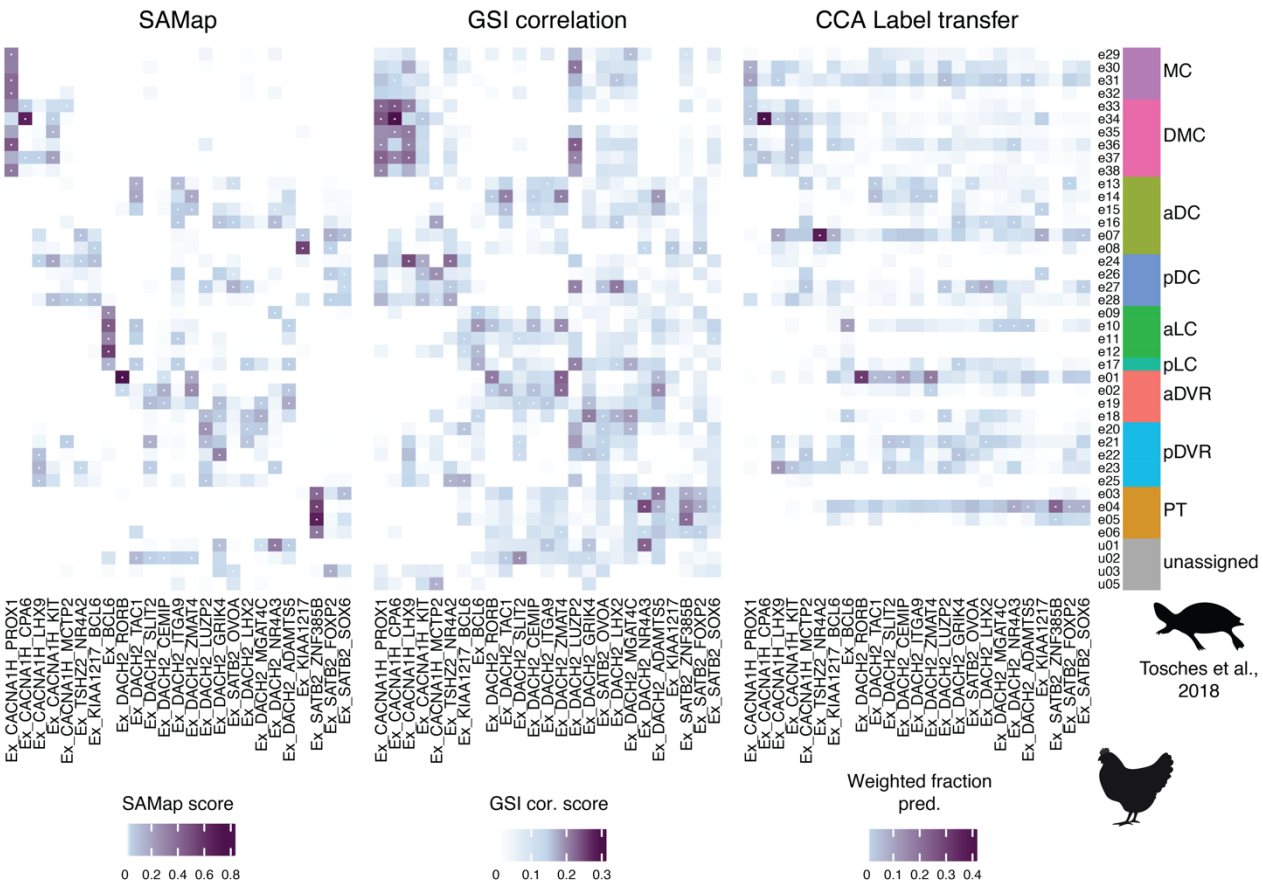

Supplementary figure 19 Comparison of excitatory neurons between chicken and turtle pallium. Comparison of excitatory supertypes in the chicken pallium to clusters of excitatory neurons in the turtle pallium from (*41*) based on three methods. White dots in tiles are shown when populations are among the top five reciprocal matches according to the chosen method. Pred, prediction; MC, medial cortex; DMC, dorsal medial cortex; aDC, anterior dorsal cortex; pDC, posterior dorsal cortex; aLC, anterior lateral cortex; pLC, posterior lateral cortex; aDVR, anterior DVR; pDVR, posterior DVR; PT, pallial thickening.

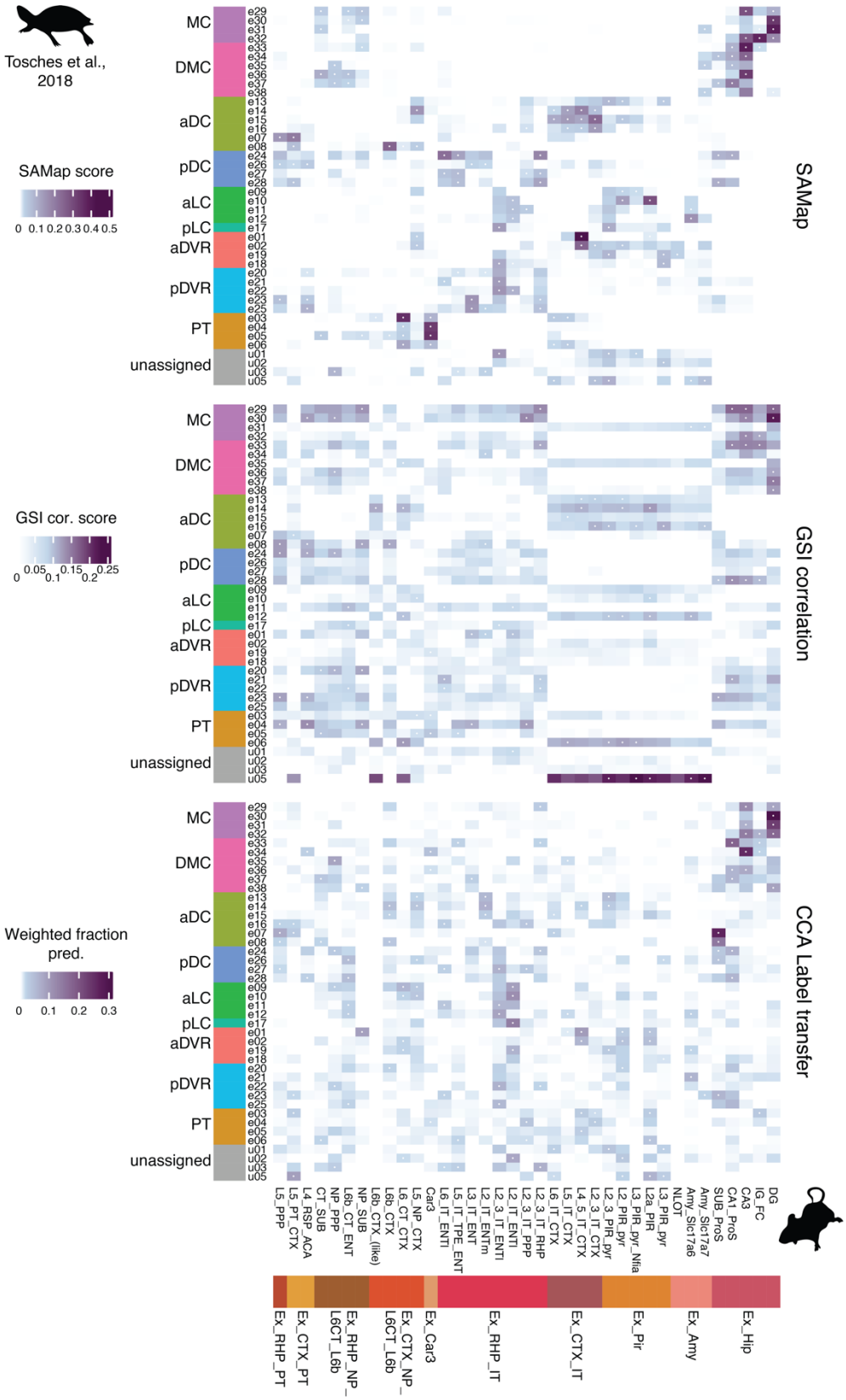

Supplementary figure 20 Comparison of excitatory neurons between mouse and turtle pallium (separate methods). Comparison between excitatory subclasses in the mouse pallium to clusters of excitatory neurons in the turtle pallium from (*41*) based on three methods. White dots in tiles are shown when populations are among the top five reciprocal matches according to the chosen method. Pred, prediction; MC, medial cortex; DMC, dorsal medial cortex; aDC, anterior dorsal cortex; pDC, posterior dorsal cortex;

aLC, anterior lateral cortex; pLC, posterior lateral cortex; aDVR, anterior DVR; pDVR, posterior DVR; PT, pallial thickening. For mouse abbreviations see List of abbreviations.

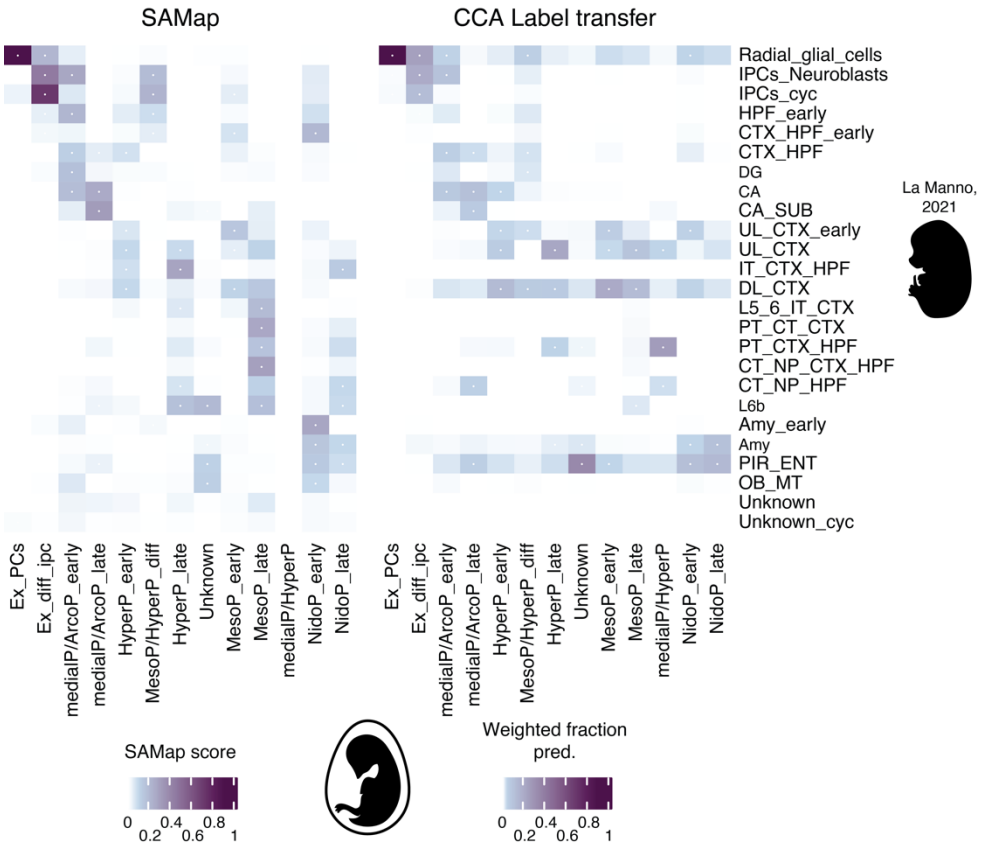

Supplementary figure 21 Comparison of excitatory lineages in the developing pallium between mouse and chicken (separate methods). Comparison between chicken pallial excitatory lineages and mouse embryonic pallial populations (data from (*80*)). Lineages comprising many cells in chick were split into early and late (pseudotime > 0.89). Comparison is based on two methods. White dots in tiles are shown when populations are among the top five reciprocal matches according to the chosen method. Pred., prediction; Amy, amygdala; CA, cornu ammonis; SUB, subiculum; CT, cortico-thalamic; NP, near-projecting; HPF, hippocampal formation; CTX, cortex; DG, dentate gyrus; DL, deep layer; IT, intra-telencephalic; OB-MT, olfactory bulb mitral tufted; PIR/ENT, piriform/entorhinal cortex; PT, pyramidal tract projecting; UL, upper layer.

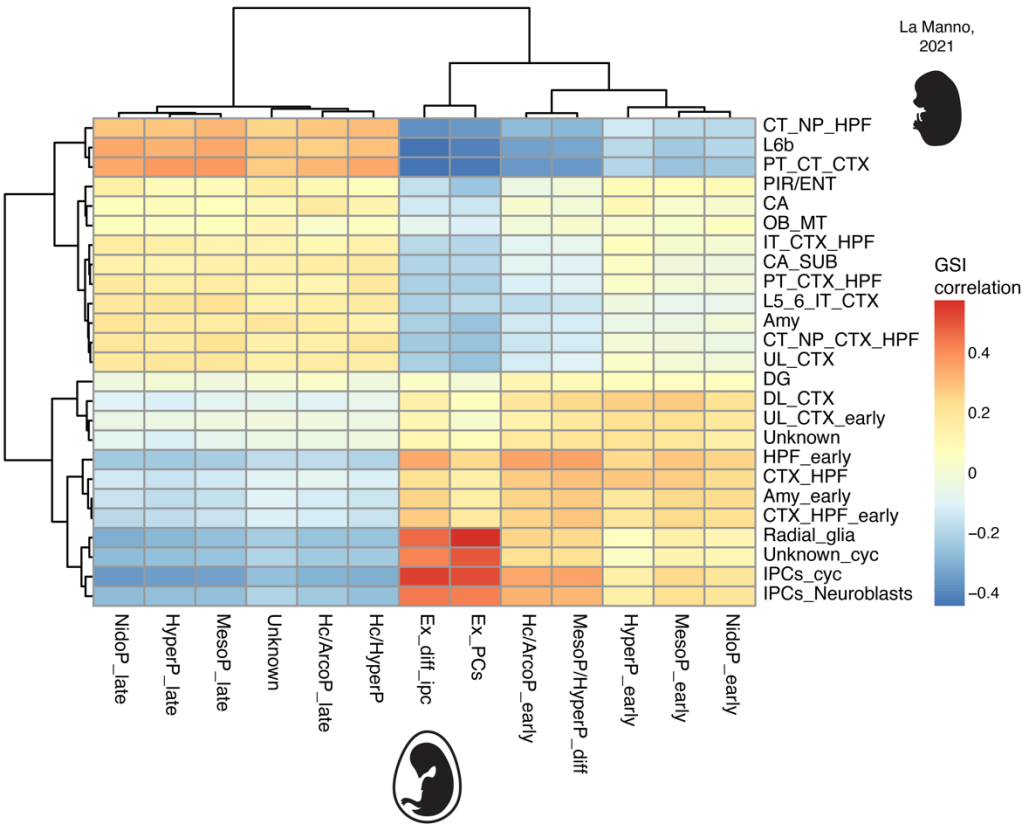

Supplementary figure 22 **Comparison of excitatory lineages in the developing pallium between mouse and chicken based on GSI correlation.** Clustered heatmap based on GSI correlation of chicken pallial excitatory lineages and mouse embryonic pallial populations (data from (*80*)).

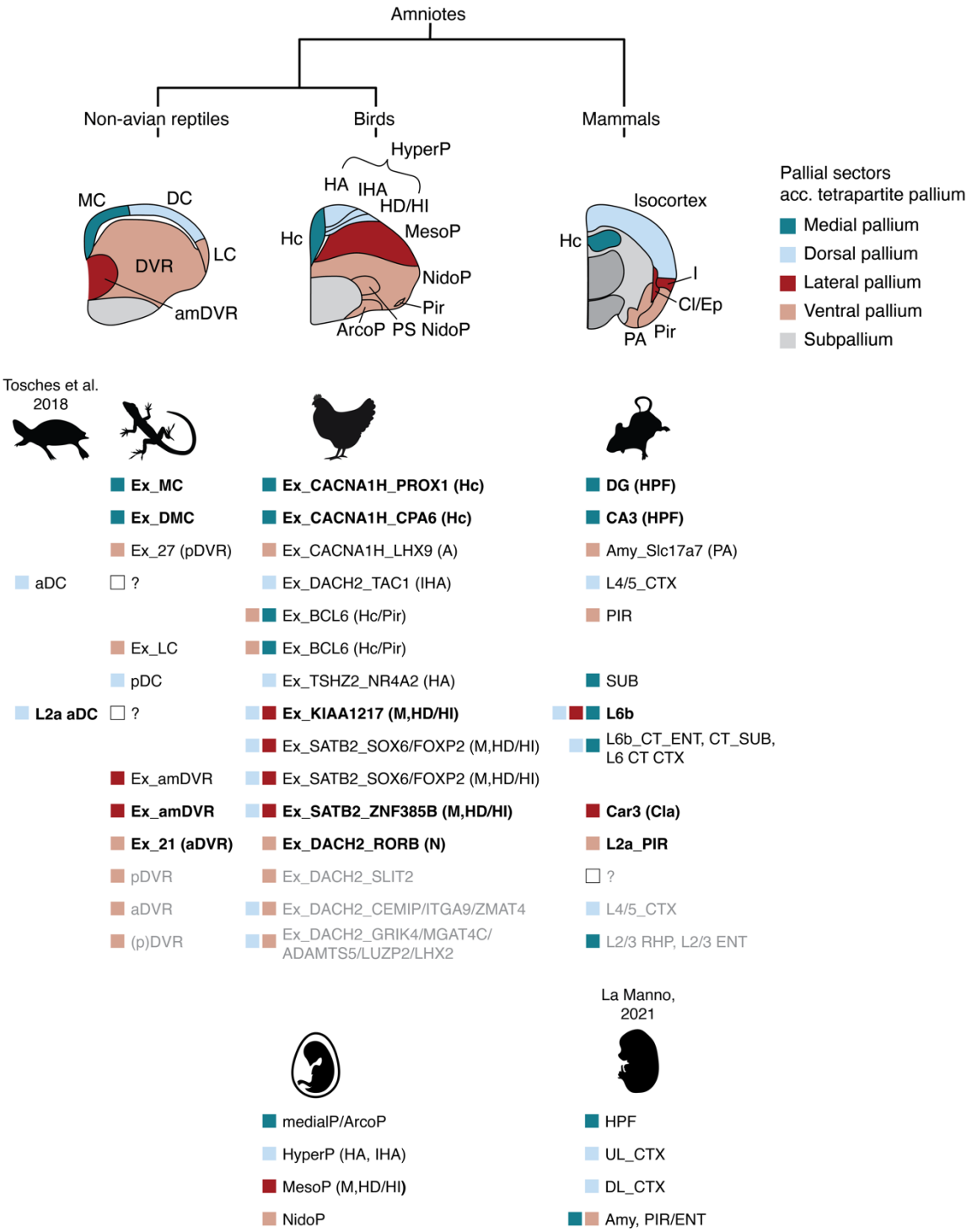

Supplementary figure 23 Homology relationships of cell types and regions. (Top) Schematic representation of coronal sections of the telencephalon in lizard (left), chicken (middle), and mouse (right). Brightly coloured areas represent the pallium divided into developmental, homologous sectors according to the tetrapartite pallium theory (*128*). Mya, million years ago; DVR, dorsal ventricular ridge; Hc, hippocampus; HA, apical hyperpallium; IHA, interstitial apical hyperpallium; HI/HD, intercalated and densocellular hyperpallium; Cla, claustrum; I, insular cortex; Pir, piriform cortex; PA, pallial amygdala. (Bottom) Identified homologous cell types. Coloured squares indicate the cell type's spatial location in the framework of the tetrapartite pallium theory. Bold text indicates homologies assigned with high confidence; grey text indicates low confidence. Cell types in the chicken pallium are listed twice, if the corresponding reptilian or mammalian populations do not correspond to each other.

7 SUPPLEMENTARY TABLES

Supplementary table 1 Genes profiled with *In Situ* sequencing.

Gene Symbol	ENSEMBL GeneID
GRIK3	ENSGALG00000002098
NTNG2	ENSGALG00000003677
CACNA1H	ENSGALG00000005215
SOX6	ENSGALG00000006074
HS3ST4	ENSGALG00000006290
OVOA	ENSGALG00000006717
ADARB2	ENSGALG00000006797
DACH2	ENSGALG00000006886
KIAA1217	ENSGALG00000007766
FOXP1	ENSGALG00000007769
SATB2	ENSGALG00000008135
RGS6	ENSGALG00000009368
FOXP2	ENSGALG00000009424
TAC1	ENSGALG00000009737
PROX1	ENSGALG00000009791
NXPH1	ENSGALG00000010711
KCNH5	ENSGALG00000011858
GRM1	ENSGALG00000012297
NR4A2	ENSGALG00000012538
PDE7B	ENSGALG00000013941
HOMER1	ENSGALG00000014813
RORB	ENSGALG00000015150
EPHA7	ENSGALG00000015593
CUX1	ENSGALG00000021636
MAF	ENSGALG00000026258
CPNE4	ENSGALG00000029235
LUZP2	ENSGALG00000030151
BCL11B	ENSGALG00000031862
BCL11A	ENSGALG00000034048
GAD1	ENSGALG00000034070
CELF2	ENSGALG00000034590
ETV1	ENSGALG00000035504
CLSTN2	ENSGALG00000037387
GRIA4	ENSGALG00000038995
MEIS2	ENSGALG00000039118
SLC17A6	ENSGALG00000039254
GAD2	ENSGALG00000040436
SYT1	ENSGALG00000041094

ANO1	ENSGALG00000041808
PCP4	ENSGALG00000022819
DPP10	ENSGALG00000012156
CNTN4	ENSGALG00000008263
HPCAL1	ENSGALG00000016443
CRIM1	ENSGALG00000032640
IL1RAPL2	ENSGALG00000008888
SST	ENSGALG00000007361
ZBTB32	ENSGALG00000038540
DAAM2	ENSGALG00000010055
OLIG2	ENSGALG00000031010
SLC1A3	ENSGALG00000003582

Supplementary table 2 Genes significantly differentially expressed between DVR and hyperpallium within Ex_DACH2_ZMAT4 supertype. Genes with negative fold change are DVR-specific.

ensembl_id	log2FoldChange	p_value_adj	gene name	biotype
ENSGALG00000030510	-5.925763	2.13E-05	NA	lincRNA
ENSGALG00000038089	-4.4386245	8.69E-05	EGFR	protein_coding
ENSGALG00000015252	-5.38E-06	1.43E-04	ST3GAL6	protein_coding
ENSGALG00000007000	-5.57E-06	1.43E-04	NR2F2	protein_coding
ENSGALG00000041042	3.68654295	2.71E-04	NA	protein_coding
ENSGALG00000010125	-8.7495738	2.71E-04	CSGALNACT1	protein_coding
ENSGALG00000007809	-4.85E-06	1.54E-03	TSHZ2	protein_coding
ENSGALG00000013616	-3.2905605	2.06E-03	OPRM1	protein_coding
ENSGALG00000009880	-3.4115366	3.05E-03	INPP4B	protein_coding
ENSGALG00000009687	-4.3767939	3.66E-03	KCNK2	protein_coding
ENSGALG00000008465	-2.5979256	6.58E-03	SORCS1	protein_coding
ENSGALG00000016017	-4.7704487	9.95E-03	SLC4A11	protein_coding
ENSGALG00000017005	-2.920003	1.10E-02	CAB39L	protein_coding
ENSGALG00000011686	-3.1026965	1.20E-02	SEMA5B	protein_coding
ENSGALG00000007140	2.8618103	1.24E-02	NRP1	protein_coding
ENSGALG00000043515	-2.90E-06	1.38E-02	KCND2	protein_coding
ENSGALG00000007927	-2.5044157	1.38E-02	CNTN6	protein_coding
XLOC-005141	-2.52E-06	2.16E-02	NA	NA
ENSGALG00000007741	-3.41E-06	2.75E-02	NA	protein_coding
ENSGALG00000023581	3.61734732	3.05E-02	NA	protein_coding
ENSGALG00000042388	-5.82E-06	3.13E-02	LAMA2	protein_coding
ENSGALG00000005215	-2.9340247	4.04E-02	CACNA1H	protein_coding
ENSGALG00000015367	-3.63E-06	4.10E-02	NECTIN3	protein_coding
ENSGALG00000012362	-2.5146389	4.70E-02	THSD7B	protein_coding

Supplementary table 3 Genes significantly differentially expressed between DVR and hyperpallium within Ex_DACH2_MGAT4C supertype. Genes with negative fold change are DVR-specific.

ensembl_id	log2FoldChange	p_value_adj	Gene name	biotype
ENSGALG00000030510	-5.4855303	2.81E-13	NA	lincRNA
ENSGALG00000007000	-4.9966249	7.08E-10	NR2F2	protein_coding
ENSGALG00000028685	-3.8597369	2.22E-06	SEMA5A	protein_coding
ENSGALG00000038543	-6.01E-06	6.36E-05	KCNH7	protein_coding
ENSGALG00000041764	-2.7455366	1.26E-03	VSTM2A	protein_coding
XLOC-029855	-3.8286221	1.93E-03	NA	NA
ENSGALG00000008998	-3.1962843	2.54E-03	FAM179A	protein_coding
ENSGALG00000007741	-3.4567984	7.09E-03	NA	protein_coding
ENSGALG00000017234	-2.6082992	1.08E-02	FOLH1	protein_coding
XLOC-022983	-3.0233015	1.77E-02	NA	NA
ENSGALG00000030151	-6.61E-06	2.12E-02	LUZP2	protein_coding
ENSGALG00000041781	-3.2488659	2.35E-02	NA	lincRNA
ENSGALG00000005215	-3.2654988	2.63E-02	CACNA1H	protein_coding
XLOC-039769	-3.14E-06	4.37E-02	NA	NA
ENSGALG00000030157	-3.4538724	4.41E-02	MCTP2	protein_coding

8 REFERENCES

1. B. Zaremba, A. Fallahshahroudi, C. Schneider, J. Schmidt, I. Sarropoulos, E. Leushkin, B. Berki, E. Van Poucke, P. Jensen, R. Senovilla-Ganzo, F. Hervas-Sotomayor, N. Trost, F. Lamanna, M. Sepp, F. García-Moreno, H. Kaessmann, Developmental origins and evolution of pallial cell types and structures in birds. *bioRxiv*, 2024.04.30.591857 (2024).

2. H. J. Jerison, *Evolution of the Brain and Intelligence* (Academic Press, 1973).

3. S. Herculano-Houzel, Brains matter, bodies maybe not: the case for examining neuron numbers irrespective of body size. *Annals of the New York Academy of Sciences* **1225**, 191–199 (2011).

4. K. Kverková, L. Marhounová, A. Polonyiová, M. Kocourek, Y. Zhang, S. Olkowicz, B. Straková, Z. Pavelková, R. Vodička, D. Frynta, P. Němec, The evolution of brain neuron numbers in amniotes. *Proceedings of the National Academy of Sciences* **119**, e2121624119 (2022).

5. S. Olkowicz, M. Kocourek, R. K. Lučan, M. Porteš, W. T. Fitch, S. Herculano-Houzel, P. Němec, Birds have primate-like numbers of neurons in the forebrain. *Proceedings of the National Academy of Sciences* **113**, 7255–7260 (2016).

6. S. Kumar, M. Suleski, J. M. Craig, A. E. Kasprowicz, M. Sanderford, M. Li, G. Stecher, S. B. Hedges, TimeTree 5: An Expanded Resource for Species Divergence Times. *Molecular Biology and Evolution* **39**, msac174 (2022).

7. W. A. Searcy, S. Nowicki, Birdsong learning, avian cognition and the evolution of language. *Animal Behaviour* **151**, 217–227 (2019).

8. C. Baan, R. Bergmüller, D. W. Smith, B. Molnar, Conflict management in free-ranging wolves, *Canis lupus*. *Animal Behaviour* **90**, 327–334 (2014).

9. O. Güntürkün, T. Bugnyar, Cognition without Cortex. *Trends in cognitive sciences* **20**, 291–303 (2016).

10. O. Güntürkün, F. Ströckens, D. Scarf, M. Colombo, Apes, feathered apes, and pigeons: differences and similarities. *Current Opinion in Behavioral Sciences* **16**, 35–40 (2017).

11. E. L. MacLean, B. Hare, C. L. Nunn, E. Addessi, F. Amici, R. C. Anderson, F. Aureli, J. M. Baker, A. E. Bania, A. M. Barnard, N. J. Boogert, E. M. Brannon, E. E. Bray, J. Bray, L. J. N. Brent, J. M. Burkart, J. Call, J. F. Cantlon, L. G. Cheke, N. S. Clayton, M. M. Delgado, L. J. DiVincenti, K. Fujita, E. Herrmann, C. Hiramatsu, L. F. Jacobs, K. E. Jordan, J. R. Laude, K. L. Leimgruber, E. J. E. Messer, A. C. de A. Moura, L. Ostojić, A. Picard, M. L. Platt, J. M. Plotnik, F. Range, S. M. Reader, R. B. Reddy, A. A. Sandel, L. R. Santos, K. Schumann, A. M. Seed, K. B. Sewall, R. C. Shaw, K. E. Slocombe, Y. Su, A. Takimoto, J. Tan, R. Tao, C. P. van Schaik, Z. Virányi, E. Visalberghi, J. C. Wade, A. Watanabe, J. Widness, J. K. Young, T. R. Zentall, Y. Zhao, The evolution of self-control. *Proceedings of the National Academy of Sciences* **111**, E2140–E2148 (2014).

12. C. Kabadayi, L. A. Taylor, A. M. P. von Bayern, M. Osvath, Ravens, New Caledonian crows and jackdaws parallel great apes in motor self-regulation despite smaller brains. *Royal Society Open Science* **3**, 160104 (2016).

13. T. Nomura, Y. Murakami, H. Gotoh, K. Ono, Reconstruction of ancestral brains: Exploring the evolutionary process of encephalization in amniotes. *Neuroscience Research* **86**, 25–36 (2014).

14. R. Nieuwenhuys, H. J. Donkelaar, C. Nicholson, *The Central Nervous System of Vertebrates* (Springer Berlin, Heidelberg, ed. 1, 1998).

15. N. Moreno, A. González, S. Rétaux, Development and evolution of the subpallium. *Seminars in Cell & Developmental Biology* **20**, 735–743 (2009).

16. F. Lamanna, F. Hervas-Sotomayor, A. P. Oel, D. Jandzik, D. Sobrido-Cameán, G. N. Santos-Durán, M. L. Martik, J. Stundl, S. A. Green, T. Brüning, K. Mößinger, J. Schmidt, C. Schneider, M. Sepp, F. Murat, J. J. Smith, M. E. Bronner, M. C. Rodicio, A. Barreiro-Iglesias, D. M. Medeiros, D. Arendt, H. Kaessmann, A lamprey neural cell type atlas illuminates the origins of the vertebrate brain. *Nat Ecol Evol* **7**, 1714–1728 (2023).

17. L. Medina, A. Abellán, Development and evolution of the pallium. *Seminars in Cell & Developmental Biology* **20**, 698–711 (2009).

18. E. D. Jarvis, O. Güntürkün, L. Bruce, A. Csillag, H. Karten, W. Kuenzel, L. Medina, G. Paxinos, D. J. Perkel, T. Shimizu, G. Striedter, J. M. Wild, G. F. Ball, J. Dugas-Ford, S. E. Durand, G. E. Hough, S. Husband, L. Kubikova, D. W. Lee, C. V. Mello, A. Powers, C. Siang, T. V. Smulders, K. Wada, S. A. White, K. Yamamoto, J. Yu, A. Reiner, A. B. Butler, Avian brains and a new understanding of vertebrate brain evolution. *Nat Rev Neurosci* **6**, 151–159 (2005).

19. J. Woych, A. O. Gurrola, A. Deryckere, E. C. B. Jaeger, E. Gumnit, G. Merello, J. Gu, A. J. Araus, N. D. Leigh, M. Yun, A. Simon, M. A. Tosches, Cell-type profiling in salamanders identifies innovations in vertebrate forebrain evolution. *Science* **377** (2022).

20. V. S. Ramachandran, Ed., *Encyclopedia of the Human Brain* (Academic Press, Amsterdam [u.a.], 2002).

21. C. Schultz, M. Engelhardt, Anatomy of the Hippocampal Formation. doi: 10.1159/000360925 (2014).

22. E. Klingler, Development and Organization of the Evolutionarily Conserved Three-Layered Olfactory Cortex. *eNeuro* **4** (2017).

23. R. Insausti, M. Muñoz-López, A. M. Insausti, E. Artacho-Pérula, The Human Periallocortex: Layer Pattern in Presubiculum, Parasubiculum and Entorhinal Cortex. A Review. *Front. Neuroanat.* **11** (2017).

24. G. Laurent, J. Fournier, M. Hemberger, C. Müller, R. Naumann, J. M. Ondracek, L. Pammer, S. Reiter, M. Shein-Idelson, M. A. Tosches, T. Yamawaki, "Cortical Evolution: Introduction to the Reptilian Cortex" in *Micro-, Meso- and Macro-Dynamics of the Brain*, G. Buzsáki, Y. Christen, Eds. (Springer International Publishing, Cham, 2016; https://doi.org/10.1007/978-3-319-28802-4_2), pp. 23–33.

25. J. R. Whitlock, A. J. Heynen, M. G. Shuler, M. F. Bear, Learning Induces Long-Term Potentiation in the Hippocampus. *Science* **313**, 1093–1097 (2006).

26. H. Eichenbaum, The role of the hippocampus in navigation is memory. *Journal of Neurophysiology* **117**, 1785–1796 (2017).

27. V. N. Nikolenko, N. A. Rizaeva, N. M. Beeraka, M. V. Oganesyan, V. A. Kudryashova, A. A. Dubovets, I. D. Borminskaya, K. V. Bulygin, M. Y. Sinelnikov, G. Aliev, The mystery of claustral neural circuits and recent updates on its role in neurodegenerative pathology. *Behavioral and Brain Functions* **17**, 8 (2021).

28. F. E. Olucha-Bordonau, L. Fortes-Marco, M. Otero-García, E. Lanuza, F. Martínez-García, "Chapter 18 - Amygdala: Structure and Function" in *The Rat Nervous System (Fourth Edition)*, G. Paxinos, Ed. (Academic Press, San Diego, 2015; https://www.sciencedirect.com/science/article/pii/B9780123742452000188), pp. 441–490.

29. Dale. Purves, S. M. (Stephen M. Williams, *Neuroscience* (Sinauer Associates, 2001; https://www.ncbi.nlm.nih.gov/books/NBK10799/).

30. A. W. Toga, *Brain Mapping : An Encyclopedic Reference* (Academic Press, London, UK, 2015; http://site.ebrary.com/id/11024951).

31. K. D. Harris, G. M. G. Shepherd, The neocortical circuit: themes and variations. *Nature Neuroscience* **18**, 170–181 (2015).

32. A. B. Butler, Z. Molnár, P. R. Manger, Apparent Absence of Claustrum in Monotremes: Implications for Forebrain Evolution in Amniotes. *Brain Behavior and Evolution* **60**, 230–240 (2002).

33. K. W. S. Ashwell, C. Hardman, G. Paxinos, The claustrum is not missing from all monotreme brains. *Brain Behav Evol* **64**, 223–241 (2004).

34. L. Krubitzer, What can monotremes tell us about brain evolution? *Philosophical Transactions of the Royal Society of London. Series B: Biological Sciences* **353**, 1127–1146 (1998).

35. L. A. Krubitzer, T. J. Prescott, The Combinatorial Creature: Cortical Phenotypes within and across Lifetimes. *Trends in neurosciences* **41**, 744–762 (2018).

36. O. Güntürkün, M. Stacho, F. Ströckens, "chapter 8 - The Brains of Reptiles and Birds" in *Evolutionary Neuroscience (Second Edition)*, J. H. Kaas, Ed. (Academic Press, London, 2020; https://www.sciencedirect.com/science/article/pii/B9780128205846000088), pp. 159–212.

37. E. D. Jarvis, J. Yu, M. V. Rivas, H. Horita, G. Feenders, O. Whitney, S. C. Jarvis, E. R. Jarvis, L. Kubikova, A. E. P. Puck, C. Siang-Bakshi, S. Martin, M. McElroy, E. Hara, J. Howard, A. Pfenning, H. Mouritsen, C. C. Chen, K. Wada, Global view of the functional molecular organization of the avian cerebrum: Mirror images and functional columns. *Journal of Comparative Neurology* **521**, 3614–3665 (2013).

38. M. Stacho, C. Herold, N. Rook, H. Wagner, M. Axer, K. Amunts, O. Güntürkün, A cortex-like canonical circuit in the avian forebrain. *Science* **369**, eabc5534 (2020).

39. O. Güntürkün, K. von Eugen, J. Packheiser, R. Pusch, Avian pallial circuits and cognition: A comparison to mammals. *Current Opinion in Neurobiology* **71**, 29–36 (2021).

40. E. Lanuza, M. Belekhova, A. Martínez-Marcos, C. Font, F. Martínez-García, Identification of the reptilian basolateral amygdala: an anatomical investigation of the afferents to the posterior dorsal ventricular ridge of the lizard. *European Journal of Neuroscience* **10**, 3517–3534 (1998).

41. M. A. Tosches, T. M. Yamawaki, R. K. Naumann, A. A. Jacobi, G. Tushev, G. Laurent, Evolution of pallium, hippocampus, and cortical cell types revealed by single-cell transcriptomics in reptiles. *Science* **360**, 881–888 (2018).

42. H. Norimoto, L. A. Fenk, H. H. Li, M. A. Tosches, T. Gallego-Flores, D. Hain, S. Reiter, R. Kobayashi, A. Macias, A. Arends, M. Klinkmann, G. Laurent, A claustrum in reptiles and its role in slow-wave sleep. *Nature* **578**, 413–418 (2020).

43. A. Reiner, D. J. Perkel, L. L. Bruce, A. B. Butler, A. Csillag, W. Kuenzel, L. Medina, G. Paxinos, T. Shimizu, G. Striedter, M. Wild, G. F. Ball, S. Durand, O. Gütürkün, D. W. Lee, C. V. Mello, A. Powers, S. A. White, G. Hough, L. Kubikova, T. V. Smulders, K. Wada, J. Dugas-Ford, S. Husband, K. Yamamoto, J. Yu, C. Siang, E. D. Jarvis, Revised nomenclature for avian telencephalon and some related brainstem nuclei. *The Journal of Comparative Neurology* **473**, 377–414 (2004).

44. L. Puelles, M. Martinez-de-la-Torre, S. Martinez, C. Watson, G. Paxinos, *The Chick Brain in Stereotaxic Coordinates and Alternate Stains* (Academic Press, 2019).

45. Y. Atoji, J. M. Wild, Afferent and efferent projections of the mesopallium in the pigeon (Columba livia). *Journal of Comparative Neurology* **520**, 717–741 (2012).

46. A. N. Iwaniuk, P. L. Hurd, The Evolution of Cerebrotypes in Birds. *Brain Behavior and Evolution* **65**, 215–230 (2005).

47. C. C. Chen, C. M. Winkler, A. R. Pfenning, E. D. Jarvis, Molecular profiling of the developing avian telencephalon: Regional timing and brain subdivision continuities. *Journal of Comparative Neurology* **521**, 3666–3701 (2013).

48. G. Gedman, B. Haase, G. Durieux, M. T. Biegler, O. Fedrigo, E. D. Jarvis, As above, so below: Whole transcriptome profiling demonstrates strong molecular similarities between avian dorsal and ventral pallial subdivisions. *Journal of Comparative Neurology* **529**, 3222–3246 (2021).

49. J. m. Wild, M. n. Williams, Rostral Wulst in passerine birds. I. Origin, course, and terminations of an avian pyramidal tract. *Journal of Comparative Neurology* **416**, 429–450 (2000).

50. A. Kriegstein, A. Alvarez-Buylla, The Glial Nature of Embryonic and Adult Neural Stem Cells. *Annual Review of Neuroscience* **32**, 149–184 (2009).

51. F. Ginhoux, S. Lim, G. Hoeffel, D. Low, T. Huber, Origin and differentiation of microglia. *Front. Cell. Neurosci.* **7** (2013).

52. K. Sharma, K. Bisht, U. B. Eyo, A Comparative Biology of Microglia Across Species. *Front. Cell Dev. Biol.* **9** (2021).

53. P. Mastorakos, D. McGavern, The anatomy and immunology of vasculature in the central nervous system. *Science Immunology* **4**, eaav0492 (2019).

54. N. Spassky, F. T. Merkle, N. Flames, A. D. Tramontin, J. M. García-Verdugo, A. Alvarez-Buylla, Adult Ependymal Cells Are Postmitotic and Are Derived from Radial Glial Cells during Embryogenesis. *J. Neurosci.* **25**, 10–18 (2005).

55. A. MacDonald, B. Lu, M. Caron, N. Caporicci-Dinucci, D. Hatrock, K. Petrecca, G. Bourque, J. A. Stratton, Single Cell Transcriptomics of Ependymal Cells Across Age, Region and Species Reveals Cilia-Related and Metal Ion Regulatory Roles as Major Conserved Ependymal Cell Functions. *Front. Cell. Neurosci.* **15** (2021).

56. C. Falcone, Evolution of astrocytes: From invertebrates to vertebrates. *Front. Cell Dev. Biol.* **10** (2022).

57. S. Marques, A. Zeisel, S. Codeluppi, D. Van Bruggen, A. M. Falcão, L. Xiao, H. Li, M. Häring, H. Hochgerner, R. A. Romanov, D. Gyllborg, A. B. Muñoz-Manchado, G. La Manno, P. Lönnerberg, E. M. Floriddia, F. Rezayee, P. Ernfors, E. Arenas, J. Hjerling-Leffler, T. Harkany, W. D. Richardson, S. Linnarsson, G. Castelo-Branco, Oligodendrocyte heterogeneity in the mouse juvenile and adult central nervous system. *Science* **352**, 1326–1329 (2016).

58. M. Bradl, H. Lassmann, Oligodendrocytes: biology and pathology. *Acta Neuropathol* **119**, 37–53 (2010).

59. B. S. Khakh, M. V. Sofroniew, Diversity of astrocyte functions and phenotypes in neural circuits. *Nature Neuroscience* **18**, 942–952 (2015).

60. J. Chen, K. E. Poskanzer, M. R. Freeman, K. R. Monk, Live-imaging of astrocyte morphogenesis and function in zebrafish neural circuits. *Nat Neurosci* **23**, 1297–1306 (2020).

61. J. P. Magnusson, C. Göritz, J. Tatarishvili, D. O. Dias, E. M. K. Smith, O. Lindvall, Z. Kokaia, J. Frisén, A latent neurogenic program in astrocytes regulated by Notch signaling in the mouse. *Science* **346**, 237–241 (2014).

62. J. P. Magnusson, M. Zamboni, G. Santopolo, J. E. Mold, M. Barrientos-Somarribas, C. Talavera-Lopez, B. Andersson, J. Frisén, Activation of a neural stem cell transcriptional program in parenchymal astrocytes. *eLife* **9**, e59733 (2020).

63. A. Buffo, F. Rossi, Origin, lineage and function of cerebellar glia. *Progress in Neurobiology* **109**, 42–63 (2013).

64. J. Wang, M. L. O'Sullivan, D. Mukherjee, V. M. Puñal, S. Farsiu, J. N. Kay, Anatomy and spatial organization of Müller glia in mouse retina. *Journal of Comparative Neurology* **525**, 1759–1777 (2017).

65. L. Valihrach, Z. Matusova, D. Zucha, R. Klassen, S. Benesova, P. Abaffy, M. Kubista, M. Anderova, Recent advances in deciphering oligodendrocyte heterogeneity with single-cell transcriptomics. *Front. Cell. Neurosci.* **16** (2022).

66. M. Y. Batiuk, A. Martirosyan, J. Wahis, F. de Vin, C. Marneffe, C. Kusserow, J. Koeppen, J. F. Viana, J. F. Oliveira, T. Voet, C. P. Ponting, T. G. Belgard, M. G. Holt, Identification of region-specific astrocyte subtypes at single cell resolution. *Nat Commun* **11**, 1220 (2020).

67. A. Zeisel, H. Hochgerner, P. Lönnerberg, A. Johnsson, F. Memic, J. van der Zwan, M. Häring, E. Braun, L. E. Borm, G. La Manno, S. Codeluppi, A. Furlan, K. Lee, N. Skene, K. D. Harris, J. Hjerling-Leffler, E. Arenas, P. Ernfors, U. Marklund, S. Linnarsson, Molecular Architecture of the Mouse Nervous System. *Cell* **174**, 999-1014.e22 (2018).

68. K. Siletti, R. Hodge, A. Mossi Albiach, K. W. Lee, S.-L. Ding, L. Hu, P. Lönnerberg, T. Bakken, T. Casper, M. Clark, N. Dee, J. Gloe, D. Hirschstein, N. V. Shapovalova, C. D. Keene, J. Nyhus, H. Tung, A. M. Yanny, E. Arenas, E. S. Lein, S. Linnarsson, Transcriptomic diversity of cell types across the adult human brain. *Science* **382**, eadd7046 (2023).

69. N. Y. Ahmed, R. Knowles, N. Dehorter, New Insights Into Cholinergic Neuron Diversity. *Front. Mol. Neurosci.* **12** (2019).

70. N. Flames, R. Pla, D. M. Gelman, J. L. R. Rubenstein, L. Puelles, O. Marín, Delineation of Multiple Subpallial Progenitor Domains by the Combinatorial Expression of Transcriptional Codes. *J. Neurosci.* **27**, 9682–9695 (2007).

71. L. Lim, D. Mi, A. Llorca, O. Marín, Development and Functional Diversification of Cortical Interneurons. *Neuron* **100**, 294–313 (2018).

72. D. Hain, T. Gallego-Flores, M. Klinkmann, A. Macias, E. Ciirdaeva, A. Arends, C. Thum, G. Tushev, F. Kretschmer, M. A. Tosches, G. Laurent, Molecular diversity and evolution of neuron types in the amniote brain. *Science (New York, N.Y.)* **377**, eabp8202 (2022).

73. S. Pandey, A. J. Moyer, S. B. Thyme, A single-cell transcriptome atlas of the maturing zebrafish telencephalon. *Genome Res.* **33**, 658–671 (2023).

74. M. Tibi, S. Biton Hayun, H. Hochgerner, Z. Lin, S. Givon, O. Ophir, T. Shay, T. Mueller, R. Segev, A. Zeisel, A telencephalon cell type atlas for goldfish reveals diversity in the evolution of spatial structure and cell types. *Science Advances* **9**, eadh7693 (2023).

75. B. M. Colquitt, D. P. Merullo, G. Konopka, T. F. Roberts, M. S. Brainard, Cellular transcriptomics reveals evolutionary identities of songbird vocal circuits. *Science* **371**, eabd9704 (2021).

76. Z. Yao, C. T. J. van Velthoven, M. Kunst, M. Zhang, D. McMillen, C. Lee, W. Jung, J. Goldy, A. Abdelhak, M. Aitken, K. Baker, P. Baker, E. Barkan, D. Bertagnolli, A. Bhandiwad, C. Bielstein, P. Bishwakarma, J. Campos, D. Carey, T. Casper, A. B. Chakka, R. Chakrabarty, S. Chavan, M. Chen, M. Clark, J. Close, K. Crichton, S. Daniel, P. DiValentin, T. Dolbeare, L. Ellingwood, E. Fiabane, T. Fliss, J. Gee, J. Gerstenberger, A. Glandon, J. Gloe, J. Gould, J. Gray, N. Guilford, J. Guzman, D. Hirschstein, W. Ho, M. Hooper, M. Huang, M. Hupp, K. Jin, M. Kroll, K. Lathia, A. Leon, S. Li, B. Long, Z. Madigan, J. Malloy, J. Malone, Z. Maltzer, N. Martin, R. McCue, R. McGinty, N. Mei, J. Melchor, E. Meyerdierks, T. Mollenkopf, S. Moonsman, T. N. Nguyen, S. Otto, T. Pham, C. Rimorin, A. Ruiz, R. Sanchez, L. Sawyer, N. Shapovalova, N. Shepard, C. Slaughterbeck, J. Sulc, M. Tieu, A. Torkelson, H. Tung, N. Valera Cuevas, S. Vance, K. Wadhwani, K. Ward, B. Levi, C. Farrell, R. Young, B. Staats, M.-Q. M. Wang, C. L. Thompson, S. Mufti, C. M. Pagan, L. Kruse, N. Dee, S. M. Sunkin, L. Esposito, M. J. Hawrylycz, J. Waters, L. Ng, K. Smith, B. Tasic, X. Zhuang, H. Zeng, A high-resolution transcriptomic and spatial atlas of cell types in the whole mouse brain. *Nature* **624**, 317–332 (2023).

77. F. Scala, D. Kobak, M. Bernabucci, Y. Bernaerts, C. R. Cadwell, J. R. Castro, L. Hartmanis, X. Jiang, S. Laturnus, E. Miranda, S. Mulherkar, Z. H. Tan, Z. Yao, H. Zeng, R. Sandberg, P. Berens, A. S. Tolias, Phenotypic variation of transcriptomic cell types in mouse motor cortex. *Nature 2020 598:7879* **598**, 144–150 (2020).

78. H. Peng, P. Xie, L. Liu, X. Kuang, Y. Wang, L. Qu, H. Gong, S. Jiang, A. Li, Z. Ruan, L. Ding, Z. Yao, C. Chen, M. Chen, T. L. Daigle, R. Dalley, Z. Ding, Y. Duan, A. Feiner, P. He, C. Hill, K. E. Hirokawa, G. Hong, L. Huang, S. Kebede, H.-C. Kuo, R. Larsen, P. Lesnar, L. Li, Q. Li, X. Li, Y. Li, Y. Li, A. Liu, D. Lu, S. Mok, L. Ng, T. N. Nguyen, Q. Ouyang, J. Pan, E. Shen, Y. Song, S. M. Sunkin, B. Tasic, M. B. Veldman, W. Wakeman, W. Wan, P. Wang, Q. Wang, T. Wang, Y. Wang, F. Xiong, W. Xiong, W. Xu, M. Ye, L. Yin, Y. Yu, J. Yuan, J. Yuan, Z. Yun, S. Zeng, S. Zhang, S. Zhao, Z. Zhao, Z. Zhou, Z. J. Huang, L. Esposito, M. J. Hawrylycz, S. A. Sorensen, X. W. Yang, Y. Zheng, Z. Gu, W. Xie, C. Koch, Q. Luo, J. A. Harris, Y. Wang, H. Zeng, Morphological diversity of single neurons in molecularly defined cell types. *Nature 2021 598:7879* **598**, 174–181 (2021).

79. R. D. Hodge, T. E. Bakken, J. A. Miller, K. A. Smith, E. R. Barkan, L. T. Graybuck, J. L. Close, B. Long, N. Johansen, O. Penn, Z. Yao, J. Eggermont, T. Höllt, B. P. Levi, S. I. Shehata, B. Aevermann, A. Beller, D. Bertagnolli, K. Brouner, T. Casper, C. Cobbs, R. Dalley, N. Dee, S.-L. Ding, R. G. Ellenbogen, O. Fong, E. Garren, J. Goldy, R. P. Gwinn, D. Hirschstein, C. D. Keene, M. Keshk, A. L. Ko, K. Lathia, A. Mahfouz, Z. Maltzer, M. McGraw, T. N. Nguyen, J. Nyhus, J. G. Ojemann, A. Oldre, S. Parry, S. Reynolds, C. Rimorin, N. V. Shapovalova, S. Somasundaram, A. Szafer, E. R. Thomsen, M. Tieu, G. Quon, R. H. Scheuermann, R. Yuste, S. M. Sunkin, B. Lelieveldt, D. Feng, L. Ng, A. Bernard, M. Hawrylycz, J. W. Phillips, B. Tasic, H. Zeng, A. R. Jones, C. Koch, E. S. Lein, Conserved cell types with divergent features in human versus mouse cortex. *Nature*, 1–8 (2019).

80. G. La Manno, K. Siletti, A. Furlan, D. Gyllborg, E. Vinsland, A. Mossi Albiach, C. Mattsson Langseth, I. Khven, A. R. Lederer, L. M. Dratva, A. Johnsson, M. Nilsson, P. Lönnerberg, S. Linnarsson, Molecular architecture of the developing mouse brain. *Nature 2021*, 1–5 (2021).

81. E. Braun, M. Danan-Gotthold, L. E. Borm, K. W. Lee, E. Vinsland, P. Lönnerberg, L. Hu, X. Li, X. He, Ž. Andrusivová, J. Lundeberg, R. A. Barker, E. Arenas, E. Sundström, S. Linnarsson, Comprehensive cell atlas of the first-trimester developing human brain. *Science* **382**, eadf1226 (2023).

82. Z. Yao, C. T. J. van Velthoven, T. N. Nguyen, J. Goldy, A. E. Sedeno-Cortes, F. Baftizadeh, D. Bertagnolli, T. Casper, M. Chiang, K. Crichton, S.-L. Ding, O. Fong, E. Garren, A. Glandon, N. W. Gouwens, J. Gray, L. T. Graybuck, M. J. Hawrylycz, D. Hirschstein, M. Kroll, K. Lathia, C. Lee, B. Levi, D. McMillen, S. Mok, T. Pham, Q. Ren, C. Rimorin, N. Shapovalova, J. Sulc, S. M. Sunkin, M. Tieu, A. Torkelson, H. Tung, K. Ward, N. Dee, K. A. Smith, B. Tasic, H. Zeng, A taxonomy of transcriptomic cell types across the isocortex and hippocampal formation. *Cell* **184**, 3222-3241.e26 (2021).

83. B. Yu, Q. Zhang, L. Lin, X. Zhou, W. Ma, S. Wen, C. Li, W. Wang, Q. Wu, X. Wang, X.-M. Li, Molecular and cellular evolution of the amygdala across species analyzed by single-nucleus transcriptome profiling. *Cell Discovery 2023 9:1* **9**, 1–22 (2023).

84. Y. Murakami, M. Ogasawara, F. Sugahara, S. Hirano, N. Satoh, S. Kuratani, Identification and expression of the lamprey Pax6 gene: evolutionary origin of the segmented brain of vertebrates. *Development* **128**, 3521–3531 (2001).

85. F. Sugahara, Y. Murakami, N. Adachi, S. Kuratani, Evolution of the regionalization and patterning of the vertebrate telencephalon: what can we learn from cyclostomes? *Current Opinion in Genetics & Development* **23**, 475–483 (2013).

86. R. Senovilla-Ganzo, F. García-Moreno, The Phylotypic Brain of Vertebrates, from Neural Tube Closure to Brain Diversification. *Brain Behavior and Evolution* **99**, 45–68 (2024).

87. F. García-Moreno, Z. Molnár, Variations of telencephalic development that paved the way for neocortical evolution. *Progress in Neurobiology* **194**, 101865 (2020).

88. T. Takahashi, R. S. Nowakowski, V. S. Caviness, The cell cycle of the pseudostratified ventricular epithelium of the embryonic murine cerebral wall. *J. Neurosci.* **15**, 6046–6057 (1995).

89. H. M. Tsai, B. B. Garber, L. M. H. Larramendi, 3H-Thymidine autoradiographic analysis of telencephalic histogenesis in the chick embryo: I. Neuronal birthdates of telencephalic compartments in situ. *Journal of Comparative Neurology* **198**, 275–292 (1981).

90. A. Cárdenas, V. Borrell, Molecular and cellular evolution of corticogenesis in amniotes. *Cellular and Molecular Life Sciences* **77**, 1435–1460 (2020).

91. M. Florio, W. B. Huttner, Neural progenitors, neurogenesis and the evolution of the neocortex. *Development (Cambridge, England)* **141**, 2182–94 (2014).

92. A. Kriegstein, S. Noctor, V. Martínez-Cerdeño, Patterns of neural stem and progenitor cell division may underlie evolutionary cortical expansion. *Nature Reviews Neuroscience* **7**, 883–890 (2006).

93. C. Dehay, W. B. Huttner, Development and evolution of the primate neocortex from a progenitor cell perspective. *Development* **151**, dev199797 (2024).

94. A. Cárdenas, A. Villalba, C. de Juan Romero, E. Picó, C. Kyrousi, A. C. Tzika, M. Tessier-Lavigne, L. Ma, M. Drukker, S. Cappello, V. Borrell, Evolution of Cortical Neurogenesis in Amniotes Controlled by Robo Signaling Levels. *Cell* **174**, 590-606.e21 (2018).

95. T. Nomura, C. Ohtaka-Maruyama, W. Yamashita, Y. Wakamatsu, Y. Murakami, F. Calegari, K. Suzuki, H. Gotoh, K. Ono, The evolution of basal progenitors in the developing non-mammalian brain. *Development* **143**, 66–74 (2016).

96. B. K. Clinton, C. L. Cunningham, A. R. Kriegstein, S. C. Noctor, V. Martínez-Cerdeño, Radial glia in the proliferative ventricular zone of the embryonic and adult turtle, Trachemys scripta elegans. *Neurogenesis* **1**, e970905 (2014).

97. F. Causeret, M. X. Moreau, A. Pierani, O. Blanquie, The multiple facets of Cajal-Retzius neurons. *Development (Cambridge)* **148** (2021).

98. J. H. Lui, D. V. Hansen, A. R. Kriegstein, Development and Evolution of the Human Neocortex. *Cell* **146**, 18–36 (2011).

99. T. Aerts, E. Seuntjens, Novel Perspectives on the Development of the Amygdala in Rodents. *Frontiers in Neuroanatomy* **15**, 98 (2021).

100. H.-T. Xu, Z. Han, P. Gao, S. He, Z. Li, W. Shi, O. Kodish, W. Shao, K. N. Brown, K. Huang, S.-H. Shi, Distinct Lineage-Dependent Structural and Functional Organization of the Hippocampus. *Cell* **157**, 1552–1564 (2014).

101. T. Nomura, M. Takahashi, Y. Hara, O. Noriko, Patterns of neurogenesis and amplitude of reelin expression are essential for making a mammalian-type cortex. *PLoS ONE* **3** (2008).

102. A. M. Goffinet, I. Bar, B. Bernier, C. Trujillo, A. Raynaud, G. Meyer, Reelin expression during embryonic brain development in lacertilian lizards. *J Comp Neurol* **414**, 533–550 (1999).

103. S. Jiménez, N. Moreno, Analysis of the Expression Pattern of Cajal-Retzius Cell Markers in the Xenopus laevis Forebrain. *Brain Behavior and Evolution* **96**, 263–282 (2021).

104. E. Rueda-Alaña, R. Senovilla-Ganzo, M. Grillo, E. Vázquez, S. Marco-Salas, T. Gallego-Flores, A. Ftara, L. Escobar, A. Benguría, A. Quintas-Gorozarri, A. Dopazo, M. Rábano, M. dM Vivanco, A. M. Aransay, D. Garrigos, Á. Toval, J. L. Ferrán, M. Nilsson, J. M. Encinas, M. De Pitta, F. García-Moreno,

Evolutionary convergence of sensory circuits in the pallium of amniotes. *bioRxiv*, 2024.04.30.591819 (2024).

105. R. N. Delgado, D. E. Allen, M. G. Keefe, W. R. Mancia Leon, R. S. Ziffra, E. E. Crouch, A. Alvarez-Buylla, T. J. Nowakowski, Individual human cortical progenitors can produce excitatory and inhibitory neurons. *Nature* **601**, 397–403 (2022).

106. S. N. Kim, V. V. Viswanadham, R. N. Doan, Y. Dou, S. Bizzotto, S. Khoshkhoo, A. Y. Huang, R. Yeh, B. Chhouk, A. Truong, K. M. Chappell, M. Beaudin, A. Barton, S. K. Akula, L. Rento, M. Lodato, J. Ganz, R. A. Szeto, P. Li, J. W. Tsai, R. S. Hill, P. J. Park, C. A. Walsh, Cell lineage analysis with somatic mutations reveals late divergence of neuronal cell types and cortical areas in human cerebral cortex. *bioRxiv*, 2023.11.06.565899 (2023).

107. Y. Hashimoto, H. Gotoh, K. Ono, T. Nomura, Differential potentials of neural progenitors for the generation of neurons and non-neuronal cells in the developing amniote brain. *Sci Rep* **9**, 4514 (2019).

108. M. Naruse, Y. Ishizaki, K. Ikenaka, A. Tanaka, S. Hitoshi, Origin of oligodendrocytes in mammalian forebrains: a revised perspective. *J Physiol Sci* **67**, 63–70 (2017).

109. A. Nishiyama, T. Shimizu, A. Sherafat, W. D. Richardson, Life-long oligodendrocyte development and plasticity. *Seminars in Cell & Developmental Biology* **116**, 25–37 (2021).

110. E. S. Akdemir, A. Y.-S. Huang, B. Deneen, Astrocytogenesis: where, when, and how. F1000Research 9:233 [Preprint] (2020). https://doi.org/10.12688/f1000research.22405.1.

111. A. M. Bond, G. Ming, H. Song, Adult Mammalian Neural Stem Cells and Neurogenesis: Five Decades Later. *Cell Stem Cell* **17**, 385–395 (2015).

112. E. A. Brenowitz, T. A. Larson, Neurogenesis in the Adult Avian Song-Control System. *Cold Spring Harb Perspect Biol* **7**, a019000 (2015).

113. M. Vellema, A. van der Linden, M. Gahr, Area-specific migration and recruitment of new neurons in the adult songbird brain. *Journal of Comparative Neurology* **518**, 1442–1459 (2010).

114. L. A. D'Amico, D. Boujard, P. Coumailleau, The Neurogenic Factor NeuroD1 Is Expressed in Post-Mitotic Cells during Juvenile and Adult Xenopus Neurogenesis and Not in Progenitor or Radial Glial Cells. *PLOS ONE* **8**, e66487 (2013).

115. S. D. Briscoe, C. B. Albertin, J. J. Rowell, C. W. Ragsdale, Neocortical Association Cell Types in the Forebrain of Birds and Alligators. *Current Biology* **28**, 686-696.e6 (2018).

116. F. García-Moreno, E. Anderton, M. Jankowska, J. Begbie, J. M. Encinas, M. Irimia, Z. Molnár, Absence of Tangentially Migrating Glutamatergic Neurons in the Developing Avian Brain. *Cell Reports* **22**, 96–109 (2018).

117. G. F. Striedter, B. P. Keefer, Cell Migration and Aggregation in the Developing Telencephalon: Pulse-Labeling Chick Embryos with Bromodeoxyuridine. *J. Neurosci.* **20**, 8021–8030 (2000).

118. K. Brodmann, Neue Ergebnisse über die vergleichende histologische Lokalisation der Grosshirnrinde mit besonderer Berücksichtigung des Stirnhirns. *Anatomischer Anzeiger* **41**, 157–216 (1912).

119. T. E. Bakken, N. L. Jorstad, Q. Hu, B. B. Lake, W. Tian, B. E. Kalmbach, M. Crow, R. D. Hodge, F. M. Krienen, S. A. Sorensen, J. Eggermont, Z. Yao, B. D. Aevermann, A. I. Aldridge, A. Bartlett, D. Bertagnolli, T. Casper, R. G. Castanon, K. Crichton, T. L. Daigle, R. Dalley, N. Dee, N. Dembrow, D. Diep, S.-L. Ding, W. Dong, R. Fang, S. Fischer, M. Goldman, J. Goldy, L. T. Graybuck, B. R. Herb, X. Hou, J. Kancherla, M. Kroll, K. Lathia, B. van Lew, Y. E. Li, C. S. Liu, H. Liu, J. D. Lucero, A. Mahurkar, D. McMillen, J. A. Miller,

M. Moussa, J. R. Nery, P. R. Nicovich, S.-Y. Niu, J. Orvis, J. K. Osteen, S. Owen, C. R. Palmer, T. Pham, N. Plongthongkum, O. Poirion, N. M. Reed, C. Rimorin, A. Rivkin, W. J. Romanow, A. E. Sedeño-Cortés, K. Siletti, S. Somasundaram, J. Sulc, M. Tieu, A. Torkelson, H. Tung, X. Wang, F. Xie, A. M. Yanny, R. Zhang, S. A. Ament, M. M. Behrens, H. C. Bravo, J. Chun, A. Dobin, J. Gillis, R. Hertzano, P. R. Hof, T. Höllt, G. D. Horwitz, C. D. Keene, P. V. Kharchenko, A. L. Ko, B. P. Lelieveldt, C. Luo, E. A. Mukamel, A. Pinto-Duarte, S. Preissl, A. Regev, B. Ren, R. H. Scheuermann, K. Smith, W. J. Spain, O. R. White, C. Koch, M. Hawrylycz, B. Tasic, E. Z. Macosko, S. A. McCarroll, J. T. Ting, H. Zeng, K. Zhang, G. Feng, J. R. Ecker, S. Linnarsson, E. S. Lein, Comparative cellular analysis of motor cortex in human, marmoset and mouse. *Nature 2021 598:7879* **598**, 111–119 (2021).

120. F. M. Krienen, M. Goldman, Q. Zhang, R. C. H. del Rosario, M. Florio, R. Machold, A. Saunders, K. Levandowski, H. Zaniewski, B. Schuman, C. Wu, A. Lutservitz, C. D. Mullally, N. Reed, E. Bien, L. Bortolin, M. Fernandez-Otero, J. D. Lin, A. Wysoker, J. Nemesh, D. Kulp, M. Burns, V. Tkachev, R. Smith, C. A. Walsh, J. Dimidschstein, B. Rudy, L. S. Kean, S. Berretta, G. Fishell, G. Feng, S. A. McCarroll, Innovations present in the primate interneuron repertoire. *Nature* **586**, 262–269 (2020).

121. J.-R. Wei, Z.-Z. Hao, C. Xu, M. Huang, L. Tang, N. Xu, R. Liu, Y. Shen, S. A. Teichmann, Z. Miao, S. Liu, Identification of visual cortex cell types and species differences using single-cell RNA sequencing. *Nat Commun* **13**, 6902 (2022).

122. E. Boldog, T. E. Bakken, R. D. Hodge, M. Novotny, B. D. Aevermann, J. Baka, S. Bordé, J. L. Close, F. Diez-Fuertes, S.-L. Ding, N. Faragó, Á. K. Kocsis, B. Kovács, Z. Maltzer, J. M. McCorrison, J. A. Miller, G. Molnár, G. Oláh, A. Ozsvár, M. Rózsa, S. I. Shehata, K. A. Smith, S. M. Sunkin, D. N. Tran, P. Venepally, A. Wall, L. G. Puskás, P. Barzó, F. J. Steemers, N. J. Schork, R. H. Scheuermann, R. S. Lasken, E. S. Lein, G. Tamás, Transcriptomic and morphophysiological evidence for a specialized human cortical GABAergic cell type. *Nature Neuroscience* **21**, 1185–1195 (2018).

123. M. T. Schmitz, K. Sandoval, C. P. Chen, M. A. Mostajo-Radji, W. W. Seeley, T. J. Nowakowski, C. J. Ye, M. F. Paredes, A. A. Pollen, The development and evolution of inhibitory neurons in primate cerebrum. *Nature* **603**, 871–877 (2022).

124. J. Berg, S. A. Sorensen, J. T. Ting, J. A. Miller, T. Chartrand, A. Buchin, T. E. Bakken, A. Budzillo, N. Dee, S.-L. Ding, N. W. Gouwens, R. D. Hodge, B. Kalmbach, C. Lee, B. R. Lee, L. Alfiler, K. Baker, E. Barkan, A. Beller, K. Berry, D. Bertagnolli, K. Bickley, J. Bomben, T. Braun, K. Brouner, T. Casper, P. Chong, K. Crichton, R. Dalley, R. de Frates, T. Desta, S. D. Lee, F. D'Orazi, N. Dotson, T. Egdorf, R. Enstrom, C. Farrell, D. Feng, O. Fong, S. Furdan, A. A. Galakhova, C. Gamlin, A. Gary, A. Glandon, J. Goldy, M. Gorham, N. A. Goriounova, S. Gratiy, L. Graybuck, H. Gu, K. Hadley, N. Hansen, T. S. Heistek, A. M. Henry, D. B. Heyer, D. Hill, C. Hill, M. Hupp, T. Jarsky, S. Kebede, L. Keene, L. Kim, M.-H. Kim, M. Kroll, C. Latimer, B. P. Levi, K. E. Link, M. Mallory, R. Mann, D. Marshall, M. Maxwell, M. McGraw, D. McMillen, E. Melief, E. J. Mertens, L. Mezei, N. Mihut, S. Mok, G. Molnar, A. Mukora, L. Ng, K. Ngo, P. R. Nicovich, J. Nyhus, G. Olah, A. Oldre, V. Omstead, A. Ozsvar, D. Park, H. Peng, T. Pham, C. A. Pom, L. Potekhina, R. Rajanbabu, S. Ransford, D. Reid, C. Rimorin, A. Ruiz, D. Sandman, J. Sulc, S. M. Sunkin, A. Szafer, V. Szemenyei, E. R. Thomsen, M. Tieu, A. Torkelson, J. Trinh, H. Tung, W. Wakeman, F. Waleboer, K. Ward, R. Wilbers, G. Williams, Z. Yao, J.-G. Yoon, C. Anastassiou, A. Arkhipov, P. Barzo, A. Bernard, C. Cobbs, P. C. de Witt Hamer, R. G. Ellenbogen, L. Esposito, M. Ferreira, R. P. Gwinn, M. J. Hawrylycz, P. R. Hof, S. Idema, A. R. Jones, C. D. Keene, A. L. Ko, G. J. Murphy, L. Ng, J. G. Ojemann, A. P. Patel, J. W. Phillips, D. L. Silbergeld, K. Smith, B. Tasic, R. Yuste, I. Segev, C. P. J. de Kock, H. D. Mansvelder, G. Tamas, H. Zeng, C. Koch, E. S. Lein, Human neocortical expansion involves glutamatergic neuron diversification. *Nature 2021 598:7879* **598**, 151–158 (2021).

125. H. J. Karten, The Organization of the Avian Telencephalon and Some Speculations on the Phylogeny of the Amniote Telencephalon. *Annals of the New York Academy of Sciences* **167**, 164–179 (1969).

126. S. D. Briscoe, C. W. Ragsdale, Homology, neocortex, and the evolution of developmental mechanisms. *Science* **362**, 190–193 (2018).

127. G. F. Striedter, The telencephalon of tetrapods in evolution. *Brain Behav Evol* **49**, 179–213 (1997).

128. L. Puelles, J. E. Sandoval, A. Ayad, R. del Corral, A. Alonso, J. L. Ferran, M. Martínez-de-la-Torre, *The Pallium in Reptiles and Birds in the Light of the Updated Tetrapartite Pallium Model* (2016)vols. 1–4.

129. L. Puelles, Current status of the hypothesis of a claustro-insular homolog in sauropsids. *Brain, Behavior and Evolution*, doi: 10.1159/000520742 (2021).

130. A. T. Kalinka, K. M. Varga, D. T. Gerrard, S. Preibisch, D. L. Corcoran, J. Jarrells, U. Ohler, C. M. Bergman, P. Tomancak, Gene expression divergence recapitulates the developmental hourglass model. *Nature* **468**, 811–814 (2010).

131. H. Hu, M. Uesaka, S. Guo, K. Shimai, T.-M. Lu, F. Li, S. Fujimoto, M. Ishikawa, S. Liu, Y. Sasagawa, G. Zhang, S. Kuratani, J.-K. Yu, T. G. Kusakabe, P. Khaitovich, N. Irie, Constrained vertebrate evolution by pleiotropic genes. *Nat Ecol Evol* **1**, 1722–1730 (2017).

132. M. Cardoso-Moreira, J. Halbert, D. Valloton, B. Velten, C. Chen, Y. Shao, A. Liechti, K. Ascenção, C. Rummel, S. Ovchinnikova, P. V. Mazin, I. Xenarios, K. Harshman, M. Mort, D. N. Cooper, C. Sandi, M. J. Soares, P. G. Ferreira, S. Afonso, M. Carneiro, J. M. A. Turner, J. L. VandeBerg, A. Fallahshahroudi, P. Jensen, R. Behr, S. Lisgo, S. Lindsay, P. Khaitovich, W. Huber, J. Baker, S. Anders, Y. E. Zhang, H. Kaessmann, Gene expression across mammalian organ development. *Nature* **571**, 505–509 (2019).

133. L. Medina, A. Abellán, E. Desfilis, Evolving Views on the Pallium. *Brain, Behavior and Evolution*, 1–19 (2021).

134. D. Arendt, J. M. Musser, C. V. H. Baker, A. Bergman, C. Cepko, D. H. Erwin, M. Pavlicev, G. Schlosser, S. Widder, M. D. Laubichler, G. P. Wagner, The origin and evolution of cell types. *Nature Reviews Genetics* **17**, 744–757 (2016).

135. R. S. Ziffra, C. N. Kim, J. M. Ross, A. Wilfert, T. N. Turner, M. Haeussler, A. M. Casella, P. F. Przytycki, K. C. Keough, D. Shin, D. Bogdanoff, A. Kreimer, K. S. Pollard, S. A. Ament, E. E. Eichler, N. Ahituv, T. J. Nowakowski, Single-cell epigenomics reveals mechanisms of human cortical development. *Nature 2021 598:7879* **598**, 205–213 (2021).

136. L. Loo, J. M. Simon, L. Xing, E. S. McCoy, J. K. Niehaus, J. Guo, E. S. Anton, M. J. Zylka, Single-cell transcriptomic analysis of mouse neocortical development. *Nature Communications* **10**, 134 (2019).

137. D. J. Di Bella, E. Habibi, R. R. Stickels, G. Scalia, J. Brown, P. Yadollahpour, S. M. Yang, C. Abbate, T. Biancalani, E. Z. Macosko, F. Chen, A. Regev, P. Arlotta, Molecular logic of cellular diversification in the mouse cerebral cortex. *Nature 2021 595:7868* **595**, 554–559 (2021).

138. T. E. Bakken, R. D. Hodge, J. A. Miller, Z. Yao, T. N. Nguyen, B. Aevermann, E. Barkan, D. Bertagnolli, T. Casper, N. Dee, E. Garren, J. Goldy, L. T. Graybuck, M. Kroll, R. S. Lasken, K. Lathia, S. Parry, C. Rimorin, R. H. Scheuermann, N. J. Schork, S. I. Shehata, M. Tieu, J. W. Phillips, A. Bernard, K. A. Smith, H. Zeng, E. S. Lein, B. Tasic, Single-nucleus and single-cell transcriptomes compared in matched cortical cell types. *PLOS ONE* **13**, e0209648 (2018).

139. J. Ding, X. Adiconis, S. K. Simmons, M. S. Kowalczyk, C. C. Hession, N. D. Marjanovic, T. K. Hughes, M. H. Wadsworth, T. Burks, L. T. Nguyen, J. Y. H. Kwon, B. Barak, W. Ge, A. J. Kedaigle, S. Carroll, S. Li, N. Hacohen, O. Rozenblatt-Rosen, A. K. Shalek, A.-C. Villani, A. Regev, J. Z. Levin, Systematic comparison of single-cell and single-nucleus RNA-sequencing methods. *Nat Biotechnol* **38**, 737–746 (2020).

140. M. Carlén, What constitutes the prefrontal cortex? *Science* **358**, 478–482 (2017).

141. A. Saunders, E. Z. Macosko, A. Wysoker, M. Goldman, F. M. Krienen, H. de Rivera, E. Bien, M. Baum, L. Bortolin, S. Wang, A. Goeva, J. Nemesh, N. Kamitaki, S. Brumbaugh, D. Kulp, S. A. McCarroll, Molecular Diversity and Specializations among the Cells of the Adult Mouse Brain. *Cell* **174**, 1015-1030.e16 (2018).

142. E. Denisenko, B. B. Guo, M. Jones, R. Hou, L. de Kock, T. Lassmann, D. Poppe, O. Clément, R. K. Simmons, R. Lister, A. R. R. Forrest, Systematic assessment of tissue dissociation and storage biases in single-cell and single-nucleus RNA-seq workflows. *Genome Biology* **21**, 130 (2020).

143. D. Mattei, A. Ivanov, M. van Oostrum, S. Pantelyushin, J. Richetto, F. Mueller, M. Beffinger, L. Schellhammer, J. vom Berg, B. Wollscheid, D. Beule, R. C. Paolicelli, U. Meyer, Enzymatic Dissociation Induces Transcriptional and Proteotype Bias in Brain Cell Populations. *International Journal of Molecular Sciences* **21**, 7944 (2020).

144. B. Cubelos, A. Sebastián-Serrano, L. Beccari, M. E. Calcagnotto, E. Cisneros, S. Kim, A. Dopazo, M. Alvarez-Dolado, J. M. Redondo, P. Bovolenta, C. A. Walsh, M. Nieto, *Cux1* and *Cux2* Regulate Dendritic Branching, Spine Morphology, and Synapses of the Upper Layer Neurons of the Cortex. *Neuron* **66**, 523–535 (2010).

145. E. A. Clark, M. Rutlin, L. S. Capano, S. Aviles, J. R. Saadon, P. Taneja, Q. Zhang, J. B. Bullis, T. Lauer, E. Myers, A. Schulmann, D. Forrest, S. B. Nelson, Cortical RORβ is required for layer 4 transcriptional identity and barrel integrity. *eLife* **9**, e52370 (2020).

146. S. Lodato, B. J. Molyneaux, E. Zuccaro, L. A. Goff, H.-H. Chen, W. Yuan, A. Meleski, E. Takahashi, S. Mahony, J. L. Rinn, D. K. Gifford, P. Arlotta, Gene co-regulation by Fezf2 selects neurotransmitter identity and connectivity of corticospinal neurons. *Nature Neuroscience* **17**, 1046–1054 (2014).

147. J. V. Nielsen, M. Thomassen, K. Møllgård, J. Noraberg, N. A. Jensen, Zbtb20 Defines a Hippocampal Neuronal Identity Through Direct Repression of Genes That Control Projection Neuron Development in the Isocortex. *Cerebral Cortex* **24**, 1216–1229 (2014).

148. T. Iwano, A. Masuda, H. Kiyonari, H. Enomoto, F. Matsuzaki, Prox1 postmitotically defines dentate gyrus cells by specifying granule cell identity over CA3 pyramidal cell fate in the hippocampus. *Development* **139**, 3051–3062 (2012).

149. L. Lambeth, M. J. Blunt, Electron-microscopic study of monotreme neuroglia. *Acta Anatomica* **93**, 115–125 (2008).

150. H. Bruguier, R. Suarez, P. Manger, A. Hoerder-Suabedissen, A. M. Shelton, D. K. Oliver, A. M. Packer, J. L. Ferran, F. García-Moreno, L. Puelles, Z. Molnár, In search of common developmental and evolutionary origin of the claustrum and subplate. *Journal of Comparative Neurology* **528**, 2956–2977 (2020).

151. T. Stuart, A. Butler, P. Hoffman, C. Hafemeister, E. Papalexi, W. M. Mauck, Y. Hao, M. Stoeckius, P. Smibert, R. Satija, Comprehensive Integration of Single-Cell Data. *Cell* **177**, 1888-1902.e21 (2019).

152. H. Scheich, G. Langner, C. Tidemann, R. B. Coles, A. Guppy, Electroreception and electrolocation in platypus. *Nature* **319**, 401–402 (1986).

153. J. E. Gregory, A. Iggo, A. K. McIntyre, U. Proske, Responses of electroreceptors in the snout of the echidna. *The Journal of Physiology* **414**, 521–538 (1989).

154. H. Hochgerner, S. Singh, M. Tibi, Z. Lin, N. Skarbianskis, I. Admati, O. Ophir, N. Reinhardt, S. Netser, S. Wagner, A. Zeisel, Neuronal types in the mouse amygdala and their transcriptional response to fear conditioning. *Nature Neuroscience 2023*, 1–13 (2023).

155. E. S. Lein, M. J. Hawrylycz, N. Ao, M. Ayres, A. Bensinger, A. Bernard, A. F. Boe, M. S. Boguski, K. S. Brockway, E. J. Byrnes, L. Chen, L. Chen, T. M. Chen, M. C. Chin, J. Chong, B. E. Crook, A. Czaplinska, C. N. Dang, S. Datta, N. R. Dee, A. L. Desaki, T. Desta, E. Diep, T. A. Dolbeare, M. J. Donelan, H. W. Dong, J. G. Dougherty, B. J. Duncan, A. J. Ebbert, G. Eichele, L. K. Estin, C. Faber, B. A. Facer, R. Fields, S. R. Fischer, T. P. Fliss, C. Frensley, S. N. Gates, K. J. Glattfelder, K. R. Halverson, M. R. Hart, J. G. Hohmann, M. P. Howell, D. P. Jeung, R. A. Johnson, P. T. Karr, R. Kawal, J. M. Kidney, R. H. Knapik, C. L. Kuan, J. H.

Lake, A. R. Laramee, K. D. Larsen, C. Lau, T. A. Lemon, A. J. Liang, Y. Liu, L. T. Luong, J. Michaels, J. J. Morgan, R. J. Morgan, M. T. Mortrud, N. F. Mosqueda, L. L. Ng, R. Ng, G. J. Orta, C. C. Overly, T. H. Pak, S. E. Parry, S. D. Pathak, O. C. Pearson, R. B. Puchalski, Z. L. Riley, H. R. Rockett, S. A. Rowland, J. J. Royall, M. J. Ruiz, N. R. Sarno, K. Schaffnit, N. V. Shapovalova, T. Sivisay, C. R. Slaughterbeck, S. C. Smith, K. A. Smith, B. I. Smith, A. J. Sodt, N. N. Stewart, K. R. Stumpf, S. M. Sunkin, M. Sutram, A. Tam, C. D. Teemer, C. Thaller, C. L. Thompson, L. R. Varnam, A. Visel, R. M. Whitlock, P. E. Wohnoutka, C. K. Wolkey, V. Y. Wong, M. Wood, M. B. Yaylaoglu, R. C. Young, B. L. Youngstrom, X. F. Yuan, B. Zhang, T. A. Zwingman, A. R. Jones, Genome-wide atlas of gene expression in the adult mouse brain. *Nature 2006 445:7124* **445**, 168–176 (2006).

156. J. Kuerbitz, M. Arnett, S. Ehrman, M. T. Williams, C. V. Vorhees, S. E. Fisher, A. N. Garratt, L. J. Muglia, R. R. Waclaw, K. Campbell, Loss of Intercalated Cells (ITCs) in the Mouse Amygdala of Tshz1 Mutants Correlates with Fear, Depression, and Social Interaction Phenotypes. *J. Neurosci.* **38**, 1160–1177 (2018).

157. Y. Zhao, O. Marín, E. Hermesz, A. Powell, N. Flames, M. Palkovits, J. L. R. Rubenstein, H. Westphal, The LIM-homeobox gene Lhx8 is required for the development of many cholinergic neurons in the mouse forebrain. *Proceedings of the National Academy of Sciences* **100**, 9005–9010 (2003).

158. R. Ke, M. Mignardi, A. Pacureanu, J. Svedlund, J. Botling, C. Wählby, M. Nilsson, In situ sequencing for RNA analysis in preserved tissue and cells. *Nat Methods* **10**, 857–860 (2013).

159. T. Biancalani, G. Scalia, L. Buffoni, R. Avasthi, Z. Lu, A. Sanger, N. Tokcan, C. R. Vanderburg, Å. Segerstolpe, M. Zhang, I. Avraham-Davidi, S. Vickovic, M. Nitzan, S. Ma, A. Subramanian, M. Lipinski, J. Buenrostro, N. B. Brown, D. Fanelli, X. Zhuang, E. Z. Macosko, A. Regev, Deep learning and alignment of spatially resolved single-cell transcriptomes with Tangram. *Nat Methods* **18**, 1352–1362 (2021).

160. M. A. Lipiec, J. Bem, K. Kozinski, C. Chakraborty, J. Urban-Ciećko, T. Zajkowski, M. Dabrowski, Ł. M. Szewczyk, A. Toval, J. L. Ferran, A. Nagalski, M. B. Wisniewska, TCF7L2 regulates postmitotic differentiation programmes and excitability patterns in the thalamus. *Development (Cambridge)* **147** (2020).

161. K. Kosaka, T. Kosaka, Secretagogin-containing neurons in the mouse main olfactory bulb. *Neuroscience Research* **77**, 16–32 (2013).

162. J. D. Fontenele-Neto, E. Kalinina, Y. Feng, L. D. Fricker, Identification and distribution of mouse carboxypeptidase A-6. *Molecular Brain Research* **137**, 132–142 (2005).

163. C. V. Mello, T. Kaser, A. A. Buckner, M. Wirthlin, P. V. Lovell, Molecular architecture of the zebra finch arcopallium. *Journal of Comparative Neurology* **527**, 2512–2556 (2019).

164. M. Bergsland, M. Werme, M. Malewicz, T. Perlmann, J. Muhr, The establishment of neuronal properties is controlled by Sox4 and Sox11. *Genes Dev.* **20**, 3475–3486 (2006).

165. S.-J. Chou, S. Tole, Lhx2, an evolutionarily conserved, multifunctional regulator of forebrain development. *Brain Research* **1705**, 1–14 (2019).

166. N. Rook, M. Stacho, A. Schwarz, V. P. Bingman, O. Güntürkün, Neuronal circuits within the homing pigeon hippocampal formation. *J of Comparative Neurology* **531**, 790–813 (2023).

167. G. F. Striedter, T. A. Marchant, S. Beydler, The "Neostriatum" Develops as Part of the Lateral Pallium in Birds. *J. Neurosci.* **18**, 5839–5849 (1998).

168. M. A. Tosches, From Cell Types to an Integrated Understanding of Brain Evolution: The Case of the Cerebral Cortex. *https://doi.org/10.1146/annurev-cellbio-120319-112654* **37** (2021).

169. M. T. Biegler, L. J. Cantin, D. L. Scarano, E. D. Jarvis, Controlling for activity-dependent genes and behavioral states is critical for determining brain relationships within and across species. *Journal of Comparative Neurology* **529**, 3206–3221 (2021).

170. A. Rodrigo Albors, G. A. Singer, E. Llorens-Bobadilla, J. Frisén, A. P. May, C. P. Ponting, K. G. Storey, An ependymal cell census identifies heterogeneous and ongoing cell maturation in the adult mouse spinal cord that changes dynamically on injury. *Developmental Cell* **58**, 239-255.e10 (2023).

171. J. F. Montiel, F. Aboitiz, Pallial patterning and the origin of the isocortex. *Frontiers in Neuroscience* **9**, 377 (2015).

172. C. Englund, A. Fink, C. Lau, D. Pham, R. A. M. Daza, A. Bulfone, T. Kowalczyk, R. F. Hevner, Pax6, Tbr2, and Tbr1 Are Expressed Sequentially by Radial Glia, Intermediate Progenitor Cells, and Postmitotic Neurons in Developing Neocortex. *J. Neurosci.* **25**, 247–251 (2005).

173. P. Taglialatela, J. M. Soria, V. Caironi, A. Moiana, S. Bertuzzi, Compromised generation of GABAergic interneurons in the brains of Vax1-/- mice. *Development* **131**, 4239–4249 (2004).

174. L. Uusküla-Reimand, M. D. Wilson, Untangling the roles of TOP2A and TOP2B in transcription and cancer. *Science Advances* **8**, eadd4920 (2022).

175. R. Ayala, T. Shu, L. H. Tsai, Trekking across the Brain: The Journey of Neuronal Migration. *Cell* **128**, 29–43 (2007).

176. I. Sarropoulos, M. Sepp, R. Frömel, K. Leiss, N. Trost, E. Leushkin, K. Okonechnikov, P. Joshi, P. Giere, L. M. Kutscher, M. Cardoso-Moreira, S. M. Pfister, H. Kaessmann, Developmental and evolutionary dynamics of cis-regulatory elements in mouse cerebellar cells. *Science* **373** (2021).

177. L. Haghverdi, M. Büttner, F. A. Wolf, F. Buettner, F. J. Theis, Diffusion pseudotime robustly reconstructs lineage branching. *Nature Methods 2016 13:10* **13**, 845–848 (2016).

178. C. Qiu, J. Cao, T. Li, S. Srivatsan, X. Huang, Systematic reconstruction of the cellular trajectories of mammalian embryogenesis. (2021).

179. E. Balaban, M. Desco, J.-J. Vaquero, Waking-like Brain Function in Embryos. *Current Biology* **22**, 852–861 (2012).

180. N. Hecker, N. Kempynck, D. Mauduit, D. Abaffyová, R. Vandepoel, S. Dieltiens, I. Sarropoulos, C. B. González-Blas, E. Leysen, R. Moors, G. Hulselmans, L. Lim, J. De Wit, V. Christiaens, S. Poovathingal, S. Aerts, Enhancer-driven cell type comparison reveals similarities between the mammalian and bird pallium. *bioRxiv*, 2024.04.17.589795 (2024).

181. A. J. Taranshansky, J. M. Musser, M. Khariton, P. Li, D. Arendt, S. R. Quake, B. Wang, Mapping single-cell atlases throughout Metazoa unravels cell type evolution. 1–42 (2020).

182. E. J. Kim, A. L. Juavinett, E. M. Kyubwa, M. W. Jacobs, E. M. Callaway, Three Types of Cortical Layer 5 Neurons That Differ in Brain-wide Connectivity and Function. *Neuron* **88**, 1253–1267 (2015).

183. S. O'Mara, The subiculum: what it does, what it might do, and what neuroanatomy has yet to tell us. *Journal of Anatomy* **207**, 271–282 (2005).

184. S. Keshavarzi, J. M. Power, E. H. H. Albers, R. K. S. Sullivan, P. Sah, Dendritic Organization of Olfactory Inputs to Medial Amygdala Neurons. *J. Neurosci.* **35**, 13020–13028 (2015).

185. A. Hoerder-Suabedissen, Z. Molnár, Development, evolution and pathology of neocortical subplate neurons. *Nat Rev Neurosci* **16**, 133–146 (2015).

186. W. Z. Wang, F. M. Oeschger, J. F. Montiel, F. García-Moreno, A. Hoerder-Suabedissen, L. Krubitzer, C. J. Ek, N. R. Saunders, K. Reim, A. Villalón, Z. Molnár, Comparative Aspects of Subplate Zone Studied with Gene Expression in Sauropsids and Mammals. *Cerebral Cortex* **21**, 2187–2203 (2011).

187. T. Shabangu, H.-L. Chen, Z. Zhuang, A. Pierani, C.-F. F. Chen, S.-J. Chou, Specific contribution of neurons from the Dbx1 lineage to the piriform cortex. *Sci Rep* **11**, 8349 (2021).

188. E. Rueda-Alaña, I. Martínez-Garay, J. M. Encinas, Z. Molnár, F. García-Moreno, Dbx1-Derived Pyramidal Neurons Are Generated Locally in the Developing Murine Neocortex. *Front. Neurosci.* **12** (2018).

189. S. Nagappan, K. M. Franks, Parallel processing by distinct classes of principal neurons in the olfactory cortex. *eLife* **10**, e73668 (2021).

190. H. Stroud, M. G. Yang, Y. N. Tsitohay, C. P. Davis, M. A. Sherman, S. Hrvatin, E. Ling, M. E. Greenberg, An Activity-Mediated Transition in Transcription in Early Postnatal Neurons. *Neuron* **107**, 874-890.e8 (2020).

191. B. E. Hegarty, G. W. Gruenhagen, Z. V. Johnson, C. M. Baker, J. T. Streelman, Spatially resolved cell atlas of the teleost telencephalon and deep homology of the vertebrate forebrain. *Commun Biol* **7**, 1–16 (2024).

192. K. Yamamoto, P. Estienne, S. Bloch, Does a Vertebrate Morphotype of Pallial Subdivisions Really Exist? *Brain Behavior and Evolution*, 1–18 (2024).

193. L. Roux, G. Buzsáki, Tasks for inhibitory interneurons in intact brain circuits. *Neuropharmacology* **88**, 10–23 (2015).

194. F. Ströckens, K. Neves, S. Kirchem, C. Schwab, S. Herculano-Houzel, O. Güntürkün, High associative neuron numbers could drive cognitive performance in corvid species. *Journal of Comparative Neurology* **530**, 1588–1605 (2022).

195. L. Puelles, *The Chick Brain in Stereotaxic Coordinates : An Atlas Featuring Neuromeric Subdivisions and Mammalian Homologies* (Academic Press, Amsterdam, 1st ed., 2007).

196. S. R. Krishnaswami, R. V. Grindberg, M. Novotny, P. Venepally, B. Lacar, K. Bhutani, S. B. Linker, S. Pham, J. A. Erwin, J. A. Miller, R. Hodge, J. K. McCarthy, M. Kelder, J. McCorrison, B. D. Aevermann, F. D. Fuertes, R. H. Scheuermann, J. Lee, E. S. Lein, N. Schork, M. J. McConnell, F. H. Gage, R. S. Lasken, Using single nuclei for RNA-seq to capture the transcriptome of postmortem neurons. *Nature Protocols* **11**, 499–524 (2016).

197. Z. Y. Wang, E. Leushkin, A. Liechti, S. Ovchinnikova, K. Mößinger, T. Brüning, C. Rummel, F. Grützner, M. Cardoso-Moreira, P. Janich, D. Gatfield, B. Diagouraga, B. de Massy, M. E. Gill, A. H. F. M. Peters, S. Anders, H. Kaessmann, Transcriptome and translatome co-evolution in mammals. *Nature*, doi: 10.1038/s41586-020-2899-z (2020).

198. A. Dobin, C. A. Davis, F. Schlesinger, J. Drenkow, C. Zaleski, S. Jha, P. Batut, M. Chaisson, T. R. Gingeras, STAR: ultrafast universal RNA-seq aligner. *Bioinformatics* **29**, 15–21 (2013).

199. B. Kaminow, D. Yunusov, A. Dobin, STARsolo: accurate, fast and versatile mapping/quantification of single-cell and single-nucleus RNA-seq data. *bioRxiv*, 2021.05.05.442755 (2021).

200. C. Hafemeister, R. Satija, Normalization and variance stabilization of single-cell RNA-seq data using regularized negative binomial regression. *Genome Biology* **20**, 296 (2019).

201. I. Korsunsky, N. Millard, J. Fan, K. Slowikowski, F. Zhang, K. Wei, Y. Baglaenko, M. Brenner, P. Loh, S. Raychaudhuri, Fast, sensitive and accurate integration of single-cell data with Harmony. *Nat Methods* **16**, 1289–1296 (2019).

202. M. Peng, B. Wamsley, A. G. Elkins, D. H. Geschwind, Y. Wei, K. Roeder, Cell type hierarchy reconstruction via reconciliation of multi-resolution cluster tree. *Nucleic Acids Research* **49**, e91–e91 (2021).

203. R. Suzuki, H. Shimodaira, Pvclust: an R package for assessing the uncertainty in hierarchical clustering. *Bioinformatics* **22**, 1540–1542 (2006).

204. C. L. Thompson, L. Ng, V. Menon, S. Martinez, C.-K. Lee, K. Glattfelder, S. M. Sunkin, A. Henry, C. Lau, C. Dang, R. Garcia-Lopez, A. Martinez-Ferre, A. Pombero, J. L. R. Rubenstein, W. B. Wakeman, J. Hohmann, N. Dee, A. J. Sodt, R. Young, K. Smith, T.-N. Nguyen, J. Kidney, L. Kuan, A. Jeromin, A. Kaykas, J. Miller, D. Page, G. Orta, A. Bernard, Z. Riley, S. Smith, P. Wohnoutka, M. J. Hawrylycz, L. Puelles, A. R. Jones, A High-Resolution Spatiotemporal Atlas of Gene Expression of the Developing Mouse Brain. *Neuron* **83**, 309–323 (2014).

205. M. I. Love, W. Huber, S. Anders, Moderated estimation of fold change and dispersion for RNA-seq data with DESeq2. *Genome Biology* **15**, 550 (2014).

206. D. M. Emms, S. Kelly, OrthoFinder: phylogenetic orthology inference for comparative genomics. *Genome Biology* **20**, 238 (2019).

207. G. Csardi, T. Nepusz, The igraph software package for complex network research. *InterJournal* **Complex Systems**, 1695 (2006).

208. Application Note: Mapping brain cell types with CARTANA in situ sequencing on the Nikon Ti2-E microscope. https://www.nature.com/articles/d42473-019-00264-8.

209. X. Qian, K. D. Harris, T. Hauling, D. Nicoloutsopoulos, A. B. Muñoz-Manchado, N. Skene, J. Hjerling-Leffler, M. Nilsson, Probabilistic cell typing enables fine mapping of closely related cell types in situ. *Nat Methods* **17**, 101–106 (2020).

210. V. Petukhov, R. J. Xu, R. A. Soldatov, P. Cadinu, K. Khodosevich, J. R. Moffitt, P. V. Kharchenko, Cell segmentation in imaging-based spatial transcriptomics. *Nat Biotechnol* **40**, 345–354 (2022).